TRANSPORTATION RESEARCH RECORD 954

Design, Evaluation, and Performance of Pavements

TRB
TRANSPORTATION RESEARCH BOARD
NATIONAL RESEARCH COUNCIL
WASHINGTON, D.C. 1984

Transportation Research Record 954
Price $13.00
Editor: Naomi Kassabian
Typists: Darlene Lawrence and Joan G. Zubal

modes
1 highway transportation
4 air transportation

subject areas
24 pavement design and performance
40 maintenance
62 soil foundations

Transportation Research Board publications are available by ordering directly from TRB. They may also be obtained on a regular basis through organizational or individual affiliation with TRB; affiliates or library subscribers are eligible for substantial discounts. For further information, write to the Transportation Research Board, National Research Council, 2101 Constitution Avenue, Washington, D.C. 20418

Printed in the United States of America

Library of Congress Cataloging in Publication Data
National Research Council. Transportation Research Board.
Design, evaluation, and performance of pavements.

(Transportation research record; 954)
1. Pavements–Addresses, essays, lectures. I. National Research Council (U.S.). Transportation Research Board. II. Series.
TE7.H5 no. 954 380.5s 84-20773 [TE250] [625.8]
ISBN 0-309-03674-7 ISSN 0361-1981

Sponsorship of Transportation Research Record 954

GROUP 2–DESIGN AND CONSTRUCTION OF TRANSPORTATION FACILITIES
Robert C. Deen, University of Kentucky, chairman

Pavement Management Section
W. Ronald Hudson, University of Texas at Austin, chairman

Committee on Rigid Pavements
Richard A. McComb, Federal Highway Administration, chairman
Ernest J. Barenberg, William E. Brewer, Larry Joe Burton, Albert J. Bush III, Richard N. Cochrane, Bert E. Colley, Raymond A. Forsyth, Ray H. Fowler, James L. Greene, Yang H. Huang, Michael P. Jones, Walter Kilareski, T.J. Larsen, B. Frank McCullough, Dennis W. Miller, John Minor, Robert G. Packard, Surendra K. Saxena, Gary Wayne Sharpe, Joe P. Sheffield, William A. Yrjanson

Committee on Flexible Pavements
R.G. Hicks, Oregon State University, chairman
James A. Sherwood, Federal Highway Administration, secretary
R.N. Doty, David C. Esch, Wade L. Gramling, Douglas I. Hanson, Newton C. Jackson, Dallas N. Little, Dennis B. Luhrs, J.W. Lyon, Jr., Joe P. Mahoney, Adrian Pelzner, William A. Phang, James A. Scherocman, James F. Shook, Eugene L. Skok, Jr., Herbert F. Southgate, William T. Stapler, Harvey J. Treybig, Harry H. Ulery, Jr., Cecil J. Van Til, Loren M. Womack, Richard J. Worch

Committee on Strength and Deformation Characteristics of Pavement Sections
Amir N. Hanna, Portland Cement Association, chairman
Gilbert Y. Baladi, Richard D. Barksdale, Stephen F. Brown, George R. Cochran, Billy G. Connor, Gaylord Cumberledge, Jacob Greenstein, Jim W. Hall, Jr., R.G. Hicks, Robert K.H. Ho, Mario S. Hoffman, Ignat V. Kalcheff, William J. Kenis, Thomas W. Kennedy, Erland Lukanen, Lufti Raad, J. Brent Rauhut, Quentin L. Robnett, Gary Wayne Sharpe, James F. Shook, Eugene L. Skok, Jr., R.N. Stubstad, Marshall R. Thompson, Mian-Chang Wang

Lawrence F. Spaine, Transportation Research Board staff

Sponsorship is indicated by a footnote at the end of each report. The organizational units, officers, and members are as of December 31, 1983.

Contents

Addresses of Authors

Ball, C.G., Construction Technology Laboratories, Portland Cement Association, 5420 Old Orchard Road, Skokie, Ill. 60077

Barenberg, E.J., Department of Civil Engineering, University of Illinois at Urbana-Champaign, 104 South Wright Street, Urbana, Ill. 61801

Barksdale, Richard D., Department of Civil Engineering, Georgia Institute of Technology, Atlanta, Ga. 30332

Basma, Adnan A., Department of Civil Engineering, University of Mississippi, University, Miss. 38677

Doddihal, S.R., H.K.E. Society Engineering College, Gulbarga, Karnatak University, Dharwar, India

Fischer, J.A., Department of Civil Engineering, University of Illinois at Urbana-Champaign, 104 South Wright Street, Urbana, Ill. 61801

George, K.P., Department of Civil Engineering, University of Mississippi, University, Miss. 38677

Houben, L.J.M., Laboratory for Road and Railroad Research, Department of Civil Engineering, Delft University of Technology, 4 Stevinweg, Delft, Netherlands

Ioannides, A.M., Department of Civil Engineering, University of Illinois at Urbana-Champaign, 104 South Wright Street, Urbana, Ill. 61801

Lary, Jo A., Department of Civil Engineering, University of Washington, Seattle, Wash. 98195

Mahoney, Joe P., Department of Civil Engineering, University of Washington, Seattle, Wash. 98195

Mamlouk, Michael S., Department of Civil Engineering, State University of New York at Buffalo, Buffalo, N.Y. 14260

Molenaar, A.A.A., Laboratory for Road and Railroad Research, Department of Civil Engineering, Delft University of Technology, 4 Stevinweg, Delft, Netherlands

Moll, H.O., Laboratory for Road and Railroad Research, Department of Civil Engineering, Delft University of Technology, 4 Stevinweg, Delft, Netherlands

Okamoto, P.A., Construction Technology Laboratories, Portland Cement Association, 5420 Old Orchard Road, Skokie, Ill. 60077

Pandey, B.B., Department of Civil Engineering, Indian Institute of Technology, Kharagpur 721302, India

Stock, A.F., Department of Civil Engineering, The University, Dundee DD1 4HN, Scotland

Tayabji, S.D., Construction Technology Laboratories, Portland Cement Asssociation, 5420 Old Orchard Road, Skokie, Ill. 60077

Thompson, M.R., Department of Civil Engineering, University of Illinois at Urbana-Champaign, 104 South Wright Street, Urbana, Ill. 61801

van Wijk, Adriaan J., Joint Highway Research Project, School of Civil Engineering, Purdue University, West Lafayette, Ind. 47907

Yu, J., Department of Civil Engineering, The University, Dundee DD1 4HN, Scotland

K_R: The Resilient Modulus of Subgrade Reaction

J.A. FISCHER, M.R. THOMPSON, A.M. IOANNIDES, and E.J. BARENBERG

ABSTRACT

The concept of the resilient modulus of subgrade reaction (K_R) is developed to account for the stress-dependent behavior of typical fine-grained subgrade soils. This new subgrade support parameter is defined as plate pressure or resilient deflection in an impulse plate load test simulated by using the finite-element program ILLI-PAVE. K_R is expressed in the same units as the standard static modulus of subgrade reaction (k), but the value of the former is significantly higher. This indicates increased stiffness in response to rapidly moving loads. Factors influencing K_R include plate size, deflection level, and subgrade type. A 30-in.-diameter plate was chosen in this study in conformity with general practice. Equations relating K_R and deflection level are developed for four broad cohesive subgrade soil types: very soft, soft, medium, and stiff. The effect of a granular subbase on K_R is also examined. The introduction of a granular layer increases K_R substantially. The importance of this effect, however, diminishes rapidly as subbase thickness exceeds 8 in. The beneficial effect of a granular subbase is consistent over the range of plate pressures investigated.

In the analysis of slab-on-grade pavements [portland cement concrete (PCC), high-strength cementitiously stabilized materials], it is necessary to idealize the characteristics of the supporting medium. In general, one of two fundamentally different hypotheses concerning the properties of the subgrade is used. In the first of these theories, the soil is regarded as an elastic, isotropic, and homogeneous semiinfinite body. The term "elastic solid" is often used to describe this idealization. The majority of current analyses that treat the subgrade as a semi-infinite, elastic half-space employ axisymmetric models. Thus they are only applicable to the interior condition, i.e., where the load is away from any edge or corner.

In the other support characterization theory, the subgrade is regarded as a flexible bed in which surface pressure is proportional to surface deflection at each point, whereas adjacent unloaded areas are not affected at all. This idealization is commonly called a dense liquid or a Winkler subgrade. The finite-element program ILLI-SLAB (1,2) employs a Winkler-type subgrade and can be used to study two-layer cracked pavement sections, load transfer by aggregate interlock or dowels or both, variable slab thickness, variable subgrade support, and complex multiwheel loading at any position on the pavement. This model has been validated and used extensively in various University of Illinois studies (1,3).

In the original version of ILLI-SLAB the modulus of subgrade reaction (k) based on the plate load test is used for subgrade characterization. This is in conformity with general engineering practice as well as several other finite-element models. In ILLI-SLAB the value of k can be varied from node to node according to a pattern specified by the user. Note that k is independent of stress or deflection level, being essentially a linear, low-stress modulus. Most subbase-subgrade support systems, however, display a load-deflection response dependent on stress level. Typically, a softer (lower k) response is exhibited at higher magnitudes of stress or deflection.

To develop suitable support relations to accommodate deflection-dependent subgrade behavior for ILLI-SLAB, various models proposed by others were reviewed in a study by the U.S. Air Force Office of Scientific Research (AFOSR) (4). Special attention was paid to those that could be used to simulate nonlinear subgrade response. Thompson and Robnett (5) proposed a resilient modulus characterization for the elastic-solid foundation that not only introduced soil nonlinearity but also, perhaps more importantly, accounted for the apparent increase in subgrade stiffness produced by rapidly moving, repeated loads. The aim of this study is to develop a similar resilient modulus characterization for the dense-liquid foundation.

Data for the development of the necessary algorithms were obtained by using ILLI-PAVE (6), an axisymmetric, resilient elastic-solid model, to simulate repeated plate load tests. Equations were derived relating K_R and deflection. Note that this is no longer k from the static plate load test but a modulus characterizing subgrade response to repeated (impulse-type) loading. The latter loading condition is considered more appropriate for moving wheel loads.

SOIL AND MATERIAL CHARACTERIZATION

General

The resilient behavior of a soil or material is an important property for pavement analysis and design. A commonly used measure of resilient response is the resilient modulus, defined as follows:

$$E_R = \sigma_D/\epsilon_r \quad (1)$$

where

E_R = resilient modulus,
σ_D = repeated deviator stress, and
ϵ_r = recoverable axial strain.

Repeated unconfined compression or triaxial testing procedures are often used to evaluate the resilient moduli of fine-grained soils and granular materials. Resilient moduli are stress dependent: Fine-grained soils experience resilient modulus decreases with increasing stress, whereas granular materials stiffen with increasing stress level.

Fine-Grained Soils

Two models of stress-dependent behavior have been proposed for the stress-softening behavior of fine-grained soils. The arithmetic model is demonstrated

in Figures 1 and 2 [AASHTO A-7-6(36)] and the semi-log model is shown in Figure 3 [AASHTO A-7-6(36)]. Extensive resilient laboratory testing, nondestructive pavement testing, and pavement analysis and design studies at the University of Illinois have indicated that the arithmetic model (Figure 1) is adequate for pavement analysis activities.

In the arithmetic model the value of the resilient modulus at the breakpoint in the bilinear curve (E_{Ri}) is a good indicator of a soil's resilient behavior. The slope values (K_1 and K_2) display less variability and influence pavement structural response to a smaller degree than E_{Ri}. Thompson and Robnett (5) developed procedures for predicting the resilient behavior of fine-grained soils based on soil classification, soil properties, and moisture content. They suggested the following regression equations relating E_{Ri} with static soil modulus (E) and unconfined compressive strength (q_u):

$$E_{Ri} = 3.36 + 1.9E \quad (2)$$

$$E_{Ri} = 0.86 + 0.307q_u \quad (3)$$

where

E_{Ri} = breakpoint resilient modulus (ksi),
E = static modulus of elasticity (ksi), and
q_u = unconfined compressive strength (psi).

These correlations indicate that E_{Ri} is substantially greater than a static E.

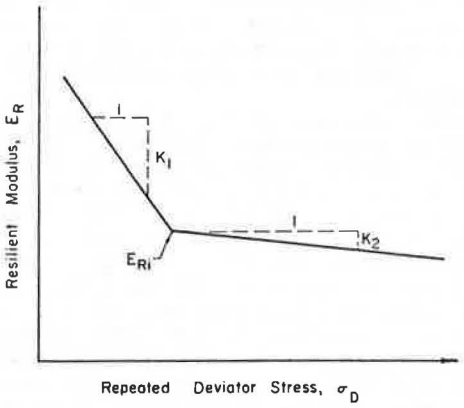

FIGURE 1 Arithmetic model for stress-dependent resilient behavior of fine-grained soils.

Granular Materials

In contrast to fine-grained soils, granular materials stiffen as the stress level increases. Repeated-load triaxial testing is used to characterize the resilient behavior of granular materials. The resilient modulus is a function of the applied stress state, defined as follows:

$$E_R = K\theta^n \quad (4)$$

where K and n are experimentally derived factors and

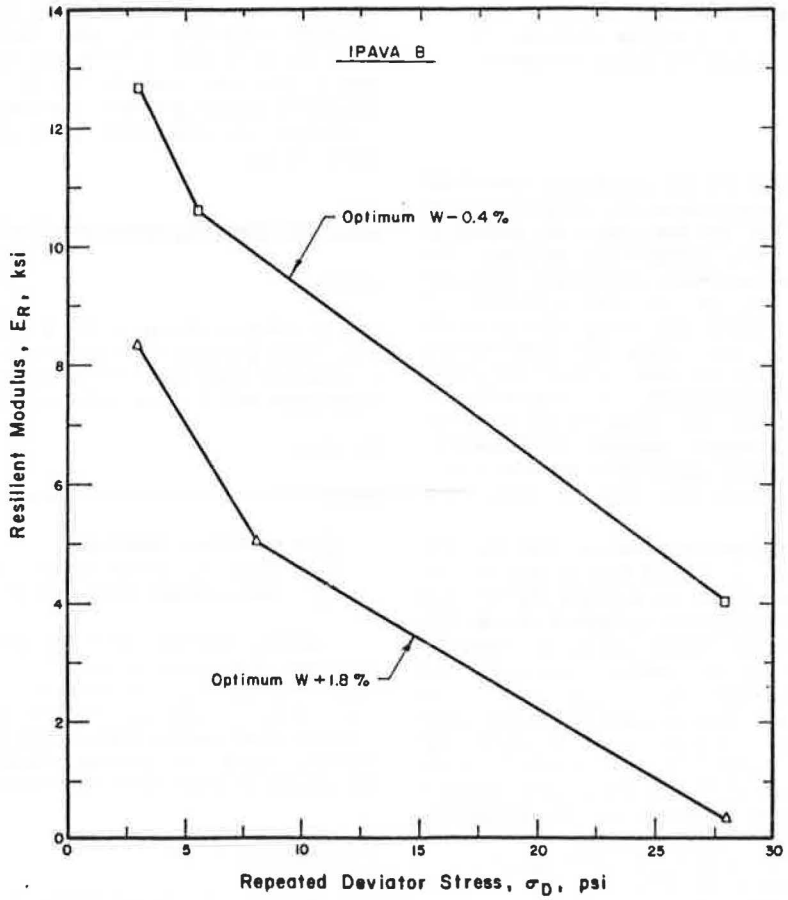

FIGURE 2 Typical stress-dependent resilient behavior of a fine-grained soil.

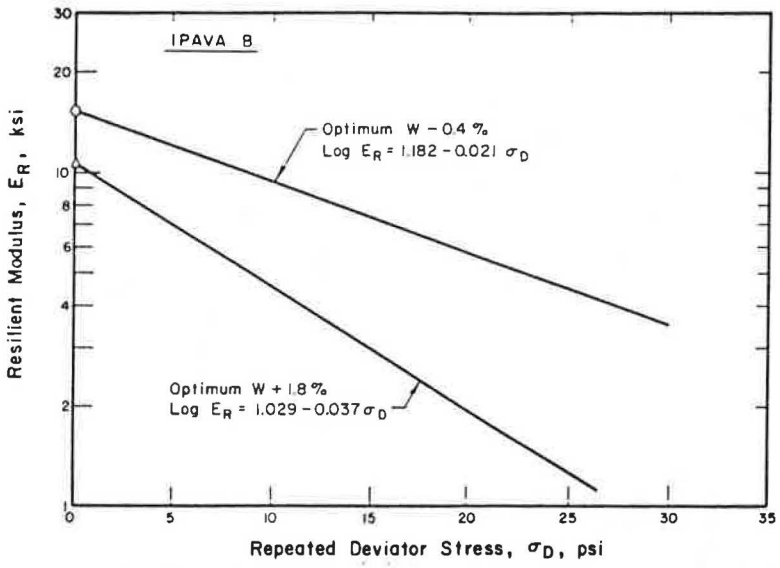

FIGURE 3 Semilog model for stress-dependent resilient behavior of a fine-grained soil.

θ is the first stress invariant ($\sigma_1 + \sigma_2 + \sigma_3$). (Note that $\theta = \sigma_1 + 2\sigma_3$ in a standard triaxial compression test.) Figure 4 is an E_R-θ relation for a sandy gravel [AASHTO A-1-b(0)].

Rada and Witczak (7) have summarized and statistically analyzed extensive published data on resilient moduli for a broad range of granular materials. The average values and ranges for K and n are given in Table 1 for several granular materials and coarse-grained soils.

Other Materials

Stabilized materials such as soil-cement, cement-aggregate mixtures, soil-lime mixtures, lime-flyash-aggregate mixtures, and similar materials that have high strength and high modulus are frequently used as base and subbase layers. These materials are normally characterized as constant-modulus materials.

RELATIONS BETWEEN K_R AND DEFLECTION

The finite-element program ILLI-PAVE (6) was used to develop the data (resilient plate load deflections) required to establish algorithms for K_R and deflection. This program considers an axisymmetric solid of revolution. Nonlinear stress-dependent material models and failure criteria for granular materials and fine-grained soils (6,8,9) are incorporated into ILLI-PAVE. The principal stresses in

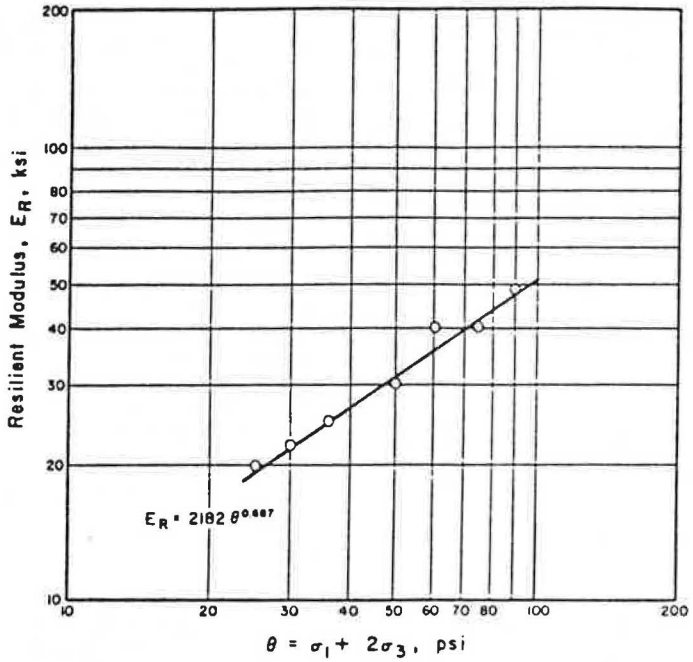

FIGURE 4 Resilient modulus versus θ for a sandy gravel.

TABLE 1 Typical Resilient Property Data *(7)*

Granular Material Type	No. of Data Points	K[a] (psi) Mean	K[a] (psi) Standard Deviation	n[a] Mean	n[a] Standard Deviation
Silty sand	8	1,620	780	0.62	0.13
Sand-gravel	37	4,480	4,300	0.53	0.17
Sand-aggregate blend	78	4,350	2,630	0.59	0.13
Crushed stone	115	7,210	7,490	0.45	0.23

[a] $E_R = K\theta^n$ where E_R is the resilient modulus (psi) and K,n are experimentally derived factors from repeated triaxial testing.

the granular and subgrade layers are modified at the end of each iteration so that they do not exceed the strength of the materials as defined by the Mohr-Coulomb theory of failure.

Studies comparing measured and ILLI-PAVE-predicted load-deformation responses, reported by Raad and Figueroa (6), Suddath and Thompson (10), Traylor (11), and Hoffman and Thompson (12), yielded favorable results. The ILLI-PAVE approach has been successfully used in developing a highway overlay design procedure for flexible pavement based on nondestructive-testing data analyses (13) as well as mechanistic thickness design procedures for secondary-road flexible pavements (14) and soil-lime layers (15).

ILLI-PAVE was used to simulate repeated plate load tests on various subgrades. The rigid plate condition was represented by a steel loading plate 4 in. thick ($E_s = 30 \times 10^6$ psi). Plate diameters of 30, 21, and 15 in. were considered for various plate pressures. For each loading condition, a resilient (recoverable) deflection was determined from the ILLI-PAVE analysis. K_R is analogous to k but is calculated by dividing the plate pressure by the calculated resilient plate deflection.

Applied plate pressures ranged from 2 psi to πc psi (c is the subgrade cohesion). Pressures larger than πc are not of practical interest, because at higher pressures significant permanent deformation (rutting) will occur in the subgrade.

Four fine-grained subgrade types (very soft, soft, medium, and stiff) were investigated. Pertinent subgrade properties and characteristics are summarized in Table 2. Relations of the resilient modulus versus repeated deviator stress level are shown in Figure 5.

Plate pressure versus resilient displacement data are presented in Figures 6 and 7. Relations of K_R versus plate deflection for the various subgrades are shown in Figures 8 through 11. The subgrades show a definite softening behavior (reduced K_R) with increasing pressures. The softening behavior

TABLE 2 Materials Property Summary

Property	Subgrade: Very Soft	Soft	Medium	Stiff	Gravel Subbase
Unit weight (pcf)	110.0	115.0	120.0	125.0	135.0
Coefficient of earth pressure at rest	0.82	0.82	0.82	0.82	0.6
Poisson's ratio	0.45	0.45	0.45	0.45	0.38
E_{Ri} (ksi)	1.00	3.02	7.68	12.34	—
E_R, model (psi)[a]	—	—	—	—	$5{,}000\theta^{0.50}$
Friction angle (degrees)	0.0	0.0	0.0	0.0	40.0
Cohesion (psi)	3.1	6.5	11.4	16.4	0.0
Estimated k[b] (psi/in.)	50	100	150	200	—

[a] $E_R = K\theta^n$ (E_R, K, and θ in psi).
[b] Standard modulus of subgrade reaction.

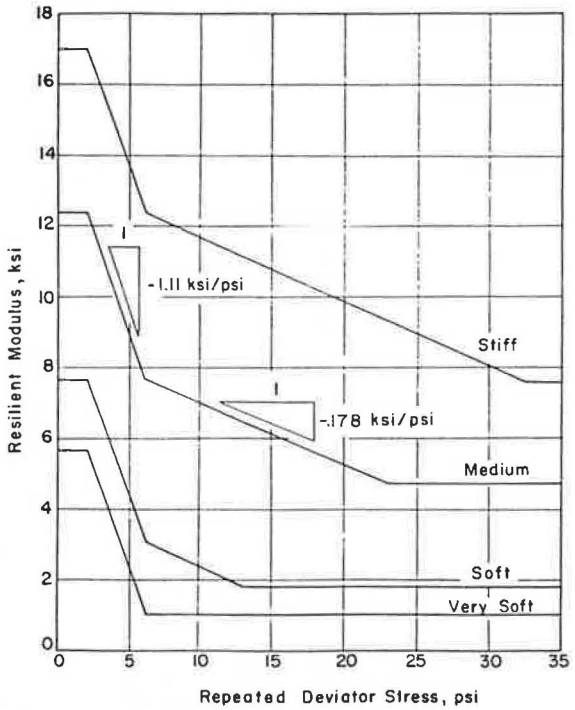

FIGURE 5 Subgrade soil material models for ILLI-PAVE analyses.

is most pronounced for the soft subgrade (Figure 9), where K_R at a pressure of πc is approximately 60 percent of K_R at 2 psi. For a given plate pressure and subgrade type, a decrease in plate size results in a stiffer plate response (K_R increases).

ALGORITHM DEVELOPMENT

A recent study by AFOSR at the University of Illinois (4) indicated that an empirical relation of plate pressure versus deflection proposed by Butterfield and Georgiadis (16) best represented the ILLI-PAVE-generated data on K_R and deflection. The basis of the equation is an idealization proposed by Burland and Lord (17). The equation is characterized by three parameters: an initial stiffness (k_0), a final stiffness (k_f), and a pressure-axis intercept (q_u) (Figure 12). The form of the equation is as follows:

$$q = q_u \left\{1 - \exp\left[-(k_0 - k_f)(w/q_u)\right]\right\} + k_f w \tag{5}$$

where w is plate deflection. The equation was modified for presenting the ILLI-PAVE data for plate pressure versus resilient displacement. A normalized deflection parameter (w/D_y) was substituted into the equation for w, where D_y represents the deflection at a plate pressure of πc psi. The resulting equation is as follows:

$$p = A_1 \left(1 - \exp\left\{-A_2\left[(w/D_y) - A_3\right]\right\}\right) + A_4\left[(w/D_y) - A_3\right] + 2 \tag{6}$$

where

p = plate pressure,
D_y = deflection factor for a given subgrade type (very soft, soft, medium, stiff), and
$A_1, A_2, \ldots$ = subgrade constants.

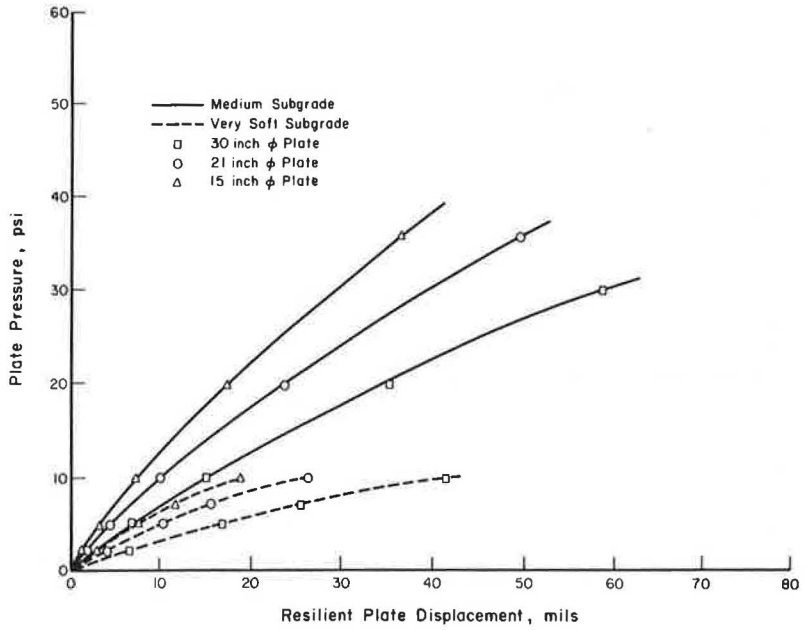

FIGURE 6 Plate pressure versus resilient displacement for medium and very soft subgrades.

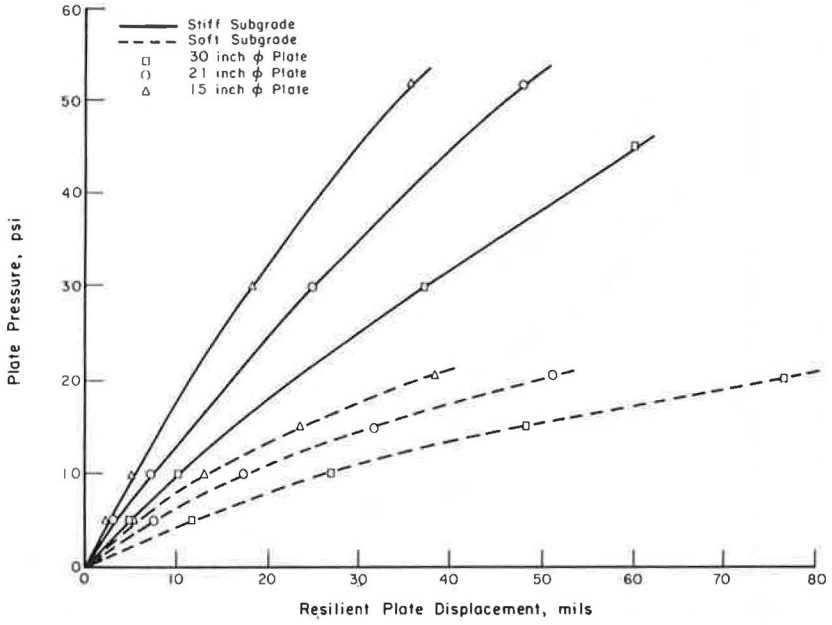

FIGURE 7 Plate pressure versus resilient displacement for stiff and soft subgrades.

If this equation is divided through by the plate deflection (w), the p/w term is K_R, the resilient modulus of subgrade reaction. The final K_R algorithm is as follows:

$$K_R = (1/w)\left[A_1\left(1 - \exp\left\{-A_2\left[(w/D_y) - A_3\right]\right\}\right) + A_4\left[(w/D_y) - A_3\right] + 2\right]$$
$$= A_5/D_y \quad \text{if } (w/D_y) < A_3 \tag{7}$$

Regression analyses were used to develop four equations, one for each subgrade type studied. The resulting equation parameters for the 30-in.-diameter plate are summarized in Table 3. Values of the correlation coefficient (R), standard error of estimate, and coefficient of variation for the equations are also presented in Table 3. To be consistent with the relations of subgrade resilient modulus versus stress level (see Figure 5), K_R is assumed to be a constant for pressures less than 2 psi.

Note that K_R obtained from these algorithms has values much greater than the corresponding static subgrade modulus (k) for any given soil. This is consistent with the observation that soils exhibit a much stiffer response when loaded by rapidly moving loads rather than by static loads. A similar observation was made regarding the relation between the values of E_{Ri} and static E.

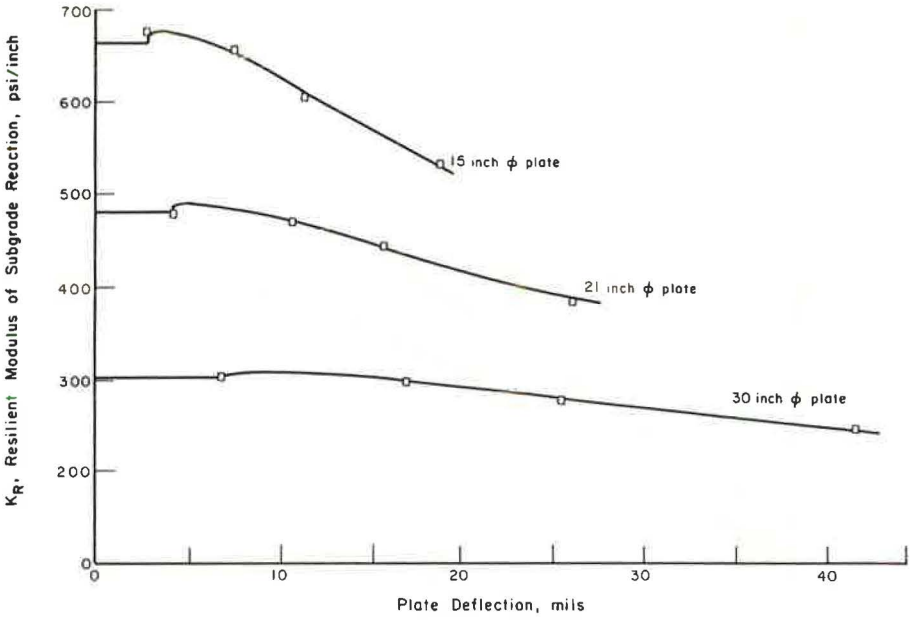

FIGURE 8 K_R versus deflection for various plate sizes (very soft subgrade).

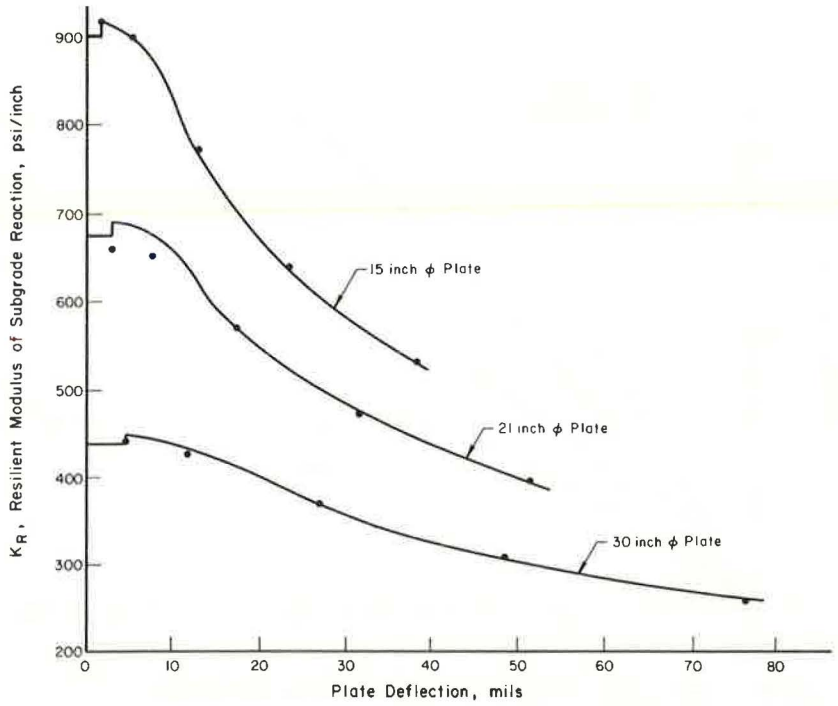

FIGURE 9 K_R versus deflection for various plate sizes (soft subgrade).

SUBBASE EFFECTS

Effect of Granular Subbase

A layer of granular material is frequently used as a subbase in PCC pavement construction. The structural contribution of the granular layer is generally acknowledged by assigning an increased design k to the combination of granular layer and subgrade (18-20).

Additional plate load tests employing a 30-in.-diameter plate on a granular subbase and subgrade soil support system were also simulated by using ILLI-PAVE. The properties of the granular subbase (gravel) are listed in Table 2. Three different granular subbase thicknesses (8, 16, and 24 in.) were considered. The applied plate pressure was 2c. Figure 13 shows the effect of granular layer thickness on K_R for each of the four subgrades. It may be concluded that the introduction of a granular

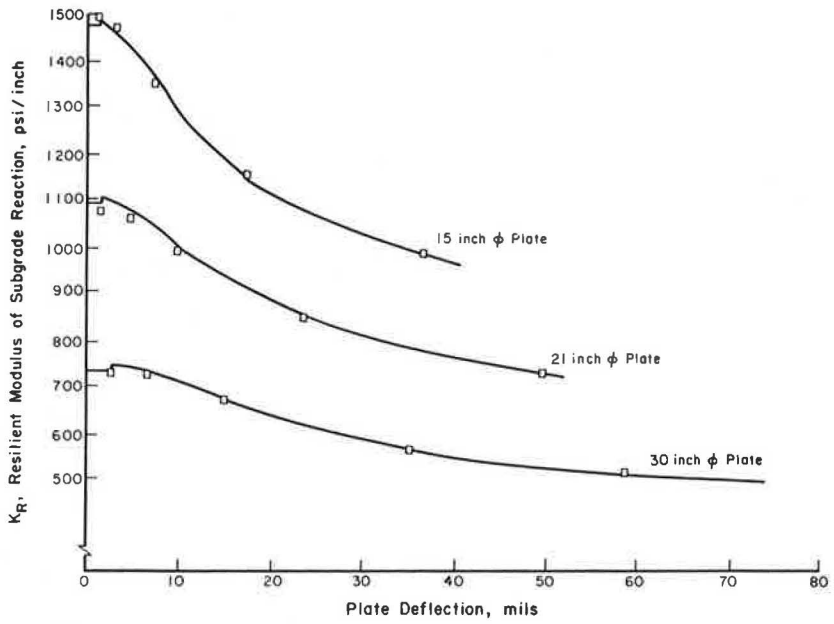

FIGURE 10 K_R **versus deflection for various plate sizes (medium subgrade).**

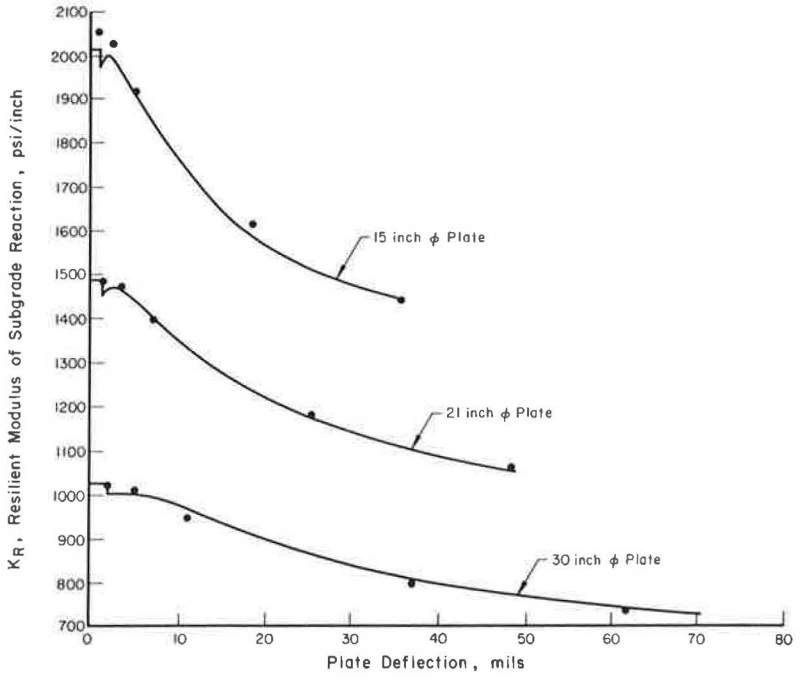

FIGURE 11 K_R **versus deflection for various plate sizes (stiff subgrade).**

TABLE 3 Regression Equation Parameters and Statistics

Subgrade	A_1	A_2	A_3	A_4	A_5	D_Y	R^a	SEE[b] (psi/in.)	Coefficient of Variation (%)
Very soft	15.0	0.80	0.1680	0.62	11.9	0.0400	0.993	3.9	1.4
Soft	9.5	2.60	0.0594	10.25	33.7	0.0782	0.995	9.1	2.5
Medium	7.0	3.74	0.0377	28.10	53.1	0.0734	0.997	9.1	1.4
Stiff	5.0	5.30	0.0282	45.90	71.0	0.0707	0.995	13.9	1.5

[a]Correlation coefficient.
[b]Standard error of estimate.

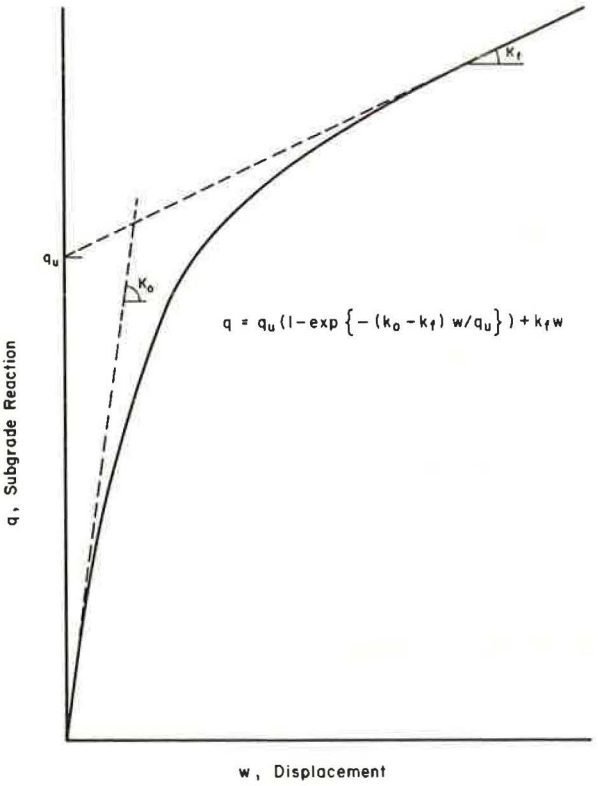

FIGURE 12 Parameters for Butterfield and Georgiadis empirical equation.

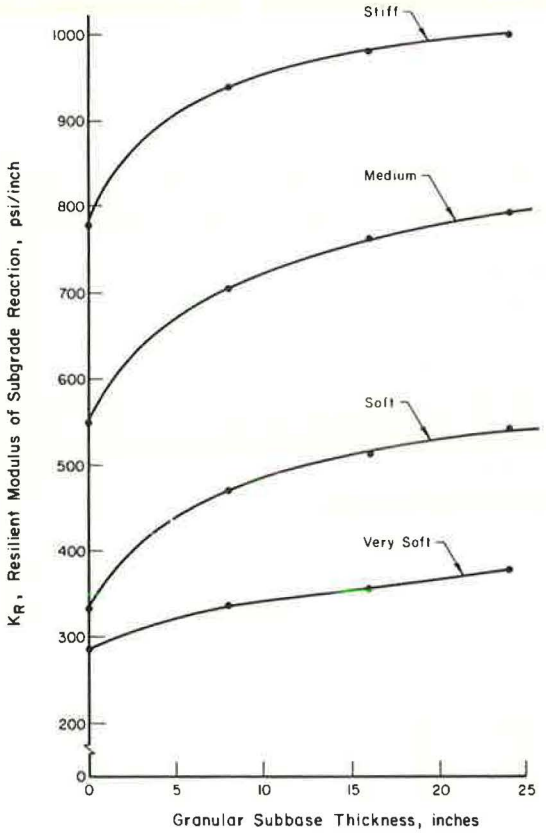

FIGURE 13 K_R versus granular subbase thickness.

subbase up to 8 in. thick has a pronounced beneficial effect on K_R. For greater thicknesses of subbase, the effect on K_R progressively decreases so that subbase thickness has only a slight effect within the 8- to 24-in. thickness range considered. The comments made in the previous section with regard to the apparently high K_R values apply here as well.

Plate pressure effects were also evaluated for an 8-in. granular subbase layer and the soft and very soft subgrade types for plate pressures of c, 2c, and πc psi. Comparative data for the no-subbase and subbase conditions shown in Figure 14 indicate that plate pressure has only a nominal effect. The stress-stiffening behavior of the granular material counteracts to some extent the stress-softening behavior of the fine-grained subgrade.

Effect of Stabilized Subbase

The effect of a subbase with high strength and modulus on a PCC pavement can be considered by increasing k for the stabilized subbase-subgrade system. This procedure is recommended by the Portland Cement Association (18,19) and the Federal Aviation Administration (20).

The ILLI-SLAB program, on the other hand, considers the stabilized subbase as a flexural subbase beneath the PCC layer. This is a more desirable procedure than using an increased k, because the elastic properties of the subbase and its degree of bonding with the PCC slab can be considered.

SUMMARY

The concept of the resilient modulus of subgrade reaction (K_R) is introduced to account for the stress-dependent behavior of typical subgrade soils. This new subgrade support parameter is defined as the pressure producing unit deflection in an impulse plate load test simulated by using the finite-element program ILLI-PAVE. K_R is expressed in the same units as the standard static modulus of subgrade reaction (k), but the value of the former is significantly higher. This indicates increased stiffness in response to rapidly moving loads.

Factors influencing K_R include plate size, deflection level, and subgrade type. A 30-in.-diameter plate was chosen in this study in conformity with general practice. Equations relating K_R and deflection level were developed for four broad cohesive subgrade soil types: very soft, soft, medium, and stiff. The effect of a granular subbase on K_R was also examined. The introduction of a granular layer increases K_R substantially. The importance of this effect, however, diminishes rapidly as subbase thickness exceeds 8 in. The beneficial effect of a granular subbase is consistent over the range of plate pressures investigated (c, 2c, and πc psi).

ACKNOWLEDGMENT

This paper was based on an AFOSR research project report (4). The project was sponsored by AFOSR, Air Force Systems Command, Bolling Air Force Base, Washington, D.C. Lt. Col. J.J. Allen was the program manager.

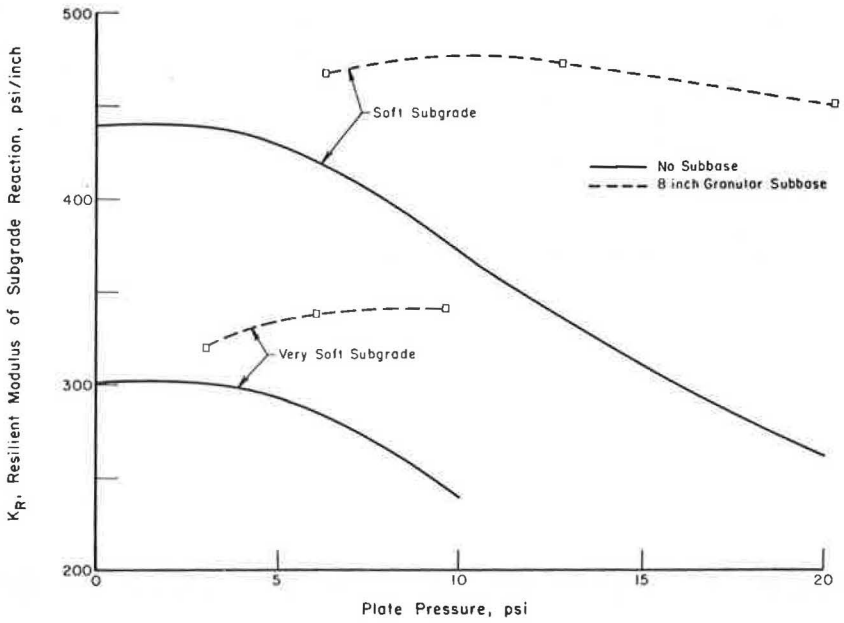

FIGURE 14 K_R versus granular subbase effects for variable plate pressures.

REFERENCES

1. A.M. Tabatabaie, E.J. Barenberg, and R.E. Smith. Longitudinal Joint Systems in Slip-Formed Rigid Pavements, Vol. 2: Analysis of Load Transfer Systems for Concrete Pavements. Report FAA-RD-79-4, II. U.S. Department of Transportation, Nov. 1979.
2. A.M. Tabatabaie and E.J. Barenberg. Longitudinal Joint Systems in Slip-Formed Rigid Pavements, Vol. 3: User's Manual. Report FAA-RD-79-4, III. U.S. Department of Transportation, Nov. 1979.
3. A.M. Tabatabaie and E.J. Barenberg. Finite-Element Analysis of Jointed or Cracked Concrete Pavements. In Transportation Research Record 671, TRB, National Research Council, Washington, D.C., 1978, pp. 11-19.
4. A.M. Ioannides, M.R. Thompson, E.J. Barenberg, and J.A. Fischer. Development of a Stress-Dependent Finite Element Slab Model. Report AFOSR-TR-83-1061. Air Force Office of Scientific Research, Air Force Systems Command, Washington, D.C., May 1983.
5. M.R. Thompson and Q.L. Robnett. Resilient Properties of Subgrade Soils. Transportation Engineering Journal of ASCE, Vol. 105, No. TE1, Jan. 1979.
6. L. Raad and J.L. Figueroa. Load Response of Transportation Support Systems. Transportation Engineering Journal of ASCE, Vol. 106, No. TE1, Jan. 1980.
7. G. Rada and M.W. Witczak. Comprehensive Evaluation of Laboratory Resilient Moduli Results for Granular Material. In Transportation Research Record 810, TRB, National Research Council, Washington, D.C., 1981, pp. 23-33.
8. J.L. Figueroa. Resilient Based Flexible Pavement Design Procedure for Secondary Roads. Ph.D. thesis. University of Illinois, Urbana, 1979.
9. M.S. Hoffman and M.R. Thompson. Mechanistic Interpretation of Nondestructive Pavement Testing Deflections. Civil Engineering Studies, Transportation Engineering Series 32, Illinois Cooperative Highway and Transportation Research Program Series 190. University of Illinois at Urbana-Champaign, June 1981.
10. L.P. Suddath and M.R. Thompson. Load-Deflection Behavior of Lime-Stabilized Layers. Technical Report M-118. Construction Engineering Research Laboratory, Champaign, Ill., 1975.
11. M.R. Traylor. Nondestructive Testing of Flexible Pavements. Ph.D. thesis. Department of Civil Engineering, University of Illinois, Urbana, 1979.
12. M.S. Hoffman and M.R. Thompson. Nondestructive Testing of Flexible Pavements--Field Testing Program Summary. Civil Engineering Studies, Transportation Engineering Series 31, Illinois Cooperative Highway and Transportation Research Program Series 188. University of Illinois at Urbana-Champaign, June 1981.
13. M.R. Thompson. Concepts for Developing a Nondestructive Based Asphalt Concrete Overlay Thickness Design Procedure. Civil Engineering Studies, Transportation Engineering Series 34, Illinois Cooperative Highway and Transportation Series 194. University of Illinois at Urbana-Champaign, June 1982.
14. J.L. Figueroa and M.R. Thompson. Simplified Structural Analyses of Flexible Pavements for Secondary Roads Based on ILLI-PAVE. In Transportation Research Record 766, TRB, National Research Council, Washington, D.C., 1980, pp. 5-10.
15. M.R. Thompson and J.L. Figueroa. Mechanistic Thickness-Design Procedure for Soil-Lime Layers. In Transportation Research Record 754, TRB, National Research Council, Washington, D.C., 1980, pp. 32-36.
16. R. Butterfield and M. Georgiadis. New Interpretation of Plate-Bearing Tests. In Transportation Research Record 810, TRB, National Research Council, Washington, D.C., 1981, pp. 60-67.
17. J.B. Burland and J.A. Lord. The Load-Deformation Behavior of Middle Chalk at Mundford, Norfolk: A Comparison Between Full Scale Perfor-

mance and In-situ and Laboratory Measurements. In In-situ Investigation of Soils and Rocks, British Geological Society, 1970.
18. R.G. Packard. Design of Concrete Airport Pavement. Engineering Bull. EB050.03P. Portland Cement Association, Skokie, Ill., 1973.
19. Thickness Design for Concrete Pavements. IS010.03P. Portland Cement Association, Skokie, Ill., 1966.
20. Airport Pavement Design and Evaluation. Advisory Circular 150/5320-60. FAA, Dec. 7, 1978.

The contents of this paper reflect the views of the authors, who are responsible for the facts and the accuracy of the data presented herein. The contents do not necessarily reflect the official views or policies of the U.S. Air Force. This paper does not constitute a standard, specification, or regulation.

Publication of this paper sponsored by Committee on Rigid Pavements.

Finite-Element Model with Stress-Dependent Support

A.M. IOANNIDES, E.J. BARENBERG, and M.R. THOMPSON

ABSTRACT

The finite-element model presented is a modified and expanded version of the model developed in 1977 for the study of jointed, slab-on-grade pavements, ILLI-SLAB. A number of modifications to the original code are described. The most important of these is the incorporation through an iterative procedure of the deflection-dependent resilient modulus of subgrade reaction (K_R). This parameter is considered more appropriate in modeling nonlinear subgrade response to rapidly moving loads. Other changes include generation of contour plots of system response, introduction of lines of symmetry, correction of the uniform subgrade stiffness matrix, specification of loaded areas in terms of global coordinates, and free-form input capability. To illustrate the impact of these innovations, results from several demonstration runs are summarized. The major effect of the proposed model is due to the higher values of K_R compared with the commonly used static k.

The determination of stresses and deflections in slab-on-grade pavements with joints or cracks or both has been a subject of major concern for several years. For many pavement structures it has been virtually impossible to obtain analytical (closed-form) solutions because of the complexity of geometry, boundary conditions, and material properties, unless certain simplifying assumptions are made. These, however, result in a modification of the characteristics of the problem. With the advent of high-speed digital computers, solution of these complex structural problems has been greatly facilitated. One of the most powerful methods that has evolved is the finite-element method. This method of analysis is widely accepted as applicable to a broad range of complex boundary-value problems in engineering.

In the calculation of stresses in slab-on-grade pavements, it is also necessary to idealize the characteristics of the supporting medium. In one of the simplest and most popular support characterization theories, the subgrade is regarded as a flexible bed with surface pressure proportional to surface deflection at each point, whereas adjacent unloaded areas are unaffected. This idealization is commonly called a dense liquid or a Winkler subgrade. Finite-element program ILLI-SLAB (1,2) employs a Winkler-type subgrade and can be used to study two-layer, cracked pavement sections, variable load transfer across joints or cracks by aggregate interlock or dowels or both, variable slab thickness, variable subgrade support, and complex multiwheel loading at any position on the pavement. This model has been validated and used extensively in various University of Illinois studies (1,3,4).

In the original version of ILLI-SLAB (1), the modulus of subgrade reaction (k) obtained from the plate load test is used for subgrade characterization. This is in conformity with general engineering practice. Several other finite-element models also use this approach (5-7). The value of k can be varied from node to node according to a pattern specified by the user at the beginning of the analysis. Note that k is assumed to be independent of stress or deflection level, being essentially a linear, low-stress modulus. Most subbase-subgrade support systems, however, display a response dependent on stress level. Typically a softer (lower-k) response is exhibited at higher magnitudes of stress or deflection.

To account for this effect, the concept of the resilient modulus of subgrade reaction (K_R) was introduced in a U.S. Air Force Office of Scientific Research (AFOSR) study (8). This is no longer the modulus k, derived from the static plate load test, but a modulus characterizing subgrade response to a repeated (impulse-type) test. The latter loading condition is considered more appropriate for the type of moving loads applied by modern-day highway and airport traffic. In the AFOSR study, relationships are developed between K_R and deflection (w) for a broad range of fine-grained soils.

In this paper a description is given of how the

deflection-dependent support relations are incorporated into ILLI-SLAB to accommodate nonlinear subgrade behavior. Several other ILLI-SLAB improvements are also presented. The impact of these innovations is assessed by using a series of demonstration runs involving typical pavement sections and loading patterns.

ILLI-SLAB

ILLI-SLAB was developed at the University of Illinois in 1977 for structural analysis of jointed one- or two-layer concrete pavements with specified levels of load transfer at the joints or cracks (1,2). The ILLI-SLAB model is based on the classical theory of a medium-thick plate on a Winkler foundation (9) and can be used to evaluate the structural response of a concrete pavement system with joints or cracks or both. It employs the plate-bending element with four nodes and 12 degrees of freedom known in the finite-element literature as ACM or RPB12 (10). The Winkler-type subgrade is modeled as a uniform distributed subgrade through an equivalent mass formulation (11). This is a much more realistic representation than the four concentrated spring elements used in other programs (5-7). A work equivalent load vector is used (10).

Various types of load transfer systems, such as dowel bars, aggregate interlock, keyways, or a combination of these, can be considered at the pavement joints with ILLI-SLAB. The model can also accommodate the effect of a stabilized base or an overlay (with either perfect bond or no bond).

MODIFICATION OF ILLI-SLAB

For the benefits of the finite-element method to be fully realized, it is highly desirable that programs using this method of analysis

1. Accept easy-to-compile, user-oriented input data restricted to the absolute minimum required and in which, where possible, potential pitfalls for the user have been eliminated;
2. Employ carefully selected default values that will reduce the amount of input data required;
3. Perform error checks, especially in the case of default values, so that errors that are concealed by the otherwise normal execution of the program will be avoided;
4. Be free of code errors;
5. Organize the output so that it is neat, meaningful, and user-oriented;
6. Incorporate skillful data-base management for the efficient utilization of available memory core;
7. Provide basic and higher-level routines; and
8. Present the results in a summary or a graphical form.

The ILLI-SLAB modifications presented in the following are aimed at providing these capabilities.

Stress-Dependent Subgrade Definition

The general expression for the relation between K_R and w as developed in this study (30-in.-diameter plate) is (8)

$$K_R = (1/w)\left[A_1\left(1 - \exp\left\{-A_2\left[(w/D_y) - A_3\right]\right\}\right) + A_4\left[(w/D_y) - A_3\right] + 2\right]$$
$$= A_5/D_y \quad \text{if } (w/D_y) < A_3 \qquad (1)$$

where A_1, A_2, A_3, A_4, A_5, and D_y are regression parameters determined from plate load tests simulated by using ILLI-PAVE (12), a stress-dependent (nonlinear) finite-element program developed at the University of Illinois. By specifying these parameters, the user can define a stress-dependent subgrade. Parameter sets for the following broad subgrade types have been developed and are now an integral part of the revised version of ILLI-SLAB:

1. Very soft (K_R = 300 psi/in.),
2. Soft (K_R = 425 psi/in.),
3. Medium (K_R = 725 psi/in.), and
4. Stiff (K_R = 1,000 psi/in.).

The figures in parentheses are recommended initial (small-deflection) values. These are significantly higher than the normally accepted static k-values, reflecting the increased subgrade stiffness that results from dynamic or rapidly moving loads.

Other options available in modified ILLI-SLAB are as follows:

1. Other: The user specifies the regression parameters individually to obtain a different relation of K_R versus w.
2. Winkler: This option is the stress-independent, uniform Winkler subgrade, available in the original version of ILLI-SLAB.
3. Springs: Support is provided by four springs at the corner of each element (stress independent). This option allows validation by direct comparison with other programs but is not recommended for general use.

An iterative procedure, which compares support values (K_R) corresponding to calculated deflections with previously assumed or determined values, is used in the modified version of ILLI-SLAB. New support values are assigned for each subsequent iteration until compatibility is achieved between support system deflections and the user-prescribed support pattern. Furthermore the new model allows the user to assign different support values to selected (or all) nodes. When one of the stress-dependent subgrade types is used, subroutine ITERATE provides a procedure for checking convergence, updating support values, and proceeding with additional iterations as necessary. Subroutine ITERATE is structured to allow easy modification of the regression equations or addition of other subgrade options. The user controls the iterative procedure by three variables:

1. ITMAX: This variable specifies the maximum number of iterations desired. Usually three iterations are sufficient; a value of ITMAX = 6 is recommended.
2. TOL1: Convergence tolerance for updated K_R compared with K_R from the previous iteration. A value of TOL1 = 0.05, i.e., 5 percent, is recommended.
3. TOL2: Convergence tolerance for percentage of nodes at which TOL1 is not satisfied. Again, a value of TOL2 = 0.05, i.e., 5 percent, is recommended. The recommended values of ITMAX, TOL1, and TOL2 are used as default values.

Contouring Capability

During a study conducted in summer 1981, the facility to generate contours of stresses and deflections was incorporated into the ILLI-SLAB package (4). This was done through auxiliary program CONT, which accepts ILLI-SLAB results as input data. Subroutine CONTOUR in this auxiliary program passes these re-

sults to a number of subroutines developed at the National Center for Atmospheric Research (NCAR). The software used in these subroutines has been developed and is made available with the restriction that NCAR be acknowledged as the source in any resulting research or publications. The most important family of NCAR subroutines used in ILLI-SLAB is CONRAN. CONRAN, the standard version, plots contour lines by using random, sparse, or irregular data sets; adds line labeling and contour dash patterns; and plots relative highs and lows. The data are triangulated and then contoured. Contouring is performed by interpolating the triangulated data. Typical contour plots are shown in Figure 1.

More Efficient Memory Core Utilization

A major problem encountered by ILLI-SLAB users is that any attempt to refine the mesh used, especially when investigation of the stability and convergence of the numerical solution is desired or when several slabs are used, faces the possibility of exceeding machine memory core capacity. This problem has been addressed by the introduction of the capability to take advantage of any symmetry lines that may exist. In the modified ILLI-SLAB version, the user has the following options:

1. No lines of symmetry exist (ISYM = 0),
2. The x-axis is a line of symmetry (ISYM = 1),
3. The y-axis is a line of symmetry (ISYM = 2), and
4. The x- and y-axes are both axes of symmetry (ISYM = 3).

Care was taken to introduce these options without imposition of a burden on the user during the preparation of the input data. Particularly undesirable are requirements to include the node numbers for the nodes along the line or lines of symmetry. In the new version of ILLI-SLAB, the various options re-

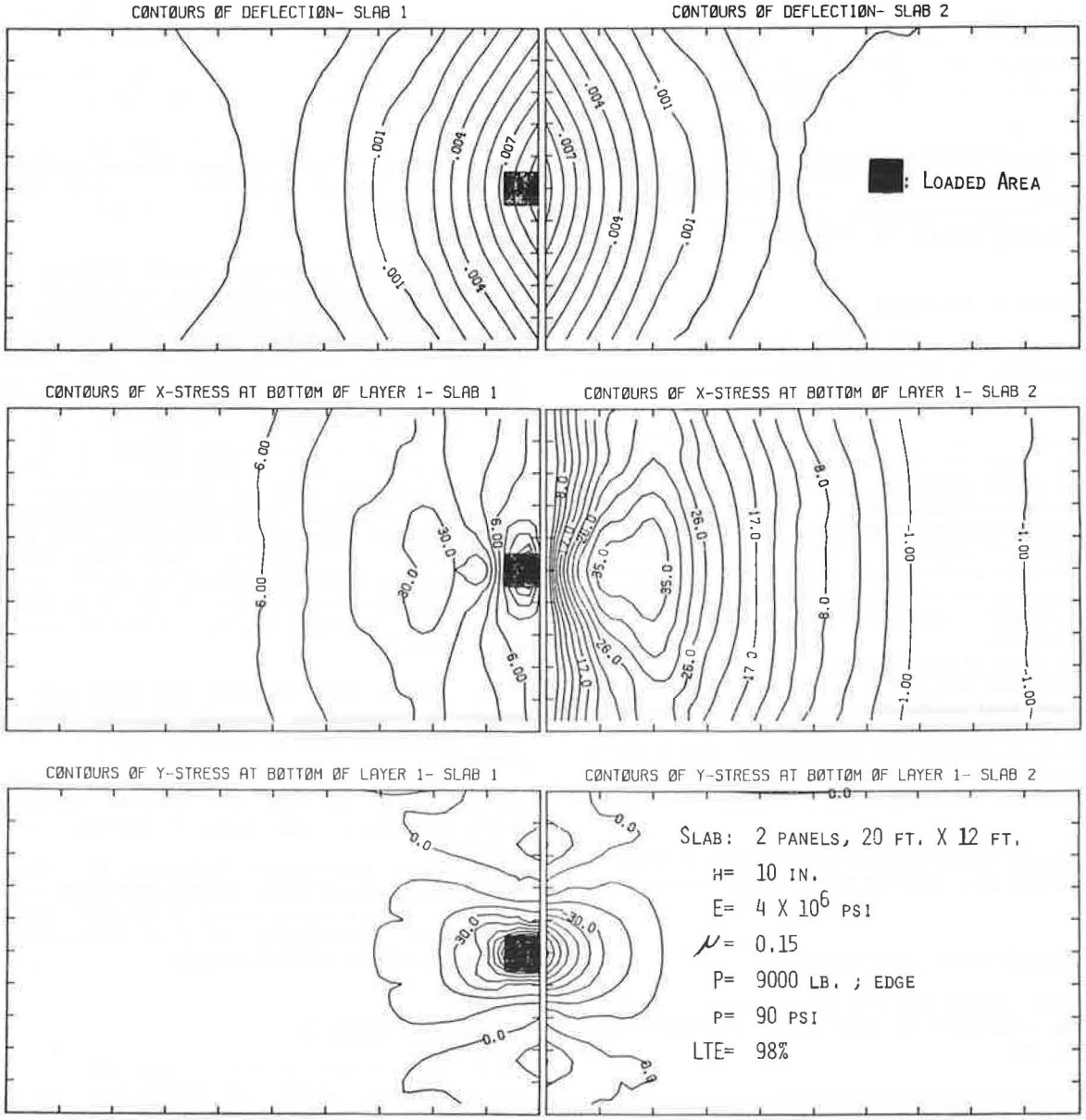

FIGURE 1 Typical contour plots.

lated with symmetry are specified by using a single input variable (ISYM), which may even be omitted if no symmetry exists.

Subgrade Stiffness Matrix Correction

One of the major advantages of ILLI-SLAB over other available programs is that the Winkler-type foundation is no longer modeled by four concentrated springs at the corners of each slab element. Through an equivalent mass formulation, a uniform distributed subgrade is provided under each element. The formulation for the derivation of the stiffness matrix for this subgrade (1) follows the same steps as the ones presented by Dawe (11), who first derived this matrix. In Dawe's equivalent mass formulation, the product of mass per unit area and plate thickness (ρh) replaces the subgrade modulus k (or K_R). Similar derivations using different sign conventions are also presented by Przemieniecki (13) and Zienkiewicz (10).

The subgrade stiffness matrix used in ILLI-SLAB was compared with each of the matrices presented in these publications, which were further compared with each other, with due allowance for differences in sign convention. The original formulation of the stiffness matrix in ILLI-SLAB (1) was thereby corrected. For earlier users of the program, the corrections in the stiffness matrix are most obvious in the results from solutions of symmetric problems, where identical responses are now obtained at corresponding points, as expected. Although the change in the results of a typical run may only range from 3 to 5 percent, it is important to have a balanced formulation to ensure the good behavior and convergence of the numerical solution.

Specification of Loaded Areas in Terms of Global Coordinates

In the original version of ILLI-SLAB, input data specifying loaded area or areas had to be in terms of local (element) coordinates. In this sytem the origin is set at the lower left corner of each element and the axes extend from 0 to 2a in the x-direction and 2b in the y-direction for a typical element of dimensions 2a x 2b. The result was that the user had to go through the following steps when the loaded areas for the problem were specified:

1. Determine the element numbers of the loaded elements adhering to a fixed numbering sequence, i.e., from bottom to top and from left to right. It should be noted that depending on the fineness of the mesh used, each loaded area (such as a wheel imprint) might apply a load on four or more elements. Thus, a large number of partially or fully loaded elements might be needed to define the loading pattern in all but the simplest situations.
2. For each of the loaded elements, determine the extent of the loaded subarea in terms of the local element coordinate system. These coordinates should then be specified, one subarea per card, together with the load intensity in each case.
3. Whenever there is a change in the finite-element mesh used, such as when the mesh is made finer, the process must be repeated.

As a result of the complexity of this process, especially when it was used, as it was, with the fixed-form input format, a large portion of all problems encountered by ILLI-SLAB users was related to specifying loading pattern data. To overcome these difficulties, subroutine SUBAREA was coded to allow input data specification in terms of the global coordinate system. In this system the origin is located at the lower left corner of the slab arrangement and the axes extend to the extreme corners of the arrangement of all the slabs in both the x- and y-directions. The advantages of this system are obvious:

1. Element numbering, although retained internally, does not enter into input data preparation;
2. Only as many loaded areas as actually exist need be specified; the global coordinates and the extent of each loaded area now acquire a more realistic physical meaning for the user; and
3. The global coordinate system is independent of the mesh used, being solely determined by the arrangement of slab or slabs analyzed.

Free-Form Input Capability

With the addition of several new subroutines, ILLI-SLAB can now accept free-form input data by using a problem-oriented language (POL) consisting of simple, easy-to-remember English-type statements. This has been made possible by accessing the SCAN library of routines developed at the Civil Engineering Systems Laboratory (CESL) at the University of Illinois (14-16). SCAN has been used as a teaching and research tool for a number of years at the University of Illinois. It is also the front end of the POLO system, including FINITE (7), and is used in a number of production systems at CESL.

Only those parameters that are different from the default values need be provided when the free-form input capability is used. This will save time in preparing the input data file and executing the program. The free-form subroutines are set up to issue diagnostic error messages before execution in the event of improper input data. These greatly facilitate debugging the input data file and are particularly useful to new users of ILLI-SLAB.

Miscellaneous Changes

In addition to providing a user-oriented input data capability, it is desirable to have a user-oriented presentation of the results from a given run. Early in this study particular attention was directed toward improving the output format by the introduction of appropriate carriage control characters, elimination of unnecessary lines of output, and replacement of these by other meaningful output information. The changes incorporated in the revised version of ILLI-SLAB are aimed at providing a well-organized, clear echo of the input file so that the parameters and loading conditions used can be easily checked as well as at giving the user a neat, usable output. Of great interest to the user is the summary of maximum values of deflection and stresses and the nodal numbers at which these occur, which is given at the end of the output.

A second group of changes involved the elimination of several code errors ("bugs") that were revealed by numerous error checks. Comparisons with FINITE show that at least the major routines of ILLI-SLAB, such as stiffness matrix assembly, inversion, and solution and determination of stresses and deflections, are free of any code errors.

TYPICAL EFFECTS WITH MODIFIED ILLI-SLAB

To illustrate the capabilities of ILLI-SLAB and the impact of the modifications described earlier, a

number of demonstration runs are presented. Two typical pavement cross sections are considered in this investigation. The first is a 10-in. portland cement concrete (PCC) pavement consisting of panels that are 20 ft square and 20 ft by 12 ft, with or without load transfer between adjacent slabs. These dimensions are typical of airport and highway pavements, respectively. The contour plots shown in Figure 1 were obtained from one of the demonstration runs with a highway pavement. For the cases involving load transfer, a second, mirror-image panel was added to the right of the panels shown in Figure 1. The second pavement section considered is a 12-in. pavement incorporating a stabilized base layer with a modulus (E) of 1.5×10^6 psi. This pavement consists of panels 15 ft by 12 ft and is typical of pavements proposed for the U.S. Air Force (USAF) alternate launch and recovery surface (ALRS) program.

The two pavement sections are loaded by a 9-kip highway load or typical USAF aircraft loading patterns, namely, the F-4, the C-130, and the F-111. A typical soft subgrade is assumed with two alternative characterizations. The first is the conventional static subgrade modulus (k), which was assigned a value of 120 to 150 psi/in. by using the WINKLER option in ILLI-SLAB. The second is the proposed resilient modulus (K_R), which was set at 425 psi/in. by using the SOFT option. Associated with the latter opinion is stress dependence, provided by the iterative scheme in ILLI-SLAB.

In an effort to clarify the picture presented by the results of these demonstration runs, three distinct effects are identified and discussed separately in the following.

Effect of Load Transfer

To investigate the impact of load transfer systems, load transfer by aggregate interlock was provided in some runs and these are compared with those in which only one panel was used. It was intended to investigate the two extreme cases, that of no load transfer efficiency (LTE = 0 percent) and that of full load transfer efficiency (LTE = 100 percent). For the latter an aggregate interlock factor (AIF) of 1×10^6 was specified, producing LTEs between 97 and 99 percent.

Under conditions of full load transfer, maximum deflection is reduced to half its value for the condition of no load transfer. The effect of load transfer on maximum bending stress is shown as a stress ratio in Table 1, which indicates that full-load-transfer stress is about 0.6 times the no-load-transfer stress. It is also observed that the proposed change to a resilient modulus subgrade characterization has only a minor effect in this respect. As expected, LTE is more pronounced (albeit only slightly) in the case of the less stiff ALRS pavement.

TABLE 1 Effect of Load Transfer

Pavement	Loading	Subgrade	Stress Ratio[a]
PCC	9-kip	k = 150 psi/in.	0.61
		SOFT	0.63
	F-4	k = 150 psi/in.	0.61
		SOFT	0.62
	C-130	SOFT	0.62
ALRS	F-4	k = 120 psi/in.	0.59
		SOFT	0.61
	C-130	SOFT	0.62

Note: All runs are for edge-loading condition. PCC = portland cement concrete; ALRS = alternate launch and recovery surface.

[a]Stress ratio = σ_{max} for LTE = 100 percent divided by σ_{max} for LTE = 0, where LTE = load transfer efficiency (deflection across joint on unloaded side divided by maximum deflection along joint on loaded side). The corresponding deflection ratio is 0.50 for LTE = 100 percent. All comparisons are for the first iteration.

Effect of Resilient Modulus Characterization

As explained earlier, it is considered that a resilient modulus subgrade characterization would be more appropriate for airfield pavement systems under transient loads than the conventional static plate load test subgrade modulus. The k-value used to characterize the subgrade in finite-element programs like ILLI-SLAB should be replaced by a stress-dependent K_R-value, which at low stress levels is substantially grater than that of the static k. In the cases analyzed in this paper, the WINKLER subgrade was assumed to have a static k-value of 120 to 150 psi/in. This is considered equivalent to the stress-dependent SOFT subgrade option in ILLI-SLAB. The low-stress-level K_R-value for this subgrade is 425 psi/in., according to the algorithms described previously.

The effect of this change is shown in Table 2 by comparing the responses of the SOFT and WINKLER subgrades in the form of deflection and stress ratios. Deflection ratios are seen to vary between 0.40 and 0.56, whereas stress ratios have values between 0.80 and 0.93. Thus, the proposed resilient modulus subgrade characterization leads to lower calculated deflections and stresses; stresses are affected to a smaller extent than deflections. Table 2 also shows that the impact of the proposed change is more significant as the load becomes more severe (C-130 instead of F-4) or if the pavement system is less stiff (ALRS rather than PCC pavement; no load transfer).

TABLE 2 Effect of Resilient Modulus

Pavement	Loading	Specified LTE (%)	Deflection[a,b] Ratio	Stress[b,c] Ratio
PCC	9-kip	0	0.53	0.91
		100	0.54	0.93
	F-4	0	0.55	0.88
		100	0.56	0.90
	C-130	100	0.49	0.81
ALRS	F-4	0	0.46	0.87
		100	0.47	0.89
	C-130	100	0.40	0.80

Note: All runs are for edge-loading condition. PCC = portland cement concrete; ALRS = alternate launch and recovery surface.

[a]Deflection ratio = maximum deflection for SOFT divided by maximum deflection for WINKLER.

[b]All comparisons are for the first iteration.

[c]Stress ratio = maximum stress for SOFT divided by maximum stress for WINKLER.

Effect of Stress Dependence: Iterative Scheme

Associated with the stress-dependent options in ILLI-SLAB, including the SOFT option employed in these demonstration runs, is an iterative scheme. In this scheme at the end of each iteration a check is performed for the compatibility of calculated deflections and assumed support pattern (i.e., K_R-values). If this compatibility is poor, a new iteration is performed after the support pattern has been updated until specified convergence tolerances are achieved. Usually no more than three iterations were required to achieve convergence within a tolerance of 5 percent.

Table 3 is an attempt to filter out the effect of the iterative scheme by presenting in terms of de-

TABLE 3 Effect of Stress Dependence

Pavement	Loading[a]	Specified LTE (%)	Deflection[b,c] Ratio	Stress[c,d] Ratio
PCC	F-4	0	1.03	1.01
		100	1.00	1.00
	C-130	0	1.10	1.05
		100	1.03	1.02
	F-111	0	1.04	1.07
ALRS	F-4	0	1.06	1.02
		100	1.01	1.00
	C-130	0	1.14	1.07
		100	1.05	1.03
	F-111	0	1.12	1.05

Note: All runs are for the SOFT subgrade and edge-loading condition. PCC = portland cement concrete; ALRS = alternate launch and recovery surface.
[a]Iterative scheme has no effect for 9-kip highway loading.
[b]Deflection ratio = maximum deflection for last iteration divided by maximum deflection for first iteration.
[c]Convergence tolerances: TOL1 = 5 percent; TOL2 = 5 percent.
[d]Stress ratio = maximum stress for last iteration divided by maximum stress for first iteration.

flection and stress ratios the responses after the first and after the last iteration. Deflection ratios range between 1.00 and 1.14, whereas stress ratios fall between 1.00 and 1.07. Thus the effect of the iterative scheme is to increase the maximum deflections and stresses obtained after the first iteration, thereby counterbalancing some of the change produced by the resilient modulus described previously.

Because the application of the iterative scheme increases execution time, it is important to draw some conclusions as to when such an increased expense is justified by the changes in response produced. Table 3 shows that the iterative scheme effect becomes substantial (i.e., 10 percent or more) for the more severe loading patterns (edge rather than interior; F-111 or C-130 rather than F-4) on the less competent pavement systems (ALRS rather than PCC section; LTE = 0 percent rather than LTE = 100 percent). The iterative scheme has no effect in the case of the 9-kip highway load, and only one iteration is required to achieve the 5 percent specified tolerance.

In general the effect of the iterative scheme is not dramatic. This may be attributed partly to the development of the algorithms used in the current version of ILLI-SLAB by simulating rigid plate load tests with ILLI-PAVE. The plates used in these tests are much stiffer than any ordinary pavement slabs, and their radius of relative stiffness (l) is much higher than the values encountered in pavement slabs. Westergaard (17) and other investigators have pointed out the effect of the radius of relative stiffness on the response of the subgrade-pavement system.

Finally Table 4 presents the combined effects of the resilient modulus and of the iterative scheme. The deflection ratios range between 0.42 and 0.57 and are in general substantially lower than the corresponding stress ratios, which lie between 0.82 and 0.93. This indicates that the impact of the proposed changes is much more significant with respect to deflections than stresses. Furthermore, the effects are more pronounced in the case of the more severe load patterns or the less competent pavement systems.

TABLE 4 Combined Effect of Proposed Changes

Pavement	Loading	Specified LTE (%)	Deflection[a] Ratio	Stress[b] Ratio
PCC	9-kip	0	0.53	0.91
		100	0.54	0.93
	F-4	0	0.57	0.89
		100	0.56	0.90
	C-130	100	0.50	0.83
ALRS	F-4	0	0.49	0.89
		100	0.47	0.90
	C-130	100	0.42	0.82

Note: All runs are for edge-loading condition. Changes consist of subgrade characterization by resilient modulus K_R (= 425 psi/in.; SOFT) instead of static subgrade modulus k (= 120 or 150 psi/in.) and stress dependence-iterative scheme. PCC = portland cement concrete; ALRS = alternate launch and recovery surface.
[a]Deflection ratio = maximum deflection after changes divided by maximum deflection before changes.
[b]Stress ratio = maximum stress after changes divided by maximum stress before changes.

SUMMARY

Classical slab-on-grade pavement analysis procedures (such as those proposed by Westergaard) cannot accommodate nonlinear subgrade support conditions, complex loading patterns, cracked sections with varying LTEs, and subbase effects. The modified ILLI-SLAB model developed in this study alleviates many of these inadequacies.

Computer program ILLI-SLAB (1), developed at the University of Illinois, offers great flexibility in modeling loading conditions (i.e., position, size, and intensity of loaded area or areas) and load transfer systems. The objective of this study was to modify the subgrade model in ILLI-SLAB from a simple, linear spring (Winkler) type to a stress-dependent (more accurately, a deflection-dependent) model, in which the resilient subgrade modulus (K_R) decreases with increasing deflection (w). Such a model was developed and incorporated into ILLI-SLAB by using an iterative scheme. According to this scheme, a selected initial value of K_R (dependent on subgrade type) is corrected after each iteration. After a number of iterations, the values of K_R before and after the last iteration differ by only a specified small percentage.

The impact of the iterative K_R model was investigated for several typical pavement systems subjected to edge loading. Some of the sections included load transfer systems. The major effect of the proposed K_R model stems from the difference between the value of the resilient subgrade modulus (initial K_R-value assigned in the iterative procedure) and the static k typically used. The effect of iterative analysis is limited and becomes more pronounced for conditions producing more severe pavement responses (thin structural sections, traffic overloads, edge loading, no load transfer).

ACKNOWLEDGMENT

This paper was based on an AFOSR research project report (8). The project was sponsored by AFOSR, Air Force Systems Command, Bolling Air Force Base, Washington, D.C. Lt. Col. J.J. Allen was the program manager.

REFERENCES

1. A.M. Tabatabaie, E.J. Barenberg, and R.E. Smith. Longitudinal Joint Systems in Slip-Formed Rigid Pavements, Vol. 2: Analysis of Load Transfer Systems for Concrete Pavements. Report FAA-RD-79-4, II. U.S. Department of Transportation, Nov. 1979.
2. A.M. Tabatabaie and E.J. Barenberg. Structural Analysis of Concrete Pavement Systems. Transportation Engineering Journal of ASCE, Vol. 106, No. TE5, Sept. 1980.
3. A.M. Tabatabaie and E.J. Barenberg. Finite-Element Analysis of Jointed or Cracked Concrete Pavements. In Transportation Research Record 671, TRB, National Research Council, Washington, D.C., 1978, pp. 11-19.

4. A.M. Ioannides. ILLI-SLAB Study, Vols. 1-4. University of Illinois at Urbana-Champaign, July 1981 (unpublished).
5. Y.T. Chou. Structural Analysis Computer Programs for Rigid Multicomponent Pavement Structures with Discontinuities--WESLIQID and WESLAYER, Report 1: Program Development and Numerical Presentations; Report 2: Manual for the WESLIQID Finite Element Program; Report 3: Manual for the WESLAYER Finite Element Program. Technical Report GL-81-6. U.S. Army Corps of Engineers Waterways Experiment Station, Vicksburg, Miss., May 1981.
6. Y.H. Huang and S.T. Wang. Finite-Element Analysis of Concrete Slabs and Its Implications for Rigid Pavement Design. In Highway Research Record 466, HRB, National Research Council, Washington, D.C., 1973, pp. 55-69.
7. L.A. Lopez, R.H. Dodds, Jr., D.R. Rehak, and J. Urzua. POLO-FINITE: A Structural Mechanics System for Linear and Nonlinear Analysis. Technical Report. University of Illinois at Urbana-Champaign and University of Kansas, Lawrence, (n.d.).
8. A.M. Ioannides, M.R. Thompson, E.J. Barenberg, and J.A. Fischer. Development of a Stress-Dependent Finite Element Slab Model. Report AFOSR-TR-83-1061. Air Force Office of Scientific Research, Air Force Systems Command, Washington, D.C., May 1983.
9. S. Timoshenko and S. Woinowsky-Krieger. Theory of Plates and Shells, 2nd ed. McGraw-Hill, New York, 1959.
10. O.C. Zienkiewicz. The Finite Element Method, 3rd ed. McGraw-Hill, New York, 1977.
11. D.J. Dawe. A Finite Element Approach to Plate Vibration Problems. Journal of Mechanical Engineering Science, Vol. 7, No. 1, 1965.
12. L. Raad and J.L. Figueroa. Load Response of Transportation Support Systems. Transportation Engineering Journal of ASCE, Vol. 106, No. TE1, Jan. 1980.
13. J.S. Przemieniecki. Theory of Matrix Structural Analysis. McGraw-Hill, New York, 1968.
14. L.A. Lopez. POLO--Problem Oriented Language Organizer. Journal of Computers and Structures, Vol. 2, 1972.
15. D.R. Rehak and L.A. Lopez. SCAN: A Tool for Translating Problem Oriented Languages. Civil Engineering Systems Laboratory, University of Illinois, Urbana-Champaign, Feb. 1982.
16. SCAN: User's Manual. Civil Engineering Systems Laboratory, University of Illinois, Urbana-Champaign, 1976.
17. H.M. Westergaard. Analytical Tools for Judging Results of Structural Tests of Concrete Pavements. Public Roads, Vol. 14, No. 10, Dec. 1933.

Publication of this paper sponsored by Committee on Rigid Pavements.

Structural Model for Concrete Block Pavement

A.A.A. MOLENAAR, H.O. MOLL, and L.J.M. HOUBEN

ABSTRACT

A structural model for the calculation of stress, strain, and deflection in a concrete block pavement is described. This model is based on the ICES STRUDL computer program that was recently extended by the introduction of a so-called RIGID BODY element. It is shown that by means of this model excellent agreement between measured and calculated deflection profiles is obtained. Furthermore, time functions were derived from the observation of 20 concrete block pavements in service. These functions show the increase of the subgrade modulus, the stiffness of the joints and the bedding layer, and the decrease in the deflection with respect to the number of equivalent 100-kN single axles. By means of ICES STRUDL and the developed time functions tentative design charts are developed in which the number of years until a given rut depth is reached is related to the initial subgrade modulus and the average daily equivalent 100-kN single axle loads. Although concrete block pavements are common in western Europe (about one-third of the paved area in the Netherlands consists of such pavements), this pavement type is not well known in the United States. Therefore a general description of the most characteristic features of concrete block pavements is given.

Concrete block paving is the most recent development in element (segmental) paving, which is built by laying down small elements on the (improved) subgrade. Element paving has been used since the Middle Ages. Wooden setts were sometimes used as elements but, especially at first, nontooled natural stone was the only pavement material that had sufficient resistance to the traffic loading by steel wheels.

After the introduction of the rubber tire at the end of the 19th century, clay bricks were applied on a large scale in the Netherlands (1,2). Because of the absence of quarries, natural stone was more expensive than bricks.

After World War II the rectangular concrete block was developed as a substitute for the rectangular brick, which was needed for the construction of houses. Concrete blocks are now used much more than bricks because of the substantially higher cost of the bricks. Outside the Netherlands bricks are hardly used. In Germany and Belgium concrete block paving has also been used on a large scale since 1950; in a number of other countries concrete blocks have been introduced hesitatingly since 1960 (3).

The profile of a concrete block pavement is shown in Figure 1 (4). For the subbase, sand or a granular

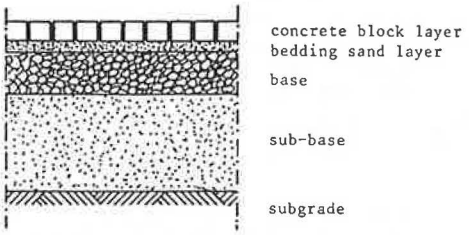

FIGURE 1 Profile of concrete block pavement.

material of higher quality is used, depending on the cost (availability) of the materials. It is important that the subbase have high permeability. The base, which is not necessary for lightly trafficked pavements (pedestrian areas, roads with hardly any trucks), may consist of granular material such as slags, natural gravels, or crushed rock (the resistance to crushing has to be high) or stabilized material, especially cement-stabilized material. A stabilized base requires special provisions for the discharge of the rainwater that percolates through the joints. The bedding sand layer, which is necessary because the subbase is too rough and often too hard, consists of stable sand (bedding sand) and sometimes fine gravel. For optimum load spreading (by friction) in the concrete block layer it is necessary not only that the joints between the blocks be narrow (2 to 3 mm) but also that they remain filled with jointing sand.

CONCRETE BLOCKS

In countries with a long tradition of concrete block paving the blocks are manufactured in plants specialized for this purpose (4). Elsewhere the blocks are often manufactured by using modified wall masonry plants (3); in general these blocks are of a lower quality.

Block Types

There are rectangular concrete blocks (with a rectangular, square, or hexagonal horizontal section) and dozens of nonrectangular (shaped) concrete blocks (3-5). A further division is made into three categories (Figure 2). Category A consists of nonrectangular blocks interlocking on all four faces; category B, nonrectangular blocks interlocking on two faces only; and category C, rectangular blocks that do not interlock.

Historically in the Netherlands rectangular blocks have been used almost exclusively. Outside

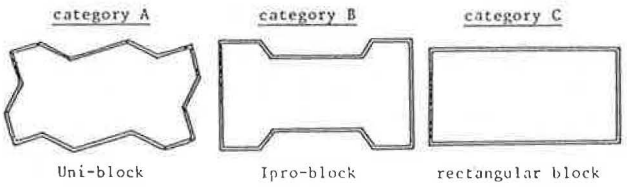

FIGURE 2 Categories of concrete blocks (with chamfer).

the Netherlands nonrectangular blocks are the most widely used, which is explained by the (presumed) better performance of such pavements, the absence of skilled paviors (nonrectangular blocks often fit together in just one way), and so forth.

In general, concrete blocks have a chamfer around the wearing face to reduce spalling, caused by blocks rotating toward one another, and to reduce differences in level between adjoining blocks in the road. Furthermore, chamfered blocks are easier to handle. The horizontal dimensions of concrete blocks are in general about 200 x 100 mm², and the thickness varies from 50 to 120 mm. The block type and the laying pattern determine the number of accessory blocks needed.

Specifications

In several countries there are specifications for concrete paving blocks (6-10). In general the specifications refer to materials, manufacturing, dimensions, dimensional tolerances, and quality (strength, durability, and so on). Most important for the pavement performance under traffic and the life of the blocks are the differences in size and the strength and the durability of the blocks.

Concrete blocks may have only slight differences in size in order to make laying and, if necessary, repairing of the block pavement easy and exact and to assure that there are narrow joints everywhere so that the permanent deformation, both vertical (rutting) and horizontal (in the direction of travel, or creep, and perpendicular to it), is limited. The horizontal differences in size in particular have to be small, and therefore most specifications call for a tolerance of about 2 mm; the tolerance for thickness is, in general, larger (up to 5 mm).

It has been widely assumed that strength and durability (in particular abrasion resistance) are interrelated. Therefore the strength requirements are higher than necessary to prevent failure of the blocks during manufacturing, transport, and processing and under traffic loading. In the countries of the Southern Hemisphere in general the strength requirements are lower than those in Europe and North America because resistance to damage by freezing and thawing is usually no problem. The lowest strength specifications mentioned in the literature are compressive strength of at last 40 N/mm² and flexural strength of at least 2.5 N/mm² (in the Netherlands flexural strength of at least 5.9 N/mm² is specified).

Properties

Because they are manufactured in steel molds, concrete blocks vary only slightly, especially in the horizontal dimensions. The strength of concrete blocks is so great that failure due to traffic loads rarely occurs; blocks with a variable width (e.g., Ipro blocks) are more susceptible to failure than blocks with a constant width. Concrete blocks are resistant to mineral oil and fuel, but they are af-

fected by inorganic acids (hydrochloric, nitric, and so on), organic acids (lactic), and vegetable and animal oils and fats. By addition of pigments concrete blocks can be given different colors. These colored blocks have functional uses (traffic markings) or are used for aesthetic reasons. Concrete blocks are sufficiently skid and abrasion resistant.

GENERAL ASPECTS OF CONCRETE BLOCK PAVING

Properties, Advantages, and Disadvantages

A concrete block pavement consists of small, precast concrete elements, which can be torn up and used again (3,4). The main advantages of concrete block paving are as follows:

1. The pavement is able to conform with the unequal settlement of the subgrade without further disintegration (cracking);
2. The subgrade remains easily accessible to underground services (cables and piping), except in the case of a stabilized subbase;
3. The blocks can be relaid (restoration of local settlement, reconstruction, and so on) easily, quickly, and with hardly any loss of material;
4. The great block strength makes a concrete block pavement (with a base) resistant to heavy and static (concentrated) loads;
5. The pavement is resistant to mineral oil and fuel;
6. The pavement can be opened to traffic immediately after construction or relaying;
7. Small and irregular surfaces can easily be paved;
8. Because concrete can be given almost any shape there are many block types, different sizes and thicknesses, and accessory blocks [half blocks, "bishop hats" for herringbone bond B (Figure 3), and so on] and therefore there are many possible applications;
9. The skid resistance remains sufficient, also because the joints tend to prevent a water film on the pavement;
10. The pavement gives diffuse light reflection, especially when uncolored or light-colored blocks are used; and
11. Application of different-colored concrete blocks, possibly laid in different patterns, offers possibilities for optical traffic-guidance markings and, from an aesthetic point of view, attractive pavements.

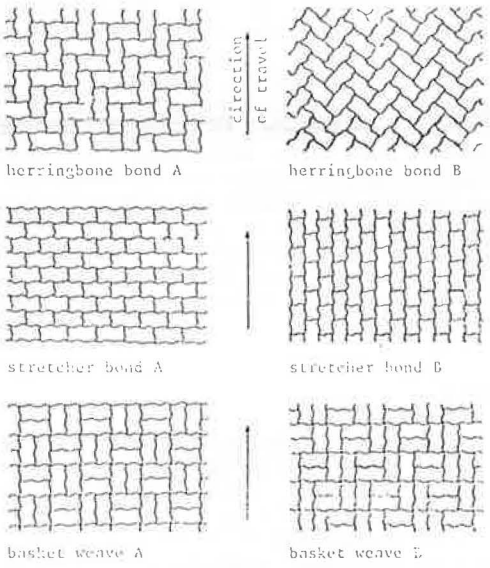

FIGURE 3 Most important laying patterns (bonds).

The most important disadvantages of concrete block paving are as follows:

1. A block pavement is not suited for vehicle speeds more than 50 to 60 km/hr because at high speed the fresh (granular) jointing sand is sucked away or, when the road surface is wet, washed away by the vehicle tires, which causes a loss of cohesion in the block layer and faster deterioration (rutting, rotating, and possibly pulling out of the blocks); furthermore, the riding quality is low.
2. The rubber of tires and the spillage of oil, soil, and so on, under traffic within some 6 to 12 months lead to a certain amount of imperviousness (luting) of the jointing sand (which leads to more load spreading in the block layer); nevertheless the joints remain more or less permeable. Therefore not only is a considerable crossfall (about 1:30) necessary, but also the drainage of the pavement requires special attention.
3. Under traffic the blocks may creep (move in the direction of travel) and they may be pressed away sideways. Because of the slight differences in the horizontal dimensions of the blocks (which means narrow joints everywhere) these movements are small, provided the joints are well filled and there is an adequate curb; the laying pattern and the block type are also important.
4. Block laying by hand, especially the traditional craft method, is rather labor intensive (which is not always a disadvantage), but the pavior has a difficult profession (injuries of the back occur frequently). The chance of injury and possibly the construction cost can be reduced by the so-called lay-down method and by mechanized block laying (in which about 1 m^2 of concrete block is laid on the prepared bedding sand layer at one time with a small machine).

Applications

Concrete block pavements are well suited to the following uses (3,4):

1. Trafficked zones in built-up regions, e.g., pedestrian walkways, residential streets, parking lots, bus stops, and fuel stations, in which frequently there are cables and piping, traffic speed is low, spillage of oil and fuel sometimes occurs, a functional division is often desired, and aesthetics can be important;
2. Trafficked zones in rural areas, especially rural roads and farmyards, in which both traffic intensity and traffic speed in general are low, but axle loads can be heavy and dirtying by such agents as soil frequently occurs (which may contribute to a fast luting of the jointing sand);
3. Industrial yards like factory grounds and container terminals, in which settlement often occurs (almost all container terminals are situated on reclaimed land in alluvial areas), the traffic loads are heavy, and the contact pressure is often high (stacked containers);
4. Small and irregular surfaces; and
5. Temporary pavements (recycling).

Laying Patterns

Concrete blocks can be laid in different patterns (bonds); the most important bonds are shown in Fig-

ure 3 (3-5). With rectangular blocks and some nonrectangular blocks (e.g., Uni blocks) all patterns can be made, but many nonrectangular blocks fit together in just one way, so these blocks can only be laid in one bond (e.g., Ipro blocks can be laid only in the stretcher bond).

The laying pattern, which can be used functionally, affects not only the horizontal movements of the blocks in the direction of travel and perpendicular to it but also the structural behavior (strength) of the block pavement under traffic. In this respect the herringbone bond is preferable to the stretcher bond and the basket weave.

AVAILABLE DESIGN METHODS

In countries with much experience in concrete block paving, the design consists of the selection of a suitable standard pavement given the traffic loads, the prevailing environmental and subgrade conditions, and the available materials. In other words design is based on the experience of the pavement engineer.

Outside western Europe a number of design methods have been developed that are partly modified for rigid and flexible pavements (11-15) or are based on the results of full-scale laboratory experiments (16-18). Until now no analytical methods were available that fully took into account the specific properties of the discontinued concrete block layer. Therefore a need was felt to develop such an analytical model so that a proper evaluation of the behavior of concrete block pavements could be made and it could be determined which factors are the key parameters that govern the behavior of such pavements. In the following sections the development of such an analytical model will be described and it will be shown how the key parameters vary with time.

MODELING OF THE CONCRETE BLOCK PAVEMENT

Even though the top layer of a concrete block pavement consists of small elements, it is tempting to analyze the concrete block pavement by means of linear elastic theory, assuming that the layers are homogeneous and isotropic. This is because graphs, tables, and computer programs are readily available for the analysis of linear elastic structures. In most cases, however, application of linear elastic theory to concrete block pavements will result in an improper description of the behavior of this pavement. This is best illustrated by Figure 4 in which a measured deflection profile and one simulated by linear elastic theory are shown. From Figure 4 one can observe that the deflection profile is rather peaked. Such a peaked profile can only be simulated by means of linear elastic theory by assuming a low elastic modulus for the concrete block layer, but even then the decay of the deflection with respect to the distance to the loading center is more gradual than the decay that is normally observed in the field. The inability of linear elastic theory to describe the deflection behavior of concrete block pavements has led to the conclusion that a better structural model for this pavement type should be used.

Finite-Element Model

In order to be able to include the discontinuities (joints) of a concrete block pavement, a finite-element program was used. For this case the ICES STRUDL program was selected because recently a special element type called the Rigid Body has become available that could be used for a proper schematization of the concrete blocks. This element was developed at the Structural Mechanics Division of the Delft University Civil Engineering Department (19).

The main features of this element are shown in Figure 5. It consists of a rigid undeformable body that is connected to other elements or other rigid bodies by means of linear springs. How this element is used with other elements in modeling a concrete block pavement is described in the following sections.

Concrete Block Layer

For this layer three assumptions were made: the blocks do not deform, no horizontal forces are transmitted by the joints, and the blocks do not rotate.

1. Deformation: In the pavement model the blocks are represented by rigid bodies because it was assumed that the deformation of the blocks themselves is negligible. This is a reasonable assumption because the Young's modulus of the concrete blocks is about 30 000 MPa, which is about 300 times larger than the Young's modulus of the bedding layer.
2. Horizontal forces: Deflection measurements on in-service concrete block pavements (20) as well as the behavior of two prototype pavements that were subjected to repeated plate loading tests (21) indicated that the shape of the deflection bowl was much like the deflection curve of a pure-shear-layer pavement. The failure mode that was observed on the prototype concrete block pavements was shear failure, and only a limited amount of bending was observed.
3. Rotation: Assuming that the concrete block layer behaves like a pure shear layer implies that no horizontal forces are transmitted in the joints and that no rotation of the blocks occurs.

The joints of the block pavement are represented in the model by linear springs (Figure 6). The underlying assumption is that the relative displacement between the blocks is so small that a linear joint stiffness is a reasonable estimate. The stiffness of these springs is denoted by k (in newtons per millimeter).

Bedding Sand Layer

As indicated in Figure 1, a bedding sand layer is constructed just beneath the block layer. In the model this layer is represented by vertical springs. This means that this layer cannot absorb bending moments either. The stiffness of these springs is represented by the bedding constant c (in newtons per cubic millimeter). Figure 7 shows the bedding sand layer.

Base, Subbase, and Subgrade

For modeling the base, subbase, and subgrade CSTG elements were used. This means that these layers are the only continuous layers in the system and that they are capable of absorbing bending moments.

Element Mesh

The element mesh that was used in the evaluation of concrete block pavements is shown in Figure 8. The

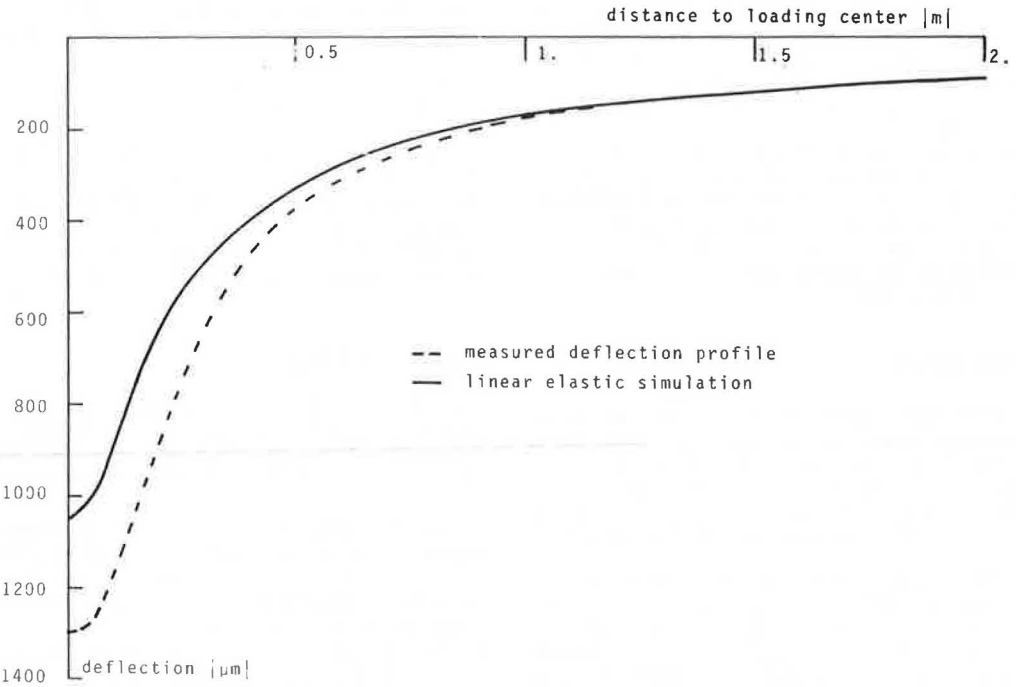

FIGURE 4 Measured deflection profile compared with profile simulated by linear elastic theory.

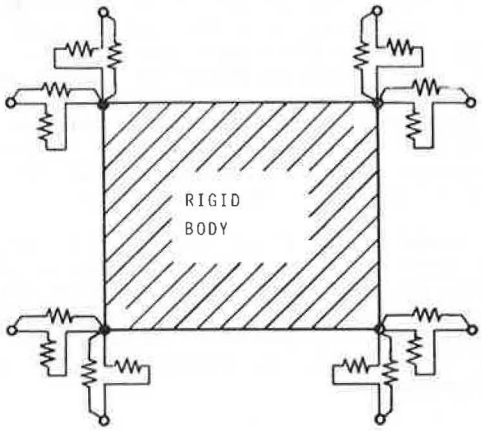

FIGURE 5 Rigid body element.

size of the rigid-body elements corresponds to a cut through herringbone bond B (see Figure 3). The calculations were made by assuming plain strain conditions. The load applied to the structure was a falling-weight-deflectometer (FWD) loading, which means a 50-kN load on a circular 0.3-m-diameter plate.

TESTING THE STRUCTURAL MODEL

The usefulness of the model was tested by simulating deflection bowls obtained from several in-service concrete block pavements. The measurements were carried out by means of the Delft University FWD (Figure 9).

It should be noted that the deflections were measured at six points that are located 0, 0.2, 0.3, 0.5, 1, and 2 m from the center of the loading plate. The deflections were measured close to the loading plate because in that region the largest de-

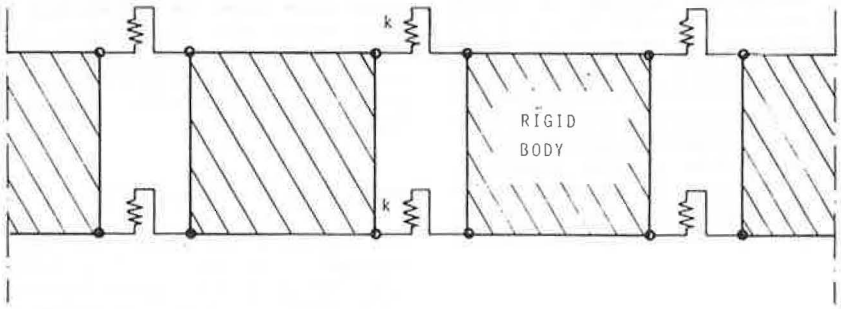

FIGURE 6 Modeling of the concrete block layer.

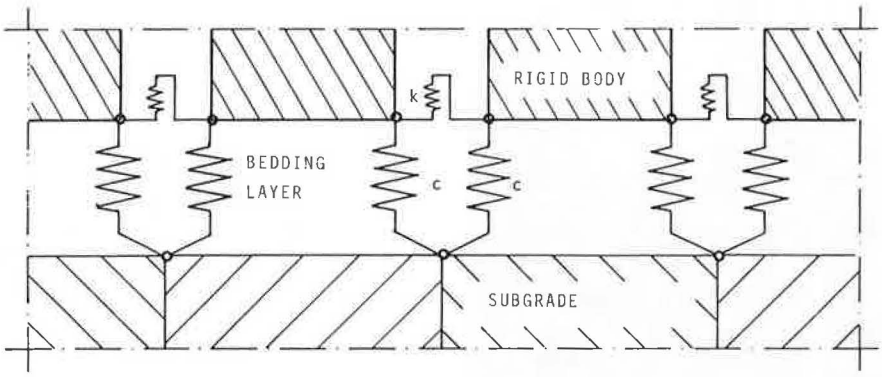

FIGURE 7 Modeling of the bedding sand layer.

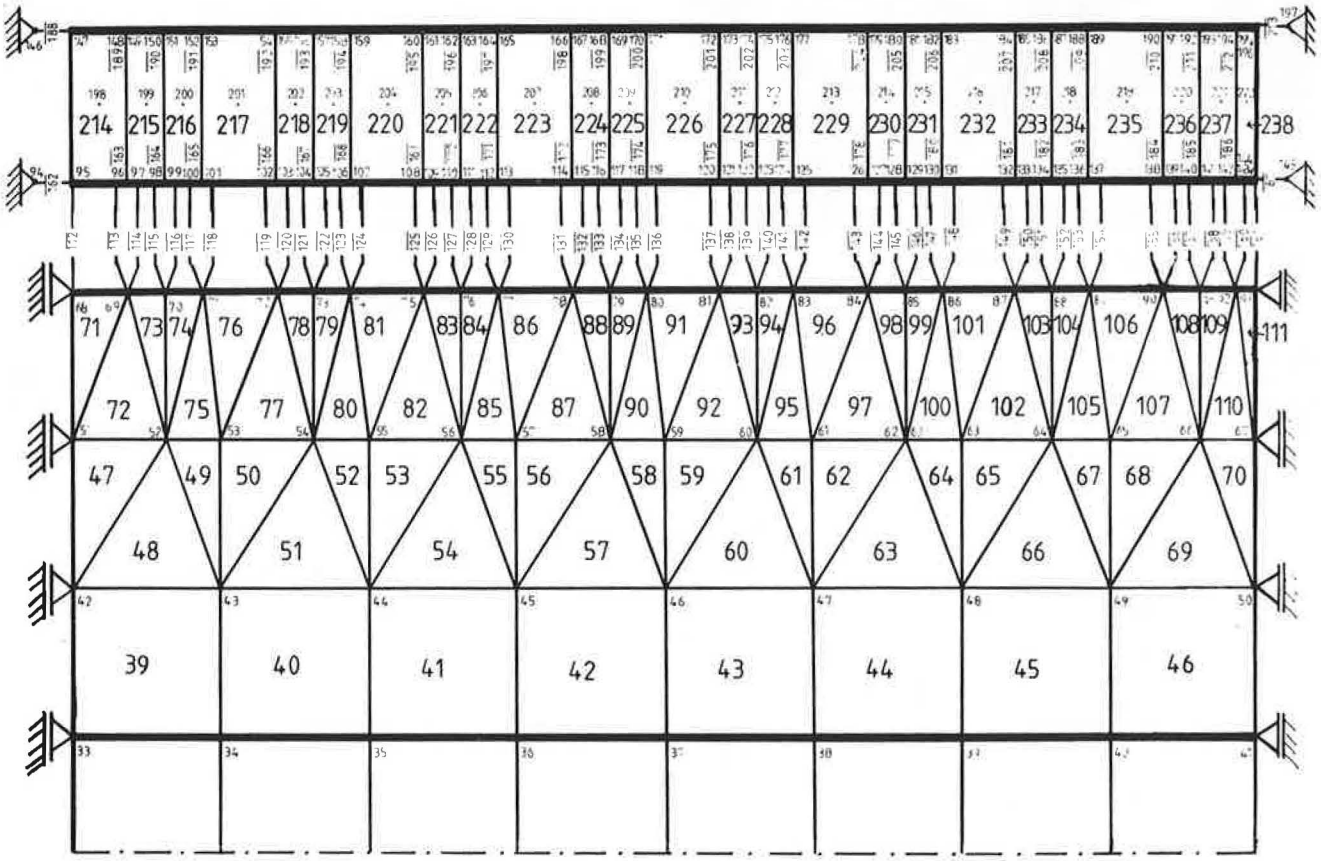

FIGURE 8 Finite-element mesh.

flection decay takes place. This decay needs to be measured accurately in order to be able to make precise estimates for k and c from the measured deflection profile.

The measured deflection profiles were simulated by means of the ICES STRUDL program in the following manner. First the subgrade modulus was calculated from the deflection measured at 2 m from the loading center by means of the following formula (22):

$$\log E = 3.868 - 1.009 \log d_2 \quad (1)$$

where E is the subgrade modulus in megapascals and d_2 is the deflection at 2 m from the loading center in micrometers (P = 50 kN). Next the joint stiffness (k) and bedding layer stiffness (c) were calculated from the measured deflection profile by means of trial and error. The resulting calculated deflection profile fitted well to the measured profiles. A typical example is shown in Figure 10 (23). Because in almost each case good correspondence between the measured and the simulated profiles could be obtained, it was concluded that the finite-ele-

FIGURE 9 Falling-weight deflectometer.

ment model adopted is indeed a proper schematization of the real pavement behavior, and it can therefore be used with confidence for design purposes. This will be discussed in a later section.

RELATION BETWEEN SURFACE CURVATURE INDEX AND STIFFNESS OF CONCRETE BLOCK JOINTS AND BEDDING LAYER

Because it is quite expensive to run the ICES STRUDL computer program, it is desirable to have a method for the selection of reasonably accurate starting values for k and c. It was therefore determined whether a first estimate of k and c could be obtained from the surface curvature index (SCI) of the measured deflection profile, because SCI is normally a good indicator of the stiffness of the pavement layers. SCI is defined here as follows:

$$SCI = d_0 - d_{0.5} \quad (2)$$

where d_0 is the deflection at the loading center of the falling weight in micrometers (P = 50 kN) and $d_{0.5}$ is the deflection at a distance of 0.5 m from the loading center in micrometers. From the results of the simulations it appeared that such relations could indeed be derived. They are given in Figures 11 and 12.

With these relations a first estimate of k and c can easily be made. If these starting values are used for k and c, normally only two or three computer runs are needed to match the calculated profile with the measured one. It is obvious that these graphs are especially useful in the evaluation of existing pavements.

STRUCTURAL PERFORMANCE OF CONCRETE BLOCK PAVEMENTS

As might be expected, rutting is the most important defect that can be observed in concrete block pavements. There is usually a considerable amount of

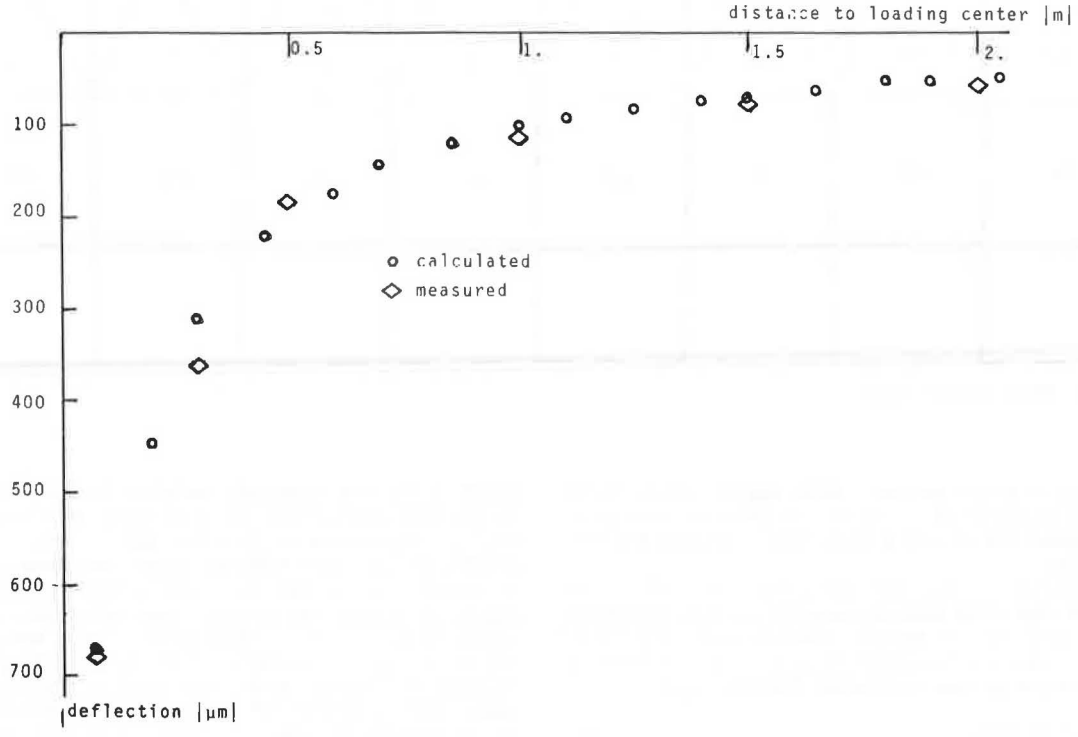

FIGURE 10 Agreement between measured and calculated deflection profiles for an in-service concrete block pavement.

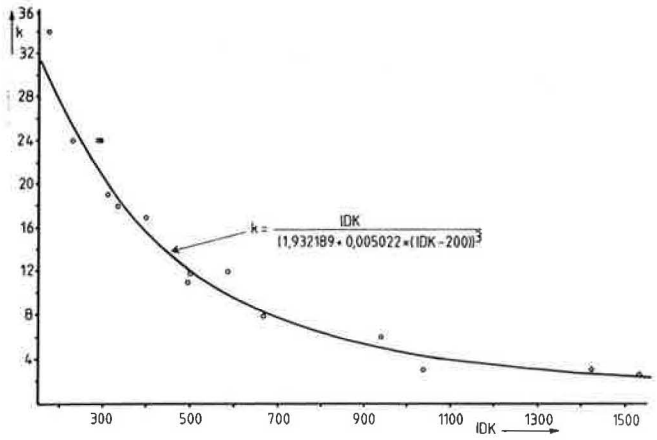

FIGURE 11 Relation between SCI and joint stiffness (k).

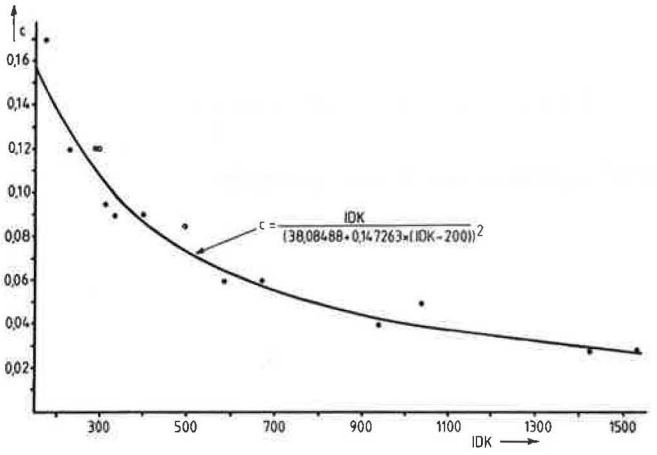

FIGURE 12 Relation between SCI and bedding layer stiffness (c).

initial rutting, which is mainly caused by postcompaction of the bedding layer, base, and subgrade. There is, however, a rapid decrease of the rutting rate with increasing number of load repetitions.

An interesting aspect of concrete block pavements is that the deflections decrease in time rather than increase, which is the case with flexible and rigid pavements. The decrease in deflection is caused by stiffening of the subgrade, base, bedding layer, and joints between the concrete blocks and is caused mainly by traffic and pollution or intrusion of fine material into the joints.

In order to be able to make a realistic design of a concrete block pavement one needs to have a proper insight into the stiffening of the construction with time. By means of a careful analysis of 20 different roads having a concrete block top layer it was possible to derive some of the most important time functions (Figures 13-16) (20,24). Figure 13 shows the increase of the subgrade modulus with respect to the number of 100-kN equivalent single axles. Figure 14 shows the decrease of the falling-weight SCI with respect to the number of 100-kN equivalent axles. It should be noted that the number of axles was not determined by means of axle-load surveys but is the best possible estimate. For instance, on most pavements the main part of the loading was caused by bus traffic; from the bus time schedule and the axle loads of the buses the total number of axle loads could be assessed. Figures 15 and 16 were obtained by combining the relations given in Figures 11, 12, and 14.

It is obvious that these time functions together with the number of equivalent axle loads are the most important parameters in the design of concrete block pavements. How they are used to develop tentative design charts is shown in the next section.

TENTATIVE DESIGN CHARTS FOR CONCRETE BLOCK PAVEMENTS

Based on the time functions for the subgrade modulus, bedding layer stiffness, and joint stiffness a number of computer runs were made with the ICES STRUDL program and subgrade E, k, and c values that are representative for different pavement ages or that occur after given numbers of load repetitions. From the calculated maximum deflection, the associated rut depth was derived by means of the following:

$$U_{pl_N} = \sum_{n=1}^{N} U_{el_n} (an^b_{n+\Delta n} - an^b_{n-\Delta n}) \quad (3)$$

where

U_{pl_N} = pavement deformation of a concrete block pavement after the design number of load applications (N),
U_{el_n} = maximum deflection occurring at the nth load repetition, and
a,b = constants.

For $n_{n+\Delta n}$, $n_{n-\Delta n}$, see Figure 17, which is a schematic representation of the above-mentioned rut-depth equation.

The rut-depth equation used is in fact the same as that developed by the Belgian Road Research Laboratory for use in the design of flexible pavements (25,26). It is modified in the sense that it takes into account the variation of the maximum deflection during the pavement life. It is obvious that the amount of rutting is dependent not only on the maximum deflection but also on the magnitude of the constants a and b. From the analysis of the 20 in-service and the two prototype concrete block pavements that were subjected to repeated plate loading tests, no accurate values for a and b could be derived. Nevertheless, it was concluded that a = 2 and b = 0.2 are reasonable estimates to be used in tentative design charts.

By using the results of the ICES STRUDL runs together with the rut-depth equation and the proposed values for a and b, charts were derived in which the number of years to a given rut depth can be determined from the average daily number of 100-kN single axle loads and the elastic modulus of the subgrade as constructed. An example of these charts is given in Figure 18, which is based on a final rut depth of 25 mm, a reasonable functional rut-depth limit. The structural rut-depth limit can be seen as 35 mm.

It should be noted that Figure 18 is not really a design chart. It is in fact a performance expectation chart; i.e., the pavement engineer is able to determine how well the concrete block pavement will perform given the prevailing subgrade conditions. If the expected pavement life is considered too low, the subgrade modulus can be improved by applying heavier compaction or by applying a base.

Efforts are now being made to determine the effect of including a base on the life of a concrete

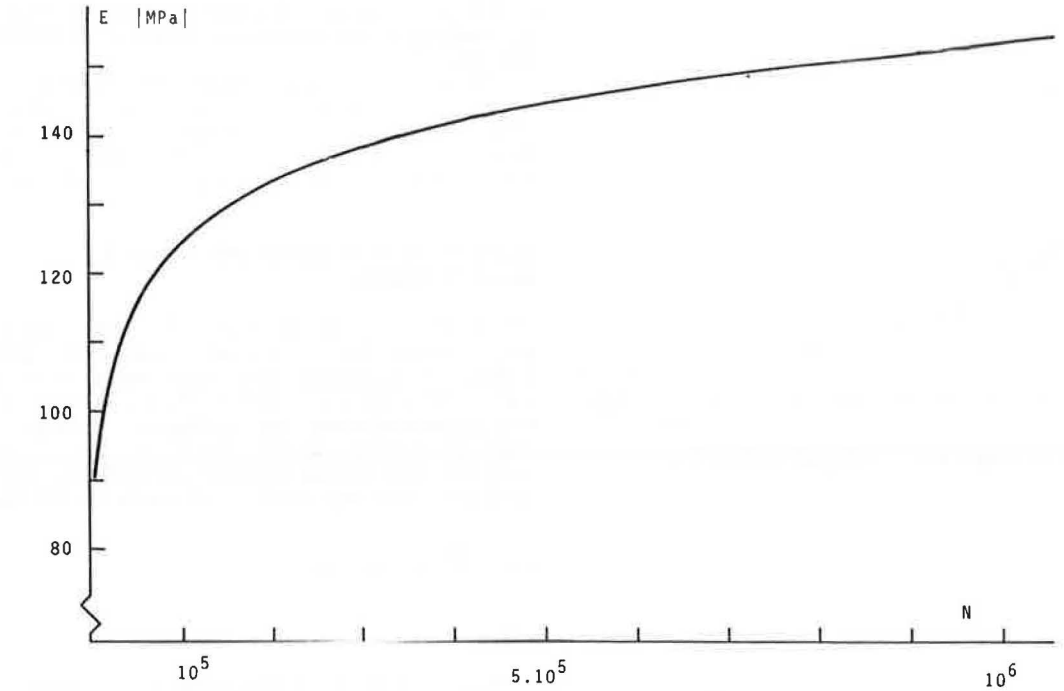

FIGURE 13 Relation between number of equivalent 100-kN single axles (N) and increase in subgrade modulus (E).

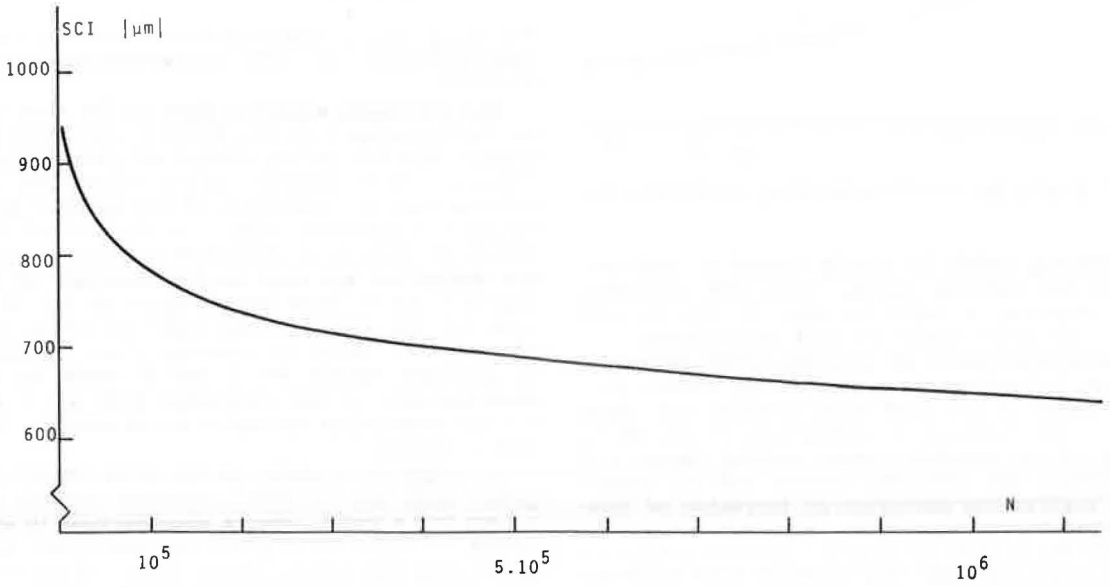

FIGURE 14 Relation between the number of equivalent 100-kN single axles (N) and decrease in SCI.

block pavement. With this determination the method presented can be used as a real design method, because then it will be possible to select base thickness and base stiffness in relation to the subgrade stiffness, number of load repetitions, and allowable rut depth.

CONCLUSIONS

Based on the results of the analysis of concrete block pavements presented here, the following main conclusions can be drawn:

1. Concrete block pavements can be modeled by means of a finite-element model consisting of rigid body elements representing the undeformable concrete blocks;

2. By means of the finite-element model an excellent correspondence between the calculated and measured deflection profiles is obtained;

3. The maximum deflection as well as SCI as measured on concrete block pavements decrease with increasing number of load repetitions, and the subgrade modulus as well as the joint stiffness and

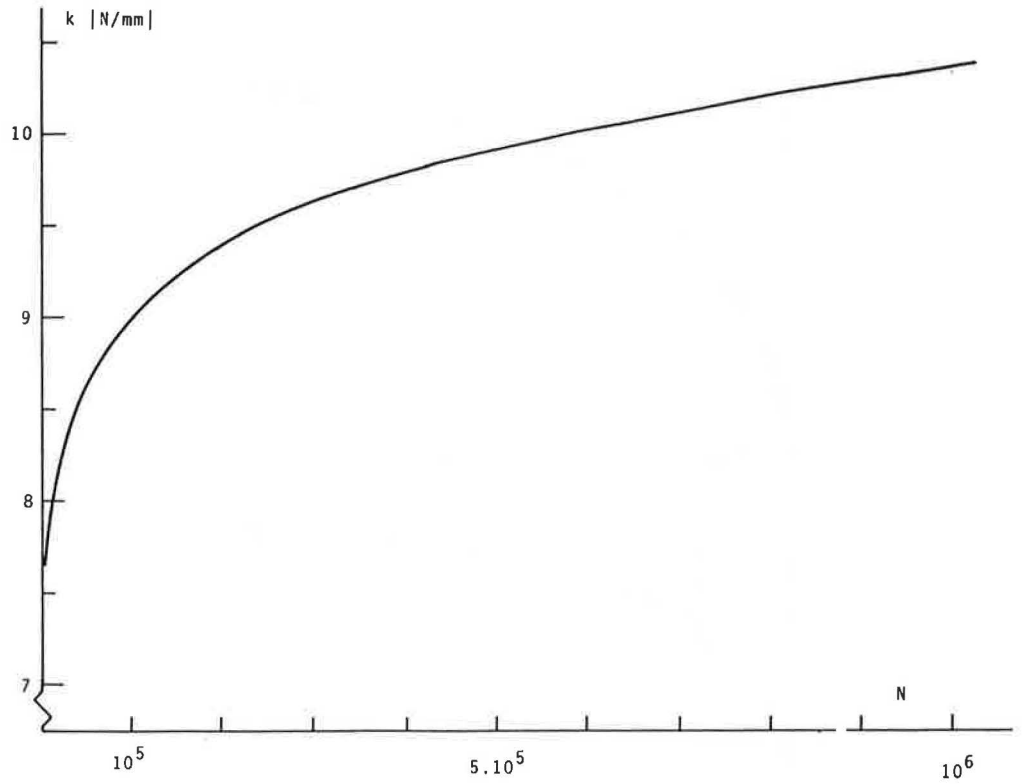

FIGURE 15 Relation between number of equivalent 100-kN single axles (N) and increase in joint stiffness (k).

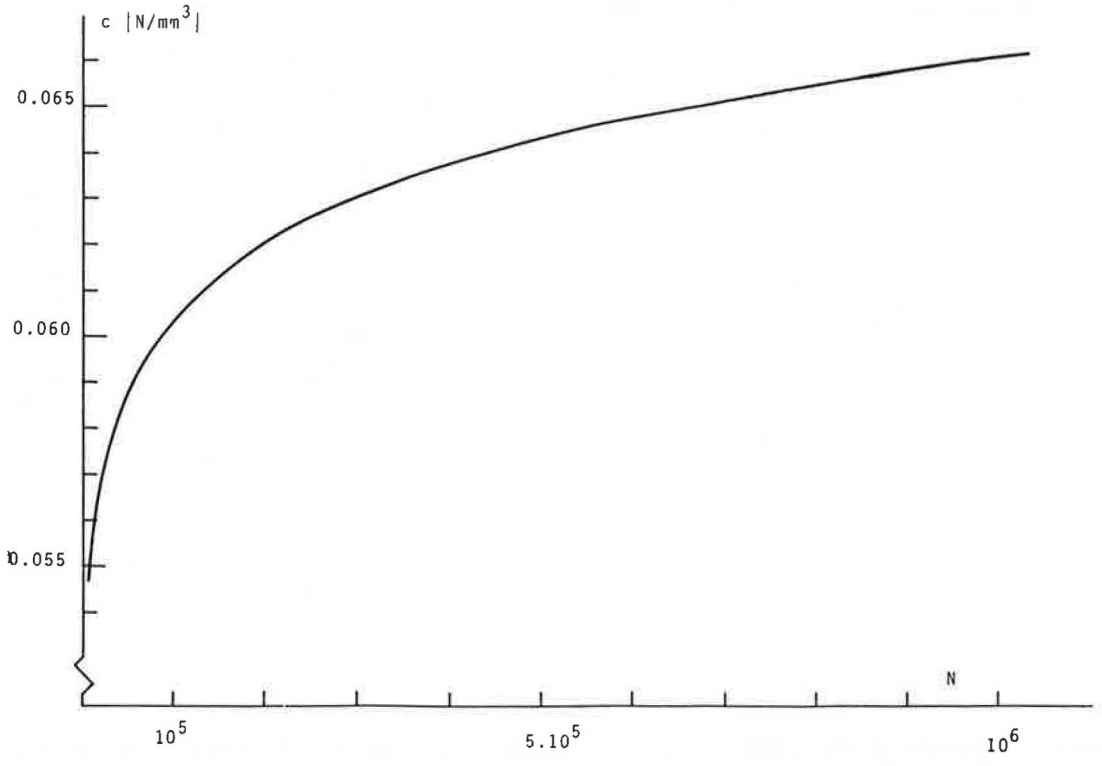

FIGURE 16 Relation between number of equivalent 100-kN single axles (N) and increase in bedding sand layer stiffness (c).

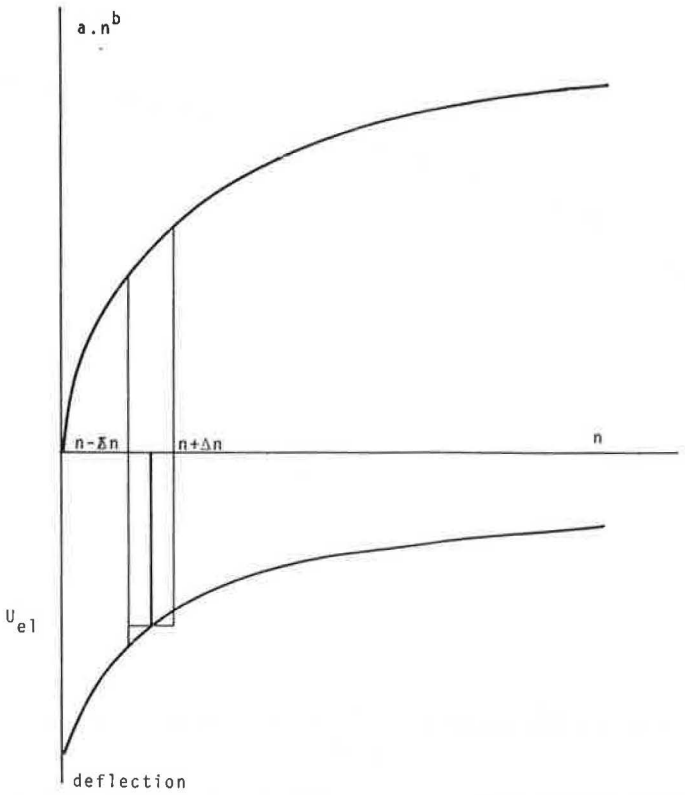

FIGURE 17 Schematic representation of the rut-depth equation.

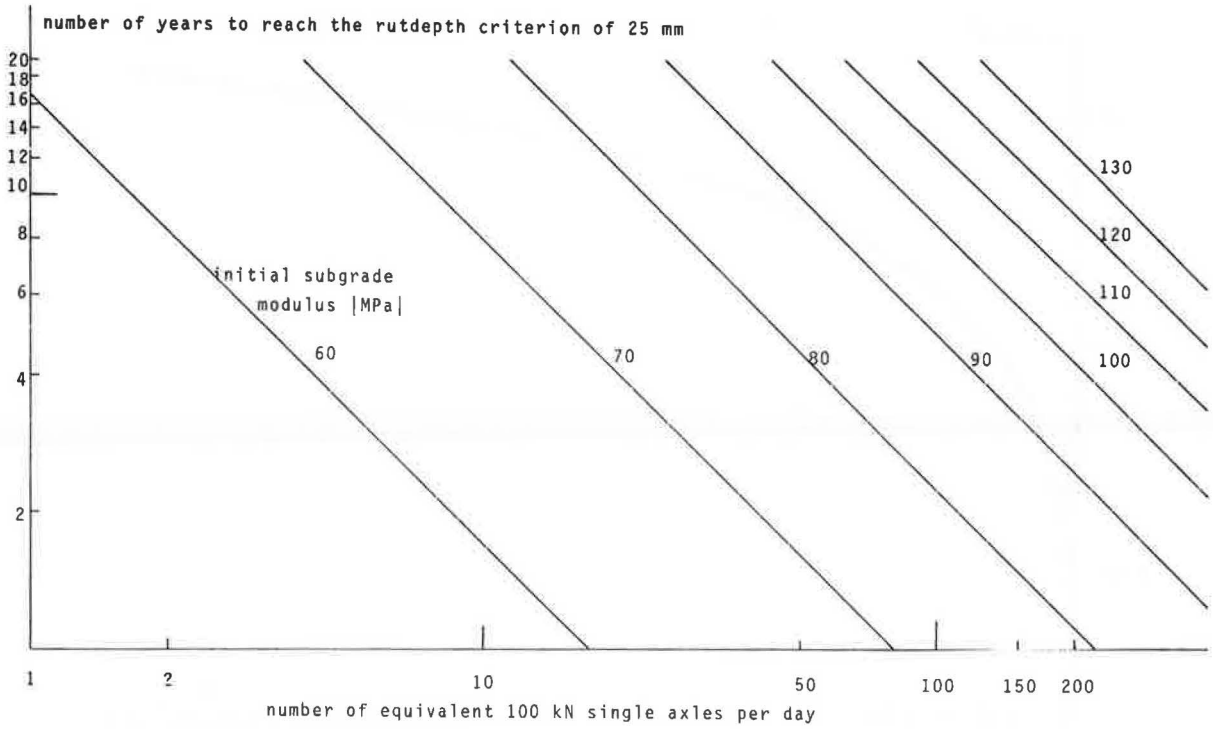

FIGURE 18 Pavement life in relation to average daily equivalent 100-kN single axle loads, initial subgrade modulus, and rut-depth criterion of 25 mm.

bedding-layer stiffness increase with increasing number of load repetitions; and

4. Based on these time functions, tentative design charts for concrete block pavements have been derived.

REFERENCES

1. L.J.M. Houben. Concrete Block Paving. Proc., Furoris Congress, University of Surinam, Paramaribo, 1982.
2. G.H. Kellersmann. Urban Block Paving in the Netherlands. Proc., First International Conference on Concrete Block Paving, University of Newcastle upon Tyne, England, 1980.
3. B. Shackel. A Review of the Technology of Interlocking Concrete Block Paving for Roads and Industrial Pavements. Technical Report RP/8/80. National Institute for Transport and Road Research, Council for Scientific and Industrial Research (CSIR), Pretoria, South Africa, 1980.
4. Bestratingen van betonstenen: Betonstraatstenen (in Dutch). Report 44. Study Centre for Road Construction (SCW), Arnhem, Netherlands, 1978.
5. FABES: Documentatiemateriaal (in Dutch). Association of Concrete Paving Block Manufacturers (FABES), Woerden, Netherlands, n.d.
6. Betonstraatstenen: Keuringseisen (in Dutch). Dutch Standard NEN 7000 (under revision). Dutch Organisation for Standardization (NNI), Delft, Netherlands, 1966.
7. Pflastersteine: Beton (in German). German Standard DIN 18501. Beuth Verlag GmbH, Berlin/Cologne, West Germany, 1979.
8. Recommended Specification for Concrete Paving Stones. Information Bull. IB019. New Zealand Portland Cement Association (NZPCA), Wellington, 1978.
9. Interim Specification for Interlocking Concrete Paving Units. Specification MA15. Cement and Concrete Association of Australia (CCAA), 1980.
10. Specification for Precast Concrete Paving Blocks. Cement and Concrete Association (CCA), Wexham Springs, and County Surveyers' Society, Interpave, England, 1980.
11. J. Knapton and S.D. Barber. U.K. Research into Concrete Block Pavements. Proc., First International Conference on Concrete Block Paving, University of Newcastle upon Tyne, England, 1980.
12. A.A. Lilley and A.J. Clark. Concrete Block Paving for Lightly Trafficked Roads and Paved Areas. Technical Report 46.024. Cement and Concrete Association, Wexham Springs, England, 1978.
13. A.A. Lilley and B.J. Walker. Concrete Block Paving for Heavily Trafficked Roads and Paved Areas. Technical Report 46.023. Cement and Concrete Association, Wexham Springs, England, 1978.
14. Interlocking Concrete Paving for Heavy Vehicular Traffic. Information Bull. IB020. New Zealand Portland Cement Association, Wellington, 1978.
15. Concrete Block Pavements: Structural Design. Publ. 115. National Concrete Masonry Association (NCMA), Herndon, Va., 1980.
16. J. Hodgkinson and C.F. Morrish. Interim Guide to the Design of Interlocking Concrete Pavements for Vehicular Traffic. Technical Note TN34. Cement and Concrete Association of Australia, 1980.
17. B. Shackel. The Evaluation and Design of Interlocking Concrete Block Pavements Subjected to Road Traffic. Technical Report RP/9/80. National Institute for Transport and Road Research, Council for Scientific and Industrial Research (CSIR), Pretoria, South Africa, 1980.
18. B. Shackel. The Design of Interlocking Concrete Block Pavements for Road Traffic. Proc., First International Conference on Concrete Block Paving, University of Newcastle upon Tyne, England, 1980.
19. A.W.M. Kok. ICES STRUDL: Rigid Bodies. Structural Mechanics Division, Department of Civil Engineering, Delft University of Technology, Delft, Netherlands, 1982.
20. G.H.A.M. Fuchs, L.J.M. Houben, and A.A.A. Molenaar. Evaluation of in Service Concrete Block Pavements (in Dutch). Report 7-83-200-5. Laboratory for Road and Railroad Research, Department of Civil Engineering, Delft University of Technology, Delft, Netherlands, 1983.
21. A.M.A.M. Van Pelt, L.J.M. Houben, and A.A.A. Molenaar. Research on the Structural Behaviour of Two Concrete Block Pavements (in Dutch). Report 7-82-200-2. Laboratory for Road and Railroad Research, Department of Civil Engineering, Delft University of Technology, Delft, Netherlands, 1982.
22. A.A.A. Molenaar and G. Van der Velden. Tables for the Calculation of Elastic Moduli from Deflection Measurements (in Dutch). Report 7-77-5-115-2. Laboratory for Road and Railroad Research, Department of Civil Engineering, Delft University of Technology, Delft, Netherlands, 1977.
23. H.O. Moll and A.A.A. Molenaar. Application of the Finite Element Method on Concrete Block Pavements (in Dutch). Memorandum 7-83-200-6-m. Laboratory for Road and Railroad Research, Department of Civil Engineering, Delft University of Technology, Delft, Netherlands, 1983.
24. L.J.M. Houben, A.A.A. Molenaar, G.H.A.M. Fuchs, and H.O. Moll. Analysis and Design of Concrete Block Pavements. To be presented at the Second International Conference on Concrete Block Paving, Delft University of Technology, Delft, Netherlands, 1984.
25. V. Veverka. Evaluation of the Rut Depth in Flexible Pavements (in Dutch). De Wegentechniek, Vol. 24, No. 23, 1979.
26. J. Verstraeten, V. Veverka, and L. Francken. Rational and Practical Designs of Asphalt Pavements to Avoid Cracking and Rutting. Proc., Fifth International Conference on the Structural Design of Asphalt Pavements, University of Michigan, Ann Arbor, 1982.

Publication of this paper sponsored by Committee on Rigid Pavements.

Effect of Concrete Shoulders on Concrete Pavement Performance

S. D. TAYABJI, C. G. BALL, and P. A. OKAMOTO

ABSTRACT

A field program of strain and deflection measurements was conducted by the Construction Technology Laboratories for the Minnesota Department of Transportation to evaluate the effects of frozen support, tied-concrete shoulders, and tridem-axle loading on concrete pavement performance. The effects of tied-concrete shoulders are presented. Field measurements were obtained at three pavement project sites located on I-90 in Minnesota. At two of these sites, a 6-in.-thick tied-concrete shoulder was used. Measurements included edge and corner deflections and edge strains. Loadings applied were a 20-kip single axle, a 34-kip tandem axle, a 42-kip tandem axle, and a 42-kip tridem axle. Theoretical analysis was also conducted by using a finite-element program to determine the effect of a tied-concrete shoulder on concrete pavement response. Field measurements and theoretical analysis indicate that concrete pavement performance is improved when a tied shoulder is used. Deflections along a tied-shoulder joint can be conservatively taken as 85 percent of those along a free edge. Based on study results and analysis of data, it is concluded that for application to the AASHTO thickness design procedure, only one-half of the design 18-kip equivalent single-axle load applications needs to be considered for concrete pavements incorporating a tied-concrete shoulder. This recommendation results in a reduction of 1 in. in the required main-line slab thickness given by the AASHTO design procedure.

A field program of strain and deflection measurements was conducted by the Construction Technology Laboratories for the Minnesota Department of Transportation (MnDOT). The objective of the measurement program was to evaluate the effects of frozen support, tied-concrete shoulders, and tridem-axle loading on concrete pavement performance. Results of the investigation are reported separately for each of the three topics. Results of the frozen-support and tridem-axle loading studies are given in reports prepared for MnDOT (1,2).

Concrete shoulders have been used adjacent to main-line concrete pavements in the United States for almost 20 years. More recently it has been noted that the use of tied shoulders has improved the performance of concrete pavements. Similarly the use of widened lanes has also resulted in improved pavement performance. The improved performance is due to reduced edge strains, reduced edge and corner deflections, and reduced water infiltration along the pavement edges.

Current thickness design methods for concrete pavements do not consider the contribution of tied shoulders and widened lanes. Use of these design methods results in the same thickness requirements for concrete pavements with or without tied shoulders or lane widening. However, both tied shoulders and widened lanes contribute to improved pavement performance by reducing deflections and stresses in the main-line pavement. Therefore it should be possible to use a less thick main-line pavement and obtain the same pavement performance as that of a thicker pavement without tied shoulders or lane widening.

A field study was sponsored during 1976 by MnDOT to evaluate the effect of tied-concrete shoulders and widened lanes. The field study involved load testing of several newly constructed concrete pavement sections with and without tied shoulders and widening. The report to MnDOT (3) showed significant reductions in pavement strains and deflections for pavements with tied shoulders and lane widening. Implementation of the study results has not been carried out because of concern that sufficient performance data gathered over a period of time were not available.

To alleviate these concerns and to obtain further field data to quantify the beneficial effects of using tied-concrete shoulders and lane widening, a follow-up study was conducted at locations included in the 1976 study. These pavement sections have experienced about 6 years of traffic. The study included field load testing, data analyses, and development of methods to facilitate incorporation of the study findings into Minnesota's concrete pavement design procedure.

Field testing was conducted during October 1982 and February 1983. This paper presents the results of field testing, analysis of results, and recommendations to incorporate study results in Minnesota's thickness design procedure.

BACKGROUND

A brief discussion is presented to highlight the important aspects of the 1976 field study (3). For this study measurements were obtained during the fall of 1976 at four pavement projects located in Minnesota. Three of these projects, projects 1, 2, and 3, were included for retesting in the current study.

Measured pavement strains are shown in Figure 1 for project 1 and in Figure 2 for project 2. The reduction in edge deflections due to the tied-concrete shoulder is shown in Figure 3 for project 1. A similar reduction in measured edge deflections due to the tied-concrete shoulder was also obtained for project 2. Based on these field measurements, laboratory slab testing, and theoretical analyses, recommendations were made for reduction in main-line slab thickness for pavements using tied-concrete shoulders. These recommendations based on edge-strain reduction are shown in Figure 4 in which the permissible thickness reduction in the outer lane due to the tied shoulder ranged from 1 to 2 in.

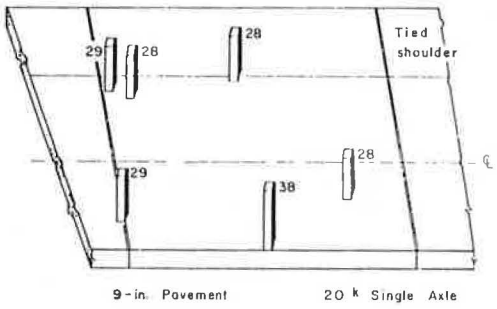

FIGURE 1 Measured strains for project 1 *(3)*.

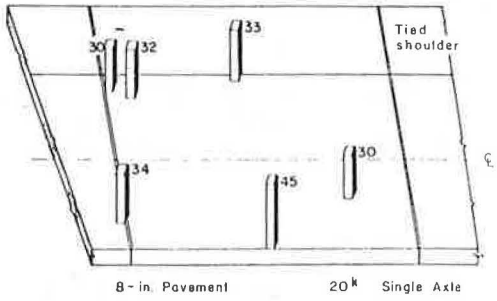

FIGURE 2 Measured strains for project 2 *(3)*.

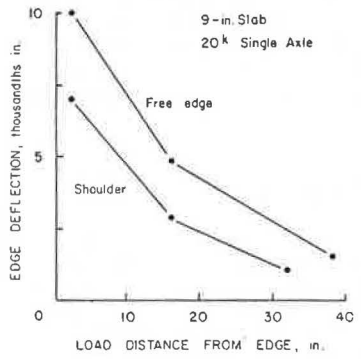

FIGURE 3 Measured edge deflection reduction due to tied shoulder at project 1 *(3)*.

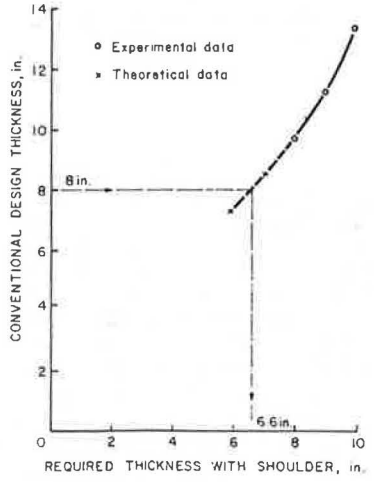

FIGURE 4 Recommended thickness reduction *(3)*.

Recent studies conducted at the University of Illinois for FHWA have also demonstrated that main-line pavement response is greatly improved by the use of tied-concrete shoulders (4). Theoretical analysis showed that calculated edge deflections and strain in the outside lane of a pavement with a tied-concrete shoulder were greatly reduced as compared with those in a pavement without a tied-concrete shoulder (4).

As part of the University of Illinois study, field measurements were made to determine joint efficiency across the outside lane shoulder joint along the I-74 and I-80 experimental portland cement concrete (PCC) shoulders (4). Joint efficiency is defined as the ratio of the deflection of the unloaded slab to the deflection of the loaded slab. Field measurements are summarized in Table 1. As shown in Table 1, shoulder sections with tied keyways on I-74 had retained joint efficiency in excess of 70 percent even after 10 years of service. It is also seen from Table 1 that the tied-shoulder sections on I-80 without keyways had much lower joint efficiencies.

TABLE 1 Field Data on I-74 and I-80 PCC Shoulders *(4)*

Project	Shoulder Design	Mean Edge Deflection (mm)		
		Traffic Lane	Shoulder	Load-Transfer Efficiency (eff)[a]
I-74[b]	Tie bars, keyway, and granular subbase	0.1143	0.1118	97.8
	Tie bars, keyway, and no subbase	0.1448	0.1016	70.2
	Keyway and granular subbase but no tie bars	0.2108	0.0330	16.0
I-80[c]	Tie bars and intermediate granular subbase	0.2311	0.0889	38.5
	Tie bars and coarse granular subbase	0.2464	0.0762	31.0
	Tie bars and no subbase	0.2159	0.1016	47.0

[a]Deflection of the unloaded slab divided by deflection of the loaded slab times 100.
[b]PCC shoulders 10 yr old.
[c]PCC shoulders 9 yr old.

Studies referred to earlier positively indicate that use of a tied-concrete shoulder with a keyway greatly improves main-line pavement performance. However, except for the MnDOT 1976 study (3), none of these studies incorporates the beneficial effect of a tied-concrete shoulder when the design slab thickness is determined for the main-line pavement.

RESEARCH OBJECTIVES

Objectives of the study were as follows:

1. To measure load-induced strains and deflections in pavement sections incorporating tied-concrete shoulders and
2. To analyze test results to establish the effects of tied-concrete shoulders on concrete pavement performance.

PAVEMENT TEST SECTIONS

Field measurements were obtained at three pavement project sites in Minnesota. These projects were included in a 1976 field study on concrete shoulders and lane widening (3). A brief description of each project follows.

Project 1: Designation State Project 2280-30 (TH-90) is a roadway 27 ft wide consisting of an inside lane 15 ft wide and an outside lane 12 ft wide with an outside tied keyed concrete shoulder 10 ft wide. Shoulders are tied at 30-in. spacing by using No. 5 tie bars 30 in. long. Shoulder thickness is 6 in. The pavement is plain concrete slabs 9 in. thick with skewed joints at a repeated random spacing of 13, 16, 14, and 19 ft. The subgrade at the site was classified as silty clay to clay loam and had a gravel subbase 5 in. thick over it. Dowel bars were placed only in the 12-ft-wide outside traffic lane. Dowels are No. 8 round bars spaced at 12 in. on centers; the first dowel is located 6 in. inward from the pavement edge. Panels selected for test are located at stations 538+65 and 540+10.

Project 2: Designation State Project 2280-30 (TH-90) is a roadway 27 ft wide and an outside tied keyed concrete shoulder 10 ft wide. Dowel size and location are the same as those for project 1. Pavement thickness is 8 in. Subgrade at the site was classified as silty clay to clay loam and had a gravel subbase 6 in. thick over it. The modulus of subgrade reaction was reported to be 270 pci. Panels selected for test are located at stations 520+55 and 521+81.

Project 3: Designation State Project 2280-31 (TH-90) is a roadway 27 ft wide with an inside lane 15 ft wide and an outside lane 12 ft wide. The pavement is reinforced concrete slabs 9 in. thick with skewed joints at a spacing of 27 ft. Subgrade at the site was classified as clay loam to silty clay loam to sandy clay loam. A gravel subbase 5 in. thick was used. Dowel bars were placed only in the 12-ft mainline pavement portion of both traffic lanes. Dowels are No. 8 round bars spaced 12 in. on centers. Panels selected for test are located at stations 985+53 and 987+11.

All three projects are located on I-90 between Albert Lea and Fairmont, Minnesota. Two test sites were selected at each project. At each site both inside and outside lanes were instrumented and monitored to evaluate pavement response. At some of the sites the panels tested in 1976 were retested. Care was taken to assure that the sites selected were representative of the project.

INSTRUMENTATION

All pavement test sections were instrumented to measure load-induced strains and deflections. In addition pavement temperature and slab curl were monitored. Curl is a change in the vertical profile of the slab resulting from changes in the slab temperature.

Strain gage and deflectometer locations for project 1 and 2 test sections are shown in Figure 5. Instrumentation locations were similar for project 3. These locations were selected to obtain the maximum values of strain and deflection for the different load positions. Curl measurements were made at deflectometer locations. Concrete temperatures were measured in instrumented test blocks placed in the subbase adjacent to the pavement.

Load Strains

Concrete strains were measured with electrical-resistance strain gages 4 in. long cemented to the pavement surface. Gages were placed at the free edge, shoulder edge, transverse joints, and joint corners and in the interior. Gage positions and loading locations shown in Figure 5 are referred to in subsequent discussions. All gages were placed in recessed grooves to protect them from direct application of wheel loads.

Load Deflections

Load deflections were measured with resistance-bridge deflectometers bolted to the pavement. Readings were referenced to encased rods driven into the subgrade to a depth of 6 ft. Construction details of the deflectometer are presented in Research and Development Bulletin D83 (5) of the Portland Cement Association.

Curl Measurements

Pavement curl was measured with 0.001-in. indicators placed at the same locations as the deflectometers. The dial indicators were bolted to the pavement and the movement was referenced to encased rods placed in the subgrade. Curl readings were taken approximately once an hour.

Temperature Measurements

Changes in pavement temperature were measured with copper-constantan thermocouples embedded in concrete blocks. The laboratory-cast blocks were 1 ft square and 8 or 9 in. thick. Thermocouples were located 0.125, 0.50, 1, 2, 4, and 6 in. from the top and 0.125 in. from the bottom surfaces. Temperature blocks were placed in the subbase adjacent to the highway at least 12 hr before testing. Air temperature was monitored with a thermocouple shaded from the direct sun.

Monitoring Equipment

Data were monitored and recorded with equipment carried in the Construction Technology Laboratories' field instrumentation van. Strain and deflection data were recorded with a high-speed computer-based data acquisition system. Twenty-two channels of instrumentation were monitored and recorded simultaneously for each vehicle loading. Computer programs were written to monitor, record, and tabulate all field data.

Temperature data were recorded with a 24-channel continuously monitoring temperature recorder. All monitoring and recording instrumentation was calibrated before testing.

TEST PROCEDURES

Strain and deflection data were recorded for a 20-kip single-axle load (SAL), 34-kip and 42-kip tandem-axle loads (TAL), and 42-kip tridem-axle load. Loading was applied with two semitrailers. One applied the 20-kip SAL and 34-kip TAL. The other applied the 42-kip TAL and 42-kip tridem-axle load. Trucks used were supplied by MnDOT. Before testing, axle weights were checked and loads were adjusted to obtain uniform distribution to the wheels.

The effects of axle weight and load location on strains and deflections were recorded with the trucks moving at creep speed along the wheel paths shown in Figure 5. Tire placements varied from 2 to 38 in. from the pavement edge. All wheel-path measurements were from the pavement edge to the outside

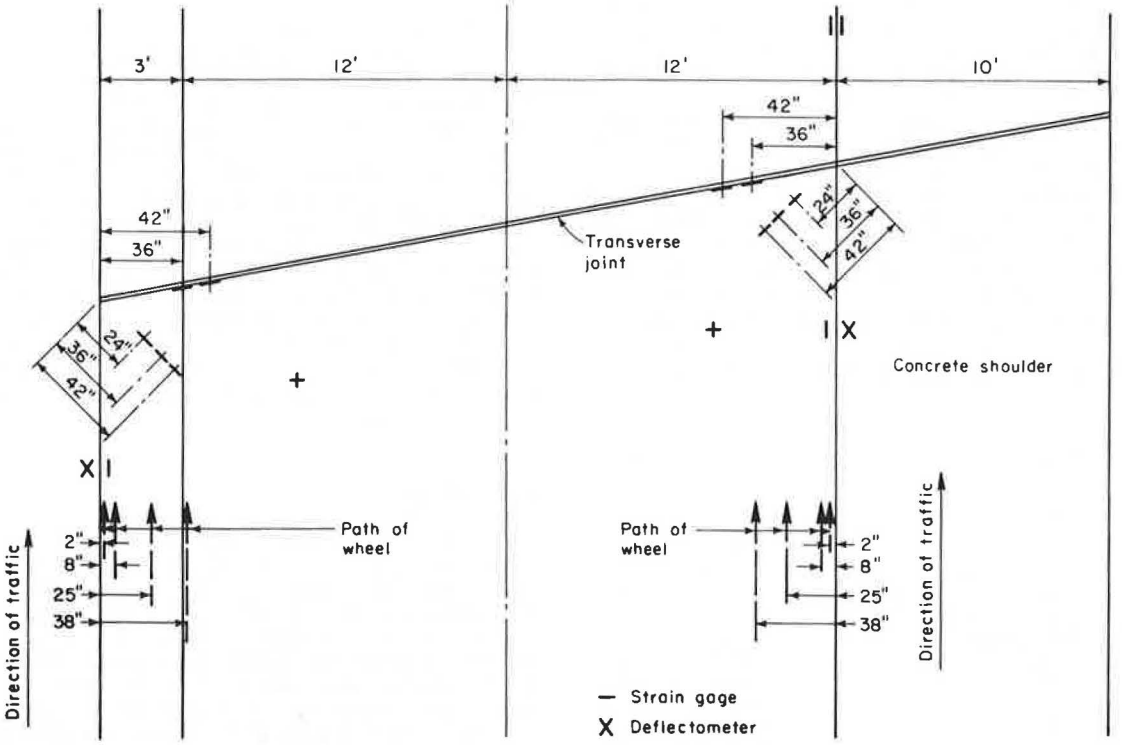

FIGURE 5 Instrumentation layout for projects 1 and 2.

edge of the tire sidewall at its maximum width. In addition, pavement curl and temperature data were obtained periodically during the day.

Test slabs from inside and outside lanes at each project site were tested on the same day. Primary readings were taken on both inside and outside lanes between approximately 11:30 a.m. and 2:00 p.m. In addition, readings were also taken on one lane before 11:30 a.m. and on the other lane after 2:00 p.m. Specific testing times were governed primarily by weather and traffic control requirements.

DATA ANALYSIS

In this section a comparison of pavement responses measured along the edges of the outside lanes and those for the inside lanes is presented for the three project sites. The outside-lane edge corresponds to a joint with a tied-concrete shoulder for projects 1 and 2. The edge of the inside lane corresponds to a free edge along the widened inside lane for projects 1 and 2. Project 3 has neither a concrete shoulder nor lane widening along the inside lane and was used as a control section to determine the influence of traffic along the outside lane.

Pavement responses reported were measured under 20-kip SAL, 34-kip and 42-kip TAL, and 42-kip tridem-axle load. Pavement responses compared are edge and corner deflections and edge strains. In addition results of theoretical analyses are presented to evaluate the effect of tied-concrete shoulders. Although measurements were obtained during October 1982 and February 1983, only the October 1982 measurements are presented and discussed in this report. Because of the frozen support, measured deflections during February 1983 were low for both the inside and outside lanes at each project site. Details of the February measurements are given elsewhere (1).

Curling and Warping Effects

Soon after concrete has been placed, drying shrinkage of the concrete begins. Drying shrinkage in a slab on grade occurs at a faster rate at the slab surface than at the slab bottom. In addition, because the subgrade and subbase may remain wet, the slab bottom remains relatively moist. Thus, total shrinkage at the bottom is less than that at the top. This differential in shrinkage results in a lifting of the slab from the subbase at edges and corners. Movements of this type resulting from moisture differentials are referred to as warping. Warping leaves slabs unsupported for distances of as much as 4 to 5 ft at slab corners and 2 to 3 ft at slab edges. Warping is almost never recoverable.

In addition to warping, a slab on grade is also subjected to curling. Curling is the change in the slab profile due to temperature differential between slab top and bottom. Curling is a daily phenomenon. Slabs curl up during the night and curl down during midday. Thus, curling deformation is additive to warping during the night and reduces the warping effect during the midday. It is believed by many engineers that the warping effect is almost never cancelled out by daytime curling and that some loss of support always exists under the slab even on hot days.

Because of curling effects, the measured deflections under load along a slab edge or a slab corner are greatly affected by the time of testing. Measured slab strains are also affected by time of

testing but at a lower level. Therefore, great care needs to be exercised in interpreting deflection and strain measurements if these measurements are made at different times of day or on different days. The usual procedure in reporting deflection measurements at a given location is to correct the measurements with respect to a reference time. The reference time is generally selected to be the time when the slab top and bottom temperatures are equal.

As discussed, temperature and curl measurements were made at each of the five test sites considered in this study. At each test site, pavement responses under load were generally measured at two different times, usually within a span of 3 hr around noon.

Figure 6 shows the variation with time of the air temperature, corner curl, and corner deflection under a 20-kip SAL at each of the five sites. It is

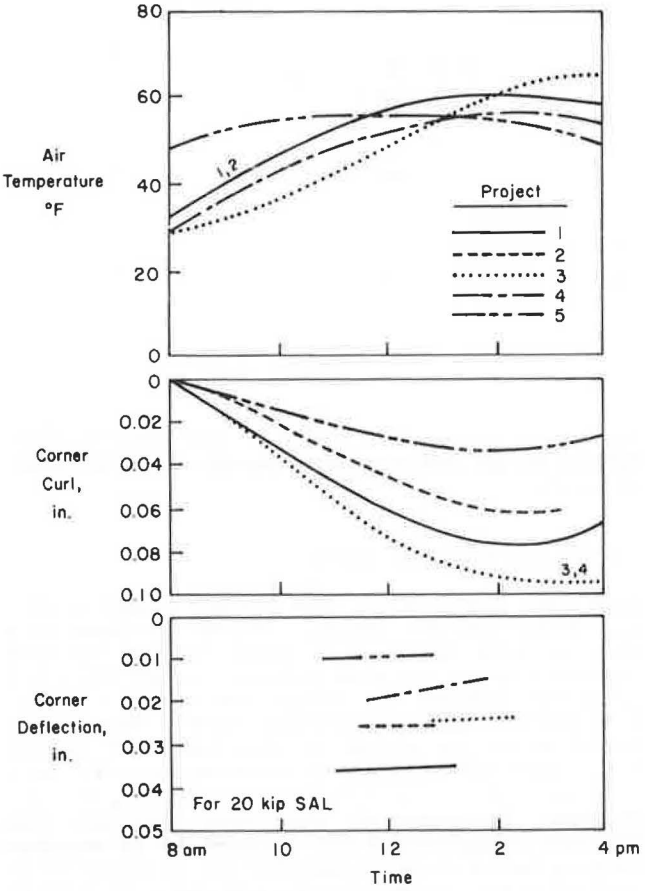

FIGURE 6 Variation of air temperature, corner curl, and deflection with time.

seen that although slabs at each site exhibit pronounced curling, the deflections under load were not greatly influenced by the time of testing between approximately 11:00 a.m. and 2:00 p.m. Similar trends were obtained for edge curl and deflections and edge strain. This is because the slabs have curled to their most downward profiles and changes from these profiles are gradual with respect to time, as shown in Figure 6. Therefore, no temperature corrections were applied to these readings. The measurements reported in this paper are the averages of the readings for the two test times and correspond to the period when each slab being tested was near its maximum downward curl.

Summary of Data

Load tests were conducted during October 1982 when air temperatures at midday were about 55°F. Pavement responses measured at each of the three sites are listed in Table 2. Edge and corner deflections and edge strains measured during October 1982 at the inside and outside lanes are listed for each of the four axle loadings. Each data point is an average of four readings made up of data taken at two different times at each of the two replicate sections at each project location. The measurements are shown in Figures 7, 8, and 9 for edge deflection, corner deflection, and edge strain, respectively. A discussion of these measurements follows. (In Figures 7-9 axles are denoted as follows: axle 1, 20-kip SAL; axle 2, 34-kip TAL; axle 3, 42-kip TAL; axle 4, 42-kip tridem-axle load. N denotes lack of reliable data.)

Edge Deflections

For project 1 measured edge deflection ranged from 0.019 in. under the 20-kip SAL to 0.029 in. under the 42-kip TAL along the outside lane and from 0.021 in. under the 20-kip SAL to 0.038 in. under the 42-kip TAL along the inside lane. As shown in Figure 7, edge deflections along the outside lane with the tied shoulder were about 75 to 90 percent of those along the untrafficked free edge of the inside lane.

For project 2 edge deflections measured along the outside lane do not show variation with different axle loads and are considerably lower than those along the free inside-lane edge. This is believed to be because of malfunctioning of the deflectometers at that location.

For the control sections at project 3 edge deflections along the free outside lane edge ranged from 96 to 115 percent of those along the untrafficked free inside lane. This indicates that the free outside-lane edge, which is subjected to a large volume of truck traffic, exhibits higher deflections than the untrafficked free inside-lane edge. This behavior is possibly caused by greater loss of support along the outside-lane edge resulting from subbase and subgrade consolidation or erosion or both. Thus, the effect of using tied-concrete shoulders at project 1 and possibly at project 2 is to significantly reduce edge deflections along the heavily traveled outside-lane edge.

Corner Deflections

For project 1 measured corner deflections ranged from 0.019 in. under the 20-kip SAL to 0.029 in. under the 42-kip TAL along the outside lane and from 0.035 in. under the 20-kip SAL to 0.051 in. under the 42-kip TAL along the inside lane. For project 2 measured corner deflections ranged from 0.021 in. under the 20-kip SAL to 0.025 in. under the 42-kip TAL along the outside lane and from 0.026 in. under the 20-kip SAL to 0.034 in. under the 42-kip TAL along the inside lane.

As shown in Figure 8, corner deflections along the outside lane with the tied shoulder as a percentage of those along the untrafficked free edge of the inside lane were about 70 to 87 percent for project 1 and about 58 to 80 percent for project 2.

For the control sections at project 3, corner deflections along the free outside-lane edge ranged from 125 to 150 percent of those along the untrafficked free inside-lane edge. These results further verify that the free outside-lane edge, which is

TABLE 2 Measured Pavement Response for Projects 1, 2, and 3

Parameter	20-kip SAL	34-kip TAL	42-kip TAL	42-kip Tridem-Axle Load
Project 1				
Inside lane				
Edge deflection (in.)	0.021	0.034	0.038	0.034
Corner deflection (in.)	0.035	0.044	0.051	0.044
Edge strain (x 10^{-6})	35	30	32	17
Outside lane				
Edge deflection (in.)	0.019	0.026	0.029	0.027
Corner deflection (in.)	0.030	0.034	0.037	0.031
Edge strain (x 10^{-6})	30	24	27	19
Shoulder strain (x 10^{-6})	3	3	8	6
Project 2				
Inside lane				
Edge deflection (in.)	0.016	0.026	0.027	0.023
Corner deflection (in.)	0.026	0.036	0.034	0.030
Edge strain (x 10^{-6})	35	32	33	18
Outside lane				
Edge deflection (in.)	0.007	0.007	0.007	0.009
Corner deflection (in.)	0.021	0.021	0.025	0.019
Edge strain (x 10^{-6})	33	31	38	20
Shoulder strain (x 10^{-6})	7	6	12	9
Project 3				
Inside lane				
Edge deflection (in.)	0.013	0.022	0.025	0.020
Corner deflection (in.)	0.024	0.030	0.032	0.026
Edge strain (x 10^{-6})	33	28	30	18
Outside lane				
Edge deflection (in.)	0.015	0.021	0.025	0.023
Corner deflection (in.)	0.036	0.040	0.040	0.034
Edge strain (x 10^{-6})	18	23	24	16

Note: All measurements were obtained during October 1982. Inside-lane measurements were taken along the edge of the 3-ft lane widening. Outside-lane measurements were taken along the joint with tied shoulder.

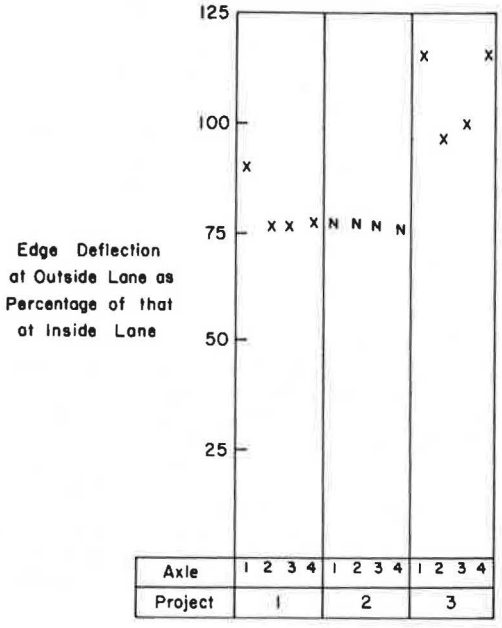

FIGURE 7 Comparison of edge deflections.

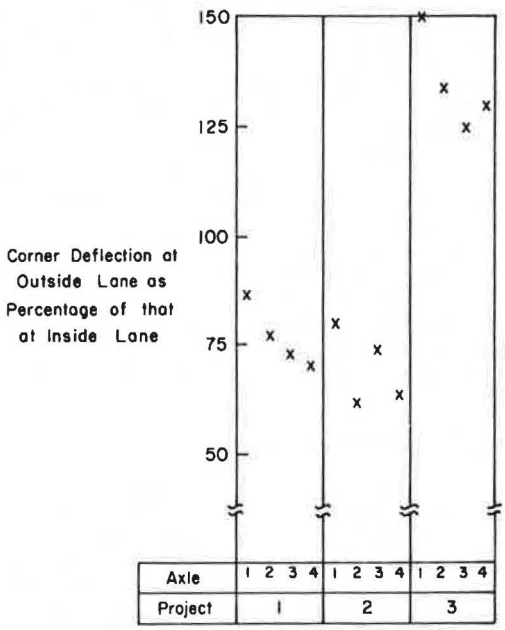

FIGURE 8 Comparison of corner deflections.

subjected to a considerable amount of traffic, exhibits higher deflections than the untrafficked free inside-lane edge.

Edge Strains

For project 1 measured edge strains ranged from 19 x 10^{-6} under the 42-kip tridem-axle load to 30 x 10^{-6} under the 20-kip SAL along the outside lane and 17 x 10^{-6} under the 42-kip tridem-axle load to 35 x 10^{-6} under the 20-kip SAL along the inside lane. For project 1 the measured tied-concrete shoulder edge strain ranged from 3 x 10^{-6} under the 20-kip SAL to 8 x 10^{-6} under the 34-kip TAL.

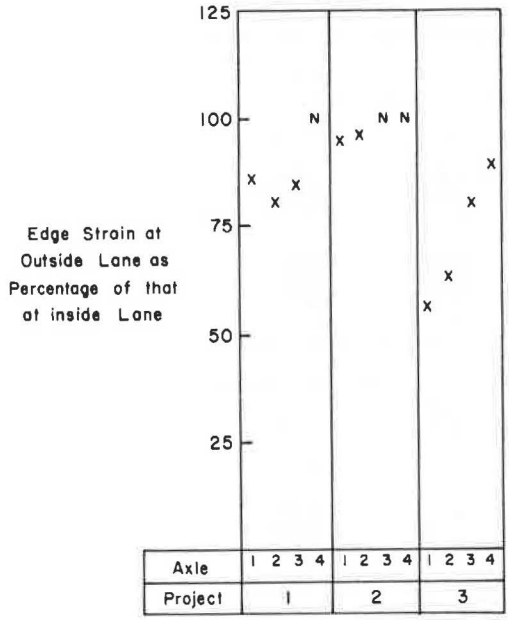

FIGURE 9 Comparison of edge strain.

For project 2 measured edge strains ranged from 20 x 10^{-6} under the 42-kip tridem-axle load to 38 x 10^{-6} under the 34-kip TAL along the outside lane and 18 x 10^{-6} under the 42-kip tridem-axle load to 35 x 10^{-6} under the 20-kip SAL along the inside lane. For project 2 measured tied-shoulder edge strain ranged from 6 x 10^{-6} under the 34-kip TAL to 12 x 10^{-6} under the 42-kip TAL.

For project 3 measured edge strains along the free outside-lane edge ranged from 55 to 89 percent of those along the untrafficked free inside-lane edge. These results are in contrast to the trend in measured deflections at project 3 in which measured deflections along the outside lane were generally greater than those measured along the inside lane.

In addition to the measurements at the three project sites reported here, similar measurements were also made at two additional project sites. These two sites did not incorporate tied shoulders or lane widening. Measurements from these two project sites are reported elsewhere (1). These measurements also indicate that corner and edge deflections as well as edge strains are larger along the trafficked free outside-lane edge as compared with those along the lightly trafficked free inside-lane edge.

Theoretical Considerations

Analyses were conducted to determine the effect of a tied-concrete shoulder on concrete pavement response. A finite-element program, JSLAB, developed by Construction Technology Laboratories for FHWA was used (6). The program can analyze a large number of jointed slabs. Joints can be modeled as doweled, aggregate interlock, or keyed. Load input is in terms of wheel loads at any location on the slabs. Loss of support, variable support, or material properties can be considered. In the program subbase and subgrade support is characterized by the modulus of subgrade support.

Analysis was conducted for a concrete pavement 9 in. thick with and without tied shoulders and with dowel bars at the transverse joints. For the case of the tied shoulder, a 6-in.-thick slab was used. Values used for the modulus of subgrade reaction were 100, 150, an 250 pci. Calculated corner deflections, edge deflections, and edge stresses are listed in Tables 3-5. For both corner and edge loadings, tire placements were 2 in. inward from the edge.

TABLE 3 Calculated Pavement Response: Corner Deflection

Shoulder Type	k (pci)	Corner Deflection (in.) 20-kip SAL	34-kip TAL	42-kip TAL	42-kip Tridem-Axle Load
Tied	100	0.025	0.026	0.032	0.026
	150	0.018	0.019	0.023	0.019
	250	0.013	0.013	0.016	0.012
None	100	0.035	0.040	0.050	0.040
	150	0.026	0.030	0.037	0.028
	250	0.019	0.020	0.025	0.019

TABLE 4 Calculated Pavement Response: Edge Deflection

Shoulder Type	k (pci)	Edge Deflection (in.) 20-kip SAL	34-kip TAL	42-kip TAL	42-kip Tridem-Axle Load
Tied	100	0.015	0.022	0.027	0.022
	150	0.012	0.016	0.020	0.016
	250	0.008	0.011	0.014	0.011
None	100	0.024	0.035	0.043	0.036
	150	0.018	0.025	0.031	0.026
	250	0.012	0.017	0.021	0.017

TABLE 5 Calculated Pavement Response: Edge Stress

Shoulder Type	k (pci)	Edge Stress (psi) 20-kip SAL	34-kip TAL	42-kip TAL	42-kip Tridem-Axle Load
Tied	100	236	180	222	114
	150	218	160	198	98
	250	199	139	172	81
None	100	286	230	284	152
	150	263	203	250	128
	250	236	172	212	103

In the computer program a tied keyway is represented by springs. For the analysis a spring stiffness value of 25,000 lb/(in. • in.) of joint length was used. This resulted in calculated joint efficiency of about 80 percent for a modulus of subgrade reaction of 250 pci to about 90 percent for a modulus of subgrade reaction of 100 pci. For this set of assumptions the ratio of calculated corner and edge deflections along a tied-shoulder joint to those along a free edge is about 65 percent. The ratio of calculated edge strains along a tied-shoulder joint to those along a free edge is about 80 percent.

Additional analysis was conducted for a 9-in.-thick slab on a subgrade with a modulus value of 250 pci and with keyway spring stiffness values of 5,000, 10,000, 15,000, and 20,000 lb/(in. • in.) of joint length. Based on these analyses, ratios of calculated deflections and strains along a tied shoulder joint to those along a free edge were determined for different values of shoulder joint efficiency (JE). These ratios are listed as follows for a main-line slab thickness of 9 in., a shoul-

der-slab thickness of 6 in., and 250 pci (JE = deflection of main-line slab divided by deflection of shoulder slab):

	Ratio (%) by JE		
Response	80 Percent	60 Percent	50 Percent
Edge deflection	65	70	75
Corner deflection	65	70	75
Edge strain	80	85	90

It should be noted that measured deflection values are much higher than calculated deflection values, even when a modulus of subgrade reaction value of 150 pci is used. Modulus of subgrade reaction values at the three locations were reported to be in excess of 250 pci. The reason for this anomaly in measured and computed deflection values is that the theoretical analysis was conducted for the case of full support under the pavement slabs. In practice there is always some loss of support along slab edges. This support loss results in higher measured slab deflections.

Analysis of Results

As indicated, it is clear that concrete pavement response is improved when a tied shoulder is used. The level of improvement, based on field testing and theoretical analyses, is summarized in Table 6, in which it can be seen that the reduction in the deflection response can be conservatively taken at 85 percent. This value corresponds to a calculated joint efficiency at the tied-shoulder joint of less than 50 percent. As discussed previously, measured joint efficiency along the shoulder sections on I-74 in Illinois, which incorporated tied keyways, had retained joint efficiency in excess of 70 percent even after 10 years of service. Therefore, properly constructed concrete pavement with tied shoulders can be expected to retain at least 50 percent joint efficiency during its design life.

TABLE 6 Improvement in Pavement Response

	Ratio of Response at Tied-Shoulder Joint to That at Free Edge (%)				
	Measured		Calculated		
Response	Project 1	Project 2	JE = 80 Percent	JE = 60 Percent	JE = 50 Percent
Edge deflection	75-90	NR[a]	65	70	75
Corner deflection	70-87	58-80	65	70	75
Edge stress	80-85	94-97	80	85	90

Note: JE = deflection of main-line slab divided by deflection of shoulder slab.
[a]Data considered not reliable.

It should be noted that the measured level of improvement shown in Table 4 is based on response of the inside-lane edge, which has been subjected to little traffic loading. Therefore, if the level of improvement had been determined based on a free longitudinal edge that had been subjected to the same amount of traffic as the outside lanes at projects 1 and 2, a greater reduction in pavement responses would have been determined for the tied-shoulder sections at projects 1 and 2.

Because pavement damage or loss of serviceability is a function of axle load magnitude and number of load repetitions, it can be concluded that a given axle would produce less deflection-related damage or loss of serviceability on a pavement with a tied shoulder than on a pavement without a tied shoulder. If a linear relationship is assumed between magnitude of axle load and pavement deflection response, an axle load (P) applied on a pavement without a tied shoulder can be considered to be equivalent to an axle load (P/0.85) applied on a pavement with a tied shoulder. Thus, based on similar deflection responses, an 18-kip SAL applied on a pavement without a tied shoulder can be considered to be equivalent to a 21-kip SAL applied on a pavement with a tied shoulder.

Application to AASHTO Design Procedure

The AASHTO Interim Guide uses the concept of traffic equivalence factors for converting mixed traffic to an equivalent number of 18-kip SALs (7). The equivalence factors, when multiplied by the number of axle loads within a given weight category, give the number of 18-kip SAL applications that have an equivalent effect on the performance of the pavement.

The AASHTO traffic equivalence factors give more weight to deflection response than to stress-type response. For example, according to the AASHTO traffic equivalence factors, presented in Table 7, tandem axles are about 2.30 to 2.50 times as damaging as a single axle weighing half as much as the tandem axles. The ratio of edge deflection under tandem axles to that under a single axle weighing half as much is about 1.64 based on theoretical analysis and about 1.90 based on field measurements. On the other hand, calculated as well as measured edge strain under tandem axles are less than those under a single axle weighing half as much as the tandem axles. Therefore, with respect to use of a tied shoulder, the reduction in deflection response is considered more significant than the reduction in strain response.

It should be further pointed out that the AASHTO design equation incorporates Spangler's equation for corner stress. For pavement and joint designs similar to that used at the AASHTO Road Test, the constant J of Spangler's equation cancels out. The constant J has a value of 3.2 for an unprotected corner. However, for pavements incorporating a tied shoulder, the value of J would be much less than 3.2 because the corner stresses would be reduced by the use of a tied shoulder. This further verifies that the AASHTO design equation would recognize the beneficial effect of a tied shoulder if the value of constant J of Spangler's equation was modified to account for use of a tied shoulder.

Thus, the establishment of a conservative level of reduction of 15 percent in the deflection response because of the use of a tied shoulder is considered valid. Similarly the assumption based on study results that an axle load (P) applied on a pavement without a tied shoulder is equivalent to an axle load (P/0.85) applied on a pavement with a tied shoulder is considered valid.

It is seen from Table 5 that for a 9-in.-thick pavement, a 21-kip SAL is 2.0 times as damaging as an 18-kip SAL. However, based on study results, a 21-kip SAL applied on a pavement with a tied shoulder can be considered to be only as damaging as an 18-kip SAL applied on a pavement without a tied shoulder. Thus, a 21-kip SAL applied on a pavement with a tied shoulder is only 1/2.0, that is, 0.5 times as damaging, as a 21-kip SAL applied on a pavement without a tied shoulder. If this logic is applied to different slab thicknesses and other axle

TABLE 7 Traffic Equivalence Factors for SALs and TALs

Axle Load		Slab Thickness D (in.)						
Kips	kN	6	7	8	9	10	11	12
Single Axle								
2	8.9	0.0002	0.0002	0.0002	0.0002	0.0002	0.0002	0.0002
4	17.8	0.003	0.002	0.002	0.002	0.002	0.002	0.002
6	26.7	0.01	0.01	0.01	0.01	0.01	0.01	0.01
8	35.6	0.04	0.04	0.03	0.03	0.03	0.03	0.03
10	44.5	0.10	0.09	0.08	0.08	0.08	0.08	0.08
12	53.4	0.20	0.19	0.18	0.18	0.18	0.17	0.17
14	62.3	0.38	0.36	0.35	0.34	0.34	0.34	0.34
16	71.2	0.63	0.62	0.61	0.60	0.60	0.60	0.60
18	80.1	1.00	1.00	1.00	1.00	1.00	1.00	1.00
20	89.0	1.51	1.52	1.55	1.57	1.58	1.58	1.59
22	97.9	2.21	2.20	2.28	2.34	2.38	2.40	2.41
24	106.8	3.16	3.10	3.23	3.36	3.45	3.50	3.53
26	115.7	4.41	4.26	4.42	4.67	4.85	4.95	5.01
28	124.6	6.05	5.76	5.92	6.29	6.61	6.81	6.92
30	133.4	8.16	7.67	7.79	8.28	8.79	9.14	9.34
32	142.3	10.81	10.06	10.10	10.70	11.43	11.99	12.35
34	151.2	14.12	13.04	12.34	13.62	14.59	15.43	16.01
36	160.1	18.20	16.69	16.41	17.12	18.33	19.52	20.39
38	169.0	23.15	21.14	20.61	21.31	22.74	24.31	25.58
40	177.9	29.11	26.49	25.65	26.29	27.91	29.90	31.64
Tandem Axles								
10	44.5	0.01	0.01	0.01	0.01	0.01	0.01	0.01
12	53.4	0.03	0.03	0.03	0.03	0.03	0.03	0.03
14	62.3	0.06	0.05	0.05	0.05	0.05	0.05	0.05
16	71.2	0.10	0.09	0.08	0.08	0.08	0.08	0.08
18	80.1	0.16	0.14	0.14	0.13	0.13	0.13	0.13
20	89.0	0.23	0.22	0.21	0.21	0.20	0.20	0.20
22	97.9	0.34	0.32	0.31	0.31	0.30	0.30	0.30
24	106.8	0.48	0.46	0.45	0.44	0.44	0.44	0.44
26	115.7	0.64	0.64	0.63	0.62	0.62	0.62	0.62
28	124.6	0.85	0.85	0.85	0.85	0.85	0.85	0.85
30	133.4	1.11	1.12	1.13	1.14	1.14	1.14	1.14
32	142.3	1.43	1.44	1.47	1.49	1.50	1.51	1.51
34	151.2	1.82	1.82	1.87	1.92	1.95	1.96	1.97
36	160.1	2.29	2.27	2.35	2.43	2.48	2.51	2.52
38	169.0	2.85	2.80	2.91	3.04	3.12	3.16	3.18
40	177.9	3.52	3.42	3.55	3.74	3.87	3.94	3.98
42	186.8	4.32	4.16	4.30	4.55	4.74	4.86	4.91
44	195.7	5.26	5.01	5.16	5.48	5.75	5.92	6.01
46	204.6	6.36	6.01	6.14	6.53	6.90	7.14	7.28
48	213.5	7.64	7.16	7.27	7.73	8.21	8.55	8.75

Note: Terminal pavement serviceability index (p_t) = 2.5.

loads, it is found that the damaging effect of a given SAL or TAL applied on a pavement with a tied shoulder is about 0.5 times that for the same axle load applied on a pavement without a tied shoulder.

For application to the AASHTO design procedure, it is recommended that the damaging effect of an axle load applied on a pavement with a tied shoulder be considered as one-half of that for the same axle load applied on a pavement without a tied shoulder. Thus, only one-half of the equivalent 18-kip SALs applied needs to be considered for thickness design of pavements with a tied shoulder.

Design Application

The following parameters are assumed:

1. Concrete modulus of rupture, 650 psi;
2. Concrete working stress, 490 psi;
3. Concrete modulus of elasticity, 4×10^6 psi, and
4. Modulus of subgrade reaction, 200 pci.

By using the design chart presented in the AASHTO Interim Guide, slab thicknesses for pavements with and without a tied shoulder are calculated as follows:

Design 18-kip SAL Applications (000,000s)	Required Pavement Thickness (in.) Without Shoulder	With Shoulder
2.5	7.6	6.6
5	8.7	7.6
10	9.7	8.7
20	10.8	9.7

Required thicknesses for pavement with tied shoulders were determined by using one-half of the design 18-kip SAL applications. It is seen that as a minimum the use of a tied shoulder allows for reduction of 1 in. in the required main-line slab thickness.

Similar results are obtained for other values of the design parameters. Therefore, it is recommended that as a minimum, the use of a tied shoulder should allow for reduction of 1 in. in the required main-line slab thickness.

Future Modifications

It should be noted that study results are based on use of a 6-in.-thick concrete shoulder. If a shoulder thickness equal to the main-line slab thickness is used, a larger reduction in main-line slab thick-

ness may be warranted. Greater thickness reduction may also be warranted if future performance of other pavements incorporating tied shoulders indicates that a level of reduction in deflection response is more than the 15 percent established in the current study.

Future modifications can be made following the procedures presented in this paper. For example, let a level of reduction in deflection response of 20 percent be established. Then following procedures presented in this paper, it is found that for application to the AASHTO design procedure, only 40 percent of the design 18-kip equivalent SAL applications needs be considered for concrete pavements incorporating tied-concrete shoulders. This would result in a reduction of 1 to 2 in. in the required main-line slab thickness given by the AASHTO design procedure.

SUMMARY

A field study was conducted to evaluate the effect of tied-concrete shoulders on concrete pavement performance. Pavement deflections and strains were measured along tied-shoulder joints and along free edges at two project locations. In addition, a theoretical analysis was performed to determine the effect of tied shoulders on concrete pavement response. Study results indicate that pavement response is improved for pavements using a tied shoulder as compared with pavements not using a tied shoulder.

Based on study results, it is concluded that for application to the AASHTO thickness design procedure, only one-half of the design 18-kip equivalent SAL applications needs be considered for concrete pavements incorporating a tied-concrete shoulder. This recommendation results in a reduction of 1 in. in the required main-line slab thickness given by the AASHTO design procedure.

ACKNOWLEDGMENT

Work was conducted by the Construction Technology Laboratories under the sponsorship of MnDOT in cooperation with FHWA. The investigation was directed by Bert E. Colley, director of the Transportation Development Department, and W. Gene Corley, director of the Engineering Development Division. Leo P. Warren, Glenn R. Korfhag, Gabriel Bodoczy, and John Hale of MnDOT provided technical coordination. Their cooperation and suggestions are gratefully acknowledged.

REFERENCES

1. C.G. Ball, S.D. Tayabji, and P. Okamoto. Effect of Frozen Support on Concrete Pavement Performance. Construction Technology Laboratories, Skokie, Ill.; Minnesota Department of Transportation, St. Paul, Oct. 1983.
2. S.D. Tayabji, C.G. Ball, and P. Okamoto. Effect of Tridem-Axle Loading on Concrete Pavement Performance. Construction Technology Laboratories, Skokie, Ill.; Minnesota Department of Transportation, St. Paul, Oct. 1983.
3. B.E. Colley et al. Evaluation of Concrete Pavement with Lane Widening, Tie Concrete Shoulders, and Thickened Pavement. Report FHWA/MN-79/06. Minnesota Department of Transportation, St. Paul, Sept. 1977.
4. J.S. Sawan et al. Structural Analysis and Design of PCC Shoulders. Report FHWA-RD-81-122. FHWA, U.S. Department of Transportation, April 1982.
5. W.J. Nowlen. Techniques and Equipment for Field Testing of Pavements. Research and Development Bull. D83. Portland Cement Association, Skokie, Ill., 1964.
6. S.D. Tayabji and B.E. Colley. Analysis of Jointed Concrete Pavements. Construction Technology Laboratories, Skokie, Ill.; FHWA, U.S. Department of Transportation, Oct. 1981.
7. Interim Guide for Design of Pavement Structures, rev. ed. AASHTO, Washington, D.C., 1981.

The opinions expressed in this paper are those of the authors and not necessarily those of the Minnesota Department of Transportation or FHWA.

Publication of this paper sponsored by Committee on Rigid Pavements.

Effect of Frozen Support and Tridem Axles on Concrete Pavement Performance

S.D. TAYABJI, C.G. BALL, and P.A. OKAMOTO

ABSTRACT

A field program of strain and deflection measurements was conducted by the Construction Technology Laboratories for the Minnesota Department of Transportation. The objective of the program was to evaluate the effects of frozen support, tied-concrete shoulders, and tridem-axle loading on concrete pavement performance. The effects of frozen support and tridem-axle loading are presented. Field measurements were obtained during October 1982 and February 1983 at five pavement project sites located on I-90 in Minnesota. Measurements included edge and corner deflections and edge strains. Loadings applied were a 20-kip single axle, a 34-kip tandem axle, a 42-kip tandem axle, and a 42-kip tridem axle. Theoretical analysis was also conducted by using a finite-element program. Study results indicate that pavement deflections and strains are greatly reduced during winter months when the support is frozen. Based on analysis of these results, it is concluded that the effect of axle loads applied during the winter can be considered to be only one-seventh as damaging as the same loads applied during the fall. Study results also indicate that for application to the AASHTO thickness design procedure, tridem axles can be considered as equivalent to a single axle weighing about 50 percent of the tridem axles and to tandem axles weighing about 80 percent of the tridem axles. Traffic equivalence factors are presented for tridem axles on concrete pavements.

A field program of strain and deflection measurements was conducted by the Construction Technology Laboratories for the Minnesota Department of Transportation (MnDOT). The objective of the measurement program was to evaluate the effect of frozen support, tied-concrete shoulders, and tridem-axle loading on concrete pavement performance. The results of the investigation of the effect of frozen support and tridem axles on concrete pavement performance are presented (1,2). Results of the tied-concrete shoulder study are given elsewhere (3).

Minnesota's current concrete pavement design procedure does not consider climatic effects. When the base, subbase, and subgrade are frozen, pavement strains and deflections due to load are smaller. Therefore, traffic-induced damage during winter months is greatly reduced. Because concrete pavement design procedures consider repeated application of traffic loading and fatigue damage, it should be possible to take advantage of the frozen support conditions in the design of concrete pavements.

Minnesota's current design procedure does not account for the effect of tridem-axle loading on pavements either. Increases in the amount of truck traffic and vehicle gross weight have led to increased need for highway maintenance. To increase trucking productivity and minimize the detrimental effects of heavier axle loading, the trucking industry is rapidly adopting the use of tridem axles in lieu of tandem axles. The rationale behind this concept is that on a gross weight basis, the tridem axles are less damaging to pavements than equally loaded tandem axles.

BACKGROUND

One of the most widely used procedures for thickness design of concrete pavements is the AASHTO Interim Guide for Design of Pavement Structures (4). The AASHTO guide is based on results of the AASHTO Road Test supplemented by existing design procedures and available theory. The AASHTO Road Test site was located about 80 miles southwest of Chicago on right-of-way that is now part of Interstate 80 near Ottawa, Illinois. Test traffic began operation in November 1958 and ended on November 30, 1961. The final axle load count was 1,114,000.

Because MnDOT has adopted the AASHTO procedure as a basis for design of concrete pavements, presentations in this paper will be referenced to the AASHTO design procedure.

Effect of Frozen Support

The AASHTO Road Test design equation for concrete pavements contained in the AASHTO guide does not provide for variations in pavement life that may result from changes in environment and weather as compared with that for the road test location. Although a regional factor is used for design of flexible pavements in the AASHTO guide, no such factor is considered in the design of concrete pavements to account for regional effects.

Effect of Tridem-Axle Loading

Most concrete pavement thickness design procedures consider the effect of mixed truck traffic. Some procedures consider the effect of different axle loads directly, as in the case of the Portland Cement Association design procedure (5). In other procedures, such as that contained in the AASHTO Interim Guide (4), mixed truck traffic is converted to a common denominator, which is an 18-kip single-axle load (SAL).

The AASHTO procedure provides for conversion of mixed traffic to an equivalent number of 18-kip SALs by use of traffic equivalence factors. However, the procedure does not contain traffic equivalence factors for tridem-axle loads nor does it contain any other provisions to consider the effect of tridem-axle loads.

Because of the increasing use of tridem axles by the trucking industry, several agencies have been studying ways to incorporate the effect of tridem-axle loads in their thickness design procedures. A

study was conducted at the Pennsylvania Transportation Research Facility to develop load equivalency factors for tridem-axle loadings on flexible pavements (6). In this study experimental pavements were subjected to approximately 55,000 repetitions of a 76-kip tridem-axle load. Study results were combined with theoretical analysis to develop equivalency factors for a range of tridem-axle loading.

In another study reported by Treybig (7) an attempt was made to relate theoretically computed concrete pavement response parameters to the AASHTO traffic equivalence factors for SALs and tandem-axle loads (TALs). However, no successful correlations were developed.

RESEARCH OBJECTIVES

The study presented in this paper was sponsored by MnDOT to compare measured pavement responses for SALs, TALs, and tridem-axle loads at five pavement sites. Field testing at these sites was conducted during October 1982 and February 1983. In this report results of field testing, analysis of results, and recommendations to incorporate study results in Minnesota's thickness design procedure for concrete pavements are presented.

Objectives of the study were as follows:

1. To measure load-induced strains and deflections in pavement sections during fall and winter periods,
2. To analyze test results to establish the effects of frozen support on concrete pavement performance, and
3. To analyze test results to establish the effects of tridem-axle loading on concrete pavement performance.

PAVEMENT TEST SECTIONS

Field measurements were obtained at five pavement project sites in Minnesota. Projects 1, 2, and 3 were included in a 1976 field study on concrete shoulders and lane widening (8). A brief description of each project follows:

Project 1: Designation State Project 2280-30 (TH-90) is a roadway 27 ft wide consisting of an inside lane 15 ft wide and an outside lane 12 ft wide with an outside tied keyed concrete shoulder 10 ft wide. Shoulders are tied at 30-in. spacing by using 30-in.-long No. 5 tie bars. Shoulder thickness is 6 in. The pavement is plain concrete slabs 9 in. thick with skewed joints at a repeated random spacing of 13, 16, 14, and 19 ft. Subgrade at the site was classified as silty clay to clay loam and had a gravel subbase 5 in. thick over it. Dowel bars were placed only in the 12-ft-wide outside traffic lane. Dowels are No. 8 round bars, spaced at 12 in. on centers; the first dowel is located 6 in. inward from the pavement edge. Panels selected for test are located at stations 538+65 and 540+10.

Project 2: Designation State Project 2280-30 (TH-90) is a roadway 27 ft wide and an outside tied keyed concrete shoulder 10 ft wide. Dowel size and location are the same as those for project 1. Pavement thickness is 8 in. Subgrade at the site was classified as silty clay to clay loam and had a gravel subbase 6 in. thick over it. The modulus of subgrade reaction was reported to be 270 pci. Panels selected for test are located at stations 520+55 and 521+81.

Project 3: Designation State Project 2280-31 (TH-90) is a roadway 27 ft wide with an inside lane 15 ft wide and an outside lane 12 ft wide. The pavement is reinforced concrete slabs 9 in. thick with skewed joints at a spacing of 27 ft. Subgrade at the site was classified as clay loam to silty clay loam to sandy clay loam. A gravel subbase 5 in. thick was used. Dowel bars were placed only in the 12-ft main-line pavement portion of both traffic lanes. Dowels are No. 8 round bars, spaced 12 in. on centers. Panels selected for test are located at stations 985+53 and 987+11.

Project 4: Designation State Project 4680-27 (TH-90) is a roadway 24 ft wide with a 12-ft inside and a 12-ft outside lane. The pavement is reinforced concrete slabs 9 in. thick with skewed joints at a spacing of 27 ft. Subgrade at the site was clay loam with an AASHTO classification of A-6. Modulus of subgrade reaction was reported to be 300 pci. A gravel subbase 6 in. thick was used. Dowel bars were placed in both the outside and inside lanes. Dowels are No. 8 round bars, spaced 12 in. on centers. Panels selected for test are located at stations 1329+52 and 1330+59.

Project 5: Designation State Project 7380-53 and 8680-57 (TH-94) is a roadway 24 ft wide with a 12-ft-wide inside lane and 12-ft-wide outside lane. The pavement is reinforced concrete slabs 9 in. thick with skewed joints at a spacing of 27 ft. Subgrade at the site was coarse sand with an AASHTO classification of A-1-b. Modulus of subgrade reaction was reported to be 700 pci. A gravel subbase 5 in. thick was used. Dowel bars were placed in both the outside and inside lanes. Dowels are No. 8 round bars, spaced 12 in. on centers. Panels selected for test are located at stations 507+93 and 509+28.

Projects 1, 2, 3, and 4 are located on I-90 between Albert Lea and Fairmont, Minnesota. Project 5 is located on I-94 near Clearwater, Minnesota.

Two test sites were selected at each project. At each site, both inside and outside lanes were instrumented and monitored to evaluate pavement response. At some of the sites for projects 1, 2, and 3, the panels tested in 1976 were retested. Care was taken to assure that the sites selected were representative of the project.

INSTRUMENTATION

All pavement test sections were instrumented to measure load-induced strains and deflections. In addition pavement temperature and slab curl were monitored. Curl is a change in the vertical profile of the slab resulting from changes in the slab temperature.

Strain gage and deflectometer locations for projects 1 and 2 test sections are shown in Figure 1. Instrumentation locations were similar for projects 3, 4, and 5. These locations were selected to obtain the maximum values of strain and deflection for the different load positions. Curl measurements were made at deflectometer locations. Concrete temperatures were measured in instrumented test blocks placed in the subbase adjacent to the pavement.

Load Strains

Concrete strains were measured with electrical-resistance strain gages 4 in. long cemented to the pavement surface. Gages were placed at the free edge, shoulder edge, transverse joints, and joint corners and in the interior. Gage positions and loading locations shown in Figure 1 are referred to

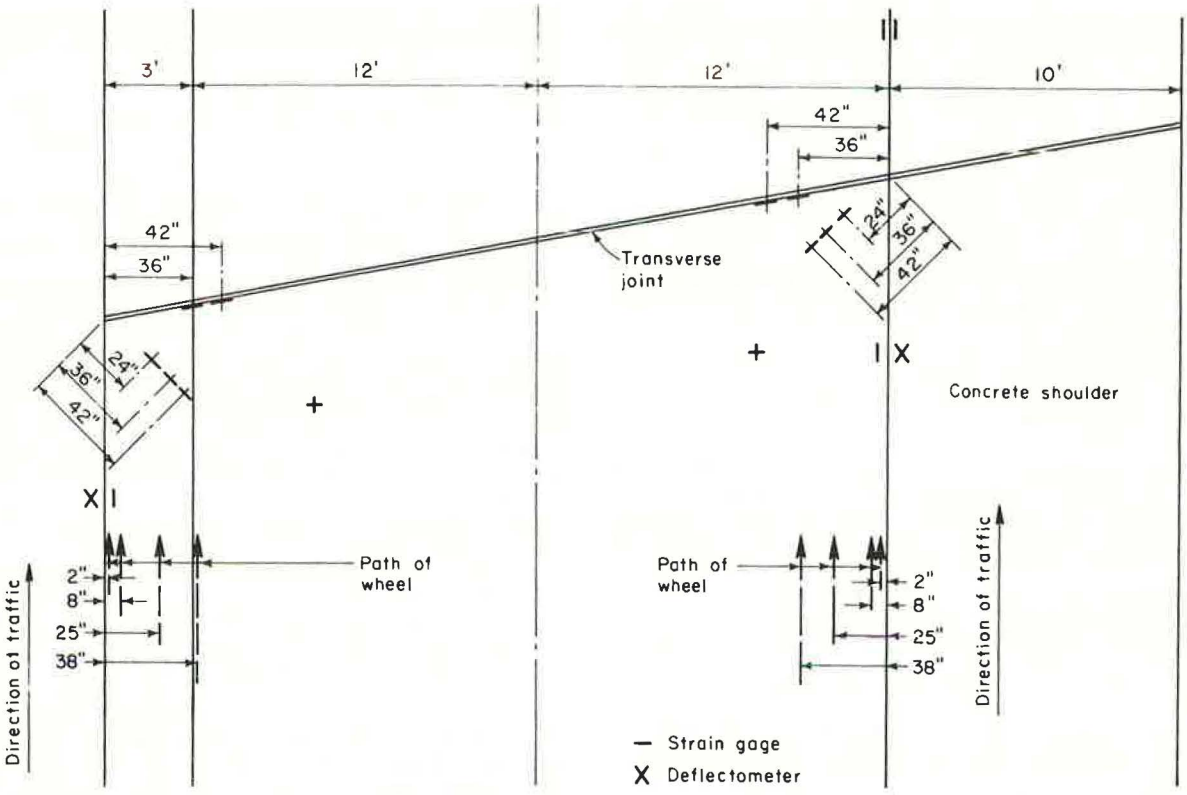

FIGURE 1 Instrumentation layout for projects 1 and 2.

in subsequent discussions. All gages were placed in recessed grooves to protect them from direct application of wheel loads.

Load Deflections

Load deflections were measured with resistance-bridge deflectometers bolted to the pavement. Readings were referenced to encased rods driven into the subgrade to a depth of 6 ft. Construction details of the deflectometer are presented in Research and Development Bulletin D83 (9) of the Portland Cement Association.

Curl Measurements

Pavement curl was measured with 0.001-in. indicators placed at the same locations as the deflectometers. The dial indicators were bolted to the pavement and the movement was referenced to encased rods placed in the subgrade. Curl readings were taken approximately once an hour.

Temperature Measurements

Changes in pavement temperature were measured with copper-constantan thermocouples embedded in concrete blocks. The laboratory-cast blocks were 1 ft square and 8 or 9 in. thick. Thermocouples were located 0.125, 0.50, 1, 2, 4, and 6 in. from the top and 0.125 in. from the bottom surfaces. Temperature blocks were placed in the subbase adjacent to the highway at least 12 hr before testing. Air temperature was monitored with a thermocouple shaded from the direct sun.

Monitoring Equipment

Data were monitored and recorded with equipment carried in the Construction Technology Laboratories' field instrumentation van. Strain and deflection data were recorded with a high-speed computer-based data acquisition system. Twenty-two channels of instrumentation were monitored and recorded simultaneously for each vehicle loading. Computer programs were written to monitor, record, and tabulate all field data. Temperature data were recorded with a 24-channel continuously monitoring temperature recorder. All monitoring and recording instrumentation was calibrated before testing.

TEST PROCEDURES

Strain and deflection data were recorded for 20-kip SALs, 34-kip and 42-kip TALs, and 42-kip tridem-axle loads. Loading was applied with the two semitrailers shown in Figure 2. One truck applied the 20-kip SALs and 34-kip TALs. The other truck applied the 42-kip TALs and 42-kip tridem-axle loadings. Trucks used were supplied by MnDOT. Before testing, axle weights were checked and loads were adjusted to obtain uniform distribution to the wheels.

The effects of axle weight and load location on strains and deflections were recorded with the trucks moving at creep speed along the wheel paths shown in Figure 1. Tire placements varied from 2 to 38 in. from the pavement edge. All wheel-path measurements were from the pavement edge to the outside edge of the tire sidewall at its maximum width. In addition, pavement curl and temperature data were obtained periodically during the day.

Inside- and outside-lane test slabs at each project site were tested on the same day. Primary read-

FIGURE 2 Trucks used: 18-kip SAL and 34-kip TAL (top), 42-kip TAL and 42-kip tridem-axle load (bottom).

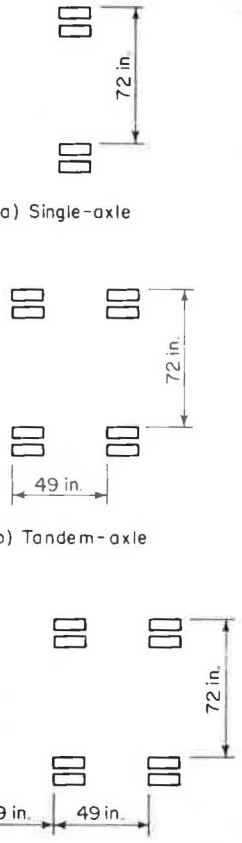

FIGURE 3 Axle configurations.

ings were taken on both inside and outside lanes between approximately 11:30 a.m. and 2:00 p.m. In addition, readings were also taken on one lane before 11:30 a.m. and on the other lane after 2:00 p.m. Specific testing times were governed primarily by weather and traffic control requirements.

DATA ANALYSIS

In this section a comparison is presented of pavement responses measured under 20-kip SALs, 34-kip and 42-kip TALs, and 42-kip tridem-axle loadings during October 1982 and February 1983. Pavement responses compared are edge and corner deflections and edge strains. In addition, results of theoretical analysis are also presented to compare pavement responses under the four different axle loads. Wheel configurations and spacings for the four axle loads used during the field testing correspond to those shown in Figure 3.

Curling and Warping Effects

Soon after concrete has been placed, drying shrinkage of the concrete begins. Drying shrinkage in a slab on grade occurs at a faster rate at the slab surface than at the slab bottom. In addition, because the subgrade and subbase may remain wet, the slab bottom remains relatively moist. Thus, total shrinkage at the bottom is less than that at the top. This differential in shrinkage results in a lifting of the slab from the subbase at edges and corners. Movements of this type resulting from moisture differentials are referred to as warping. Warping leaves slabs unsupported for distances of as much as 4 to 5 ft at slab corners and 2 to 3 ft at slab edges. Warping is almost never recoverable.

In addition to warping, a slab on grade is also subjected to curling. Curling is the change in the slab profile due to temperature differential between slab top and bottom. Curling is a daily phenomenon. Slabs curl up during the night and curl down during the midday. Thus, curling deformation is additive to warping during the night and reduces the warping effect during the midday. It is believed by many engineers that the warping effect is almost never cancelled out by daytime curling and that some loss of support always exists under the slab even for hot days.

Because of curling effects, the measured deflections under load along a slab edge or a slab corner are greatly affected by the time of testing. Measured slab strains are also affected by time of testing but at a lower level. Therefore, great care needs to be exercised in interpreting deflection and strain measurements if they are made at different times of a day or on different days. The usual procedure in reporting deflection measurements at a given location is to correct the measurements with respect to a reference time. The reference time is generally selected to be the time when the slab top and bottom temperatures are equal.

As discussed, temperature and curl measurements were made at each of the five test sites considered in this study. At each test site, pavement responses under load were generally measured at two different times, usually within a span of 3 hr around noon.

Figure 4 shows the variation with time of the air temperature, corner curl, and corner deflection under a 20-kip SAL at each of the five sites.

It is seen that although slabs at each site exhibit pronounced curling, the deflections under load were not greatly influenced by the time of testing between approximately 11:00 a.m. and 2:00 p.m. Similar trends were obtained for edge curl and deflections and edge strain. This is because the slabs have curled to their most downward profiles and change from these profiles is gradual with respect to time, as shown in Figure 4. Therefore, no temperature corrections were applied to these readings. The measurements reported in this paper are the averages of the readings for the two test times and correspond to the period when each slab being tested was near its maximum downward curl.

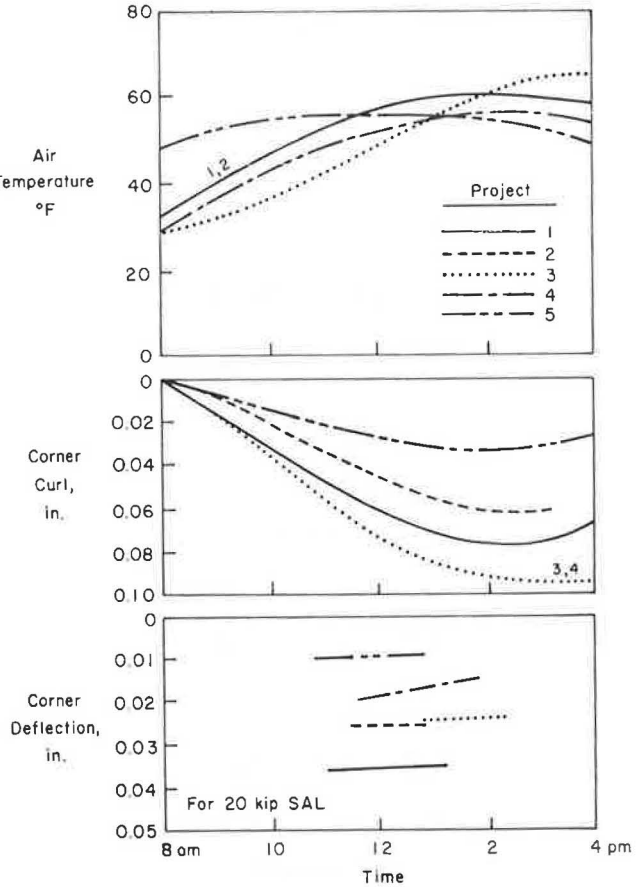

FIGURE 4 Variation of air temperature, corner curl, and deflection with time.

Summary of Data

Load tests were conducted during October 1982 when air temperatures at midday were about 55°F and during February 1983 when air temperatures at midday were about 20 to 30°F.

Pavement response measured at each of the five sites is given in Table 1. Edge and corner deflections and edge strains measured during October 1982 and February 1983 at inside and outside lanes for each of the four axle loadings are listed. Each data point is an average of four readings made up of data taken at two different times at each of the two replicate sections at each project location.

EFFECT OF FROZEN SUPPORT

This section considers the effect of frozen support on concrete pavement performance. The February measurements are shown as a percentage of the October measurements in Figures 5, 6, and 7 for edge deflection, corner deflection, and edge strain, respectively. (Axles are defined as follows in Figures 5-7: axle 1, 20-kip SAL; axle 2, 34-kip TAL; axle 3, 42-kip TAL; axle 4, 42-kip tridem-axle load. Lane I is the inside lane; lane O the outside lane. N denotes lack of reliable data.)

Measured Edge Deflections

As shown in Figure 5, edge deflections measured during February generally ranged from 15 to 25 percent of edge deflections measured during October. Under the 20-kip SAL, edge deflections ranged from 0.007 in. at project 5 to 0.021 in. at project 1 during October and from 0.001 in. at project 5 to 0.004 in. at project 1 during February.

It should be noted that at project 2, edge deflections measured along the outside lane do not show any variation with different axle loads. This is believed to be because of malfunctioning of the deflectometers at this location.

Measured Corner Deflections

As shown in Figure 6, corner deflections measured during February generally ranged from 5 to 15 percent of corner deflections measured during October. Under the 20-kip SAL, corner deflections ranged from 0.010 in. at project 5 to 0.035 in. at project 1 during October and from 0.001 in. at Project 5 to 0.004 in. at project 1 during February.

Measured Edge Strains

As shown in Figure 7, edge strains measured during February generally ranged from 20 to 60 percent of edge strains measured during October. Under the 20-kip SAL, edge strains ranged from 19×10^{-6} at the inside lane of project 5 to 35×10^{-6} at the inside lane of project 1 during October. Edge strains under the 20-kip SAL ranged from 9×10^{-6} at the inside lane of project 5 to 18×10^{-6} at the inside lane of project 1 during February.

Theoretical Considerations

Analysis was conducted to determine the effect of the subbase and subgrade support on pavement response. A finite-element program, JSLAB, developed by Construction Technology Laboratories for FHWA was used (10). The program can analyze a large number of jointed slabs. Joints can be modeled as doweled, aggregate interlock, or keyed. Load input is in terms of wheel loads at any location on the slabs. Loss of support, variable support, or material properties can be considered. In the program subbase and subgrade support is characterized by the modulus of subgrade support. Thus, the effect of a frozen support can be considered by using a high value for the modulus of subgrade reaction.

The analysis was conducted for a concrete pavement 9 in. thick with and without a tied shoulder and with dowel bars at transverse joints. For the case of a tied shoulder, a slab 6 in. thick was used. Values used for the modulus of subgrade reaction were 100, 150, 250, 1,000, and 2,000 pci. Calculated corner deflections, edge deflections, and edge stresses are listed in Tables 2-4. For both corner and edge loadings, tire placements were 2 in. inward from the edge.

The calculations verify that although a stiffer subbase and subgrade support will produce a large reduction in slab deflections, the corresponding decrease in slab edge stresses is not so large. For example, edge deflection for a support value of 2,000 pci is reduced to about 25 to 35 percent of that for a support value of 250 pci. However, edge stress for a support value of 2,000 pci is reduced to only about 50 to 70 percent of that for a support value of 250 pci. These calculations and field measurements indicate that during winter months, the support value under a concrete pavement can be expected to exceed 1,000 pci. For this condition, edge

TABLE 1 Measured Pavement Response at Projects 1 Through 5

Parameter	20-kip SAL		34-kip TAL		42-kip TAL		42-kip Tridem-Axle Load	
	Fall	Winter	Fall	Winter	Fall	Winter	Fall	Winter
Project 1								
Inside lane								
Edge deflection (in.)	0.021	0.004	0.034	0.006	0.038	0.008	0.034	0.007
Corner deflection (in.)	0.035	0.004	0.044	0.006	0.051	0.007	0.044	0.006
Edge strain (x 10^{-6})	35	18	30	23	32	17	17	10
Outside lane								
Edge deflection (in.)	0.019	0.004	0.026	0.006	0.029	0.007	0.027	0.007
Corner deflection (in.)	0.030	0.003	0.034	0.005	0.037	0.005	0.031	0.005
Edge strain (x 10^{-6})	30	18	24	18	27	14	19	12
Project 2								
Inside lane								
Edge deflection (in.)	0.016	0.003	0.026	0.004	0.027	0.005	0.023	0.005
Corner deflection (in.)	0.026	0.002	0.036	0.004	0.034	0.004	0.030	0.004
Edge strain (x 10^{-6})	35	12	32	13	33	17	18	9
Outside lane								
Edge deflection (in.)	0.007	0.002	0.007	0.003	0.007	0.003	0.009	0.003
Corner deflection (in.)	0.021	0.003	0.021	0.004	0.025	0.003	0.019	0.002
Edge strain (x 10^{-6})	33	11	31	9	38	9	20	5
Project 3								
Inside lane								
Edge deflection (in.)	0.013	0.002	0.022	0.004	0.025	0.004	0.020	0.004
Corner deflection (in.)	0.024	0.002	0.030	0.003	0.032	0.003	0.026	0.003
Edge strain (x 10^{-6})	33	–	28	–	30	–	18	–
Outside lane								
Edge deflection (in.)	0.015	0.003	0.021	0.003	0.025	0.004	0.023	0.004
Corner deflection (in.)	0.036	0.002	0.040	0.002	0.040	0.002	0.034	0.002
Edge strain (x 10^{-6})	18	–	23	–	24	–	16	–
Project 4								
Inside lane								
Edge deflection (in.)	0.013	0.002	0.020	0.002	0.020	0.002	0.018	0.002
Corner deflection (in.)	0.017	0.002	0.022	0.002	0.024	0.002	0.019	0.001
Edge strain (x 10^{-6})	31	13	27	13	27	–	17	–
Outside lane								
Edge deflection (in.)	0.013	0.002	0.018	0.002	0.021	0.002	0.019	0.002
Corner deflection (in.)	0.022	0.002	0.026	0.002	0.027	0.002	0.024	0.001
Edge strain (x 10^{-6})	–	13	–	13	–	–	–	–
Project 5								
Inside lane								
Edge deflection (in.)	0.007	0.001	0.010	0.002	0.009	0.002	0.007	0.002
Corner deflection (in.)	0.010	0.001	0.011	0.001	0.010	0.002	0.008	0.002
Edge strain (x 10^{-6})	19	9	19	10	20	3	14	–
Outside lane								
Edge deflection (in.)	0.007	0.002	0.008	0.002	0.008	0.002	0.007	0.002
Corner deflection (in.)	0.013	0.002	0.013	0.003	0.012	0.002	0.010	0.003
Edge strain (x 10^{-6})	31	14	23	12	26	6	17	2

Note: Inside-lane measurements were taken along the edge of the 3-ft lane widening. Outside-lane measurements were taken along the joint with tied shoulder. Fall measurements were obtained during October 1982; winter measurements were obtained during February 1983.

and corner deflections for a 34-kip TAL would be less than 0.004 in. and edge stresses for a 20-kip SAL would be less than 150 psi.

It should be noted that deflection values measured during October were much higher than calculated deflection values, even when a modulus of subgrade reaction of 150 pci was used. Modulus of subgrade reaction values at the five locations were reported to be in excess of 250 pci. The reason for the anomaly in measured and computed deflection values is that the theoretical analysis was conducted for the case of full support under the pavement slabs. In practice, there is always some loss of support along slab edges. This support loss results in higher measured slab deflections.

Analysis of Results

As indicated, it is clear that concrete pavement responses for the case of frozen support were much smaller compared with those obtained when the support was not frozen. The greatly improved deflection response is considered to be caused by the frozen subgrade and subbase and also a lower level of slab warping. Slab warping is lower during winter months because of the higher moisture content at the surface of the concrete slab. The effect of less slab warping is less loss of support along slab edges. From the field testing conducted at the five project locations, the following values indicate the improvement in pavement response during February as

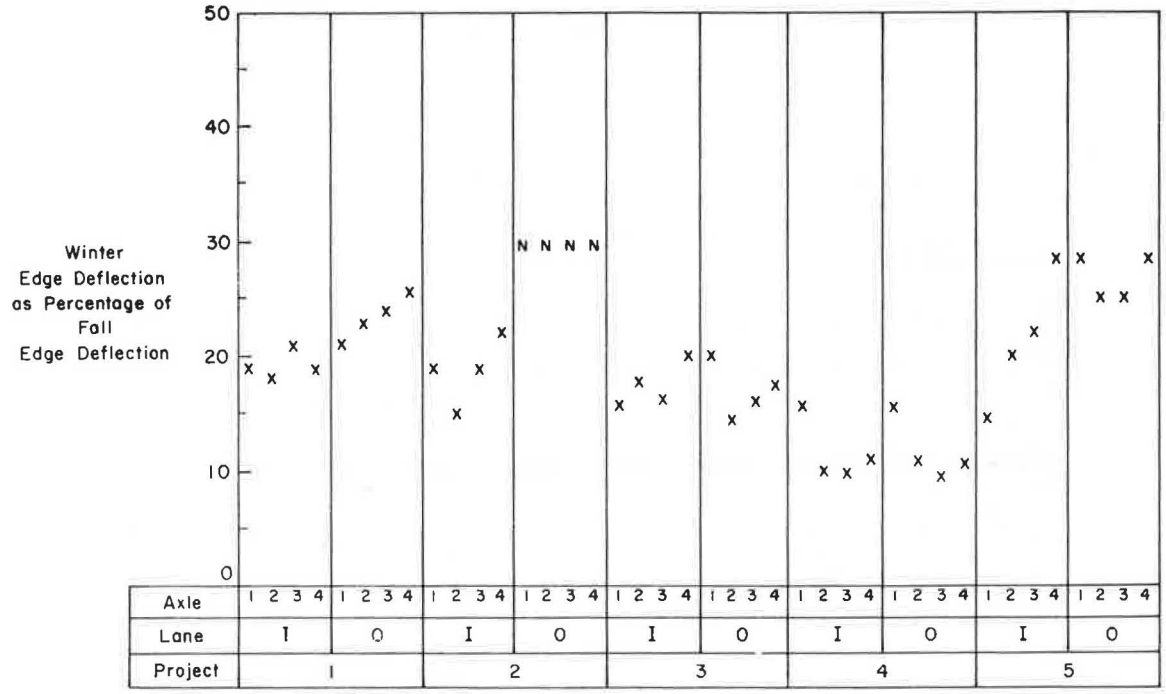

FIGURE 5 Comparison of winter and fall edge deflections.

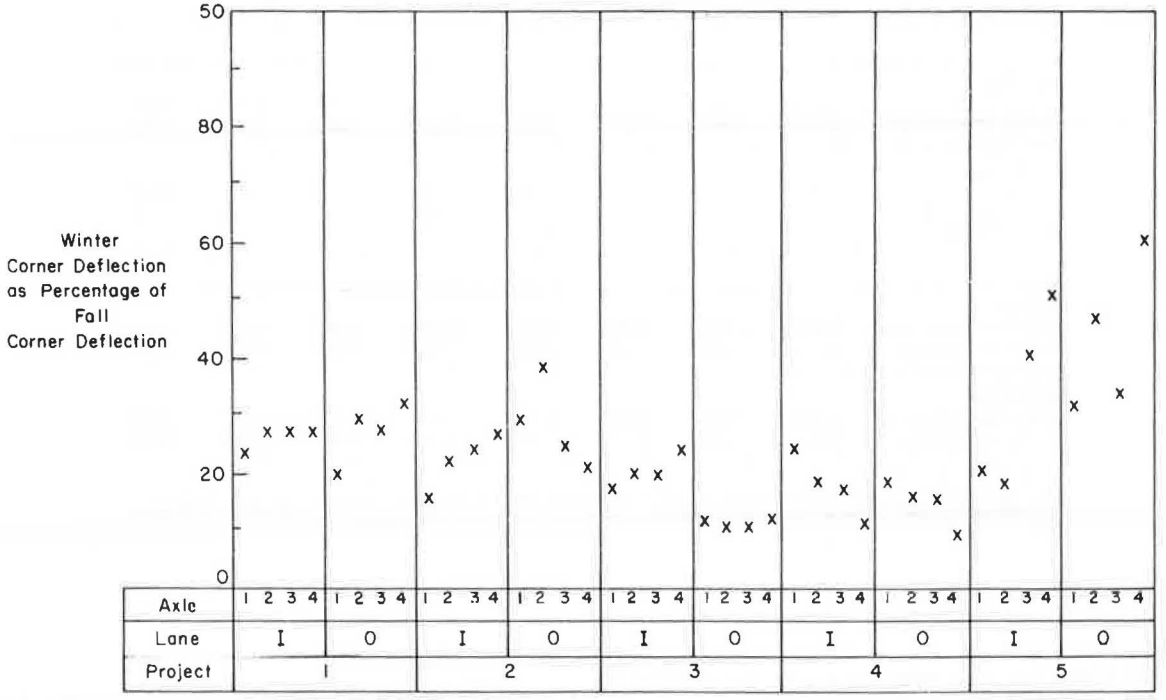

FIGURE 6 Comparison of winter and fall corner deflections.

compared with that in October (A = value calculated for k of 2,000 pci as percentage of value for k of 250 pci; B = measured value during February as percentage of October measurement):

A (%)	Pavement Response	B (%)
25-30	Corner deflection	15
25-35	Edge deflection	25
50-70	Edge stress	60

For consideration of the effects of frozen support in the thickness design for concrete pavements, it is recommended that 60 percent be used as the maximum level of improvement in pavement response from fall to winter. This recognizes that deflections as well as stresses are important in assessing pavement performance.

Because pavement damage or loss in serviceability is a function of axle load magnitude and number of load repetitions, it can be concluded that a given

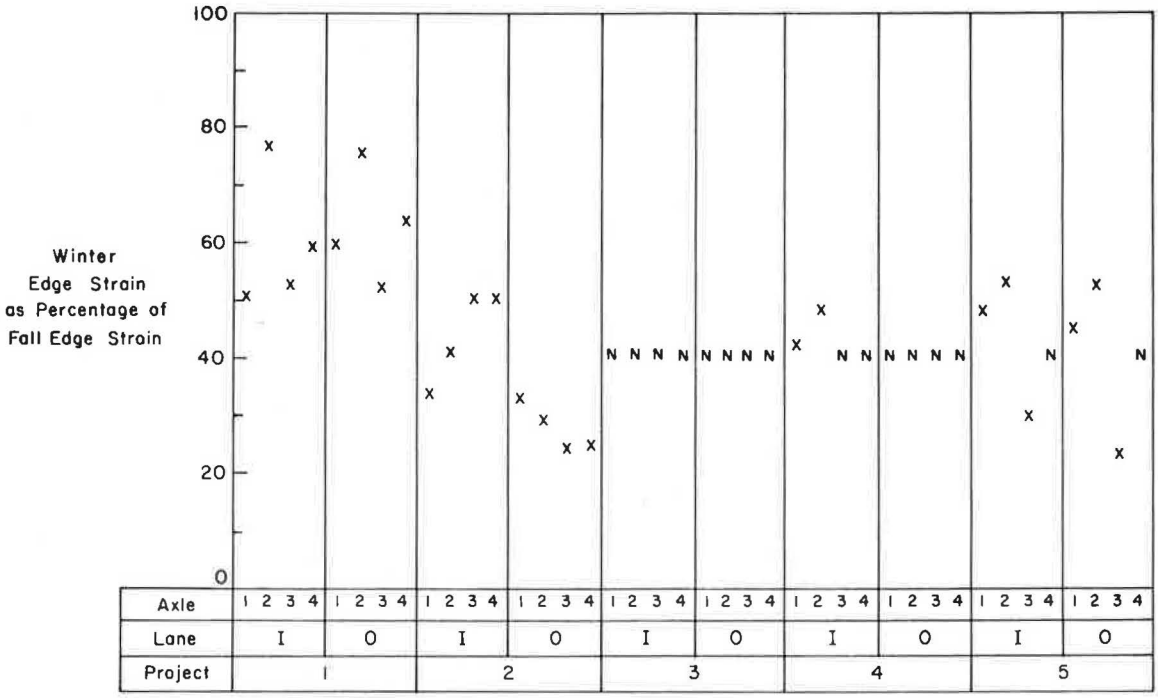

FIGURE 7 Comparison of winter and fall edge strains.

TABLE 2 Calculated Pavement Response: Corner Deflection

Shoulder Type	k (pci)	Corner Deflection (in.) 20-kip SAL	34-kip TAL	42-kip TAL	42-kip Tridem-Axle Load
Tied	100	0.025	0.026	0.032	0.026
	150	0.018	0.019	0.023	0.019
	250	0.013	0.013	0.016	0.012
	1,000	0.006	0.005	0.006	0.004
	2,000	0.004	0.004	0.004	0.003
None	100	0.035	0.040	0.050	0.040
	150	0.026	0.030	0.037	0.028
	250	0.019	0.020	0.025	0.019
	1,000	0.008	0.007	0.009	0.007

TABLE 3 Calculated Pavement Response: Edge Deflection

Shoulder Type	k (pci)	Edge Deflection (in.) 20-kip SAL	34-kip TAL	42-kip TAL	42-kip Tridem-Axle Load
Tied	100	0.015	0.022	0.027	0.022
	150	0.012	0.016	0.020	0.016
	250	0.008	0.011	0.014	0.011
	1,000	0.004	0.004	0.005	0.004
	2,000	0.003	0.003	0.004	0.003
None	100	0.024	0.035	0.043	0.036
	150	0.018	0.025	0.031	0.026
	250	0.012	0.017	0.021	0.017
	1,000	0.005	0.006	0.007	0.005

axle load would produce less damage or loss of serviceability during the winter as compared with that in the fall. If a linear relationship is assumed between magnitude of axle load and pavement response, an axle load (P) applied during the winter is equivalent to an axle load (0.6P) applied during the fall.

TABLE 4 Calculated Pavement Response: Edge Stress

Shoulder Type	k (pci)	Edge Stress (psi) 20-kip SAL	34-kip TAL	42-kip TAL	42-kip Tridem-Axle Load
Tied	100	236	180	222	114
	150	218	160	198	98
	250	199	139	172	81
	1,000	157	102	126	55
	2,000	138	85	103	42
None	100	286	230	284	152
	150	263	203	250	128
	250	236	172	212	103
	1,000	178	116	143	63

Application to AASHTO Design Procedure

The AASHTO Interim Guide uses the concept of traffic equivalence factors for converting mixed traffic to an equivalent number of 18-kip SALs. The equivalence factors, when multiplied by the number of axle loads within a given weight category, give the number of 18-kip SALs that have an equivalent effect on the performance of the pavement.

Traffic equivalence factors for concrete pavements are given in Table 5 for SALs and TALs. It may be seen that for a pavement 9 in. thick, a 30-kip SAL is 8.28 times as damaging as an 18-kip SAL. However, based on measured pavement response, a 30-kip SAL applied during a winter month can be considered to be only as damaging as an 18-kip SAL applied during the fall. Thus, a 30-kip SAL applied during the winter months is only 1/8.28, that is, 0.12 times as damaging as a 30-kip SAL applied during the fall. Applying this logic to different slab thicknesses and other axle loads, it is found that the damaging effect of a given SAL or TAL applied in the winter is about one-seventh to one-ninth of that for the same axle load applied during the fall.

For design purposes it is recommended that the

TABLE 5 Traffic Equivalence Factors for Single and Tandem Axles

Axle Load		Slab Thickness D (in.)						
Kips	kN	6	7	8	9	10	11	12
Single Axle								
2	8.9	0.0002	0.0002	0.0002	0.0002	0.0002	0.0002	0.0002
4	17.8	0.003	0.002	0.002	0.002	0.002	0.002	0.002
6	26.7	0.01	0.01	0.01	0.01	0.01	0.01	0.01
8	35.6	0.04	0.04	0.03	0.03	0.03	0.03	0.03
10	44.5	0.10	0.09	0.08	0.08	0.08	0.08	0.08
12	53.4	0.20	0.19	0.18	0.18	0.18	0.17	0.17
14	62.3	0.38	0.36	0.35	0.34	0.34	0.34	0.34
16	71.2	0.63	0.62	0.61	0.60	0.60	0.60	0.60
18	80.1	1.00	1.00	1.00	1.00	1.00	1.00	1.00
20	89.0	1.51	1.52	1.55	1.57	1.58	1.58	1.59
22	97.9	2.21	2.20	2.28	2.34	2.38	2.40	2.41
24	106.8	3.16	3.10	3.23	3.36	3.45	3.50	3.53
26	115.7	4.41	4.26	4.42	4.67	4.85	4.95	5.01
28	124.6	6.05	5.76	5.92	6.29	6.61	6.81	6.92
30	133.4	8.16	7.67	7.79	8.28	8.79	9.14	9.34
32	142.3	10.81	10.06	10.10	10.70	11.43	11.99	12.35
34	151.2	14.12	13.04	12.34	13.62	14.59	15.43	16.01
36	160.1	18.20	16.69	16.41	17.12	18.33	19.52	20.39
38	169.0	23.15	21.14	20.61	21.31	22.74	24.31	25.58
40	177.9	29.11	26.49	25.65	26.29	27.91	29.90	31.64
Tandem Axles								
10	44.5	0.01	0.01	0.01	0.01	0.01	0.01	0.01
12	53.4	0.03	0.03	0.03	0.03	0.03	0.03	0.03
14	62.3	0.06	0.05	0.05	0.05	0.05	0.05	0.05
16	71.2	0.10	0.09	0.08	0.08	0.08	0.08	0.08
18	80.1	0.16	0.14	0.14	0.13	0.13	0.13	0.13
20	89.0	0.23	0.22	0.21	0.21	0.20	0.20	0.20
22	97.9	0.34	0.32	0.31	0.31	0.30	0.30	0.30
24	106.8	0.48	0.46	0.45	0.44	0.44	0.44	0.44
26	115.7	0.64	0.64	0.63	0.62	0.62	0.62	0.62
28	124.6	0.85	0.85	0.85	0.85	0.85	0.85	0.85
30	133.4	1.11	1.12	1.13	1.14	1.14	1.14	1.14
32	142.3	1.43	1.44	1.47	1.49	1.50	1.51	1.51
34	151.2	1.82	1.82	1.87	1.92	1.95	1.96	1.97
36	160.1	2.29	2.27	2.35	2.43	2.48	2.51	2.52
38	169.0	2.85	2.80	2.91	3.04	3.12	3.16	3.18
40	177.9	3.52	3.42	3.55	3.74	3.87	3.94	3.98
42	186.8	4.32	4.16	4.30	4.55	4.74	4.86	4.91
44	195.7	5.26	5.01	5.16	5.48	5.75	5.92	6.01
46	204.6	6.36	6.01	6.14	6.53	6.90	7.14	7.28
48	213.5	7.64	7.16	7.27	7.73	8.21	8.55	8.75

Note: Terminal pavement serviceability index (p_t) = 2.5.

damaging effect of an axle load applied during the winter be considered to be one-seventh of that for the same axle load applied during the fall. Thus, only one-seventh of the equivalent 18-kip SALs applied during the winter months needs to be considered for thickness design. If traffic is considered to be uniformly distributed over the 12-month period and if only one-seventh of the winter period traffic is considered applicable, only 79 percent of the total design value of the equivalent 18-kip SALs needs to be considered for thickness design.

However, it should be noted that the current AASHTO design procedure already has built into it the effect of frozen support, because the AASHTO Road Test was conducted over a period of two winters. Study results presented in this report can be implemented into the AASHTO design procedure if the difference in severity and duration of winter conditions between Ottawa, Illinois, and the state of Minnesota can be established.

Application to Other Design Procedures

Results of this study have direct application to design procedures that are based on considerations of stresses or deflections or both under each axle-load group of mixed traffic. For example, the Portland Cement Association thickness design for concrete pavements is based on fatigue consumed under mixed traffic (7). In this procedure fatigue consumption is computed for each axle-load group and summed to determine total fatigue consumption during the design period.

To apply study results to such a procedure, fatigue consumption would be determined separately for winter periods and for nonwinter periods. For nonwinter periods the conventional procedure would be used. For winter periods fatigue consumption computation would incorporate use of a stiff support.

EFFECT OF TRIDEM-AXLE LOADING

In this section the effect of tridem-axle loading is considered. Although measurements were obtained during October 1982 and February 1983, only the October 1982 measurements are discussed in this section. Because of the frozen support, measured deflections during February 1983 were low for each axle type. The measurements listed in Table 1 for October 1982 are shown as a percentage of the 42-kip tridem-axle load measurements in Figures 8, 9, and 10 for edge deflection, corner deflection, and edge strain, respectively. (Axles are defined as follows in Figures 8-10: axle 1, 20-kip SAL; axle 2, 34-kip TAL; axle 3, 42-kip TAL; axle 4, 42-kip tridem-axle load. Lane I is the inside lane; lane O, the outside lane. N denotes lack of reliable data.)

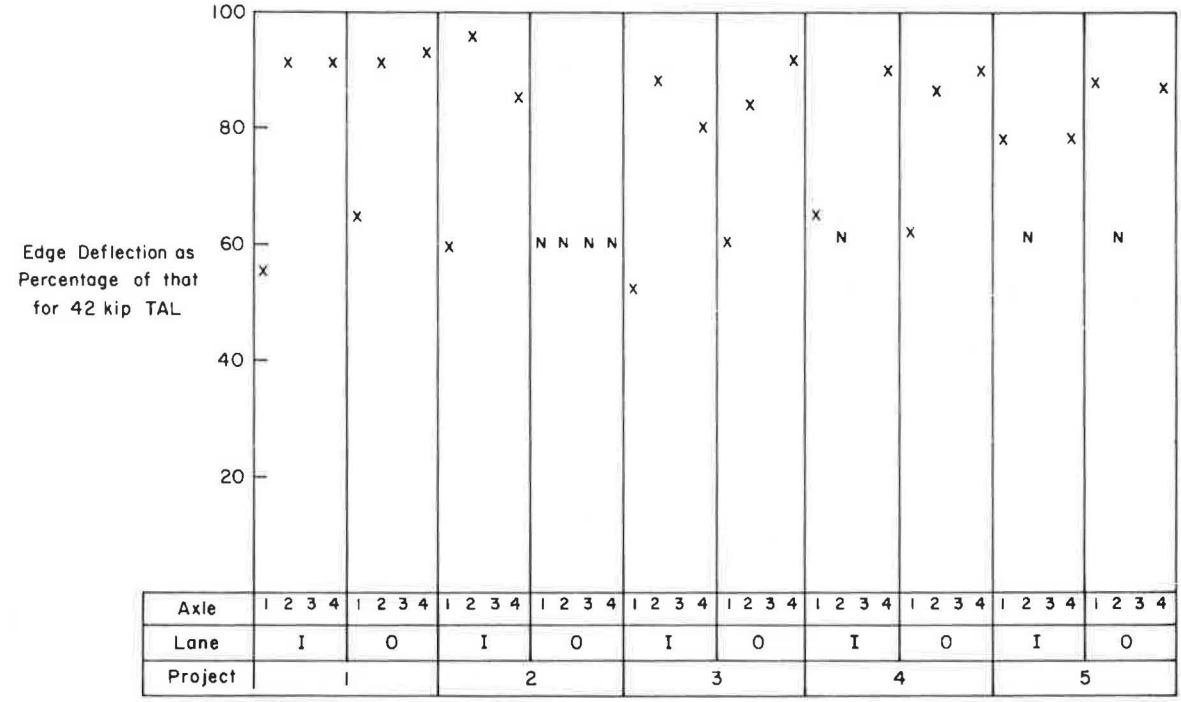

FIGURE 8 Edge deflections as percentage of those for 42-kip TAL.

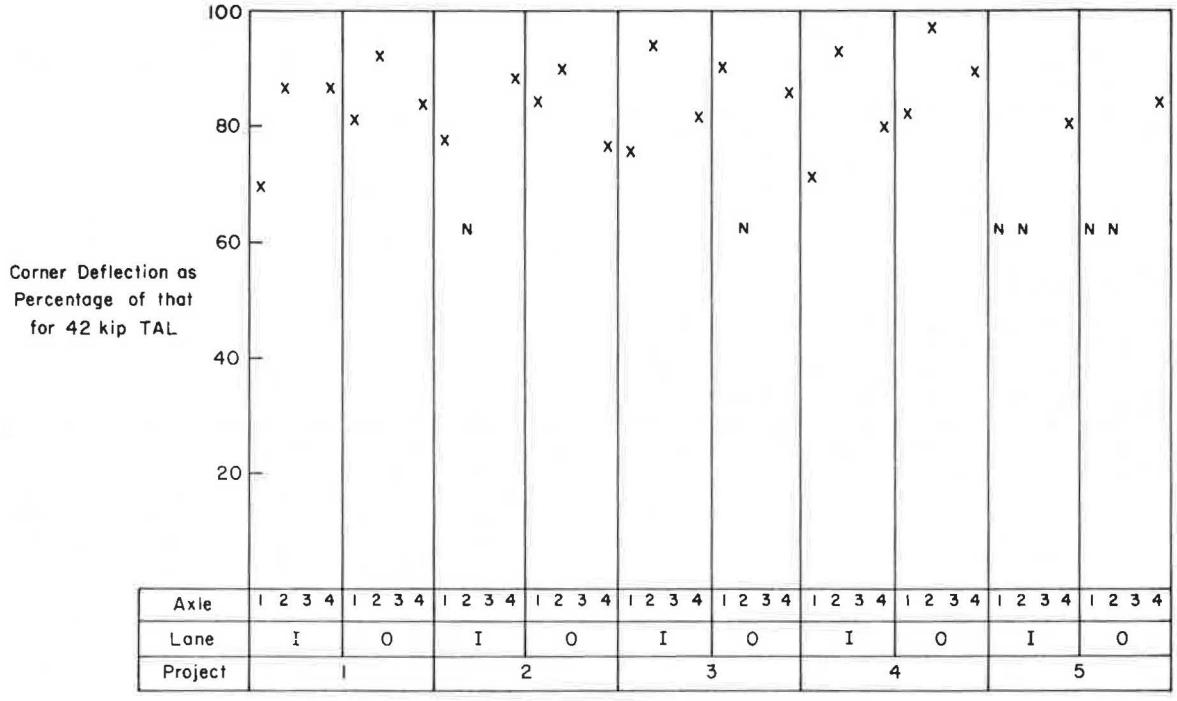

FIGURE 9 Corner deflections as percentage of those for 42-kip TAL.

Measured Edge Deflections

As shown in Figure 8, edge deflections measured during the fall period under the 42-kip tridem-axle loads ranged from 78 to 93 percent of those for the 42-kip TALs. At 7 of the 10 sections, edge deflections under the tridem-axle loads were less than 90 percent of those under the 42-kip TALs. As a comparison, the 34-kip TALs produced edge deflections between 84 to 96 percent of those for the 42-kip TALs. Theoretically, the 34-kip TALs should produce edge deflections about 80 percent of those produced under the 42-kip TALs.

It should be noted that at project 2, edge deflections measured along the outside lane do not show any variation with different axle loads. This is believed to be because of malfunctioning of the deflectometers at this location.

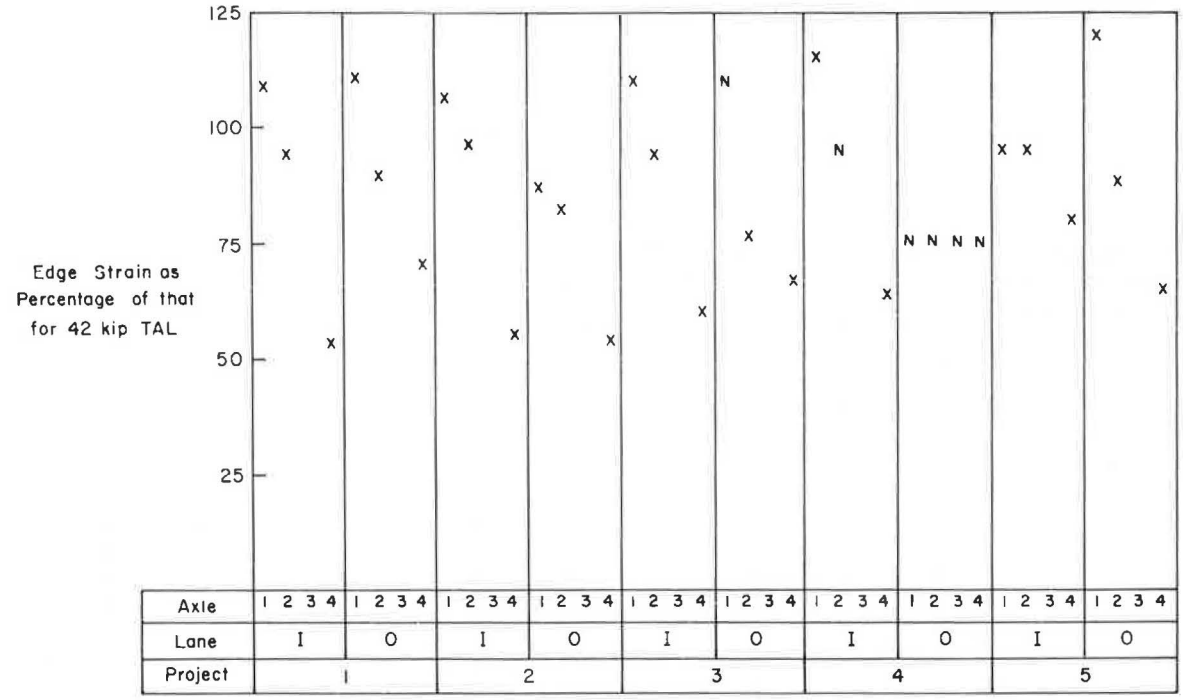

FIGURE 10 Edge strains as percentage of those for 42-kip TAL.

Measured Corner Deflections

As shown in Figure 9, corner deflections measured during the fall period under the 42-kip TALs ranged from 76 to 90 percent of those for the 42-kip TALs. The 34-kip TALs produced corner deflections between 86 and 96 percent of those for the 42-kip TALs. As in the case of edge deflections, theoretically the 34-kip TALs should produce corner deflections about 80 percent of those produced under the 42-kip TALs.

Measured Edge Strains

As shown in Figure 10, edge strains measured during the fall period under the 42-kip tridem-axle loads ranged from 53 to 69 percent of those for the 42-kip TALs. The 34-kip TALs produced edge strains between 82 and 97 percent of those for the 42-kip TALs. Theoretically, edge strain for the 34-kip TALs should be about 80 percent of those for the 42-kip TALs.

Theoretical Considerations

Calculated pavement responses for the different axle loads are given in Tables 2-4. A summary of these calculated results is given in Table 6 as a percentage of values obtained for the 42-kip TALs. As shown in Table 6, calculated slab deflections and strains under the 42-kip tridem-axle loads are much less than those for the 42-kip TALs and in fact are equal to or less than those for the 34-kip TALs. Of the four cases of axle loading considered, the 42-kip TALs resulted in the highest calculated edge and corner deflections and the 20-kip SALs produced the highest calculated edge strains.

When the effects on pavement response of different axle types are compared, the profiles for deflections and strains along the slab edge should also be considered. Figure 11 shows calculated edge deflection profiles for the 20-kip SALs, 34-kip TALs, and the 42-kip tridem-axle loads. As shown,

TABLE 6 Calculated Pavement Response as Percentage of That for 42-Kip TALs

Shoulder Type	Response Type	Percentage of Response by Axle Load: 20-kip SAL	34-kip TAL	42-kip Tridem-Axle Load
Tied	Edge deflection	58	81	81
	Corner deflection	79	81	80
	Edge strain	111	81	49
None	Edge deflection	57	81	83
	Corner deflection	69	81	80
	Edge strain	106	81	51

the shapes of the deflection profiles are similar for the three cases. Figure 12 shows the calculated corner deflection profiles for the tridem-axle loads. The deflection basin length under the tridem-axle loads is almost twice as long as that for the SALs and about 1.5 times as long as that for the TALs.

Profiles for calculated edge strain for the three cases of axle loads are shown in Figure 13. For this case there is a marked difference between the responses under the three different types of axle loads. The SAL exhibits a single peak, the TAL exhibits two peaks, and the tridem-axle load produces three peaks. These peaks are produced under each axle.

Analysis of Results

It has been shown that pavement response under the 42-kip tridem-axle loads is less severe than that for the 42-kip TALs. In fact, the response for the 42-kip tridem-axle loads was equal to or less severe than that for the 34-kip TALs.

According to the AASHTO traffic equivalence factors, presented in Table 5, tandem axles are about

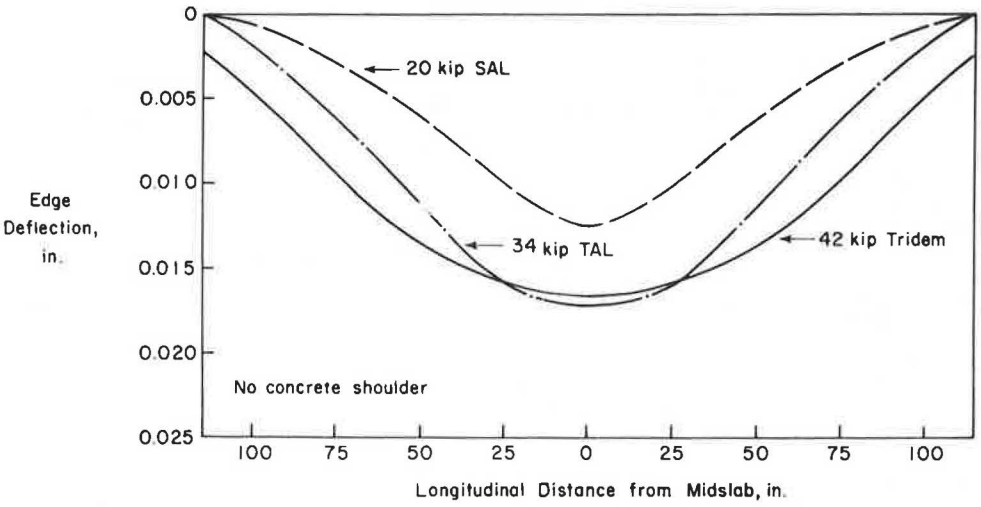

FIGURE 11 Calculated edge deflection profiles.

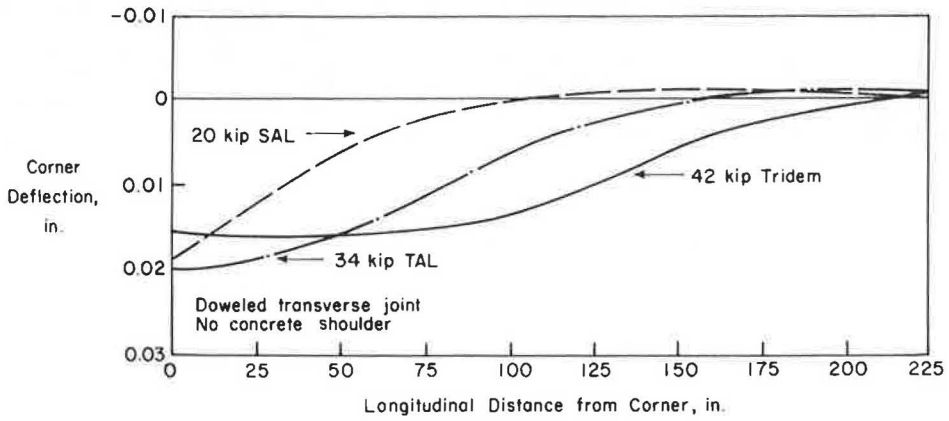

FIGURE 12 Calculated corner deflection profiles.

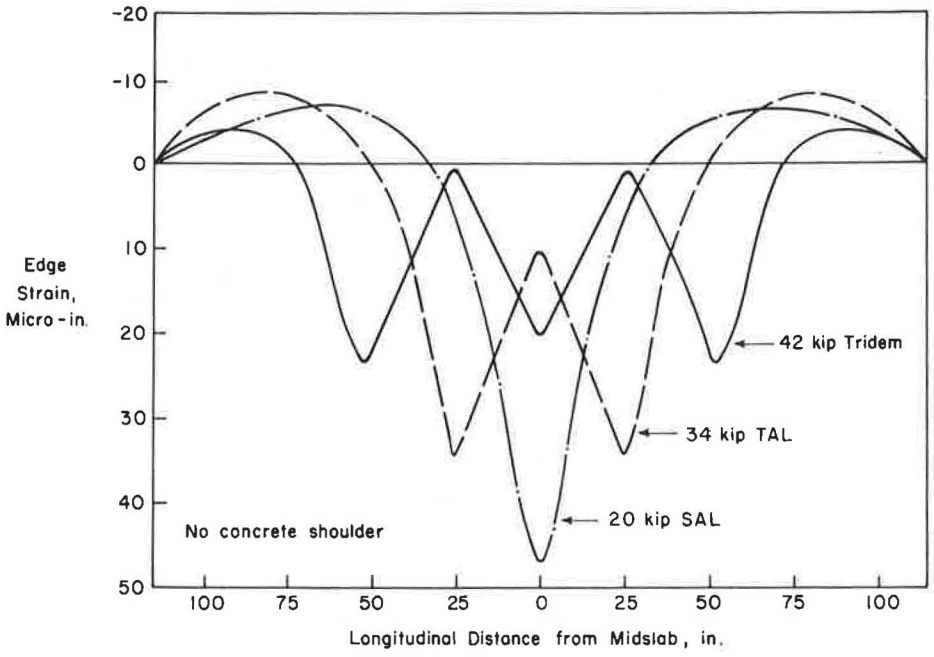

FIGURE 13 Calculated edge strain profiles.

2.30 to 2.50 times as damaging as a single axle weighing half as much as the tandem axles. The ratio of edge deflection under tandem axles to that under a single axle weighing half as much as the tandem axles is about 1.64 based on theoretical analysis and about 1.60 to 1.90 based on field measurements. On the other hand, calculated as well as measured edge strain under tandem axles are less than the edge strains under a single axle weighing half as much as the tandem axles. Thus, it can be seen that the AASHTO traffic equivalence factors give more weight to edge deflection response than any other response parameter when the effects of single and tandem axles are compared.

The ratio of edge deflection under a tridem axle to that under a single axle weighing one-third as much as the tridem axle is about 2.0 based on theoretical analysis and about 2.0 to 2.2 based on field measurements. By extrapolation, it is found that the ratio of edge deflection under a tridem axle to that under a single axle weighing 40 percent as much as the tridem axle is about 1.65 based on theoretical analysis and about 1.65 to 1.80 based on field measurements. Therefore, if proportionality is assumed between deflections and performance, a tridem axle can be considered about 2.30 to 2.50 times as damaging as a single axle weighing 40 percent as much as the tridem axle. As an example, a 50-kip tridem axle would be considered 2.30 to 2.50 times as damaging as a 20-kip single axle.

Based on this reasoning, traffic equivalence factors for tridem axles were developed for concrete pavements. These factors are listed in Table 7 and are considered tentative. The factors were developed by considering a tridem axle to be 2.40 times as damaging as a single axle weighing 40 percent as much as the tridem axle. The factors for each axle-load group were then established by using traffic equivalence factors for a single axle on a slab 9 in. thick that has a terminal serviceability of 2.5. A comparison of traffic equivalence factors for the single axles, tandem axles, and tridem axles is given in Figure 14. The factors for tridem axles presented in Table 7 and Figure 14 are considered applicable to slab thicknesses of 7 through 10 in.

TABLE 7 Traffic Equivalence Factors for Tridem Axles

Tridem-Axle Load (kips)	Traffic Equivalence Factor	Tridem-Axle Load (kips)	Traffic Equivalence Factor
30	0.43	46	2.64
32	0.55	48	3.12
34	0.70	50	3.77
36	0.91	52	4.32
38	1.20	54	5.04
40	1.44	56	6.00
42	1.68	58	7.20
44	2.16	60	8.06

Note: Terminal pavement serviceability index (p_t) = 2.5.

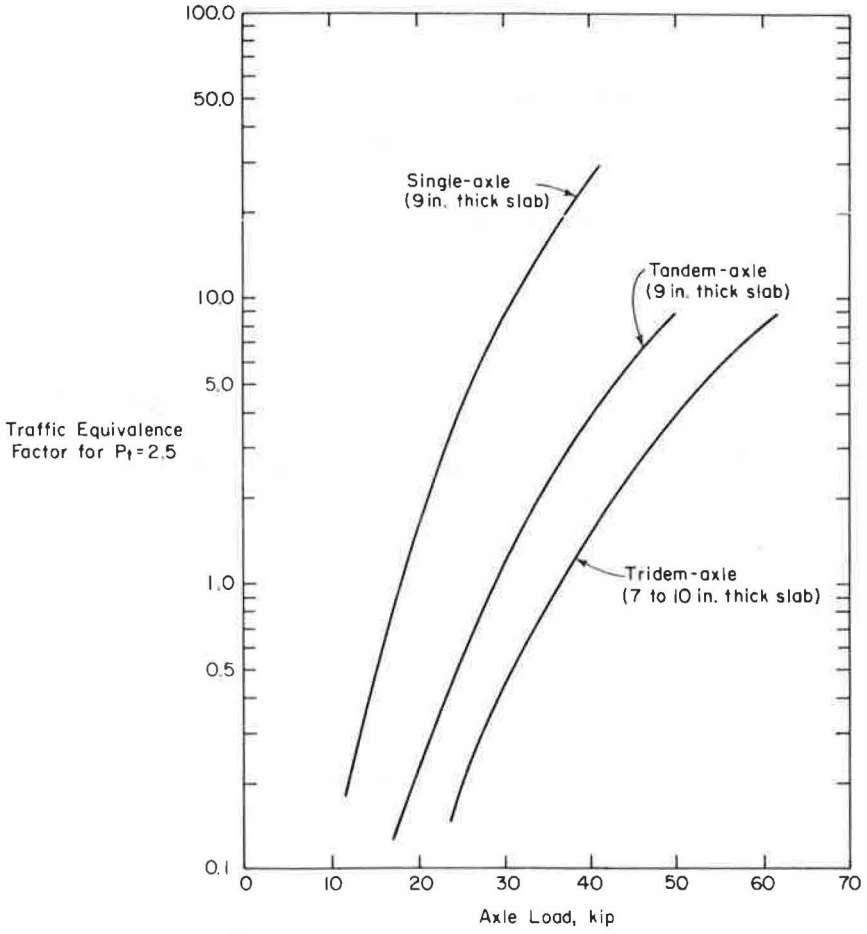

FIGURE 14 Comparison of traffic equivalence factors.

SUMMARY

A field study was conducted to evaluate the effect of frozen support and tridem-axle loading on concrete pavement performance. Pavement deflections and strains were measured during the fall and the winter at five project locations.

Study results indicate that pavement deflections and strains are greatly reduced during winter months when the support is frozen. Based on analysis of these results, it is concluded that the damaging effect of axle loads applied during the winter when the support is frozen can be considered to be only one-seventh as damaging as the same loads applied during the fall.

Study results also indicate that pavement deflections and strains are greatly reduced for a 42-kip tridem-axle loading as compared with those for 42-kip TALs. In fact, measured and calculated corner and edge deflections under 42-kip tridem-axle loadings were almost equal to or less than those for 34-kip TALs. Measured and calculated edge strains for a 42-kip tridem-axle loading were considerably lower than those for a 34-kip TAL.

Based on study results, it is concluded that for application to the AASHTO thickness design procedure, a tridem axle can be considered as equivalent to a single axle weighing about 50 percent of the tridem axle and to tandem axles weighing about 80 percent of the tridem axle. Traffic equivalence factors were developed for tridem axles on concrete pavements. These factors are tentative but may be considered for use in lieu of other field data on the effects of tridem axles on concrete pavement response.

ACKNOWLEDGMENT

Work was conducted by the Construction Technology Laboratories under the sponsorship of MnDOT in cooperation with FHWA. The investigation was directed by Bert E. Colley, director of the Transportation Development Department, and W. Gene Corley, director of the Engineering Development Division. Leo P. Warren, Glenn R. Korfhage, Gabriel Bodoczy, and John Hale of MnDOT provided technical coordination. Their cooperation and suggestions are gratefully acknowledged.

REFERENCES

1. S.D. Tayabji, C.G. Ball, and P. Okamoto. Effect of Tridem-Axle Loading on Concrete Pavement Performance. Construction Technology Laboratories, Skokie, Ill.; Minnesota Department of Transportation, St. Paul, Oct. 1983.
2. C.G. Ball, S.D. Tayabji, and P. Okamoto. Effect of Frozen Support on Concrete Pavement Performance. Construction Technology Laboratories, Skokie, Ill.; Minnesota Department of Transportation, St. Paul, Oct. 1983.
3. S.D. Tayabji, C.G. Ball, and P. Okamoto. Effect of Concrete Shoulders on Concrete Pavement Performance. Construction Technology Laboratories, Skokie, Ill.; Minnesota Department of Transportation, St. Paul, July 1983.
4. Interim Guide for Design of Pavement Structures, rev. ed. AASHTO, Washington, D.C., 1981.
5. Thickness Design for Concrete Pavements. Publ. IS10. Portland Cement Association, Skokie, Ill., 1966.
6. M.C. Wang and R.P. Anderson. Load Equivalency Factors of Triaxle Loadings for Flexible Pavements. In Transportation Research Record 810, TRB, National Research Council, Washington, D.C., 1981, pp. 42-49.
7. H.J. Treybig. Equivalency Factor Development for Multiple Axle Configurations. In Transportation Research Record 949, TRB, National Research Council, Washington, D.C., 1983, pp. 32-44.
8. B.E. Colley et al. Evaluation of Concrete Pavement with Lane Widening, Tie Concrete Shoulders, and Thickened Pavement. Report FHWA/MN-79/06. Minnesota Department of Transportation, St. Paul, Sept. 1977.
9. W.J. Nowlen. Techniques and Equipment for Field Testing of Pavements. Research and Development Bull. D83. Portland Cement Association, Skokie, Ill., 1964.
10. S.D. Tayabji and B.E. Colley. Analysis of Jointed Concrete Pavements. Construction Technology Laboratories, Skokie, Ill.; FHWA, U.S. Department of Transportation, Oct. 1981.

The opinions expressed in this paper are those of the authors and not necessarily those of the Minnesota Department of Transportation or FHWA.

Publication of this paper sponsored by Committee on Rigid Pavements.

Environmental Factors in Flexible Pavement Design

ADNAN A. BASMA and K.P. GEORGE

ABSTRACT

The principal objective of this research was to study the influence of the environment on the thickness of flexible pavements. Environmental variables considered include general soil conditions and temperature effects. As identified in previous studies, six climatic zones were recognized. Weather information and soil properties were collected for 175 typical stations covering the continental United States, excluding Alaska. Based on the criteria of rutting of 1.25 cm (0.5 in.) and thermal cracking of 115 m/1000 m^2 (35 ft/1,000 ft^2), appropriate asphalt-cement grades were selected for each station. To consider the interaction of temperature and modulus with fatigue damage, the concept of effective modulus was introduced. The effective modulus calculated by using the appropriate asphalt grade was found to be nearly constant within a zone but varied considerably from one zone to another. A sensitivity analysis was performed on the AASHO flexible pavement design equation, the purpose of which was to determine the effect of the regional factor and the soil support value on the structural number. After these two items had been combined with the change in the layer coefficient due to modulus change, their overall effect on pavement thickness was evaluated. The ratio of the thickness required at a given station to that required at reference conditions [namely, asphalt effective modulus of 34.5 kPa (5×10^3 psi), regional factor of 1.0, and soil support value of 5.0] is defined as the depth factor. The depth factor ranged from as low as 0.45 in Florida, parts of Mississippi, Alabama, Georgia, and the Carolinas to as high as 1.60 in regions of Montana, North Dakota, and South Dakota. The higher the depth factor, the more severe the influence of environment on pavement performance. Examples to illustrate how the depth factor may be incorporated into the AASHO flexible design are given.

In the design of flexible pavements, traffic load and environment are the most influential factors in the determination of pavement thickness. Before the AASHO Road Test, most pavements were designed with regard to traffic alone, with little if any consideration for the environment. Since the introduction of the AASHO pavement design (1), however, more emphasis has been placed on environmental effects. For example, the AASHO flexible model, which is written symbolically as follows, presents in equational form the design relationship between the important variables:

$$\log W = 9.36 \log(SN + 1) - 0.20 + \log\left[(c_0 - p)/(c_0 - 1.5)\right] \div \left\{0.40 + \left[1{,}094/(SN + 1)^{5.19}\right]\right\} + 0.37756\,(SSV - 3.0) - 0.97 \log(R_f) \quad (1)$$

where

W = total number of 80-kN (18-kip) equivalent axle loads (EALs),
SN = weighted structural number,
c_0 = initial serviceability index,
p = terminal serviceability index,
SSV = soil support value, and
R_f = regional factor.

Buick (2) studied the significance of these variables and showed that besides traffic, SSV and R_f are most important in the formulated thickness function.

Following the AASHO study (1) several attempts were made to investigate the climatic effect on pavements, first in four climatic zones, then later in six climatic zones (Figure 1). The effect of the surrounding environment on the pavement performance, however, has not yet been quantified to any degree.

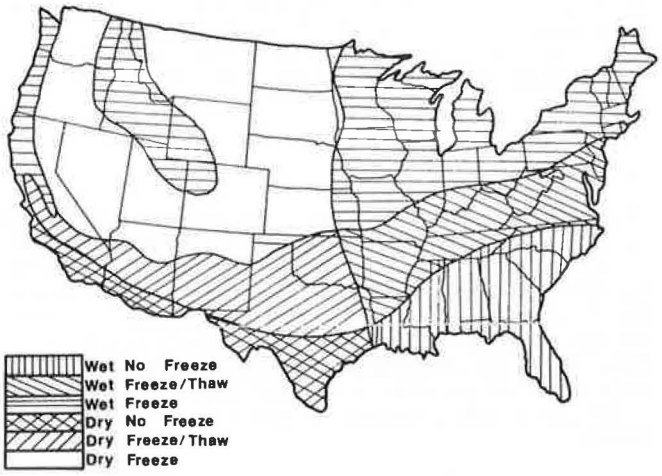

FIGURE 1 Climatic zones of the United States *(3)*.

Environmental variables can include such inputs as general soil conditions, moisture, and air temperature variation around and within the pavement structure. In this study, the environmental variables are limited to soil and climatic conditions.

This investigation was motivated by the provisions of section 137(a) of the Surface Transportation Assistance Act of 1982, which, in part, calls for a study to make specific recommendations for changing the apportionment formulas to take into account weather-related factors. "The study shall analyze current conditions and factors including, but not limited to, volume and mix of traffic, weight and size of vehicles, environmental, geographical and meteorological conditions in various states...." Environmental and geographical effects on flexible pavements are analyzed in this paper.

The objective of this study was to show how the environmental factors affect the thickness requirement of flexible pavements. The AASHO Interim Guide equation for flexible pavement (Equation 1) provided the basic structural design model. Through a system-

atic sensitivity analysis of the AASHO equation with respect to the most significant environmental factors (such as modulus of asphalt concrete, SSV, and R_f), their impact on the equation was evaluated and quantified. In order to portray the severity of environment nationwide, the concept of a depth factor is introduced and discussed.

GENERAL FRAMEWORK

A combination of existing design procedure (1), weather information from the U.S. Weather Bureau (4), and a soil map for the contiguous United States (5) was used in developing the flexible-pavement thickness requirements for the entire United States. The AASHO flexible-pavement equation (Equation 1) forms the basis for structural design. This equation relates traffic repetitions and SN; SSV and R_f are secondary variables. One tacit assumption in the design equation is that asphalt concrete, regardless of location or climate or both, will have the same stiffness (modulus) as that encountered in the AASHO Road Test. That the AASHO design procedure does not take into account the variations in the asphalt-concrete modulus is considered a major drawback of the method. In order to overcome this deficiency, a weighted average modulus is introduced in the first part of the study. Because asphalt grade plays a crucial role in the modulus of the asphalt mixture, a rational method was developed to select the appropriate asphalt grade.

In the second part of the study, the overall effect of environment on pavement structural thickness is evaluated by performing (a) a sensitivity analysis of the AASHO equation with respect to the SSV and R_f and (b) a sensitivity analysis to illustrate the role of the effective modulus in the thickness design. The overall effect of environment on structural design is obtained by combining items (a) and (b) to give rise to what is defined in this paper as the depth factor.

CLIMATIC EFFECT ON ASPHALT LAYER

The effect of climate on the asphalt layer is well documented in that the asphalt modulus fluctuates substantially with ambient temperature. Therefore it is customary to specify softer-grade asphalt in colder climates to reduce thermal cracking and harder-grade asphalt in warmer climates to reduce rutting. There is as yet no complete procedure for selecting the asphalt grade appropriate to the climate except for a graphical solution proposed in premium pavement design to minimize low-temperature cracking (6). Not only low-temperature cracking but also excessive rutting must be taken into account in the asphalt selection process; accordingly, the graphical plot of Von Quintus et al. is modified as in Figure 2. In the development of this nomograph two criteria are specified: the thermal cracking is not to exceed 115 m/1000 m² (35 ft/1,000 ft²) and rutting is to be no more than 1.25 cm (0.5 in.).

Asphalt-Grade Selection to Minimize Thermal Cracking

Von Quintus et al. used the TC-1 program (7) in developing the asphalt-grade selection chart. We too have used this program because it provides the capability of estimating low-temperature cracking and material properties for asphalt-concrete surfaces. By using the program for asphalt of a given penetration index, the relation between low-temperature cracking and expected minimum pavement temperature can be obtained. Subsequently this relation was plotted in nomographical form as shown on the right-hand side of Figure 2.

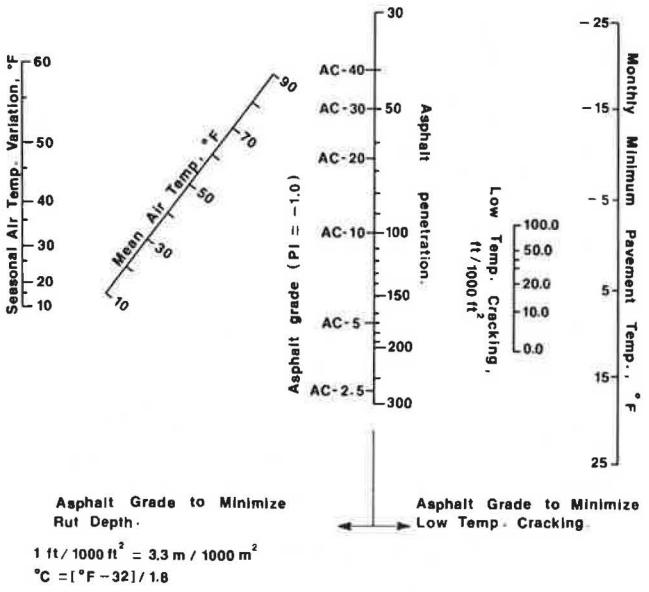

FIGURE 2 Asphalt-concrete grade selection to minimize rut depth and low-temperature cracking.

Asphalt-Grade Selection to Minimize Rutting

Climatologically representative stations were selected throughout the United States, and pertinent air temperature data were gathered for those stations from U.S. Weather Bureau records. AASHO flexible pavement designs were prepared for typical subgrade conditions. With the VESYS computer program, the asphalt penetration grade required for each station was determined, with the stipulated criterion that rutting be no more than 1.25 cm. In other words a relation was established between the mean air temperature in combination with seasonal variations and the asphalt grade, and it is nomographed on the left-hand side of Figure 2.

Asphalt Selection to Minimize Both Cracking and Rutting

Employing the nomographs in Figure 2, we want to determine the appropriate asphalt grades for the entire country. To accomplish this, such weather data as the mean air temperature and monthly mean air temperature variation at some 175 typical stations covering the entire United States were gathered from U.S. Weather Bureau records. These temperature data were used in a graph proposed by Von Quintus et al. (6) to estimate the expected minimum temperature of the pavement at each station. With the minimum pavement temperature and the criterion of thermal cracking no more than 115 m/1000 m² the minimum penetration and therefore the asphalt grade are obtained from Figure 2. The maximum allowable penetration to satisfy the rutting criterion is obtained by placing the appropriate ambient temperature information on the left-hand side of Figure 2. A grade of asphalt that will provide penetration no less than that required to prevent low-temperature cracking and no more than that required to prevent rutting is construed to be the right grade for that station. Plot-

ting all of the 175 points on a map enabled the identification of five zones of asphalt-concrete-grade asphalt (see Figure 3). Note that for this study a penetration index (PI) of -1.0 is used.

When the asphalt grade is known for each region, it is desirable to calculate a representative modulus for each climatic zone; this topic is discussed in the next section.

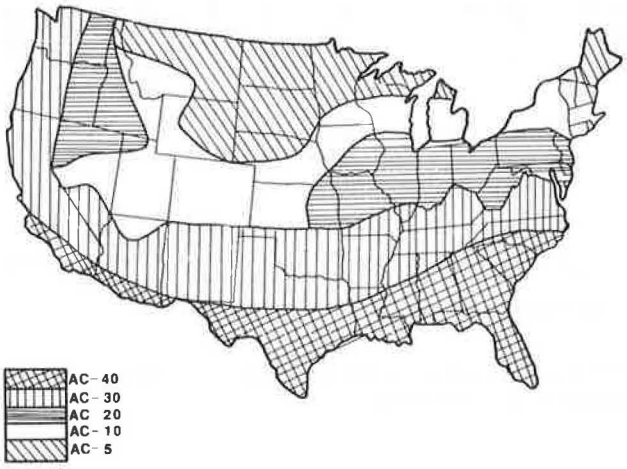

FIGURE 3 Recommended asphalt-concrete grades for the United States.

Effective Modulus Related to Climatic Zones

Variations in climate and ambient temperature produce significant changes in the modulus of asphalt-concrete materials. Von Quintus et al. (6) developed a procedure that includes a weighted mean asphalt-concrete modulus for each asphalt cement type and climate. The terms "effective modulus" or "weighted mean asphalt-concrete modulus" were developed to designate the effects of temperature variations on fatigue cracking. These effects cannot be adequately determined by simply averaging the asphalt-concrete modulus over all seasons because of the interaction of temperature and modulus with the fatigue damage produced in the pavement. The effective modulus is defined mathematically by the following equation (6):

$$E_e = \sum_{i=1}^{n} E_i \times FF(E_i) / \sum_{i=1}^{n} FF(E_i) \quad (2)$$

where E_e is the effective modulus and E_i is the modulus during the ith period (season). $FF(E_i)$ is termed the fatigue factor, defined as follows:

$$FF(E_i) = d_f(E_i)/d_f(34.5 \times 10^5 \text{ kPa}) \quad (3)$$

where $d_f(E_i)$ is the unit damage caused by a single application of 18-kip axle load at modulus E_i corresponding to temperature T_i. In Equation 2, n = 4 if the temperature variations are averaged, so that four seasonal temperatures are considered, or n = 12 if the variations are expressed on a month-by-month basis.

The fatigue factor is related to modulus E_i; this relationship is expressed by the following empirical equation:

$$\log FF(E_i) = -1.9427 \log E_i + 1.3553 \quad (4)$$

where E_i is the asphalt-concrete modulus (psi x 10^5). It should be noted from Equations 3 and 4 that $FF(34.5 \times 10^5 \text{ kPa}) = 1.0$, because a modulus of 34.5×10^5 kPa was used as a reference.

After an asphalt grade has been selected and the seasonal pavement temperature estimated, one can evaluate the seasonal asphalt-concrete modulus for each station. If the seasonal effective modulus is substituted in Equation 4, the effective modulus for each station can be estimated by using Equation 2. Sample calculations of E_e are given elsewhere (6). Interestingly enough, the effective modulus, as listed in Table 1, exhibited little variation within a zone, even with the different asphalt grades specified in Figure 3. That fatigue sensitivity of asphalt also enters into the effective-modulus calculation partly accounts for the seemingly anomalous result. The mix properties for estimating the temperature-dependent modulus and in turn the effective modulus of Table 1 are listed as follows:

TABLE 1 Calculated Effective Modulus in Various Climatic Zones

Zone	Asphalt Grade	Effective Modulus (psi x 10^5)
Wet no-freeze	AC-40	8.40
Wet freeze and thaw	AC-30	5.30
Wet freeze	AC-20	4.42
	AC-10	4.43
	AC-5	4.27
Dry no-freeze	AC-40	4.90
Dry freeze and thaw	AC-30	3.30
Dry freeze	AC-5	2.50
	AC-10	2.40
	AC-30	2.90

Note: 1 psi = 6.895 kPa.

Property	Value
Percent asphalt by weight	5
Percent air voids	5
Percent passing No. 200 sieve	5
Loading frequency	10 Hz
PI	-1.0

The data in Table 1 clearly show that the pavement location and the prevailing climate indeed have a significant effect on the asphalt modulus. For example, the effective modulus in a wet no-freeze region may be three times as large as that in a dry freeze region. How this variation affects the thickness design is discussed in a later section.

ENVIRONMENTAL EFFECT ON PAVEMENT THICKNESS

Effect of SSV and R_f on SN

To quantify the effect of the environment on the pavement thickness, the researchers performed a sensitivity analysis of the AASHO design equation (Equation 1). This analysis clearly identified the individual and combined effects of the AASHO design parameters on SN. The design parameters considered were SSV and R_f in addition to the effective modulus. Excluded in this analysis were such other parameters as traffic and initial and final serviceability indices.

The combined effect of all of the variables on the weighted SN is best expressed by the following equation of total differential:

$$dSN = (\partial SN/\partial c_0)\,dc_0 + (\partial SN/\partial p)\,dp + (\partial SN/\partial W)\,dW + (\partial SN/\partial SSV)\,dSSV + (\partial SN/\partial R_f)\,dR_f \quad (5a)$$

If the initial and final serviceability indices are kept constant, $dp = 0$ and $dc_0 = 0$. In addition, because this study is concerned with environmental variables only, the wheel-load term also drops out. With these modifications, Equation 5a becomes as follows:

$$dSN = (\partial SN/\partial SSV)\,dSSV + (\partial SN/\partial R_f)\,dR_f \quad (5b)$$

The first-order partial derivatives of the weighted SN with respect to SSV and R_f were presented by Buick (2) as follows:

$$\partial SN/\partial SSV = 0.3775/(\partial\phi/\partial SN) \quad (6)$$

$$\partial SN/\partial R_f = (-0.4166/R_f)/(\partial\phi/\partial SN) \quad (7)$$

where $\partial\phi/\partial SN$ is defined by the function shown below:

$$\partial\phi/\partial SN = [4.065/(SN+1)] + \log[(c_0 - p)/(c_0 - 1.5)]\left\{5{,}677.9\,(SN+1)^{4.19}/[0.4(SN+1)^{5.19} + 1{,}094]^2\right\} \quad (8)$$

with $c_0 = 4.0$, $p = 2.5$, and $\log[(c_0 - p)/(c_0 - 1.5)] = -0.2218$.

Proportional change in SN may be expressed by using Equation 5b as follows:

$$\Delta SN/SN = [(\partial SN/\partial SSV)/SN]\,dSSV + [(\partial SN/\partial R_f)/SN]\,dR_f \quad (9)$$

When the value of $[(\partial SN/\partial SSV)/SN]$ was evaluated for $1 < SN < 6$, it was found to vary between 0.19 and 0.11; the average was 0.13. In other words SN increases by an average of 13 percent for a unit decrease of SSV. With an SSV of 5.0 as a base value and $[(\partial SN \div \partial SSV)/SN] = 0.13$, the values for $[(\partial SN \div \partial SSV)/SN]dSSV$ and the soil support value factor (FSSV) are given in Table 2.

With a similar approach, the values of $[(\partial SN/\partial R_f) \div SN]R_f$ are computed as listed in Table 3 for $R_f = 1.0$ as a reference. For the range of $1 < SN < 6$ the average value was found to be -0.16, which was used to compute the influence factor (FR_f), as defined in Equation 10.

TABLE 2 Soil Support Value Factor

SSV	dSSV	$[(\partial SN/\partial SSV)/SN]\,dSSV$	FSSV
2.0	+3.0	0.39	1.39
3.0	+2.0	0.26	1.26
4.0	+1.0	0.13	1.13
5.0[a]	0.0	0.00	1.00
6.0	-1.0	-0.13	0.87
7.0	-2.0	-0.26	0.74
8.0	-3.0	-0.39	0.61
9.0	-4.0	-0.52	0.48

Note: SSV = soil support value; dSSV = change in SSV from reference value; FSSV = soil support value factor.
[a]Reference soil support value.

TABLE 3 Values of $[(\partial SN/\partial R_f)/SN]\,R_f$ for Different Values of SN

SN	$\partial SN/\partial R_f$	$[(\partial SN/\partial R_f)/SN]\,R_f$
1.0	-0.21	-0.21
2.0	-0.33	-0.17
3.0	-0.49	-0.16
4.0	-0.62	-0.15
5.0	-0.70	-0.14
6.0	-0.77	-0.13

Influence factors for SSV and R_f, respectively, are defined as follows:

$$FSSV = 1 + [(\partial SN/\partial SSV)/SN]\,dSSV$$

$$FR_f = 1 + [(\partial SN/\partial R_f)/SN]\,dR_f \quad (10)$$

Equation 9 could be simplified to read as follows:

$$\Delta SN/SN = (FSSV + FR_f) - 2 \quad (11)$$

Equation 11 is an explicit expression for the change in SN as a function of FSSV and FR_f. The values of FSSV and FR_f are given in Tables 2 and 4, respectively.

TABLE 4 Influence Factor of R_f

R_f	dR_f	$[(\partial SN/\partial R_f)/SN]\,dR_f$	FR_f
1.0[a]	0.0	0.0	1.00
2.0	-1.0	+0.08	1.08
3.0	-2.0	+0.11	1.11

Note: dR_f = change in R_f from reference value; FR_f = influence factor of R_f.
[a]R_f reference value.

In order to assign FSSV for various sections of the United States, soil deposits were identified and strength characteristics of each soil were estimated. A map of this general nature has been compiled by Woods (5) as shown in Figure 4. The general

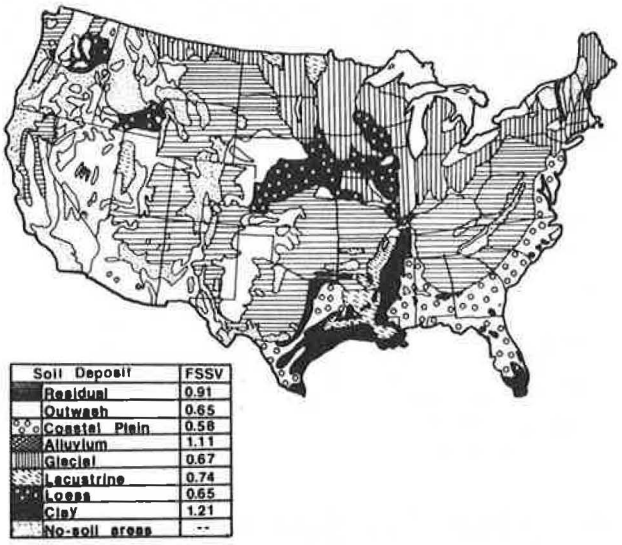

FIGURE 4 FSSV for soil deposits in the United States.

soil description given by Woods has made it possible to estimate such strength parameters as California bearing ratio (CBR) and from that the SSV (5,8). When the SSV values are known, data in Table 2 may be employed to derive FSSV for each soil deposit, as tabulated in the inset to Figure 4. The interpretation of this map is that under similar traffic conditions regions with higher FSSV values call for thicker pavements on account of the abundance of weaker subgrade soils. A similar interpretation could be offered for the FR_f. From the range of values of the latter (1.0 to 1.11), it could be concluded that R_f exerts a relatively small influence on the thickness of flexible pavements.

Effect of Asphalt-Concrete Modulus on SN

Yet another sensitivity analysis was performed to study how effective modulus influences pavement thickness. With the AASHO suggested values (1) of the asphalt layer coefficient for different asphalt-concrete moduli, a regression analysis was performed to relate mathematically a_1 (asphalt layer coefficient) to E_1 (asphalt modulus), which yielded the following equation:

$$a_1 = 0.22691E_1^{0.4260} \quad R^2 = 0.993, SE = 0.051 \tag{12}$$

for $1.0 < E_1 < 10.0$ where E_1 is in units of 10^5 psi (1 psi = 6.895 kPa).

In order to study the effect of modulus on flexible pavement design, the modulus factor (MF) is defined as the ratio of layer coefficient evaluated at the reference modulus of 34.5 x 10^5 kPa to that at an arbitrary modulus. That is,

$$MF_B = a_{1*}/a_{1B} \tag{13a}$$

where a_{1*} and a_{1B} are layer coefficients evaluated at the reference value and at an arbitrary value, E_B. According to Equation 12, the layer coefficient bears an explicit relation to the asphalt modulus. Substitution for a_{1*} and a_{1B} from Equation 12 results in the following:

$$MF_B = 1.983/E_B^{0.426} \tag{13b}$$

Note that Equation 13b is valid for a reference modulus of 34.5 x 10^5 kPa. By using Equation 13b, MFs for typical values of modulus are listed in Table 5. The significance of MF is the same as that of FSSV or FR_f in that larger MF-values indicate thicker pavements. As can be seen from Table 5, larger MF-values result solely from lower effective moduli of asphalt.

TABLE 5 Values of MF for Different Moduli

Asphalt-Concrete Modulus E_1 (psi)	MF (E_1)	Asphalt-Concrete Modulus E_1 (psi)	MF (E_1)
200,000	1.48	600,000	0.92
300,000	1.24	700,000	0.86
400,000	1.10	800,000	0.82
500,000[a]	1.00	900,000	0.78

Note: 1 psi = 6.895 kPa.

[a]Asphalt-concrete reference modulus.

Combined Effects of Asphalt Modulus, SSV, and R_f on Asphalt-Concrete Thickness

Although an explicit expression to estimate pavement thickness considering all of the environmental factors is desired, for purposes of this study it suffices to determine the relative asphalt thickness with respect to a chosen set of reference values: effective modulus = 34.5 x 10^5 kPa, SSV = 5.0, and R_f = 1.0.

Considering the general case of an asphalt pavement, the change in asphalt thickness between stations B and * (with reference values) ($\Delta h_{B/*}$) can be estimated as follows:

$$\Delta h_{B/*} = (h_B - h_*)/h_* \tag{14}$$

where h_B and h_* are asphalt thickness at B and *.

For a full-depth pavement, Equation 14 may be written as follows:

$$\Delta h_{B/*} = [(SN_B/a_{1B}) - (SN_*/a_{1*})]/(SN_*/a_{1*}) \tag{15}$$

If the overall change in SN from station * to B is defined as ΔSN,

$$SN_B = SN_* + \Delta SN \tag{16}$$

If Equations 13a and 16 are substituted into Equation 15, the following is obtained:

$$\Delta h_{B/*} = MF\,[1 + (\Delta SN/SN_*)] - 1 \tag{17}$$

The depth factor (DF) is defined as the ratio of asphalt thickness at station B to that at station * with reference environmental conditions. That is,

$$DF_B = h_B/h_* \tag{18}$$

By using the simple relation $h_B = h_* + \Delta h_{B/*}$ as well as Equation 17 in Equation 18, the following is obtained:

$$DF_B = \{MF_B[1 + (\Delta SN/SN)]\} \tag{19}$$

Note that MF_B, the modulus factor corresponding to the effective modulus at B, has finally been calculated (see Table 5). In addition, with values of $\Delta SN/SN$ evaluated from Equation 11, the depth factor for a given station can be explicitly calculated. A map of the United States listing values of DF for the whole country is presented in Figure 5.

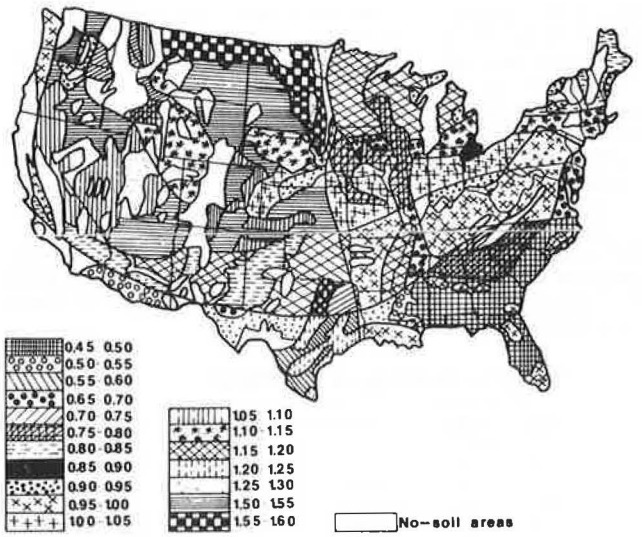

FIGURE 5 DF values for the United States.

It is significant that the DF boundaries coincide with those of the soil map of Figure 4 and the climatic zonal map of Figure 1; the climatic zones perhaps exert a greater influence than does soil on DF. The latter assertion can be substantiated by comparing DFs in Figure 5: DF varies from as low as 0.45 in Florida, parts of Mississippi, Alabama, Georgia, and the Carolinas, where the effective modulus is 58.0 x 10^5 kPa (8.4 x 10^5 psi), to as high as 1.60 in regions of Montana, North Dakota, and South Dakota, where, in fact, the effective modulus is the lowest, namely, 17.2 x 10^5 kPa (2.5 x 10^5 psi).

DF is a convenient index that portrays how severe the environment is with regard to pavement life.

Asphalt-concrete pavements need to be thicker in regions where the DF is greater than 1 than in regions where the DF is less than 1.

CONCLUDING REMARKS

In order to adequately account for the effects of the environment in the AASHO flexible pavement design, the influence of climatic variables in the design is evaluated by a sensitivity analysis. The effect of ambient temperature on asphalt-concrete stiffness is also incorporated into the final version of the environmental factor referred to in this report as DF. A DF map of the United States (Figure 5) is included for ready reference.

Higher DFs resulted from either poor subgrade soil or a relatively small effective modulus or both. DF is a convenient index for assessing the influence of environment on flexible pavement in that the higher the depth factor, the more severe the environment is for pavement performance. Therefore, federal agencies will find that DF can be an effective measure in allocating funds for construction and maintenance of highway systems throughout the country.

Because DF is a measure of environmental severity with regard to pavement performance, the AASHO design procedure could be updated by incorporating the DF concept. As pointed out earlier, it includes not only the effect of SSV and R_f on SN but also the climatic effect on the asphalt layer coefficient (a_1). Two examples are presented in the following to illustrate how DF could be incorporated into the AASHO design procedure. The data normally required for AASHO design, along with other special information for both examples, are listed in Table 6.

TABLE 6 Input Data for Pavement Design Examples

Item	Example 1	Example 2
Mean air temperature (°C)	7	20
Climatic zone	Dry freeze	Wet no-freeze
Asphalt-cement grade	AC-5	AC-40
Effective modulus E_e (kPa)	17.2×10^5	58.0×10^5
Effective asphalt layer coefficient a_{1e}	0.38	0.56
AASHO asphalt layer coefficient a_1	0.42	0.42
AASHO regional factor	3.0	1.0
AASHO mean SSV	6.5	9.0
Traffic (80-kN EALs)	3×10^6	6×10^6
Depth factor	1.23	0.47
Gravel base thickness h_2 (cm)	25.4	0.0

Note: 1 cm = 0.39 in.; 1 kPa = 0.145 psi; $t°C = (t°F - 32)/1.8$; 1kN = 0.2 kip.

Example 1: Huron, South Dakota

Thickness for Standard Conditions

Enter Figure 6 with $W = 3 \times 10^6$ 18-kip EALs and $h_2 = 25.4$ cm (10.0 in.) to obtain the asphalt layer thickness for reference conditions, $h_{1R} = 14.2$ cm (5.6 in.). Figure 6 was prepared by using the AASHO design charts with inputs of $R_f = 1.0$ and SSV = 5.0 along with $E_e = 34.5 \times 10^5$ kPa (reference values). Note that the asphalt layer thickness can also be computed by using Equation 20, which is the regression equation developed from the data in Figure 6:

$$h_{1R} = [4.62 \exp(-0.061 h_2)] \times W^{0.161 \exp(0.0354 h_2)} \quad R^2 = 0.970, SE = 0.10 \quad (20)$$

where h_2 is the gravel base thickness in inches.

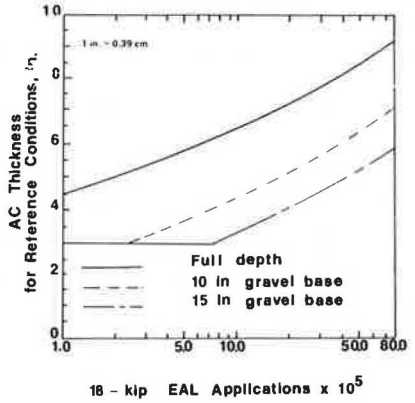

FIGURE 6 Asphalt-concrete thickness for the reference conditions versus traffic with and without gravel base.

Asphalt Thickness for Huron, South Dakota

Multiply h_{1R} by the depth factor to get the asphalt thickness; $h_1 = 1.23 \times 14.2$ cm = 17.5 cm (6.9 in.). The required pavement thickness, therefore, is 17.5 cm of asphalt concrete and 25.4 cm of gravel base.

Example 2: Tallahassee, Florida

Thickness for Standard Conditions

With $W = 6 \times 10^6$ 18-kip EAL and no base specified, from Figure 6 or Equation 20, $h_{1R} = 22.4$ cm (8.8 in.).

Asphalt Thickness for Tallahassee, Florida

As in example 1, $h_1 = 0.47 \times 22.4$ cm = 10.5 cm (4.2 in.). The required pavement thickness is 10.5 cm (4.2 in.) of full-depth asphalt concrete.

Comparison between the AASHO design and the AASHO modification with DF results in the data given in Table 7. From these examples two observations deserve mention:

1. If the AASHO design were to be followed along with the AASHO-recommended layer coefficient for asphalt concrete ($a_1 = 0.42$), the pavement in Huron, South Dakota, would have been underdesigned by approximately 1.78 cm (0.7 in.) and would have had a shorter life than that anticipated. This result would have been expected because DF is greater than 1.0. On the other hand, the pavement in Tallahassee, Florida, is overdesigned by nearly 3.8 cm (1.5 in.). A low DF of 0.47 reflects this.

TABLE 7 Comparison of Structural Designs

Location	Pavement Component	Pavement Thickness (cm) A	B	C
Huron, S.D. (DF = 1.23)	Asphalt concrete	15.7	17.3	17.5
	Gravel base	25.4	25.4	25.4
Tallahassee, Fla. (DF = 0.47)	Asphalt concrete	14.5	10.9	10.6
	Gravel base	0.0	0.0	0.0

Note: A = AASHO SN with $a_1 = 0.42$, p = 2.5; B = AASHO SN with variable a_{1e} [layer coefficient corresponding to the effective modulus (Equation 12)], p = 2.5; C = AASHO design with DF modification, p = 2.5. 1 cm = 0.39 in.

2. Had the effect of climate been included in the AASHO design by judiciously varying the effective asphalt layer coefficent as a function of effective modulus, a correct pavement design would have been obtained. The good agreement between the designs in the last two columns of Table 7 confirms this assertion.

These examples reaffirm the previous conclusions: namely, that the DF concept is a useful measure in assessing the relative effect of environment on pavement and that this concept could serve as a guide for personnel who allocate federal funds to projects in various parts of the country.

REFERENCES

1. Interim Guide for the Design of Pavement Structures. AASHTO, Washington, D.C., 1974.
2. T.R. Buick. Analysis and Synthesis of Highway Pavement Design. Joint Highway Research Project, Purdue University, West Lafayette, Ind., 1968.
3. S.H. Carpenter, M.I. Darter, and B.J. Dempsey. Evaluation of Pavement Systems for Moisture-Accelerated Distress. In Transportation Research Record 705, TRB, National Research Council, Washington, D.C., 1979, pp. 7-13.
4. Climatological Data National Summary, 1941-1970. Weather Bureau, U.S. Commerce Department, 1970.
5. K.B. Woods and C.W. Lovell, Jr. Distribution of Soils in North America. In Highway Engineering Handbook, Section 9, McGraw Hill, New York, 1960.
6. H.L. Von Quintus, F.N. Finn, W.R. Hudson, and F.L. Roberts. Flexible and Composite Structures for Premium Pavements, Vols. 1 and 2. Report FHWA-RD-80. FHWA, U.S. Department of Transportation, Dec. 1979.
7. M.Y. Shahin. Design System for Minimizing Asphalt Concrete Thermal Cracking. Proc., Fourth International Conference on Structural Design of Asphalt Pavements, University of Michigan, Ann Arbor, Aug. 1977.
8. E.J. Yoder and M.W. Witczak. Principles of Pavement Design, 2nd ed. Wiley, New York, 1975.

Publication of this paper sponsored by Committee on Flexible Pavements.

Seasonal Load Limit Determined by the Criterion of Uniform Failure Rate

MICHAEL S. MAMLOUK

ABSTRACT

Efficient performance of our highway system requires rational optimization of its use within the constraints of the adopted strategy. During the spring-thaw season in the northern part of the United States many highway agencies reduce the maximum load limits on some roads in an attempt to preserve the pavement serviceability. The selection of such a reduced load limit is not well defined now. A rational method has been developed that suggests that the load limit should be reduced in such a way to maintain a uniform rate of pavement deterioration throughout the year. The method considers various types of pavement failure such as fatigue cracking, rutting, and roughness and combines them by using the AASHO serviceability index. If the properties of the pavement materials are determined, mechanistic approaches can be used to predict the failure trend and to adjust the axle load limit to maintain the uniformity of this trend. A computer program LOADLMT has been developed in order to determine the optimum seasonal axle load limit on flexible pavements under various conditions. The use of the method was verified on a typical road under typical traffic distribution, material properties, and environmental conditions. The adoption of a seasonal load limit determined by this method indicates a large extension of the useful life of the road. The concept of this method is compared with other criteria currently used.

With the rapid aging of highway pavements, the public demand for higher levels of service, and the escalating rates for labor, equipment, and materials, highway operations should be performed according to a scientifically based procedure. A good understanding of the pavement behavior under various conditions and a rational optimization of such behavior within the constraints of the adopted strategy would result in efficient road performance.

The deterioration of pavement because of traffic and aging causes the serviceability of the road to decrease. The rate of decrease of serviceability varies depending on the amount of traffic, material properties, and environmental conditions. During

the spring-thaw season in the northern part of the United States the strength and stiffness of the subgrade soils and the unbound granular layers within the pavement section are decreased because of the increased moisture content that results from the melting ice. The loss of bearing capacity during the spring-thaw period is a recognized effect of frost action that severely impairs the performance of pavements. Under the same traffic conditions the permanent loss in pavement serviceability during a brief period in the spring may equal or exceed the loss during the rest of the year (1). One of the methods used by many highway agencies to preserve pavement serviceability on low-volume roads is to impose a low maximum load limit during the spring break-up period. The seasonal load limit is recognized by highway agencies; however, the selection process, which is the subject of this paper, is not well rationalized.

BACKGROUND

At this time the magnitude of the seasonal load limits, the dates of their imposition, and the duration of the restricted period are usually based on local experience (2). Empirical as well as mechanistic methods have been developed recently in at attempt to rationalize the criteria for a seasonal load limit. An empirical approach was introduced in NCHRP Report 76 (3) in which pavement deflection measurements were used. It was suggested that a load-limit restriction be imposed during the critical season in regions with a mean freezing index exceeding 200 degree-days and in which the average normal Dynaflect surface curvature index (SCI) measured during the previous fall exceeded 0.35 milli-in. The selection of the load-limit value is based on the assumption that the maximum safe axle load (L_s) that can be applied to a given highway during the critical period is inversely proportional to the maximum (peak) SCI measured during that period:

$$L_s = k/\text{maximum SCI} \quad (1)$$

where the constant k is equal to 6.3 and the maximum SCI is twice the normal SCI. Although this method is relatively simple and nondestructive, it does not relate the load-limit criteria directly to pavement damage. The method is also based on observations and correlations developed for specific in-service pavements that do not necessarily represent pavements in other regions. Therefore, the method is restricted to the soil types and conditions considered in the original investigation. For example, the maximum and the normal SCI values were linearly related, which may not be the case with other soil types and conditions.

Another common method used by some highway agencies is to limit the axle load based on the criterion of maintaining equal pavement surface deflection measured by a deflection-measuring device such as the Benkelman beam or the Dynaflect during the spring-thaw and summer-fall conditions. Although the method is also simple and nondestructive, it does not relate the load limit directly to pavement failures such as fatigue cracking, rutting, or roughness (slope variance). By reviewing the different factors affecting various modes of flexible pavement failure, fatigue cracking can be related to the number and magnitude of load repetitions, the horizontal strain at the bottom of the asphalt-bound layer, pavement temperature, and the fatigue properties of the asphalt-bound materials. Rutting, on the other hand, is the accumulation of permanent deformation with the increase in the number of wheel-load repetitions. Each increment of permanent deformation is a function of the deflection response, the number of previous repetitions, and the permanent deformation properties of the system. Moreover, roughness is a function of variability of the material properties and poor construction control. Therefore, the concept of controlling the load limit to obtain equal pavement surface deflections (recoverable or permanent or both) in the spring-thaw and summer-fall conditions measured by a deflection-measuring device does not necessarily produce the same rate of failure consumption.

A more rational mechanistic approach was developed (2) that assumes that the flexible pavement damage is due to fatigue cracking of the asphalt-bound layer. In this method, the maximum axle load allowed during the spring-thaw period is restricted to that which produces a horizontal (critical) tensile strain at the bottom of the asphalt-bound layer equal to the strain produced by the maximum legal axle load that is allowed during the normal summer-fall period. It is further assumed that if the number of heavy axle loads does not vary seasonably, the selected criterion will result in a uniform rate of damage and fatigue life consumption throughout the year. The study suggests the use of an elastic-layer computer program to calculate the horizontal tensile strain previously mentioned. The study also estimates the saving in the remaining pavement service life if the proposed load-limit method is used with respect to the remaining life when the equal-surface-deflection method is used or when no special seasonal load limit is imposed.

Although the fatigue-based criterion for seasonal load limit discussed earlier (2) is more rational than empirical approaches, some assumptions are oversimplified and are not fully justified, as discussed in the following:

1. It was assumed that the thaw weakening affects the fatigue behavior of the pavement only. Obviously slope variance and rutting are also affected by thaw weakening. In fact, slope variance and rutting contribute to flexible pavement serviceability more than fatigue cracking (4). The fatigue-based criterion may be efficient if previous experience shows that fatigue cracking is the critical type of failure for the specific condition.
2. All axle loads were implicitly assumed to have one magnitude, which was the maximum axle load limit. No consideration was given to the actual axle load distribution, although different axle loads contribute to pavement failure.
3. Only single axle loads were considered, and no consideration was given to tandem axle loads.
4. In the calculation of the remaining fatigue life under various seasonal load limits, it was assumed that the monthly number of axles remains the same during the year even when a lower axle load limit is imposed during the spring-thaw season. In fact, when a low axle load limit is imposed, some heavy trucks select other routes, which results in reducing the number of axles on the road.
5. The study assumed linear-elastic material properties, which do not represent the true material behavior and which neglect any permanent deformation (rutting and slope variance).

It is important to impose a seasonal load limit that optimizes the use of the road and its remaining useful life on a rational basis. If too low a load limit is imposed, the pavement may last longer but the use of the road might not be efficient as far as transportation is concerned. On the other hand, a load limit equal to or close to the normal load limit may result in fast pavement deterioration. A new concept, the criterion of uniform failure rate for

TABLE 1 Material Properties for Summer-Fall and Spring-Thaw Conditions

Material Property	Summer-Fall Conditions[a]				Spring-Thaw Conditions[b]			
	Surface	Base	Subbase	Subgrade	Surface	Base	Subbase	Subgrade
Modulus (psi)	532,000	20,000	10,000	5,000	900,000	20,000	10,000	3,000
Poisson's ratio	0.35	0.40	0.40	0.45	0.35	0.40	0.40	0.45
Fatigue properties								
K_1	0.918×10^{-2}	–	–	–	0.932×10^{-5}	–	–	–
K_2	3.08	–	–	–	3.14	–	–	–
Permanent deformation properties								
μ	0.06	0.04	0.05	0.06	0.035	0.04	0.05	0.07
α	0.75	0.75	0.75	0.85	0.75	0.75	0.75	0.65

Note: For detailed testing procedure, see report on VESYS program *(5)*.
[a]Average values for June through February.
[b]Average values for March and April.

TABLE 2 Current Axle Load Distribution in the Design Lane

Single Axle		Tandem Axle	
Axle Load (kips)	No./Day	Axle Load (kips)	No./Day
22	30	36	35
20	35	34	40
18	50	32	60
16	65	30	70
14	70	28	50
12	60	26	50
10	50	24	30

Note: Current daily 18-kip EALs = 500; traffic growth rate = 3 percent per year.

a 2-month period with both summer-fall and spring-thaw conditions and to adjust the spring load limit to maintain the difference in PSI within a tolerance of 0.1. It was found that the maximum single-axle and tandem-axle loads during the spring-thaw period should be 14 and 28 kips, respectively. In this case the change in the serviceability index during the 2 months of spring thaw was 0.103, whereas the corresponding change during 2 months within the summer-fall period was 0.025, a difference of 0.078.

The original VESYS computer program (5) was further used to investigate the trend of pavement failure with and without the seasonal load limit. The trends of the failure components--fatigue cracking index, rut depth, and slope variance--in the two cases are shown in Figures 4, 5, and 6. On the other hand, the trends of the serviceability index in the two cases are shown in Figure 7. It is noted that the trends of the individual pavement failure types are not uniform under the seasonal load limit condition. However, the trend of serviceability index under this condition is uniform, as shown in Figure 7. Also, if the terminal serviceability index is 2, the pavement is expected to reach the end of its useful life after 3.3 years without the seasonal load limit, whereas it is expected to last for 7 years with the seasonal load limit.

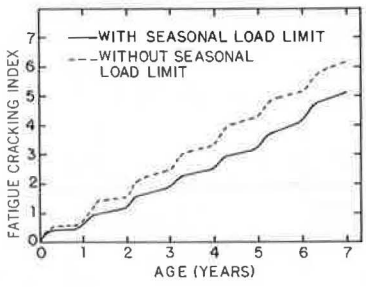

FIGURE 4 Fatigue cracking index versus age with and without seasonal load limit.

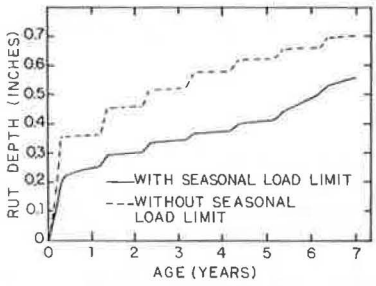

FIGURE 5 Rut depth versus age with and without seasonal load limit.

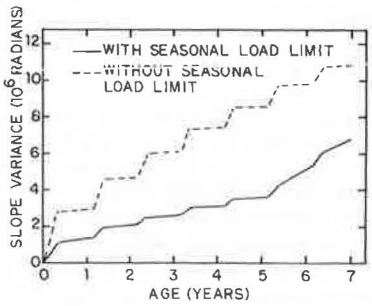

FIGURE 6 Slope variance versus age with and without seasonal load limit.

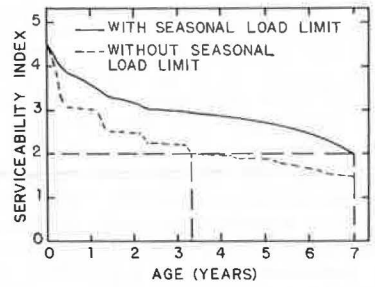

FIGURE 7 Serviceability index versus age with and without seasonal load limit.

In this example a comparison was made between the criterion of uniform failure rate and the equal deflection and the fatigue-based criteria by using the VESYS computer program. The results indicate that if the equal deflection criterion is used, a seasonal single-axle load limit of 18 kips should be imposed. On the other hand, if the fatigue-based criterion is used, no special seasonal load limit should be imposed because the horizontal tensile strains at the bottom of the asphalt-bound layer under the assumed properties for the spring-thaw and summer-fall conditions are close. Obviously this comparison is applicable for this example only. In general the criterion of uniform failure rate should provide more conservative seasonal load limits than those obtained by the fatigue-based criterion because the former considers various types of pavement failure and not just fatigue cracking.

CONCLUSION

Because of the weakening process in the pavement structure during the spring-thaw period it is necessary to impose a low load limit during that period for many secondary roads in the United States. A rational method of selecting this load limit is discussed and compared with other empirical and mechanistic methods. In this method the load limit should be reduced in such a way to maintain a uniform rate of pavement failure throughout the year. Various pavement failure types should be considered, such as fatigue cracking, rutting, and roughness. If the properties of the pavement materials under the summer-fall and spring-thaw conditions are determined, mechanistic techniques can be used to predict the failure trend and to adjust the axle load limit to maintain the uniformity of the pavement failure rate. In this study the computer program LOADLMT has been developed by modifying the FHWA computer program VESYS-3-A in order to determine the optimum seasonal axle load limit. The use of the method was verified by determining the seasonal load limit for a typical road under typical traffic distribution, material properties, and environmental conditions. The adoption of the seasonal load limit by using this method indicates a large extension of the useful life of the pavement. The results were compared with those obtained with other criteria. It is believed that the results obtained from this method would be more accurate than those from other methods. Although the proposed method is sophisticated, its use is justified in view of the escalating rate of highway maintenance.

REFERENCES

1. Roadway Design in Seasonal Frost Area. NCHRP Synthesis of Highway Practice 26. TRB, National Research Council, Washington, D.C., 1974, 104 pp.
2. J.H. Hardcastle, R.P. Lottman, and T. Buu. Fatigue-Based Criteria for Seasonal Load Limit Selection. In Transportation Research Record 918, TRB, National Research Council, Washington, D.C., 1983, pp. 22-30.
3. F.H. Scrivner, R. Peohl, W.M. Moore, and M.B. Phillips. Detecting Seasonal Changes in Load-Carrying Capabilities of Flexible Pavements. NCHRP Report 76. HRB, National Research Council, Washington, D.C., 1969, 37 pp.
4. E.J. Yoder and M.W. Witczak. Principles of Pavement Design, 2nd ed. Wiley, New York, 1975.
5. W.J. Kenis. Predictive Design Procedures, VESYS User's Manual--An Interim Design Method for Flexible Pavements Using VESYS Structural Subsystem. Final Report. FHWA, U.S. Department of Transportation, Jan. 1978, 128 pp.

Publication of this paper sponsored by Committee on Flexible Pavements.

Use of Surface Deflection for Pavement Design and Evaluation

A.F. STOCK and J. YU

ABSTRACT

Most current mechanistic pavement design methods are based on strain calculated at the bottom of the asphalt layer and the top of the subgrade. Because the only part of a pavement that is reasonably accessible when construction has been completed is the surface, it is virtually impossible to verify for a design that the parameters have actually been met. The ability of the engineer to check the design will therefore be greatly enhanced if a parameter based on surface deflection can be used. The development of just such a parameter, which has been called the tangent slope, is reported. This parameter is the slope of the tangent drawn from the point of maximum deflection of the pavement to graze its surface. A sensitivity analysis is reported in which the tangent slope is compared with several other parameters based on surface deflection as well as the conventional asphalt and subgrade strains. The calibration by back analysis of the tangent slope against current practice is presented so that it can be used as a design parameter, although its principal use may be as a tool for the structural evaluation of existing pavements and for validating designs.

Mechanistic pavement design techniques for asphalt pavements have been developed to a degree that permits their application with a significant measure of confidence. The Fourth International Conference on the Structural Design of Asphalt Pavements (1) in 1977 was a milestone in the development of these methods; it was devoted almost entirely to the presentation of complete design systems or subsystems. Although mechanistic design is a reality and has been for some years, it is not widely accepted or applied.

One of the reasons for this is the difficulty of checking in the short term that the response of the pavement structure is as predicted. When the principles of structural design are applied to most structural problems, it is relatively easy to check a prediction of the response of the structure against a measured response. Deformation at preselected points is usually a convenient parameter. Mechanistic design of pavements uses response parameters that are difficult to measure. For example, the two most widely used parameters, selected on the basis of a considerable volume of research, are tensile strain at the bottom of the asphalt layer and vertical strain on the subgrade. They are difficult to measure, and so a designer who would like reassurance with regard to the precision of his calculations cannot obtain it.

In addition, pavements are designed for a life measured in terms of many years. Thus traditional validation of mechanistic design methods by full-scale trials will require many years of observation of many pavements.

On both national and international scales, changes in economic conditions have become relatively rapid, and most countries are facing an economic recession. The consequences of this for pavement engineers appear to be that heavy vehicles become heavier and that the resources available for the maintenance of the pavements are decreasing. Thus, in order to maintain and reconstruct the highway network pavement engineers need to use the flexibility in terms of material selection and structural design available to them through the application of mechanistic techniques to flexible pavements.

It is therefore necessary to develop design parameters that can be checked in the traditional manner, by comparing a prediction with a measurement. The only part of a completed pavement readily available for inspection is the surface. So it would seem appropriate to attempt to develop a relationship between pavement life and some characteristics of the deflected shape of the surface of a loaded pavement that is sensitive to structural parameters such as layer thickness and material properties.

Research carried out in an attempt to develop a parameter to meet the requirement of sensitivity based on an analysis of the shape of the surface of a loaded pavement is reported here.

SURFACE DEFLECTION PARAMETERS FOR PAVEMENTS

The best-known surface deflection parameter is the maximum deflection of a point on the surface as measured by the Benkelman beam or similar device. However, the limitations of this single parameter, i.e., that two different pavements may have the same maximum deflection but different deflection profiles, are well known and are shown in Figure 1. Because it is accepted that the strain in the asphalt is an important parameter in the definition of its performance and that this strain is related to the shape of the deflected surface, the inability of a single deflection measurement to differentiate between the two pavements as described earlier is a serious deficiency.

Recognition of this problem has led to the development of several alternative parameters. A literature review undertaken at the start of this research yielded the following parameters:

1. Radius of curvature (R),
2. Deflection ratio (DR),
3. Spreadability (SP),
4. Bending index (BI),
5. Radius of influence (RI), and
6. Slope of deflection (SD).

Formulas for determining these parameters and their sources are presented in Table 1.

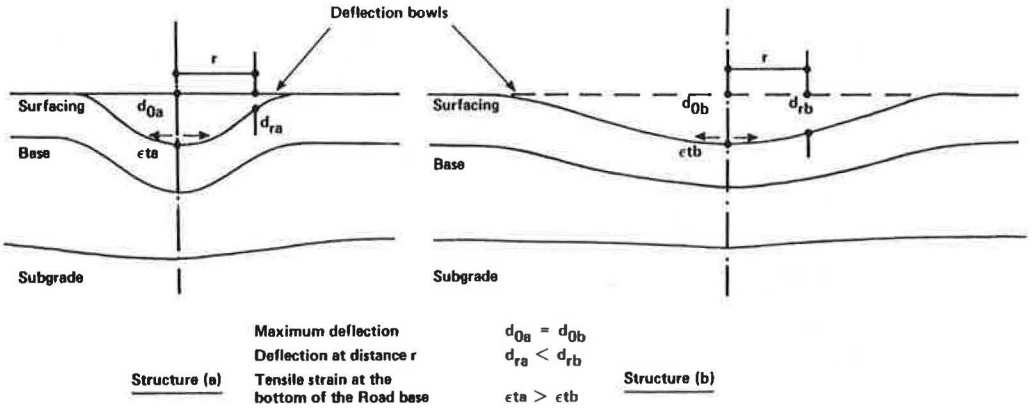

FIGURE 1 Pavements with same maximum deflections but different deflection profiles.

TABLE 1 Parameters Based on Surface Deflection

Parameter	Formula	Source
Radius of curvature[a]	$R = r^2/2d_0[(d_0/d_r) - 1]$	Miura and Tobe *(2)*
Deflection ratio[b]	$DR = d_r/d_0$	Claessen et al. *(3)*
Spreadability[c]	$SP = [(d_0 + d_1 + d_2)/3d_0] \times 100$	Rufford *(4)*
Bending index	$BI = d_0/a$	Hveem *(5)*
Radius of influence	$RI = R^1/d_0$	Ford and Bisselt *(6)*
Slope of deflection[d]	$SD = \tan^{-1}[(d_0 - d_r)/r]$	Kung *(7)*

Note: r = radial distance from center of load; d = deflection (0 = center of load, r = radial distance, 1,2 = locations 1 and 2); a = one-fourth length of deflection basin; R^1 = distance from point of maximum deflection to where curve becomes tangential to horizontal.
[a] r and radius for $d_r = 127$ mm.
[b] Radius for $d_r = 600$ mm.
[c] d_1 and d_2 measured at 300 and 600 mm from the load, respectively.
[d] r and radius for $d_r = 610$ mm.

Development

Development of the parameter described in the following is based on the assumption that elastic-layer analysis, which is widely used for mechanistic design, will be used for the prediction. Because elastic-layer analysis provides a reliable representation of the slope of the deflected surface but can be in error with regard to the magnitude of the deflections (R. Koole, unpublished data), it is necessary that parameters developed take account of this. That is, deflection-based parameters should describe the shape of the surface and be independent of the absolute magnitude of the deflection at any point.

Preliminary analysis of pavement structures with the BISTRO (8) program indicated that if a dual-wheel load is considered, the location of the point of maximum deflection is not consistently beneath one of the wheel loads. It could occur between the two. Also, if the locations of the points of maximum deflection at given radii from the load are plotted, they cannot be connected by a straight line, which indicates that near the dual-wheel load the deflected surface has an inconveniently complex shape.

As a result of this preliminary investigation of the surface under dual wheels and because many devices used for pavement evaluation apply loads through one point only, the investigation was restricted to surfaces loaded by one point only.

Definition

Preliminary investigation indicated that the slope of a line drawn outward from the point of maximum deflection to touch but not intersect the surface would meet the requirement of describing the deflected shape and be independent of the absolute magnitude of the deflection.

This line may be considered a tangent to the surface and hence the pavement response parameter has been labeled the tangent slope (TS). Figure 2 shows the parameter.

The tangent slope can be expressed as follows:

$$TS = (dmax - dx)/x \quad (1)$$

where

dmax = maximum deflection (mm),
dx = deflection at the tangent point (B) (mm), and
x = distance of the tangent point from the point of maximum deflection (m).

CALCULATION PROCEDURE

The procedure for calculating the slope of the tangent is as follows. The deflection of the surface under a dynamic load is measured. A curve to describe the deflected surface is fitted through the measured deflections. This function is then solved simultaneously with the equation of a straight line, the tangent. Because the coordinates of the point of maximum deflection and of the tangent point are known, the slope of the line joining these two points, that is, the tangent slope, can be calculated.

Measurement of Surface Deflection

It is desirable to measure the surface deflection at as many points as possible. This will permit greater flexibility in fitting a curve to the measurements and will provide a more precise curve. However, the device currently available for the measurement of surface deflection has a limited number of sensors, and so for practical reasons it is desirable to define the minimum number of measuring points that will produce satisfactory data. It is also necessary

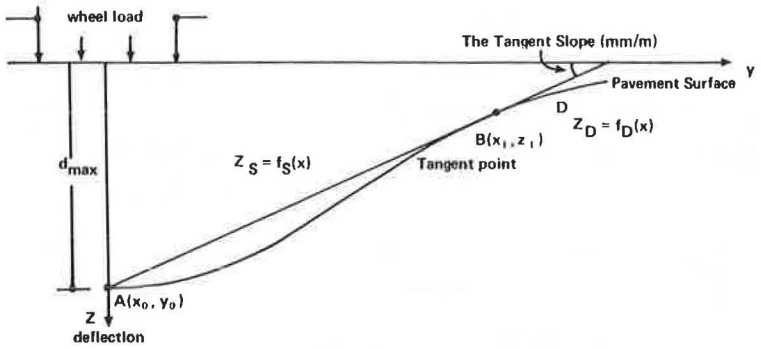

FIGURE 2 Tangent slope.

to obtain some information with regard to the preferred location of the sensor. These two questions were examined by calculating a deflected slope for pavements with a wide range of material properties and layer thicknesses. Sensitivity analyses were then undertaken to assess the effect of measuring deflections at a limited number of points and to define a practical maximum distance from the load for the farthest measuring point.

Deflection profiles were calculated for a large number of pavement structures ranging from relatively flexible layers to stiff ones. This analysis indicated that tangent points would not be more than 1.2 m from the load, which set a practical limit for the location of the farthest measuring point. Because the spacing and number of measuring points are pertinent to fitting a curve to the surface, this will be discussed in the next section.

Fitting a Curve to Deflected Surface

A curve-fitting routine that employs Chebyshev polynomials was selected to represent the deflected surface of the pavement (9). This system has particular advantages in that it can avoid some of the difficulties encountered in solving ill-conditioned simultaneous equations that are sometimes encountered with least-squares curve fitting and also can eliminate situations that may lead to loss of numerical accuracy.

With regard to curve fitting, it is necessary to have data at more points than the order of the polynomial. Ideally the number of measurement points should be at least twice the order of the polynomial; the minimum requirement is one more than the order. Thus for convenience and economy with respect to measuring the surface deflection it is advantageous to determine the lowest-order polynomial that provides a reasonable representation of the shape of the surface. In order to provide information on which to base a decision with respect to the order of polynomial required, the deflection data calculated for several structures were analyzed.

In order to assess goodness of fit the root-mean-square value of the residuals (RMSR) was examined. As the order of the polynomial increases, the RMSR decreases to a fairly constant value. Use of a polynomial with higher order than the first one with the low RMSR will not effectively improve the representation of the data and will increase the risk of unnecessary fluctuations between the data points.

This study examined polynomials of the third, fourth, and fifth order. It was concluded that little improvement in precision was obtained by using functions above the third order. In addition the value of the tangent slope did not change appreciably when the polynomial order was changed. Thus a third-order polynomial should be sufficient for most purposes. This permits a minimum of four measurements of surface deflection for the derivation of the tangent slope. However, reliability and precision will be improved if measurements are made at more points.

In order to calculate the tangent slope it is necessary to locate the tangent point. This is done by using the equation of the curve representing the deflected surface and the equation of the tangent (Equations 2 and 3):

$$Z_d = f_d(x) \tag{2}$$

$$Z_s = f_s(x) \tag{3}$$

The following conditions are necessary for the solution:

1. The slope of the curve at the tangent point must equal the slope of the straight line; i.e., $dz_s/dx = dz_d/dx$ at $x_1 z_1$;
2. The curve must pass through the point x, z: $z_d = z_1 = f_d(x_1)$.

There are two difficulties that may arise when this method is used for calculating the tangent slope. The first is the possibility that more than one tangent point exists. This will be caused by fluctuations between data points when high-order polynomials are used. This difficulty should not arise with the low-order polynomials recommended, and the danger can be further reduced by using more than the minimum number of measurement points.

The second problem may arise if the tangent point is further than 1.2 m from the load. If this is so, the maximum deflection will be small and the tangent slope will not be affected significantly by assuming that the tangent point is 1.2 m from the load.

COMPARISON OF PAVEMENT RESPONSE PARAMETERS

A sensitivity analysis was undertaken to compare various response parameters with the tangent slope. The following parameters were selected from Table 1: radius of curvature, deflection ratio, spreadability, and slope of deflection.

In addition the two commonly used response parameters, tensile strain at the bottom of the bituminous layer (ET) and vertical strain on the subgrade (EV), were included with the maximum resilient deflection (dmax). The sensitivity of these response parameters was investigated with respect to a simple three-layer structure of asphalt, unbound material, and subgrade; the principal structural variables

were the thickness of the asphalt, the stiffness of the asphalt, the modulus of the subgrade, and the magnitude of the applied load. Two thicknesses of granular layer, 200 and 700 mm, were also used for the study, but because this variation had little effect on most of the parameters concerned, the results have been omitted from the discussion. In Figure 3 the structures studied are summarized.

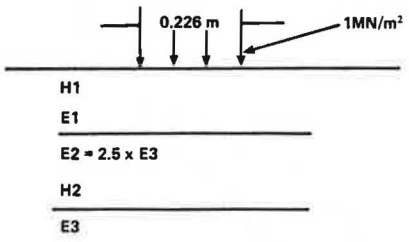

H2	0.2		
Parameters / Structures	H1 (m)	E1 (MN/m²)	E3 (MN/m²)
1	A	5000	30
2	0.24	B	30
3	0.24	5000	C
4(D)	0.24	5000	30

A : H1 varied : 0.12, 0.18, 0.24, 0.2, 0.26 m
B : E1 varied : 3000, 5000, 7000, 9000, 1100 MN/m**2
C : E3 varied : 30, 55, 80, 120, 150 MN/m**2
D : Applied stress varied : 0.7, 1.0, 1.35, 1.75, 2.0 MN/m**2

FIGURE 3 Pavement structures used in study of sensitivity of several evaluation parameters.

In order to compare the individual parameters that have a range of dimensions and magnitudes, it was necessary to transform them into dimensionless parameters. This was accomplished by defining the parameter sensitivity (S) as follows:

$$S = [|P_1 - P_i|/P_m] \times 100 \quad (4)$$

where

P_1 = the first value of the response parameter,
P_i = the ith value of the response parameter, and
P_m = the maximum value of the response parameter for the structural variable under consideration.

This transformation ensures that the parameter sensitivity is always an increasing curve and that no value of S exceeds 100 percent and permits a comparison of the rate of change of the parameter independent of its magnitude. The results of this study are plotted in Figures 4 to 7 and will be discussed in the following.

Thickness of Asphalt Layer

The sensitivity of the various parameters is plotted as a function of the thickness of the asphalt layer in Figure 4. The rate of change of sensitivity of all parameters decreases as the thickness increases. The response parameters are clearly ranked with the tensile strain in the asphalt and the slope of deflection; the tangent slope is the most sensitive and spreadability the least.

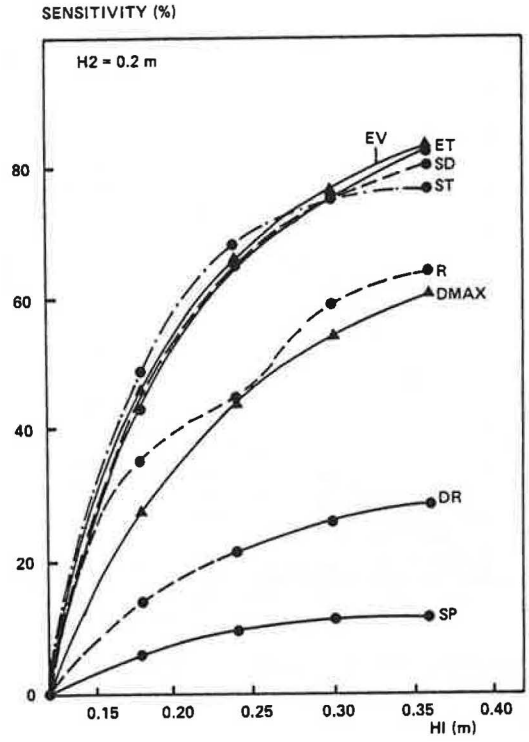

FIGURE 4 Sensitivity as function of asphalt stiffness in structure 1.

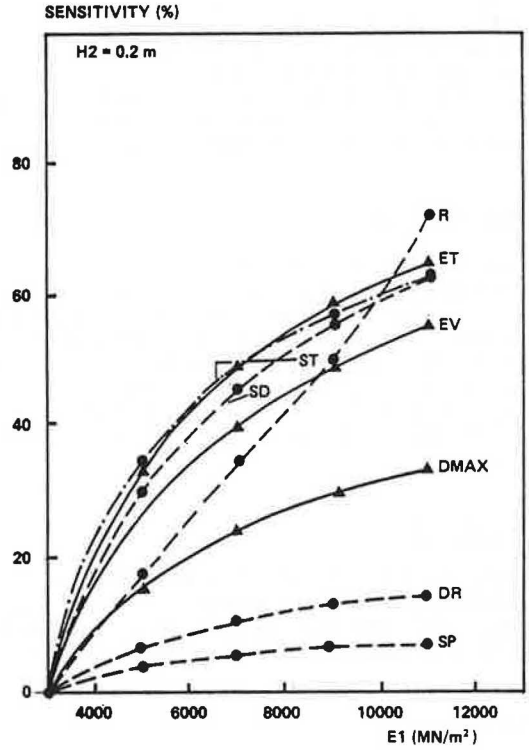

FIGURE 5 Sensitivity as function of asphalt stiffness in structure 2.

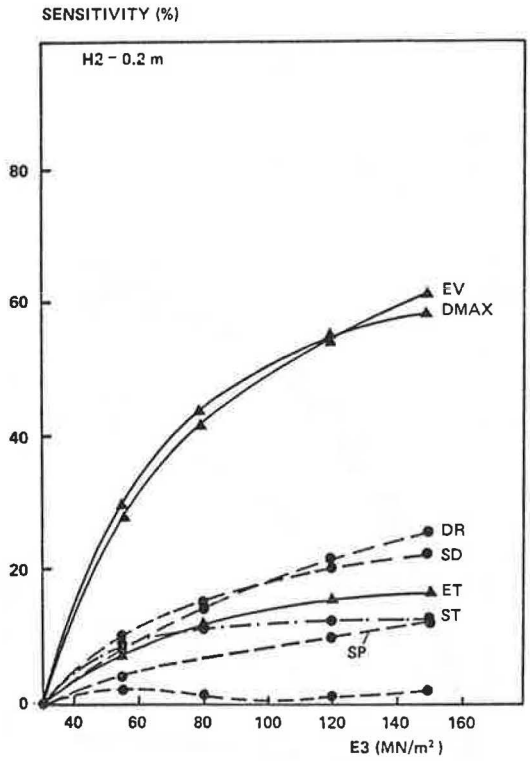

FIGURE 6 Sensitivity as function of subgrade modulus in structure 3.

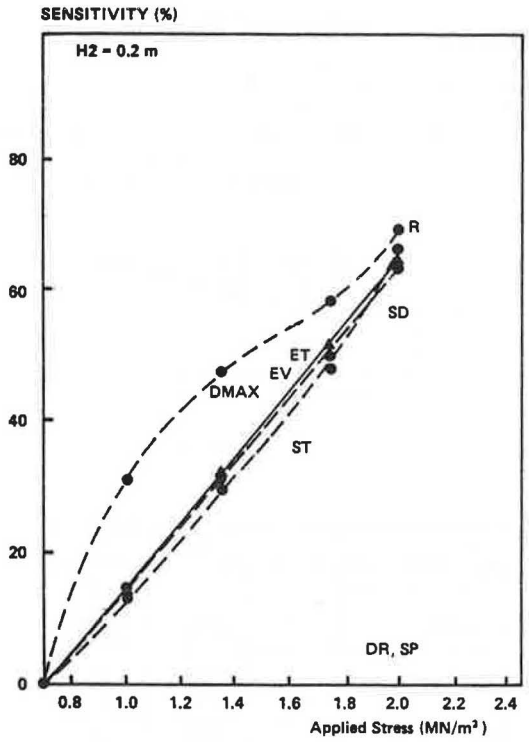

FIGURE 7 Sensitivity as function of applied stress in structure 4.

Stiffness of Asphalt Layer

Figure 5 is a plot of sensitivity as a function of the stiffness of the asphalt layer. With the exception of the radius of curvature, the response parameters are ranked in the same order as those for sensitivity to the asphalt layer thickness, although they tend to fall into distinct groups. The radius of curvature exhibits the useful characteristic of a uniform rate of change with respect to asphalt stiffness and is most sensitive to stiffness at the maximum value selected for this study.

Subgrade Stiffness

The nonlinear model for granular material proposed by Stock and Brown (10) was used for this part of the study. Figure 6 indicates that most parameters are insensitive to variation of subgrade moduli. The exceptions are maximum deflection and the vertical strain on the subgrade. It is particularly noticeable that the radius of curvature hardly changes at all throughout the wide range of subgrade moduli studied.

Applied Stress

As shown in Figure 7, all the parameters calculated show virtually identical sensitivity to the applied load with the exception of the radius of curvature, which is more sensitive except at high stresses.

DISCUSSION

It is clear that none of the eight parameters considered is sensitive to all the structural variables considered. In general spreadability and deflection ratio are insensitive. The two strain parameters are consistently sensitive to the structural parameters investigated, although they are of course difficult to verify in a full-scale structure. Radius of curvature appears to be useful with respect to asphalt thickness and stiffness and applied stress. However, its total insensitivity to subgrade modulus eliminates it as a parameter in its own right.

The tangent slope generally compares well with the other parameters, although it is relatively insensitive to subgrade modulus. However, if it is used in conjunction with maximum deflection, which must be measured in order to calculate the tangent slope, this deficiency is eliminated. An especially successful combination of parameters is radius of curvature and maximum deflection.

CALIBRATION OF TANGENT SLOPE AGAINST CURRENT PRACTICE

In order to improve the value of the tangent slope as a parameter for pavement assessment, it was calibrated against RN29 (11) structures by a process of back analysis. This procedure has been adopted by other research workers and has been widely used for the development of the subgrade strain criteria (12).

RN29 permits three types of base material for pavements: unbound granular material (13), bitumen macadam (14), and hot rolled asphalt (15). Figure 8 is a plot of tangent slope against design life for each of the three types of structures.

CONCLUSIONS

None of the response parameters compared in this study is sensitive to variations in all the possible

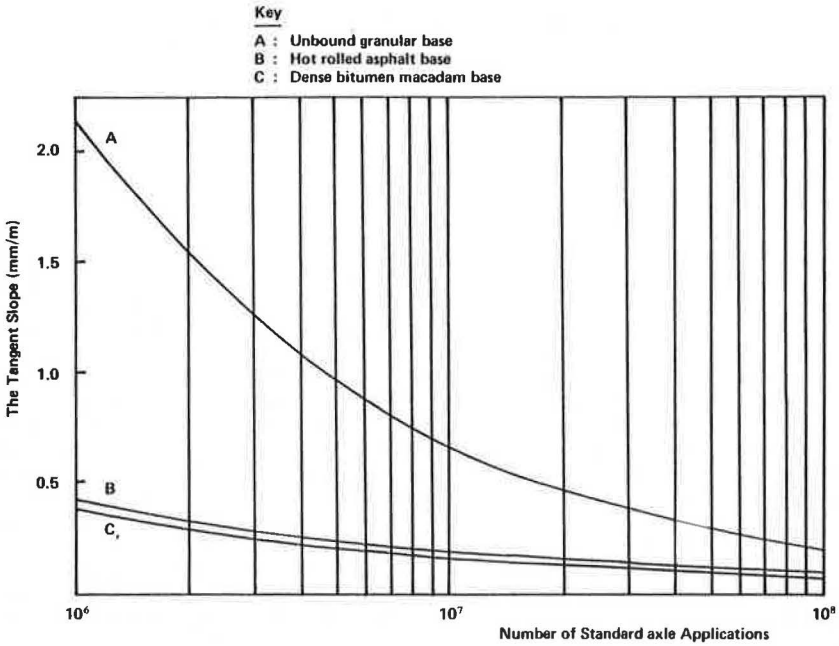

FIGURE 8 Tangent-slope values for typical RN29 structures.

structural parameters in a pavement. The tangent-slope response parameter is adequately sensitive to most structural parameters. It includes variations in both maximum deflection and the shape of the deflected surface and can therefore describe a pavement unambiguously.

ACKNOWLEDGMENT

The authors would like to thank Imperial Chemical Industries, Ltd., for financial and technical assistance during this project. The support of A.E. Vardy, head of the Department of Civil Engineering at Dundee University, is also acknowledged, as is the assistance of the Computing Centre.

REFERENCES

1. Proc., Fourth International Conference on the Structural Design of Asphalt Pavements. University of Michigan, Ann Arbor, 1977.
2. Y. Miura and R. Tobe. Evaluation of Existing Pavements Based on Deflection and Radius of Curvature and Overlay Design. Proc., Fourth International Conference on the Structural Design of Asphalt Pavements, University of Michigan, Ann Arbor, 1977.
3. A.I.M. Claessen, C.P. Valkering, and R. Ditmarsch. Pavement Evaluation with the Falling Weight Deflectometer. Proc., AAPT, Vol. 45, 1976.
4. P.G. Rufford. A Pavement Analysis and Structural Design Procedure Based on Deflection. Proc., Fourth International Conference on the Structural Design of Asphalt Pavements, University of Michigan, Ann Arbor, 1977.
5. F.N. Hveem. Pavement Deflection and Fatigue Failures. Bull. 114. HRB, National Research Council, Washington, D.C., 1955, pp. 43-73.
6. M.C. Ford, Jr., and J.R. Bisselt. Flexible Pavement Performance Studies in Arkansas. Bull. 321. HRB, National Research Council, Washington, D.C., 1962, pp. 1-15.
7. K.Y. Kung. A New Method in Correlation Studies of Pavement Deflection and Cracking. Proc., Second International Conference on the Structural Design of Asphalt Pavements, University of Michigan, Ann Arbor, 1967.
8. M.G.F. Peutz, A. Jones, and H.P.M. van Kempen. Computer Program BISTRO: Layered Systems under Normal Loads. External Report. Koniniklijke/Shell Laboratorium, Amsterdam, Netherlands, 1967.
9. M.G. Cox and J.G. Hayes. Curve Fitting: A Guide and Suite of Algorithms for the Non-Specialist User. Report NAC26. National Physical Laboratory, Teddington, Middlesex, England, 1973.
10. A.F. Stock and S.F. Brown. The Nonlinear Characterization of Granular Materials for Asphalt Pavement Design. In Transportation Research Record 755, TRB, National Research Council, Washington, D.C., 1980, pp. 14-20.
11. A Guide to the Structural Design of Pavements for New Roads, 3rd ed. TRRL Road Note 29. U.K. Transport and Road Research Laboratory, Crowthorne, Berkshire, England, 1970.
12. S.F. Brown, P.S. Pell, and A.F. Stock. The Application of Simplified Fundamental Design Procedures for Flexible Pavements. Proc., Fourth International Conference on the Structural Design of Asphalt Pavements, University of Michigan, Ann Arbor, 1977.
13. Specification for Road and Bridgeworks. TRRL, Crowthorne, Berkshire, England, 1969.
14. Coated Macadam for Roads and Other Paved Areas. B.S. 4987. British Standards Institution, London, 1973.
15. B.S. 594. British Standards Institution, London, 1973.

Publication of this paper sponsored by Committee on Flexible Pavements.

Structural Comparison of Two Cold Recycled Pavement Layers

ADRIAAN J. van WIJK

ABSTRACT

The structural strengths of two cold recycled pavements are compared. One recycled pavement section was built with foamed asphalt as a binder and the other with emulsion as a binder. Cores and deflection measurements were taken at different times after construction. The comparisons were based on results of tests on the cores, Dynaflect deflections, and strength indicators as well as developed AASHTO layer coefficients. The comparisons showed that the stiffness and strength of both recycled sections increased during the first 400 days after construction. The strength of the foamed-asphalt section increased more rapidly than that of the emulsion section during the first 250 days. The strengths and stiffnesses of the foamed-asphalt recycled section were slightly higher than those of the emulsion recycled section during most of the evaluation period, but the differences were small. Ranges of layer coefficients were developed that can be used in design of similar layers. These ranges indicate that the two recycled layers should perform about the same. The initial cost will therefore be the controlling factor in an economic analysis of these two types of recycled pavements.

Recycling of pavements has received widespread attention during the last 7 or 8 years, mainly because of energy and financial restraints. Recycling has the potential of reducing highway construction and rehabilitation costs. Actual cost savings can be evaluated only if the performance of the recycled section is known, because a proper economic evaluation can be conducted only when the initial as well as the life-cycle costs are known. An estimate of the performance of a pavement is essential in the effective comparison of alternatives and in pavement management. The major disadvantage of recycling, especially cold-asphalt recycling, is that relatively little is known about the performance of these layers. Practitioners (1,2) and researchers (3,4) recognize this problem. High-priority research needs in asphalt recycling involve the determination of material coefficients or the establishment of some limiting allowable strain or stress criteria. There are currently no such material coefficients or criteria available (3).

The determination of the performance of a recycled pavement is by no means an easy task. The performance is complex and influenced by a large number of factors. The performance of many of the conventional pavements is still not well understood. Performance of recycled pavements can be better understood and, it is hoped, predicted by further research and the monitoring of existing recycled pavements.

The structural strength of a pavement is an important indicator of its performance. The strength of a pavement material can be expressed in terms of resilient modulus (stiffness), Marshall stability, Hveem R-value, or deflection characteristics. These indicators have not been related directly to the performance of a layer, although some general relations have been developed (5). These indicators can be used successfully to compare the strength of the pavement layers but not to predict pavement life. The structural or layer coefficient used in the AASHTO design method for flexible pavements is currently the best single indicator of the performance of a pavement layer, although it is not perfect.

The AASHTO design method for flexible pavements is used by the majority of states in the United States (6). An equation relates the number of equivalent axle load applications to the structural number (SN) of the pavement. SN is an indication of the strength of the pavement. It is basically the sum of the strengths of the individual pavement layers. The higher the SN, the larger the number of loads that the pavement can accommodate before failure for given soil support and environmental conditions. The number of axle loads to failure can further be related to the number of years before functional failure will occur. The strength of the individual pavement layers is expressed in the AASHTO design method as the structural coefficient (a). Structural coefficients are dependent on a variety of factors, e.g., layer thickness, position in the pavement, thickness, and strength of surrounding layers, besides the strength of the layer itself. Coefficients range from about 0.05 for sandy-clay subbases to about 0.44 for hot-asphalt surface mixtures. The higher the coefficient, the greater the strength of the layer and the better it will perform.

RECYCLED PAVEMENT SECTIONS

The two cold recycled pavements compared in this paper were built during August and September 1981. The sections are contiguous and subjected to the same traffic and environmental conditions. Similar construction methods were used. The only difference was the binders used in the recycling: foamed asphalt and asphalt emulsion. A good comparison can therefore be drawn between the foamed-asphalt and emulsion cold recycled pavement sections.

After 5 in. (125 mm) of initial asphalt pavement had been removed, it was mixed with the binder and additional aggregate and relaid during recycling (7,8). A layer 1 in. (25 mm) thick of the initial pavement layer was left to protect the subbase during construction. The 5.5-in. (140-mm) recycled layer was overlaid with a 1.25-in. (40-mm) hot asphalt surface. Foamed asphalt was used on 4.2 miles (6.7 km) and emulsion on the remaining 4.7 miles (7.5 km). Various types of tests were conducted at approximately 10 days (September 1981), 250 days (May 1982), 375 days (September 1982), and 610 days (May 1983) after construction on the foamed-asphalt section. Similar tests were conducted at approximately 40 days (September 1981), 275 days (May 1982), 400

days (September 1982), and 640 days (May 1983) after construction on the emulsion section. The tests consisted of deflection measurements and the laboratory testing of core samples. The recycled pavement system further consisted of a granular subbase of approximately 4.5 in. (115 mm) on top of a sandy-silt subgrade.

STRUCTURAL COMPARISON

The main purpose of the structural comparison was to evaluate the performance of the two layers. A knowledge of the performance of the two recycled layers will assist pavement designers in future designs and the economic evaluation of such pavements. The layer coefficients are the most valuable in this regard.

Laboratory Strength Tests

Cores 4 in. (100 mm) in diameter and randomly selected were taken 10 and 375 days after construction on the foamed-asphalt recycled section and 400 days after construction on the emulsion recycled section. A large number of cores were broken to such an extent that they could not be tested. Only perfect samples were used. Strength characteristics were evaluated by means of resilient moduli, Marshall stabilities, and Hveem R-values. All tests were conducted at about 73°F (21°C) as specified by the Asphalt Institute for cold mixtures. The results are summarized in Table 1. Because only the unbroken cores could be used to determine the properties discussed, the average values obtained from these cores will probably be higher than the actual values. This will not influence comparisons between the recycled layers, however. Only a small number of specimens could be obtained to determine the Marshall stability, and the results should therefore be used with caution.

The asphalt mixture design methods proposed by the Asphalt Institute (9) usually specify a minimum Marshall stability and Hveem R-value among other parameters such as flow, coating, and so on, for cold asphalt mixtures. These specifications do not indicate what the service life of the pavement layers will be. This has to be accomplished by pavement design methods. The specifications only ensure that the layers will be stable under various traffic and environmental conditions. The foamed-asphalt and emulsion recycled mixtures both exceeded the required strengths.

The Marshall stability has been correlated with the structural coefficients for base courses (5), but because this was done for mixtures at 140°F (60°C), the relationships cannot be used here. What can be used is the increase in the structural coefficient as the Marshall stability increases. The foamed-asphalt mixture therefore appears to have a slightly higher strength based on performance if only the average values are considered. The differences in average values are, however, not significant at $\alpha = 0.05$ (t-test). The structural coefficients can therefore be assumed to be the same after 400 days, based on the Marshall stability.

The resilient moduli also have to be correlated with the structural coefficients and are used in mechanistic design procedures. By using the correlation of Van Til et al. (5) developed for asphalt-treated bases, the structural coefficient of the foamed-asphalt recycled layer increased from a value 10 days after construction of 0.10 to a value 375 days after construction of 0.26. A correlation by Tia (10) shows an increase from 0.25 to 0.38 for the foamed asphalt. The resilient moduli of the foamed-asphalt and emulsion sections are the same 400 days after construction at $\alpha = 0.05$ and the structural coefficients, based on these relations, will therefore be the same for the two layers.

The estimates from the laboratory test results indicated that the structural coefficients of the foamed-asphalt section increased after construction. Not enough information is available to discuss the rate of increase. The coefficients of the emulsion and foamed-asphalt sections are essentially the same approximately 400 days after construction.

Deflection Measurements

A Dynaflect was used to measure deflections of the pavement after construction at the indicated times in both lanes. The Dynaflect is widely used to measure pavement deflections (11,12). Properties of the deflection basin (Figure 1) used in the evaluation of the recycled layers were as follows:

1. Dynaflect maximum deflection (DMD) is the deflection at the center between the two steel wheels. This deflection can be converted to the Benkelman beam deflection by multiplying it by 20.63 (13). Other correlations are also available (11,14, 15). They all give basically the same answers.
2. Surface curvature index (SCI) is an indication of the stiffness of the surface course. SCI is defined as the difference between the deflections of the first and the second sensors.
3. The spreadability (SPD) is defined as the sum of the deflections of the five sensors divided by five times the maximum deflection and expressed as a percentage. The SPD is indicative of the distribution of loads by the pavement to the underlying layers.

High values of SPD but low values of DMD and SCI indicate stiff (or strong) upper layers. All three of these indicators are strongly influenced by factors other than the properties of the surface and base-course layers, e.g., subgrade strength and thickness of layers, and have not been correlated directly with material strength parameters, e.g., resilient moduli or structural coefficients. Another problem with the use of deflections to compare pavements at different times is that deflections are influenced by the asphalt temperature and the subgrade moisture

TABLE 1 Results of Laboratory Strength Tests

Specimen	Time after Construction (days)	Resilient Modulus			Marshall Stability			Hveem R-Value		
		N	Avg (psi)	SD (psi)	N	Avg (lb)	SD (lb)	N	Avg	SD
Foamed asphalt	10	43	97,400	26,100	12	1,960	1,050	25	78.3	9.2
Foamed asphalt	375	12	333,000	84,000	3	2,900	100	10	82.0	9.0
Emulsion	400	14	247,000	82,000	5	3,300	790	11	84.5	5.6

Note: SD = standard deviation; N = number of samples; 1 lb = 4.448 N; 1 psi = 6.89 kPa.

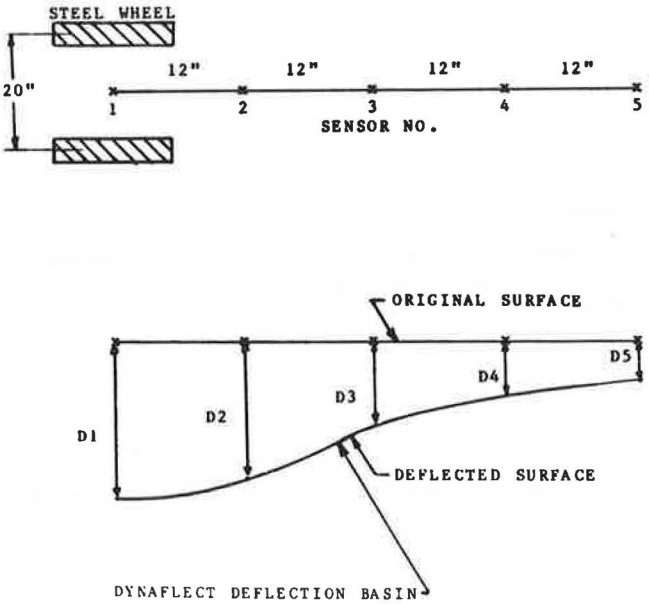

FIGURE 1 Dynaflect deflection basin.

content. Researchers in Kentucky (16) developed a method to adjust pavement deflections based on the asphalt pavement temperature. Because reliable pavement temperatures were not available, general correlations developed by Metwali (12) for Indiana were used. With these relations the DMD and SCI could be adjusted to a reference date (and thus a reference temperature and subgrade moisture content) based on the month of the year. The month after construction, September, was used as a reference. Metwali concluded that the DMD and SCI were influenced by seasons, but that the spreadability was not. Figures 2 to 4 show these changes in DMD, SCI, and SPD, respectively. All three indicators show that the stiffness of both sections increased during the first 400 days after construction because of densification under traffic and curing of the mixtures. The foamed-asphalt section was stiffer than the emulsion section. The rate of increase in stiffness, as indicated by DMD and SCI, was slightly higher for the foamed-asphalt section during the first 400 days. After that the rates of change in stiffness were almost equal. The stiffness (DMD, SCI) and load transfer capacity (SPD) of both sections decreased after about 400 days.

Both sections are in what Vaswani called the elastic phase of the pavement life (17). In this phase the consolidation or densification is almost negligible and the pavement layers behave more or less elastically. The deflections and stiffness indicators remain almost constant. The length of this phase depends on the type of material used, the traffic, and the environmental conditions. In Virginia this phase lasts about 5 years (17). The elastic phase is preceded by the consolidation phase in which the pavement layers, in this case the recycled layers, consolidate or densify. This phase lasted about 400 days (13 months) for both recycled pavements. Bandyopadhyay (4), in a study on recycled pavements in Kansas, found that the performance (and stiffness) of most recycled pavements improved during the first 7 or 8 months, after which they deteriorated. The elastic phase is followed by failure due to fatigue, in which cracks appear in the wheel path. The foamed-asphalt and emulsion sections are not yet in this phase.

Structural Layer Coefficients

Various methods can be and have been used to determine structural coefficients of pavement materials, but the most widely used are those based on the strains or deformations in the pavement and on the fatigue life of the material. The elastic-layer theory or finite-element method can be used to simulate the stresses, strains, and deformations in the pavement. The structural coefficients can be determined by comparing the strains, deformations, and fatigue life of the recycled pavement with those of a similar pavement with a standard AASHTO hot mixed asphalt layer in place of the recycled layer. The tensile strain at the bottom of the asphalt layer, the subgrade deformation, the maximum deformation at the surface, and the maximum compressive strain on top of the subgrade have been correlated with the number of load applications to failure (N_f). The tensile strain is an indicator of fatigue of the pavement. The deformations and compressive strain are indicators of the permanent deformation or rutting of the pavement. High permanent deformations lead to functional and eventually structural failure of the pavement. Functional failure can be defined

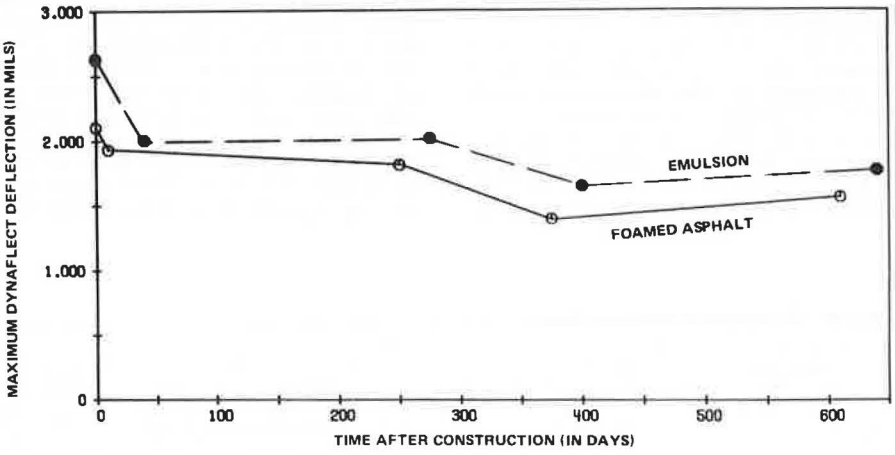

FIGURE 2 Comparison of DMDs.

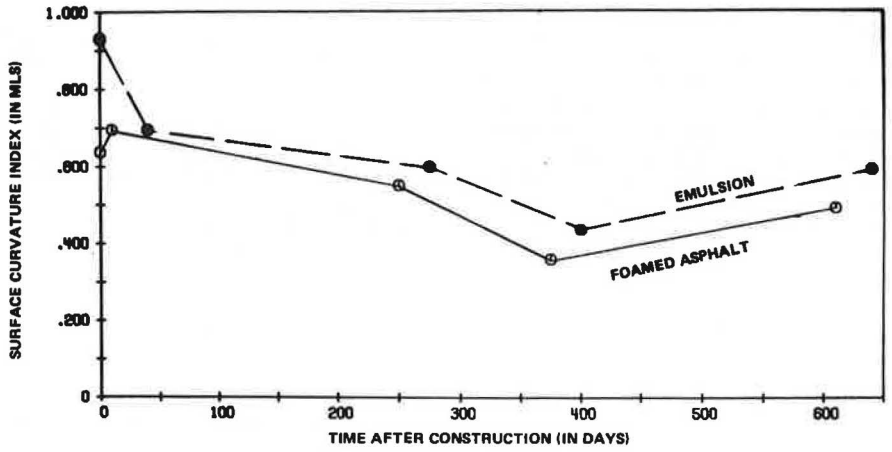

FIGURE 3 Comparison of SCIs.

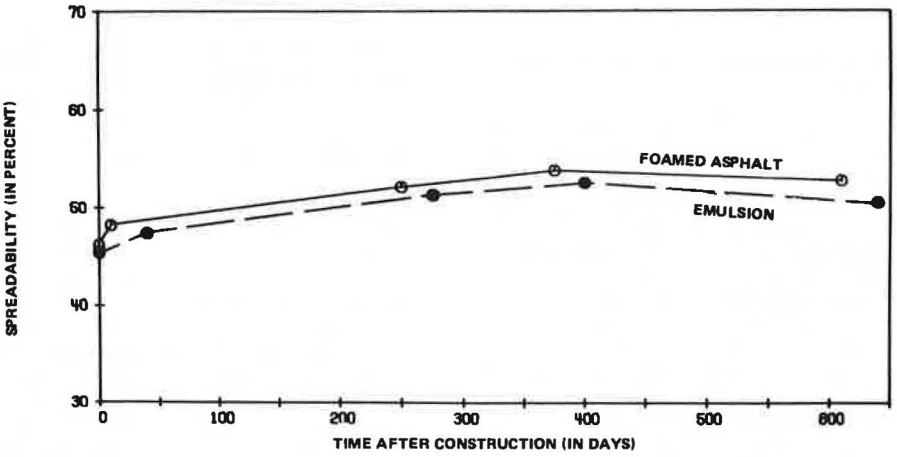

FIGURE 4 Comparison of SPDs.

as the condition at which the pavement will not be able to carry out its intended function without causing discomfort to passengers and high stresses on the vehicle, e.g., ruts. Different materials will have different load repetitions to failure. Pavements with the same number of load applications to failure will have the same service life and SN for similar climatic conditions, subgrade soil, and present serviceability indices according to the AASHTO design method. By replacing only the recycled layer with a standard AASHTO hot mixed asphalt layer the coefficients and thicknesses of the other layers will remain the same. Therefore

$$SN' = SN \quad (1)$$

where SN is the structural number of the pavement with the AASHTO layer and SN' is the structural number of the pavement with the recycled layer.

$$a' = a^*h/h' \quad (2)$$

where

a' = structural coefficient of the recycled layer used as a base,
a* = structural coefficient of the AASHTO asphalt layer = 0.44,
h' = thickness of the recycled layer, and
h = thickness of the AASHTO asphalt layer to give the same strain, deformation, or fatigue life.

The structural coefficient of a layer is influenced by the properties of the surrounding layers, the age of the pavement, the magnitude and frequency of load, the elastic parameters, and the thickness of the layer. The most important single factor is the elastic modulus of the layer in question. The best prediction of the true structural coefficients would be obtained if the in situ material properties and thicknesses of the pavement layers as well as the fatigue characteristics of all the layers were known. The strain or deformation criterion used in comparing the recycled layer with the standard AASHTO hot mixed asphalt layer should be the one that predicts the shortest service life and thus controls the performance. A large amount of testing is unfortunately necessary to obtain the necessary information.

A detailed description of the determination of the structural coefficients of the foamed-asphalt section is given elsewhere (18). The same method was used to determine the coefficients of the emulsion section. The first step was to determine the in situ elastic moduli of all the layers in the pavement at

the different times the deflection measurements were taken. The layer thicknesses were measured before and during construction. Values of Poisson's ratio were assumed for the layers and they were assumed to remain constant. Constant elastic moduli were used for the asphalt layers. The granular subbase material and subgrade are stress-sensitive, and relationships obtained from the literature were used to relate stress in the pavement to the modulus of the layer. The relationships were of the following forms:

Granular material:

$$M_r = k_1 \theta^{k_2} \quad (3)$$

Subgrade material (clayey):

$$M_r = k_3 \sigma_d^{k_4} \quad (4)$$

where

M_r = resilient modulus,
θ = bulk stress,
σ_d = deviator stress, and
$k_1, \ldots, k_4$ = laboratory-developed coefficients.

Different coefficients were used for the different times of the year that the deflection measurements were taken.

A computer program based on the elastic-layer theory was used in this analysis to calculate the stresses, strains, and deformations in the pavement. This program, called BISTRO, uses constant elastic modulus values, and the moduli of the subbase and subgrade were adjusted manually after each run to incorporate their stress-sensitive behavior. A stiff subgrade layer was also introduced in the hypothetical pavement to simulate the pavement system more accurately. These methods have also been used by other researchers (19). An iteration process was used to determine the layer properties. In this iteration process the responses of the Dynaflect deflection basin were predicted by the program and compared with those from the actual deflection basin. With the layer thicknesses as well as modulus-strain relationships for the subbase and subgrade layers known, the moduli of the asphalt recycled and the surface layers could be determined through the iteration. A double wheel load of 9,000 lb (40 kN) at a pressure of 80 psi (550 kPa) was used in the program to induce the strains and deflections in the pavement system. The wheel spacing was 13 in. (330 mm). This is the same load as that used in the Benkelman beam test. These deflections, calculated by the program, were adjusted to Dynaflect deflections with the correlation factor mentioned earlier, because the Dynaflect applies a different load to the pavement system. The iteration process was terminated when the predicted deflection basin closely approximated the actual basin.

The tensile strains at the bottom of the asphalt layers, the compressive subgrade strain, and the maximum and subgrade deflections (Figure 5) were calculated with the properties of the recycled pavement known. These maximum strains were calculated under one of the wheels. The maximum strain does not always occur under one of the wheels, but the accuracy is sufficient for this study.

The next step was to replace the recycled layer with a standard AASHTO hot mixed asphalt layer and to calculate the required strains and deformations for different layer thicknesses. The moduli of the AASHTO layer were adjusted according to the average temperature observed each time the deflection readings were taken.

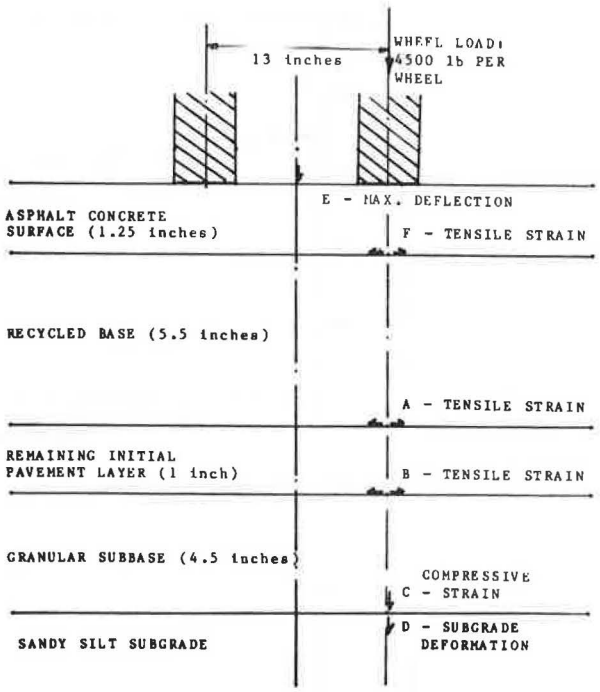

FIGURE 5 Pavement cross section.

The maximum surface deflection (20), the subgrade deflection (21), and the maximum compressive strain (20,22) have been correlated with the number of load repetitions to failure. The maximum tensile strain at the bottom of the asphalt layers has also been used to compare the recycled with the AASHTO layer. The same tensile strains will give the same performance only if the materials have the same fatigue characteristics. This will be the case for the remaining initial pavement layer, because it appears in both the recycled pavement and the pavement with the AASHTO layer. A certain tensile strain in the recycled layer will not indicate the same performance in the AASHTO layer, because their fatigue characteristics differ. The fatigue relationships are usually in the form of

$$N_f = k_1 (1/\epsilon_r)^{k_2} \quad (5)$$

where

N_f = number of loads to failure,
ϵ_r = maximum tensile strain, and
k_1, k_2 = coefficients.

Fatigue relationships were not developed for the recycled materials used in the construction of the road, nor are general relationships available for recycled materials. Relationships obtained from the literature for asphalt-stabilized base courses by Barksdale (23) and for asphalt base courses by Finn (24) were used for both the foamed-asphalt and emulsion recycled layers. Further relationships developed by Chevron (25) for emulsion mixes were used for the emulsion recycled layer, and relationships developed by Little and Epps (26) for foamed-asphalt mixtures were used for the foamed-asphalt recycled layer. The AASHTO layer was represented by two relationships, one each by Finn and by Witczak (27). Fatigue-life combinations that predicted coefficients of more than 0.50 or less than 0.05 were not considered to be applicable to the recycled layers

and were deleted in the final analysis. Any of the strains, deformations, or fatigue characteristics can be used as a criterion to determine the coefficients, but the criterion that predicts the shortest service life will control the performance. The coefficients are sensitive to the criterion used, and unless the exact relationship of the criterion to the fatigue life for all the layers is known, a single coefficient cannot be determined. The relationships used were developed for materials not necessarily the same as those in this study. Various relationships were therefore used to develop a range of coefficients rather than a single coefficient for each recycled layer in this study. The following criteria were used in the development of these ranges:

1. The subgrade compressive strain, because it has been used widely in similar analyses;
2. The subgrade deformation, because it predicts the shortest service life;
3. The tensile strain at the bottom of the remaining initial pavement layer, which represents the maximum tensile strain in the asphalt layers and is independent of the fatigue life, because the same layer is used in the recycled pavement and the pavement with the AASHTO layer;
4. Three fatigue-life combinations (X2, Y1, and Y3), which gave coefficients between 0.05 and 0.50; the combinations used were as follows:
   a. The Finn relationship for the AASHTO layer with the Finn relationship for asphalt base courses (X2),
   b. The Witczak relationship for the AASHTO layer with the Barksdale relationship for the recycled layers (Y1), and
   c. The Witczak relationship for the AASHTO layer with the Little relationship for the foamed-asphalt recycled layer and the Chevron relationship for the emulsion layer (Y3).

The maximum deflection was found to be only a fair indicator of the structural strength or performance of the pavement (28).

Figures 6 and 7 show the comparison of the layer coefficients of the foamed-asphalt and emulsion recycled layers based on the maximum compressive strain in the subgrade and the maximum strain in the asphalt layers, respectively. Both Figures 6 and 7 show the same trends. The layer coefficients of the foamed-asphalt section increased rapidly during the first 250 days after construction. After 250 days they decreased slightly. The coefficients of the emulsion section increased the most between 250 and 400 days after construction, after which they also decreased slightly. Figure 8 gives the midpoints and the ranges of the coefficients determined by the six criteria listed (asphalt tensile strain, subgrade compressive strain and deformation, and three fatigue-life combinations). The coefficients of the two sections are basically the same from about 400 days after construction. The emulsion section took longer to reach its maximum strength and the strength increased more than the strength of the foamed-asphalt recycled layer. Coefficients for design purposes can be obtained from Figure 8. It is difficult to predict what the average layer coefficient over the life of the pavement will be with the limited information. The coefficient should be within the ranges of the coefficients determined for the sections after consolidation took place, that is, 400 days after construction. The coefficients to be used within the range depend on the pavement designer. Average values can be obtained by combining the ranges obtained at approximately 400 and 600 days after construction to get a new range and then taking the midpoint of this range. Such a procedure gave a layer coefficient of 0.31 for the foamed-as-phalt recycled layer and 0.29 for the emulsion recycled layer. It should be noted that these coefficients were developed for specific recycled layers. Caution should be exercised when they are used for other recycled layers.

CONCLUSIONS

All the strength indicators showed a rapid increase in strength during approximately the first 400 days after construction for both the foamed-asphalt and emulsion recycled sections. The rate of increase varied. The foamed-asphalt section gained most of its strength during the first 250 days, whereas the emulsion layer increased in strength gradually during the first 400 days. The strength as indicated by the deflection parameters showed that the foamed-asphalt layer had slightly higher strengths throughout the analysis period than the emulsion layer, but the differences were small. Full consolidation or densification was reached for both recycled layers during the first 400 days after construction.

The layer coefficient is the best single indica-

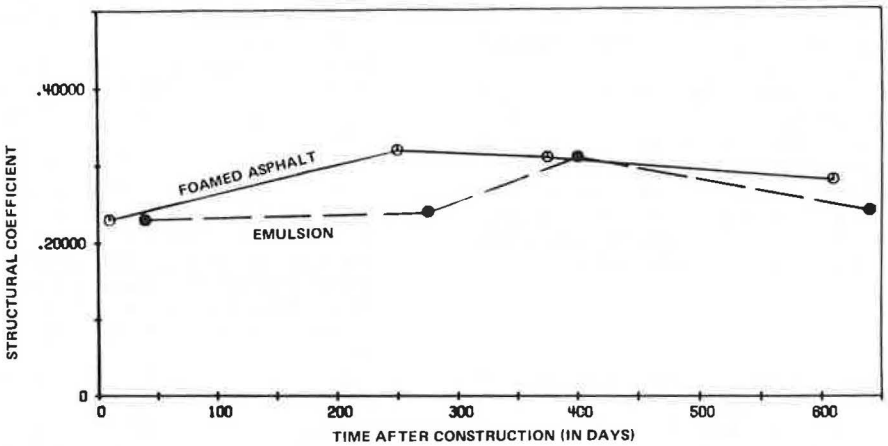

FIGURE 6 Comparison of layer coefficients: subgrade strain.

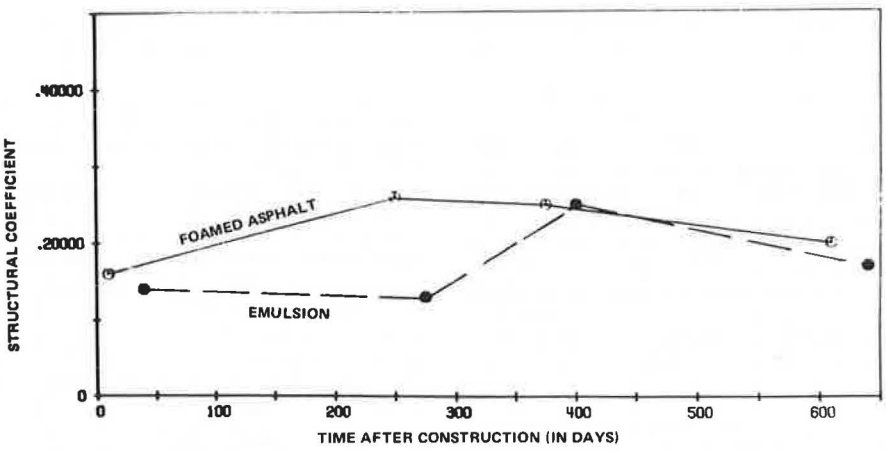

FIGURE 7 Comparison of layer coefficients: asphalt tensile strain.

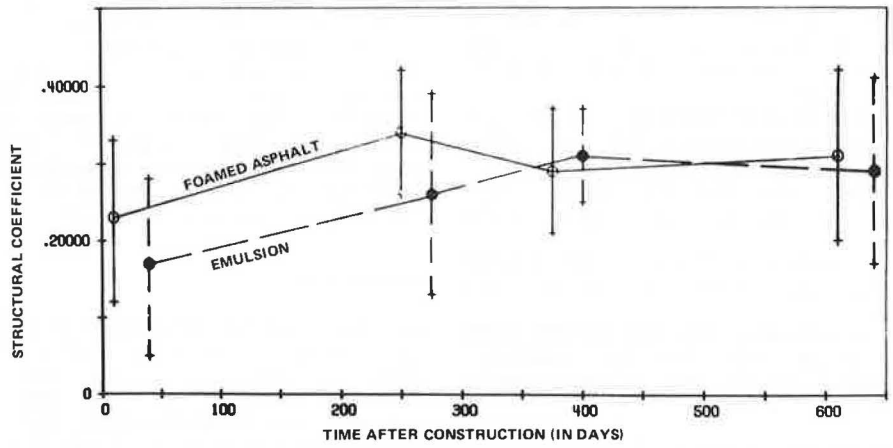

FIGURE 8 Comparison of layer coefficients: all criteria.

tor of the pavement performance. Figure 8 gives ranges of layer coefficients that can be used in the selection of layer coefficients for recycled layers similar to these used in the analysis. The midpoints are 0.31 and 0.29 for the foamed-asphalt and the emulsion recycled layers, respectively. Coefficients on the lower side of the range should be used in design, because both materials are new and their behavior has not been studied extensively. The structural coefficients of the foamed-asphalt recycled layer range from 0.20 to 0.42 and of the emulsion recycled layer from 0.17 to 0.41.

The coefficients are virtually the same, which indicates that the performances of the two recycled sections should be the same. The practical implication of the same performances is that any of the two binders, foamed asphalt or emulsion, can be used in cold recycling, because they will have the same service life. The most economical binder to use would be the one that has the lowest initial cost.

ACKNOWLEDGMENT

The research was sponsored through the Joint Highway Research Project by the Indiana Department of Highways. The author wishes to thank K.J. Kercher and the personnel of the Research and Training Section of the Indiana Department of Highways for their cooperation in obtaining the cores and deflection measurements. The author also acknowledges the invaluable guidance and support of L.E. Wood and the late E.J. Yoder from Purdue University on this project.

REFERENCES

1. J.C. Bennett. Cold Recycling of Asphalt Pavement: Warrick County, Indiana. Interim Report. Indiana Department of Highways, Indianapolis, Sept. 1981.
2. Recycling Asphalt Pavements: New Hampshire. Demonstration Project 39, Report FHWA-DP-39-33. FHWA, U.S. Department of Transportation, April 1982.
3. Pavement Recycling: Summary of Two Conferences. Final Report FHWA-TS-82-224. FHWA, U.S. Department of Transportation, April 1982.
4. S.S. Bandyopadhyay. Structural Performance Evaluation of Recycled Pavements Utilizing Dynamic Deflection Measurements. In Transportation Research Record 888, TRB, National Research Council, Washington, D.C., 1982, pp. 38-42.
5. C.J. Van Til, B.F. McCullough, B.A. Vallerga, and G. Hicks. Evaluation of AASHO Interim Guides for Design of Pavement Structures. NCHRP Report 128. TRB, National Research Council, Washington, D.C., 1972.
6. E.L. Skok, R.N. Doty, F.N. Finn, and J.W. Lyon.

Traffic Factors Used in Flexible Pavement Design. Transportation Research Circular 240. TRB, National Research Council, Washington, D.C., April 1982.
7. A.J. Van Wijk and L.E. Wood. Construction of a Recycled Pavement Using Foamed Asphalt. Proc., Canadian Technical Asphalt Association Meeting, Edmonton, Alberta, Canada, Nov. 1982.
8. A.J. Van Wijk, L.E. Wood, and K.J. Kercher. Construction of Cold Recycled Pavements Using Emulsion as Binder. Proc., Conference on Asphalt Pavements in Southern Africa, Cape Town, South Africa, March 1984.
9. A Basic Asphalt Emulsion Manual. Manual Series 19. Asphalt Institute, College Park, Md., March 1979.
10. M. Tia. Characterization of Cold-Recycled Asphalt Mixtures. Research Report JHRP-82-5. Joint Highway Research Project, Purdue University, West Lafayette, Ind., 1982.
11. F.H. Scriver, R. Peohl, W.M. Moore, and M.B. Phillips. Detecting Seasonal Changes in Load-Carrying Capabilities of Flexible Pavements. NCHRP Report 76. TRB, National Research Council, Washington, D.C., 1969.
12. E.S.W. Metwali. Framework for a Pavement Evaluation System. Research Report JHRP-81-T. Joint Highway Research Project, Purdue University, West Lafayette, Ind., 1981.
13. J.A. Epps, D.N. Little, R.J. Holmgreen, R.L. Terrel, and W.B. Ledbetter. Guidelines for Recycled Pavement Materials. NCHRP Report 224. TRB, National Research Council, Washington, D.C., 1980.
14. Asphaltic Concrete Overlays of Rigid and Flexible Pavements. Final Report. Louisiana Department of Transportation and Development, Baton Rouge, 1980.
15. Asphalt Overlays and Pavement Rehabilitation. Manual Series 17. Asphalt Institute, College Park, Md., Nov. 1977.
16. H.F. Southgate and R.C. Deen. Temperature Distribution within Asphalt Pavements and Its Relationship to Pavement Deflection. In Transportation Research Record 291, TRB, National Research Council, Washington, D.C., 1970, pp. 116-127.
17. N.K. Vaswani. Design of Pavements Using Deflection Equations from the AASHO Road Test Results. In Transportation Research Record 239, TRB, National Research Council, Washington, D.C., 1968, pp. 76-94.
18. A.J. Van Wijk, E.J. Yoder, and L.E. Wood. The Determination of Structural Equivalency Factors of Recycled Layers Using Field Data. In Transportation Research Record 898, TRB, National Research Council, Washington, D.C., 1983, pp. 122-131.
19. D.R. Luhr and B.F. McCullough. Structural Analysis of AASHO Road Test Flexible Pavements for Performance Evaluation. In Transportation Research Record 888, TRB, National Research Council, Washington, D.C., 1982, pp. 63-69.
20. D.N. Little and J.A. Epps. Effects of Recycling Agents on Structural Performance of Recycled Asphalt Concrete Materials. Proc., AAPT, 1982.
21. M.C. Wang. Performance Analysis for Flexible Pavements with Stabilized Bases. In Transportation Research Record 888, TRB, National Research Council, Washington, D.C., 1982, pp. 70-76.
22. E.J. Yoder and M.W. Witczak. Principles of Pavement Design, 2nd ed. Wiley, New York, 1974.
23. R.D. Barksdale. Development of Equipment and Techniques for Evaluating Fatigue and Rutting Characteristics of Asphalt Concrete Mixes. School of Civil Engineering, Georgia Institute of Technology, Atlanta, June 1977.
24. F.N. Finn, C. Saraf, and R. Kulkarni. Development of Structural Subsystems. Final Report, NCHRP Project 1-10B. NCHRP, in preparation.
25. Bitumen Mix Manual. Chevron Asphalt Research Co., Richmond, Calif., 1975.
26. D.N. Little, J.W. Button, and J.A. Epps. Structural Properties of Laboratory Mixtures of Foamed Asphalt and Marginal Aggregates. Presented at 60th Annual Meeting of the Transportation Research Board, Washington, D.C., 1981.
27. M.W. Witczak. Design of Full-Depth Asphalt Airfield Pavements. Proc., Third International Conference on Structural Design of Asphalt Pavements, University of Michigan, Ann Arbor, 1972.
28. H.J. Treybig. Equivalent Factor Development for Multiple Axle Configurations. In Transportation Research Record 949, TRB, National Research Council, Washington, D.C., 1983, pp. 32-44.

The opinions expressed in this paper are those of the author, who is responsible for the facts and the accuracy of the data presented.

Publication of this paper sponsored by Committee on Flexible Pavements.

Performance of Crushed-Stone Base Courses

RICHARD D. BARKSDALE

ABSTRACT

Twelve full-scale, instrumented pavement sections were tested to failure in a special laboratory facility under closely controlled environmental conditions. Seven of the pavement sections were loaded to more than 1 million repetitions and five of these sections to more than 2 million repetitions. A 6.5-kip (29-kN) uniform circular loading was applied to the surface and systematically moved to prevent a punching failure. Pavements tested consisted of five conventional sections having crushed-stone bases, five full-depth asphalt-concrete sections, and two inverted sections. The inverted sections consisted of a crushed-stone base sandwiched between a lower cement-stabilized layer and an upper asphalt-concrete layer. Conventional sections were tested with two thicknesses of base and three base gradations. The crushed-stone base sections were found to give excellent performance when covered with asphalt concrete 3.5 in. (89 mm) thick. Good performance of the engineered crushed-stone base is attributed to (a) a uniform, high degree of density (100 percent of AASHTO T-180), (b) use of a well-graded crushed stone with 1- to 2-in. (25- to 50-mm) top size that has only 4 to 5 percent passing the No. 200 sieve, (c) practically no segregation, and (d) a relatively thin asphalt-concrete surfacing.

The rising cost of petroleum products dictates the use of more materials that are low energy intensive and relatively inexpensive such as unstabilized crushed stone. There is therefore an important need to formally study the performance of granular bases in large-scale test sections taking advantage of recent advances in materials technology and modern instrumentation.

In this study the use of crushed-stone base is evaluated as an alternative to the deep strength asphalt-concrete construction now used by the Georgia Department of Transportation (GDOT) in flexible pavements. Twelve large-scale pavement sections were tested to determine whether engineered crushed stone can be successfully used to replace at least a portion of asphalt concrete in the base course. A summary of the full-depth asphalt-concrete, crushed-stone-base, and inverted sections tested is given in Table 1.

The inverted sections tested are not described in any detail; these results will be described in a subsequent paper. With the exception of test sections 3 and 4, between 0.15 and 4.4 million repetitions were applied to each section (Table 1). All tests were conducted in an enclosed constant-temperature environment at 78 to 80°F (25.6 to 26.7°C) over a period of 2 to 4 months.

TEST FACILITY

The pit in which the tests were performed was 8 ft (2.4 m) wide, 12 ft (3.7 m) long, and 5 ft (1.5 m) deep (Figure 1). To study a maximum number of base variables a different structural section was constructed at each end of the pit to give two tests for each complete filling of the pit. Emphasis was placed during construction of the test sections on achieving uniform material properties and meeting GDOT material specifications.

An air-over-oil cyclic loading system was developed to apply 6.5 to 7.5 kips (29.4 to 33.4 kN) to the pavement in 0.17 sec to simulate a slowly moving, heavy wheel loading. About 70 to 90 load pulses per minute were transmitted to the pavement surface through a water-filled circular rubber bladder. The diameter of the 6.5-kip load applied to the surface was 9.1 in. (231 mm). The resulting peak pressure was about 100 psi (689 kN/m^2), uniformly distributed over the pavement surface. Loading was conducted 5 to 6 days a week, 24 hr a day.

Cyclic Loading System

In the hybrid air-over-oil pneumatic loading system, oil was sandwiched between a small [4 in. (102 mm) in diameter] free-floating aluminum piston on the top and a large [12 in. (305 mm) in diameter] aluminum piston on the bottom. Air pressure applied to the top of the small piston was transmitted undiminished to the large lower piston, giving a large force that was applied to the loading bladder resting on the pavement surface. A push rod transmits this force from the lower piston to the loading bladder. To develop the repeated loading, air was cyclically applied to the top of the upper cylinder by using a solenoid valve system and an electronic timer.

The bladder essentially consisted of a thin steel ring covered with a rubber diaphragm on the top and bottom. A constant seating loading was maintained between load applications to prevent a shock loading.

To prevent a localized punching failure from occurring during the test, the repeated loading was applied at a primary load position and six secondary positions located symmetrically around the edge of the primary position (Figure 2). In all tests load was applied in the ratio of five repetitions at the primary position to each repetition applied at any individual secondary position. The basic pattern was to apply 100,000 repetitions at the primary position and 20,000 repetitions to each secondary position; this number, however, was reduced in the early phases of most tests; in a few tests greater numbers of load repetitions were applied in the later phases of testing (1).

The pavement was subjected to a cyclic loading of 6.5 kips up to 2 x 10^6 repetitions. To decrease the time required to cause the failure of strong pavement sections, the loading was increased to 7.5 kips after 2 x 10^6 repetitions. In sections 11 and 12 the load was maintained at 6.5 kips throughout the test. In this series, however, 200,000 load rep-

TABLE 1 Construction and Performance Summary of Pavement Sections Tested

Section Number	Asphalt-Concrete Thickness (in.)	Crushed-Stone Thickness (in.)	Repetitions to Failure (000,000s)	Failure Mode[a]	Comments
1	3.5	12.0	3.0 3.5	Fatigue and rutting	Tested to 2.4 million repetitions; failure extrapolated
2	3.5	8.0	1.0	Rutting	—
3	9.0	None	0.010	Rutting (1 in.)	Bad asphalt: asphalt-concrete content, 5.9 percent; flow, 15.4; stability, 1,870 lb; γ_D = 145.1 pcf
4	6.5	None	0.010	Rutting (1 in.)	
5	9.0	None	0.13	Rutting	Rutting failure primarily in asphalt concrete
6	6.5	None	0.44	Rutting	
7	7.0	None	0.15	Rutting	Direct comparison of crushed-stone and full-depth sections
8	3.5	8.0	0.55	Rutting	
9	3.5	8.0[b]	2.4	Fatigue	δ_p = 0.28 in. at 2.9 million repetitions
10	3.5	8.0[c]	2.9	Fatigue	δ_p = 0.34 in. at 2.9 million repetitions
11	3.5	8.0	3.6	Fatigue and rutting	6.0-in. soil cement subbase[d]
12	3.5	8.0	4.4	Fatigue and rutting	6.0-in. cement-stabilized stone subbase[e]

Note: 1 in. = 25 mm. 1 lb = 0.45 kg. 1 pcf = 16 kg/m^3. 1 psi = 6.89 kN/m^2.
[a]A fatigue failure is defined as class 2 cracking; a rutting failure is defined as a 0.5-in. (12-mm) rut depth.
[b]Coarse-gradation base.
[c]Fine-gradation base.
[d]28-day unconfined compressive strength of 214 psi.
[e]28-day unconfined compressive strength of 1,146 psi.

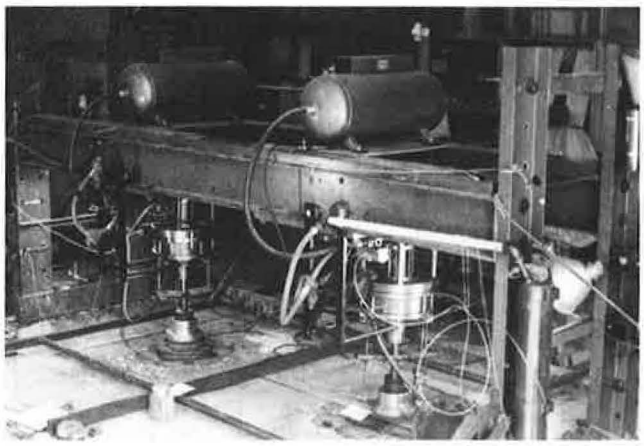

FIGURE 1 General view of pit test facility including load frame, air-over-oil loading system, and loading bladder.

etitions were applied at the primary load position in the latter stages of testing; use of this pattern of loading greatly increased the number of repetitions that could be applied during a given 24-hr day.

Reaction Frame

A reaction frame extended horizontally across the pit in the long direction about 3 ft (0.9 m) above the surface of the pavement (Figure 1). The loading system was attached to the load frame by means of a horizontally oriented thrust plate 1 in. (25 mm) thick and 26 x 33 in. (660 x 838 mm) in size. Rapid positioning by hand of the loading system at seven fixed load locations on the thrust plate was achieved by using seven sets of bolt holes to support the load system. Movement of the load cylinder from one fixed load position to another was easily accomplished by a special carriage that hung from

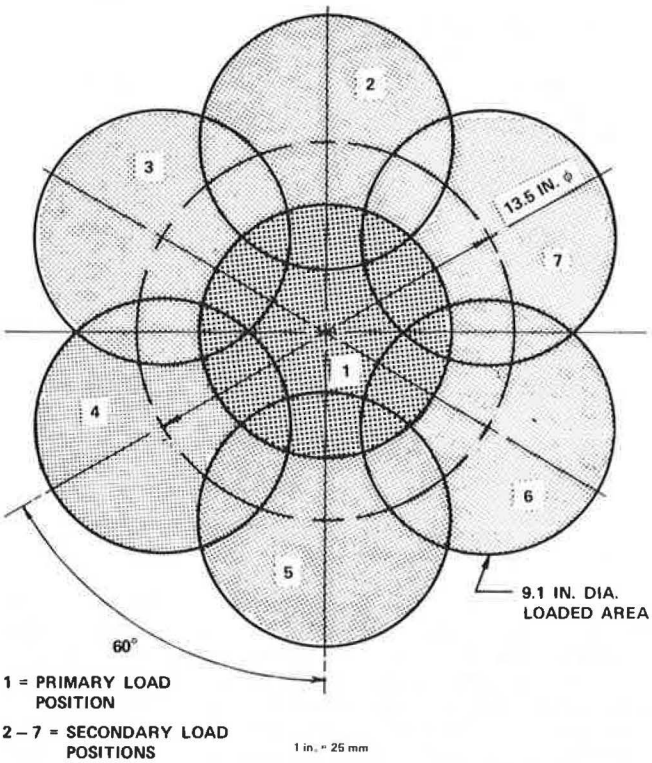

FIGURE 2 Load positions used in test section loading.

the reaction beams. The carriage rolled along the reaction beam on four wheels and temporarily supported the load cylinder during movement.

Instrumentation

The test sections were extensively instrumented to define the response of the pavement system. Typical-

ly 19 to 24 Bison-type strain sensors were installed to measure both resilient and permanent deformations throughout the pavement section (Figure 3). Small diaphragm-type pressure cells were used to measure vertical stress on the subgrade. Resilient surface deflections were measured by using linear variable differential transducers (LVDTs). Permanent deformations of the pavement surface were measured from a string line by using a metal scale. All instrumentation was carefully calibrated. A detailed description of the instrumentation is given elsewhere (1).

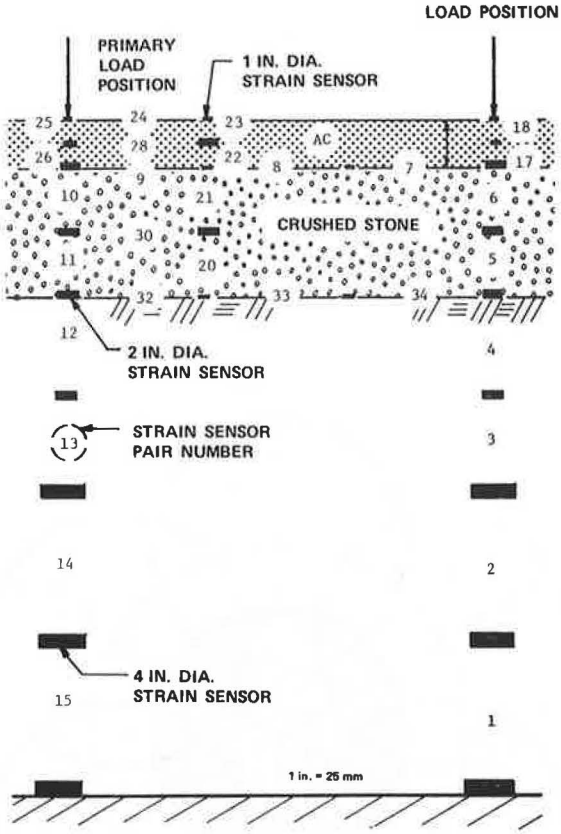

FIGURE 3 Bison strain sensor layout used in section 8, crushed-stone base.

TEST-SECTION CONSTRUCTION AND MATERIAL PROPERTIES

All test sections were constructed by using the same standardized procedures found to give consistent, reproducible results. After being tested to failure, each section was completely removed from the pit and new sections were constructed from the bottom of the subgrade up. Only the silty-sand subgrade soil was reused; after each test the subgrade soil was removed from the pit, stored, remixed, and then placed and recompacted in the pit.

Subgrade

The micaceous silty-sand subgrade was uniformly blended in a small Barber-Green pugmill in small batches. Before blending, the material was weighed, and the water content of each batch was determined by using a Speedy moisture meter. During mixing, the water required to bring the moisture content to optimum was added. The soil subgrade was placed in approximately 2-in. (51-mm) lifts and compacted with five to seven passes of a Jay-12 vibrating base compactor. A Wacker compactor was also sometimes used. A spring-loaded static penetrometer helped in controlling the density of each soil lift; the actual density was determined by using a thin-wall drive-tube sample. The subgrade of all sections had a uniform dynamic cone penetration resistance equivalent to a standard penetration test value of seven to eight blows per foot (23 to 26 blows per meter).

A uniform micaceous silty-sand subgrade about 50 in. (1270 mm) thick was used in all tests. The average maximum dry density (AASHTO T-99) was 105 pcf (16.5 kN/m³), and the optimum water content was about 18.5 percent. The subgrade was compacted in lifts 2 in. thick to an average of 98 percent (σ = 1.5 percent) of AASHTO T-99 density at a moisture content of 20.4 percent (σ = 0.5 percent), which was 2 percent above the optimum value. The micaceous silty sand had an average GDOT volume change of 38.5 percent and a clay content of 20 percent. It was nonplastic and had 85 percent passing the No. 40 sieve and 39 percent passing the No. 200 sieve. The micaceous silty sand had a laboratory resilient modulus of about 900 psi (6200 kN/m²) for a deviator stress greater than about 2.5 psi (17.2 kN/m²), as shown in Figure 4; confining pressure and moisture

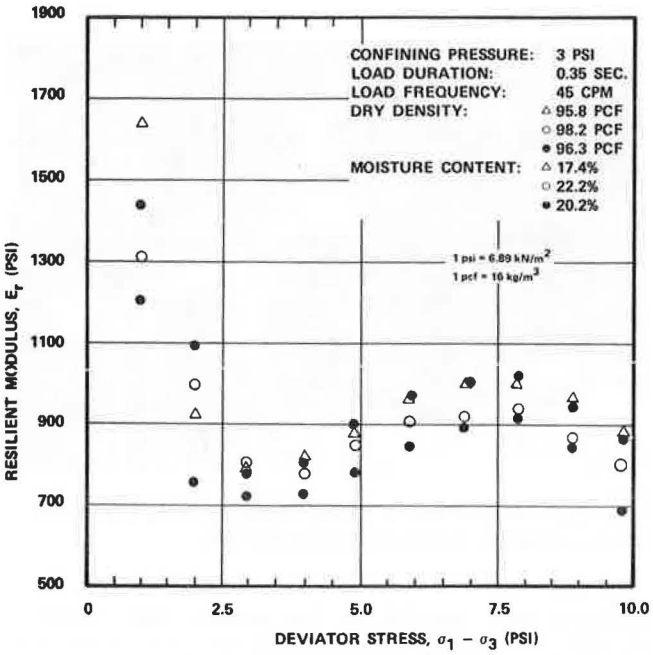

FIGURE 4 Influence of deviator stress and moisture content on resilient modulus of micaceous silty-sand subgrade.

content had only a minor effect on the resilient modulus. A low resilient modulus typically from 1,000 to 3,000 psi (6890 to 20 000 kN/m²) is common in highly micaceous Piedmont soils.

Crushed-Stone Base

The crushed-stone base was constructed by blending together in the pugmill No. 5, No. 57, and No. 810 crushed granite gneiss stone to give the desired gradations. After pugmilling, the stone was bottom-dumped into a special bucket. The bucket was moved by a crane to the desired location and once again bottom-dumped. Use of separate sizes of stone, pug-

milling, and bottom-dumping resulted in a uniform, homogeneous blend having a minimum amount of segregation after placement.

The sand-replacement method was used to determine the density of test sections 1 and 2. This method caused excessive disturbance of the crushed-stone base. The density of all subsequent unstabilized granular bases was therefore determined by a GDOT inspector by using a nuclear density gage. The average density of all sections (except 11 and 12) was 100 percent of AASHTO T-180; little variation was observed between sections. The unstabilized crushed-stone bases used in the inverted sections (11 and 12) were constructed over a rigid cement-stabilized layer. As a result, the density obtained in the crushed stone in these bases was greater than that in the other granular base sections, 105 percent of AASHTO T-180.

Stone gradations used are given in Table 2. The resilient response of the standard-gradation stone base is given in Figure 5 and the plastic response in Figure 6.

Asphalt Concrete

Either a GDOT B or a GDOT modified-B binder was used for the full thickness of the asphalt-concrete layer. The asphalt concrete was transported from the plant to the test facility in an enclosed, heavily insulated plywood box. At the time of delivery to the test facility, the temperature of the asphalt was between 290 and 300°F (143 to 149°C). The asphalt concrete was quickly weighed out, placed in the pit, leveled, and compacted by using a small two-wheel vibrating maintenance roller. The asphalt concrete was placed in lifts about 1.75 in. (44.4 mm) thick and rolled in each direction. A light prime coat of RC-70 was sprayed on the surface of the stone before the asphalt concrete was placed.

The mix designs and extraction test results are shown in Table 3. The stone used was a granite gneiss (obtained from two different quarries) that had the following typical gradation as defined by the extraction tests: 97 to 100 percent passing the 1-in. (25-mm) sieve, 62 to 85 percent passing the 3/8-in. (9.5-mm) sieve, 48 to 60 percent passing the No. 4 (4.75-mm) sieve, and 4 to 8 percent passing the No. 200 (75-μm) sieve.

TEST SECTION FINDINGS

General Comparison

Table 1 gives a general summary of the performance of the sections tested in this study. Sections 3 and 4 failed prematurely by rutting because of a high asphalt content. Both rutting and fatigue failures occurred in the tests. Sections 1, 11, and 12 failed in a combined fatigue and rutting mode. (Section 1 was tested to 2.4 million load repetitions; failure would have occurred at about 3 million to 3.5 million repetitions.) Sections 2 through 8 failed in rutting, and sections 9 and 10 failed in fatigue.

A fatigue failure was defined as the initiation of class 2 cracking. Only fine hairline cracks, which were hard to see, developed in sections considered to have undergone a fatigue failure. Numerous instances of the healing of these cracks were observed throughout the study when the load was placed over them.

A rutting failure was defined as an average rut depth of 0.5 in. (12 mm) measured from a fixed string line; rutting occurring during the first 1,000 repetitions was not included. Of significance is the finding that the sections surviving more than 2 million repetitions failed in fatigue or were close to a fatigue failure. In contrast, sections having relatively short lives failed in rutting. Thus, these test results are a good illustration of the importance of preventing excessive rutting in all layers.

The relatively early failure of the full-depth sections (sections 5-7) in rutting compared with the crushed-stone base sections (sections 1, 2, and 8-10) appears to be caused by (a) application of the heavy loading in a reasonably concentrated pattern, (b) important contributions of rutting from the weak subgrade beneath the relatively thin, full-depth as-

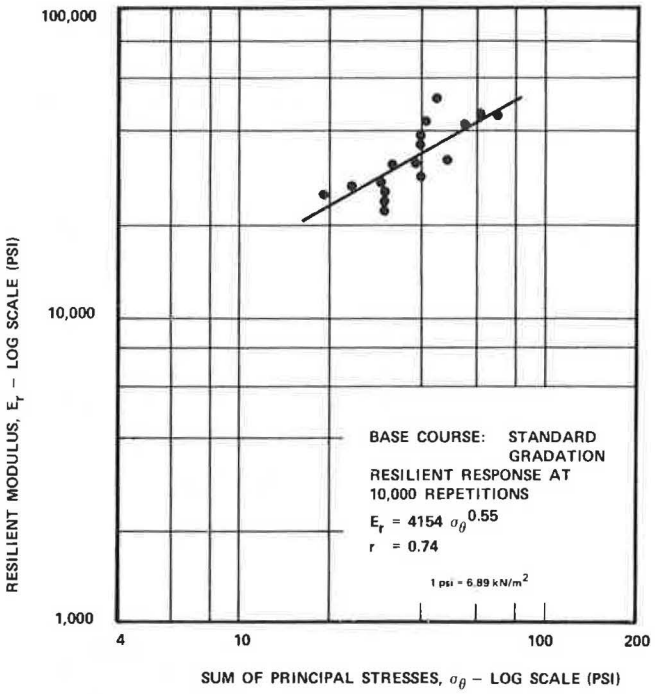

FIGURE 5 Influence of stress state on resilient modulus of crushed-stone base material, standard gradation.

TABLE 2 Crushed-Stone Base-Course Gradations and AASHTO T-180 Maximum Dry Densities

Base	Cumulative Percent Passing by Sieve Size											γ_{max}[b] (pcf)
	1 1/2 in.	1 in.	3/4 in.	3/8 in.	No. 4	No. 8	No. 10	No. 50	No. 60	No. 100	No. 200	
Standard[a]	100	98	83	61	43		31	13			4	137.0
Fine[a]	100	99	92	64	44		31		11		4	139.5
Coarse[a]	98	83	69		40	31	29		10		4	141.5
2-in. Fuller curve	98	82	69		39	31	29		12		4	–

Note: 1 in. = 25 mm. 1 pcf = 16 kg/m³.

[a]The standard-gradation base was used in sections 1, 2, 8, 11, and 12; the fine-graded base in section 10; and the coarse-graded base in section 9.
[b]AASHTO T-180 maximum dry density.

phalt concrete (the subgrade was located closer to the surface than the crushed-stone section and apparently as a result made a larger contribution to rutting), and (c) slightly higher asphalt content of the full-depth sections than that of the crushed-stone base sections (Table 3).

Permanent Deformation

In each test section, the pavement surface beneath the center of the primary load position underwent a continual up-and-down movement of permanent deformation (Figure 7). The surface underwent permanent downward movement when the load was in the primary load position and upward movement when the load was in a secondary position. This cyclic movement was caused by important lateral shear flow of material in all layers back and forth beneath the loaded regions. Net movement of the center (primary load position) was gradually downward as shown in Figure 7.

The distribution of permanent deformation in a full-depth and a crushed-stone base section is compared in Figure 8 after 300,000 load applications. In the asphalt-concrete layers of both sections the permanent deformation was approximately equally distributed between the top and bottom halves of the asphalt-concrete layer. In the full-depth asphalt-concrete section, 67 percent of the total permanent deformation occurred in the asphalt-concrete and 33 percent in the subgrade. In the crushed-stone section, 55 percent of the permanent deformation occurred in the asphalt-concrete surfacing, which was 3.5 in. (89 mm) thick; 10 percent in the crushed stone; and 35 percent in the subgrade. At equal depths more permanent rutting appeared to occur in the upper part of the subgrade beneath the full-depth asphalt-concrete section than in the crushed-stone section.

Going from a 12-in. (305-mm) crushed-stone base to an 8-in. (203-mm) crushed-stone base resulted in an increase in percentage of total rutting in the subgrade from 20 to 39 percent. At the same time, the percentage of rutting in the asphalt surfacing dropped from 59 to 34 percent; rutting in the stone base only increased from 21 to 27 percent of the total. Both this comparison and the previous one indicate that rutting can be relatively small in a properly designed and constructed crushed-stone base under conditions in which water is not a problem in the base. As illustrated in Figure 9, for the crushed-stone bases studied, typically 60 to 70 percent of the rutting occurring in the stone base developed in the upper half of the base. Finally, little difference in rutting was observed within the base between the sections having the coarse- and fine-gradation stone bases (sections 9 and 10) as shown in Figure 9. The gradation of both these sections below the No. 40 sieve was, however, essentially the same; only 4.2 to 4.4 percent passed the No. 200 sieve (Table 2). More total rutting did develop in the fine-gradation base section (section 10) than in the coarse base section. The difference, however, was primarily caused by rutting in the subgrade.

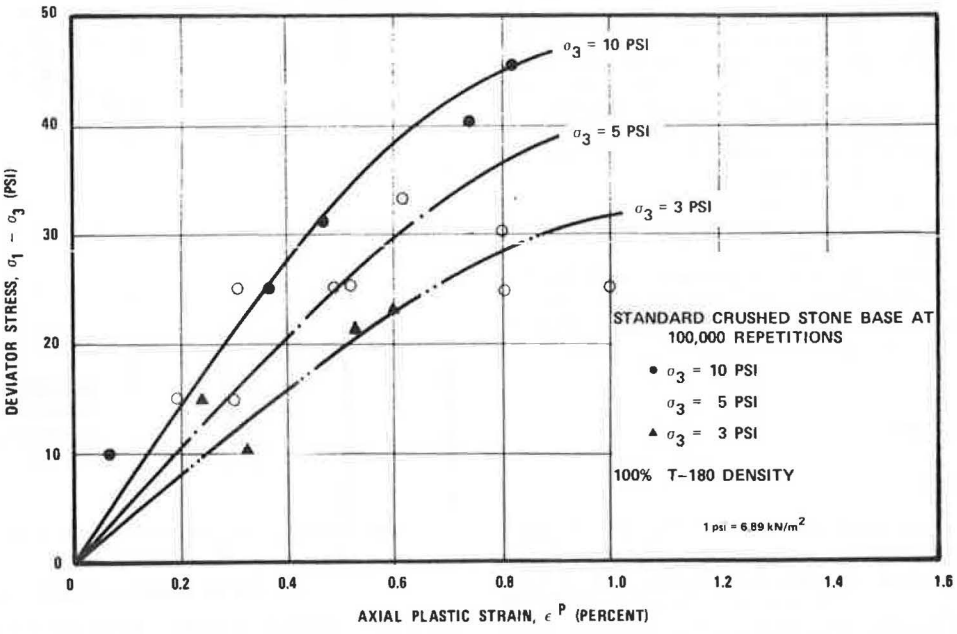

FIGURE 6 Influence of deviator stress and confining pressure on plastic strain in standard-gradation crushed-stone base.

Resilient Response

Resilient strains were measured by using Bison strain coil pairs (Figure 3). Hence the resilient strains given are the average strain occurring between the two coils and not a peak (maximum) value that occurs at a point; the difference, however, between the two values should be relatively small.

The typical variation of resilient strain response with number of load repetitions is given in Figure 10 for section 10; as indicated, the strains typically decreased after 10,000 to 100,000 repetitions. They then underwent an important increase after about 1 million load applications, which indicated reduction in the structural integrity of the pavement.

Comparison of Theory and Observed Response

A comparison of calculated and typical measured resilient response is given in Table 4. The response

TABLE 3 Fifty-Blow Marshall Mix Designs for Test Sections: AC-20 Asphalt Cement

Section	50-Blow Marshall Mix Design[a]					Constructed	
	Optimum Asphalt Concrete (%)	Flow (0.01 in.)	Stability (lb)	Air Voids (%)	γ (pcf)	Asphalt Concrete (%)	γ (pcf)
1,2	4.9	9.6	2,500	4.5	146.0	4.61	143.7
3,4	4.9	9.6	2,500	4.5	146.0	5.9	145.1
5,6	5.2	10.6	2,150	4.5	145.5	5.44[b]	145.3
7,8	5.2	10.6	2,150	4.5	145.5	4.92[c]	145.0
9,10	5.0	10.1	2,950	5.0	148.0	4.90	148.0
11,12	5.2	9.0	2,300	4.0	146.0	–	99.2[c]

Note: 1 in. = 25 mm. 1 lb = 0.45 kg. 1 pcf = 16 kg/m^3.
[a]Resilient modulus of 70,000 psi, 95°F, sections 7 and 8; bending stiffness of 380,000 psi, 80°F, sections 1 and 2; both tests on reheated asphalt concrete.
[b]Section 5 had a measured asphalt content of 5.71 percent and section 6, 5.17 percent; section 7 had 5.60 percent and section 8 had 4.23 percent; the actual difference in asphalt-concrete content was probably less because each pair of sections was constructed at the same time.
[c]Percent maximum from nuclear-density tests.

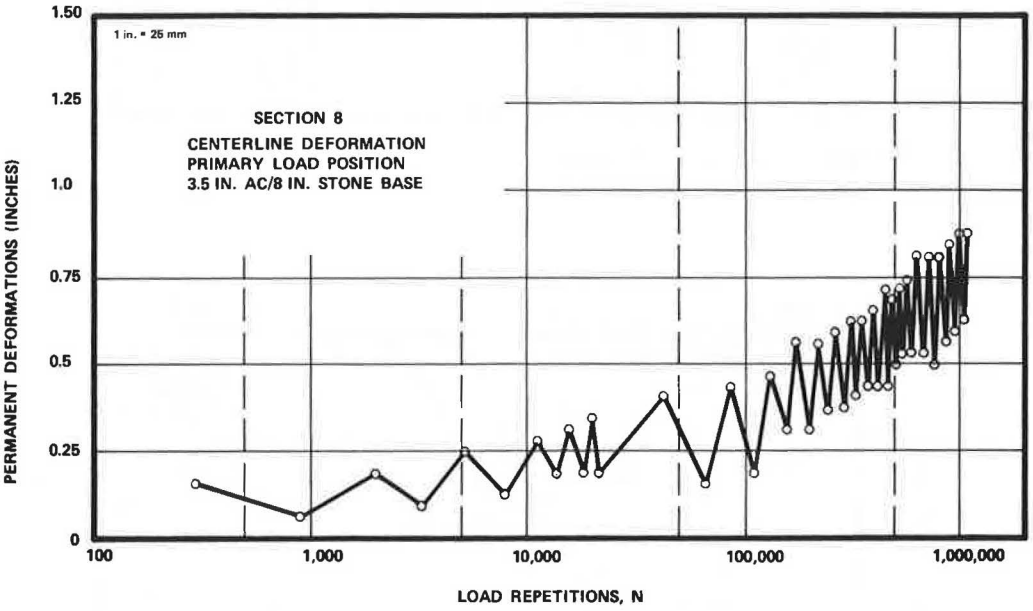

FIGURE 7 Variation of centerline deformation with number of load repetitions, section 8.

was calculated by assuming the layers to be isotropic, linear-elastic, homogeneous, and semiinfinite in horizontal extent (2). Linear-elastic theory of this type is usually used in mechanistic design methods. Because pavements are neither linear elastic nor isotropic, a good match of all measured variables should not be expected.

The laboratory-measured resilient moduli were adjusted to give an approximate best overall fit of the observed strain, deflection, and stress response of the pavement systems. For a reasonably good overall fit of the observed response, the resilient moduli of the subgrade, crushed-stone base, and surfacing were taken to be about 2,800 psi (19.3 MN/m^2), 15,000 psi (103 MN/m^2), and 4 to 8 x 10^5 psi (2756 to 5512 MN/m^2), respectively.

The moduli values used generally give deflections that are somewhat larger than those measured but give a reasonably good prediction of the tensile strain measured in the bottom of the asphalt-concrete surfacing.

The theoretical vertical stress on the subgrade is considerably smaller than the measured values. Some overmeasurement of vertical stress may certainly have occurred in the investigation. The pressure cells, however, were calibrated in the same subgrade soil, and the effect of dynamic loading was found by calibration to be small. Therefore it is felt that the existing stresses were indeed greater than those predicted by theory. The finding (Table 4) that the measured vertical strains on the subgrade for the full-depth and stone base sections were about 50 percent greater than predicted also tends to indicate larger subgrade stresses.

The resilient modulus used to characterize the subgrade was about three times the value indicated by the repeated-load triaxial tests. Disturbance and remolding effects and the short time for which the laboratory test specimens are subjected to σ_3 may partially account for this important difference. Previous work with the micaceous silty sands of the Piedmont have indicated similar problems with laboratory-evaluated moduli (3).

Fatigue Behavior

Crushed-stone base sections 9 through 12 failed in fatigue or a combined fatigue-rutting failure. The fatigue relationship obtained from these data points

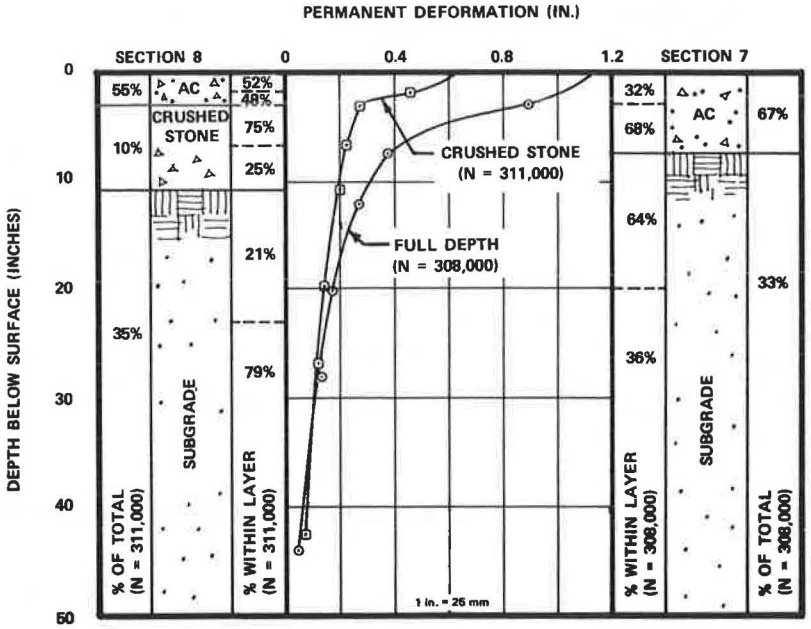

FIGURE 8 Comparison of distribution of permanent deformation in full-depth section 7 and crushed-stone section 8.

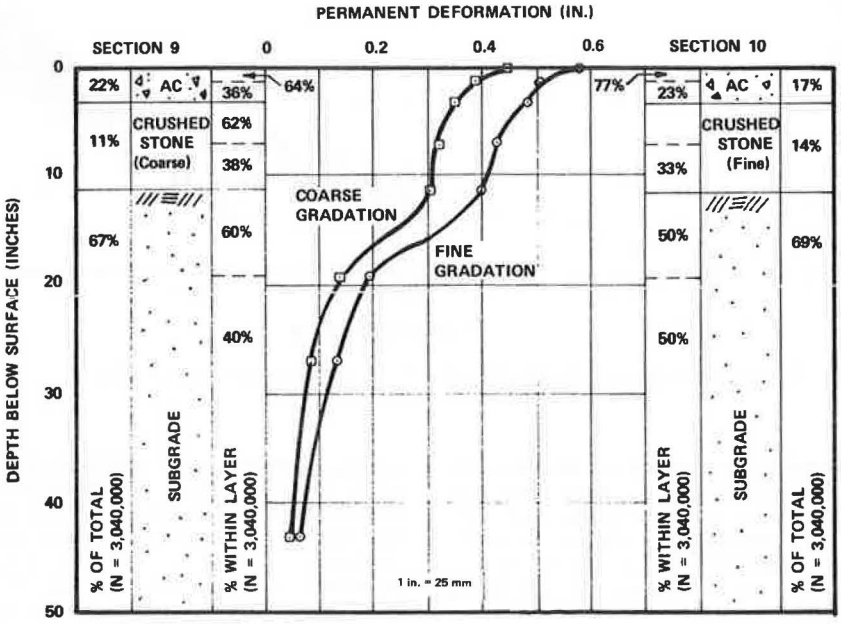

FIGURE 9 Comparison of distribution of permanent deformation in coarse- and fine-gradation crushed-stone base pavements, sections 9 and 10.

for 79°F (26.1°C), $N_f = 0.00108\varepsilon_t^{-2.695}$, was found where N_f is the number of repetitions to cause fatigue failure and ε_t is the tensile strain in the bottom of the asphalt-concrete layer. This fatigue relationship is for a temperature of 79°F, fine hairline cracking, and the assumption that each load application caused the same amount of damage. The relatively concentrated pattern of loading is felt to be more severe than would normally occur for a highway pavement.

The observed fatigue curve, corrected to 70°F (21.1°C), is located above the fatigue curves summarized by Rauhut and Kennedy (4), as shown in Figure 11. The high fatigue curve is probably partly caused by use of a thin bituminous surfacing and a high-quality crushed-stone base. The points fall between the curves developed by Barksdale (5) for a 3-in. and 9.8-in. thickness of asphalt-concrete surfacing.

Influence of Crushed-Stone Base Thickness

Increasing the thickness of the crushed-stone base from 8 in. to 12 in. increased the life of the pavement by a factor of almost 3 (compare sections 1 and

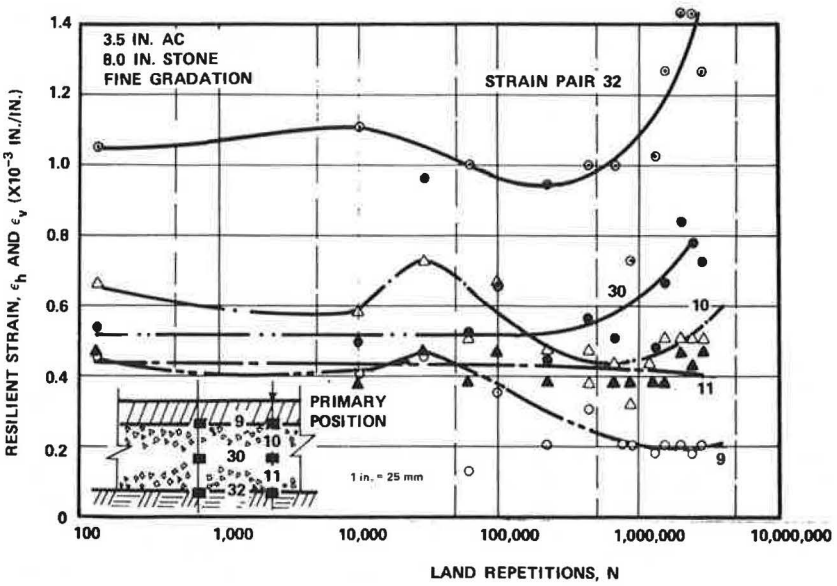

FIGURE 10 Variation of resilient strain with load repetitions, section 10.

TABLE 4 Comparison of Measured and Theoretical Stresses, Strains, and Deflections by Using Final Material Parameters

Pavement Design	Vertical Stress on Subgrade (psi)		Tangential Strain at Bottom of Asphalt Concrete ($\mu\epsilon$)		Surface Displacement (mils)		Vertical Subgrade Strain ($\mu\epsilon$)	
	Typical Measured	Theoretical	Typical Measured	Theoretical	Typical Measured	Theoretical	Typical Measured	Theoretical
Full-depth (9-in.) asphalt concrete	8.7	2.5	308	280	14	17	1,380	852
Asphalt concrete (3.5 in.) on 8-in. crushed-stone base	6.8-11.2	4.0	270-390	352	23	29	2,030	1,450
Asphalt concrete (3.5 in.) on 8.7-in. crushed-stone base on 5.8-in. cement-treated crusher run	3.5	2.1	272	262	17	15	340	463
Asphalt concrete (3.7 in.) on 8.9-in. crushed-stone base on 6.0-in. cement-treated subgrade	3.2	2.5	324	276	26	19	390	649

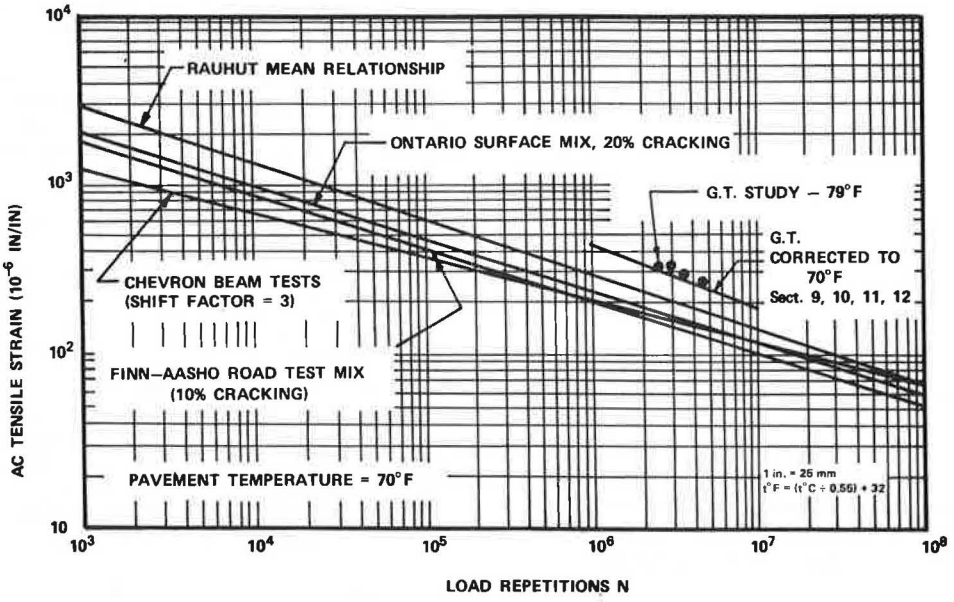

FIGURE 11 Comparison of observed fatigue performance with relationships summarized by Rauhut and Kennedy *(4)*.

2, Table 1). The AASHO Road Test results also indicated a similar significant beneficial effect of a small increase in base-course thickness (6). As the base thickness becomes greater, however, the beneficial effect of increasing thickness probably decreases, as indicated by an analytical study (1).

Influence of Crushed-Stone Base Gradation

Excellent performance was obtained from the granular-base pavements that had both the coarse gradation (section 9) and the fine gradation (section 10). Both these sections failed in fatigue rather than in rutting at a higher number of repetitions than two other 8-in. crushed-stone base pavements (sections 2 and 8). The fatigue life of the fine-gradation base section was about 20 percent greater than the fatigue life of the coarse base section. On the other hand, rutting in the fine-gradation base section was 21 percent greater than in the section having a coarsely graded granular base section. These differences are reasonably minor considering the possible variation.

The somewhat limited test results indicate for the relatively narrow range of gradations tested that gradation has a reasonably minor influence on performance provided the section is compacted to 100 percent of AASHTO T-180 density and little segregation is allowed to occur. All three crushed-stone base gradations, however, had a top size of 1 to 2 in. (25 to 51 mm), 40 to 44 percent passing the No. 4 sieve, and 4 to 5 percent fines.

Influence of Asphalt Content

Permanent deformation in the B and modified-B binder mixes was found to increase dramatically as the asphalt content increased, as shown in Figure 12, which is based on the permanent deformation occurring in the upper 3.5 in. (89 mm) of both full-depth and crushed-stone base sections at 10,000 load repetitions. Because the permanent deformations in most sections were small at 10,000 repetitions, Figure 12 indicates general trends of the influence of asphalt content on rutting.

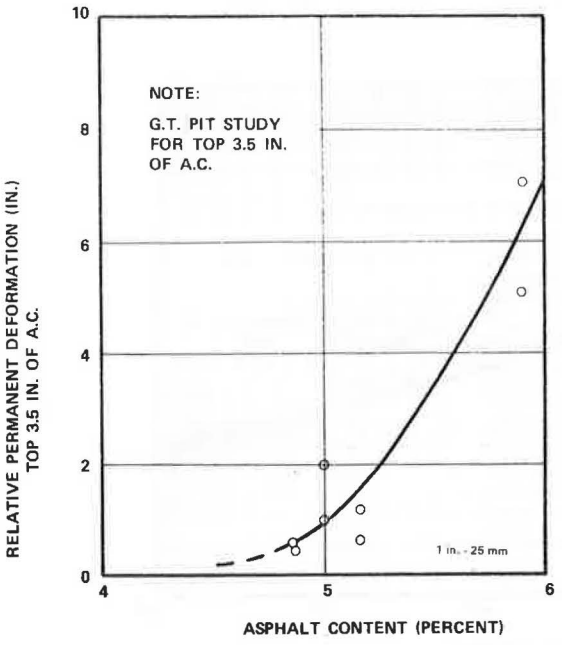

FIGURE 12 Approximate relative rutting in asphalt concrete as function of asphalt content: B and modified-B binder.

The results of these full-scale laboratory studies indicate that the 50-blow Marshall mix design method gives approximately the correct asphalt content. Use of greater asphalt content to increase fatigue life, which is sometimes advocated, does not appear to be justified for heavily loaded sections based on these findings. For heavy traffic and warm summer temperatures, the optimum asphalt content may even be slightly less than the Marshall value.

Permanent Subgrade Deformation

The same resilient micaceous silty-sand subgrade was used beneath all test sections. As previously discussed, the subgrade was removed and recompacted at the same density and moisture content for each test. Figure 13 shows that an increase in base thickness causes a decrease in permanent subgrade deformation. As the base thickness increases, however, the rate at which the deformation decreases becomes less.

A 9-kip (40-kN) dual-wheel load would cause about 1.4 times more rutting than that shown in Figure 13. This extrapolation is based on theory and the plastic strain response obtained from repeated-load triaxial tests. Finally, these studies indicated that the full-depth asphalt-concrete sections were no more effective in reducing subgrade rutting per inch of base than the unstabilized crushed-stone base.

Base-Course Coefficients

The full-scale laboratory tests show that excellent performance can be obtained by using relatively thin asphalt-concrete surfacings and properly constructed crushed-stone bases. The crushed-stone base sections outperformed the full-depth sections in every test series. A higher asphalt content in the full-depth sections probably accounted for most of the poor performance of the full-depth sections.

Based on the observed fatigue and strain response of the pavement, one application of the 6.5-kip circular load used in this study is approximately equivalent to 0.58 applications of a 9-kip dual-wheel load. Now assume an AASHTO Interim Guide (7,8) layer coefficient a_1 of 0.44 for the 3.5-in. asphalt-concrete surfacing and a soil support value of 3.5 (which is greater than would be generally used in Georgia for Piedmont soils). A regional factor of 0.5 assumes that no environmental effects occurred during the study. For this conservative set of assumptions, the average calculated AASHTO Interim Guide crushed-stone base-course coefficient a_2 is 0.19. Based on the results of this study and observed field response (1), a base-course coefficient of 0.18 was recommended for total pavement thicknesses less than 15 in. (381 mm); this is slightly less than the maximum structural thickness used in this study. The engineered crushed-stone base should be compacted to at least 100 percent AASHTO T-180 density and have a gradation approximately similar to that of the stone used in this study. Also, segregation should be minimized during construction and adequate drainage provided.

CONCLUSIONS

The test results show that engineered crushed-stone base sections having relatively thin asphalt-con-

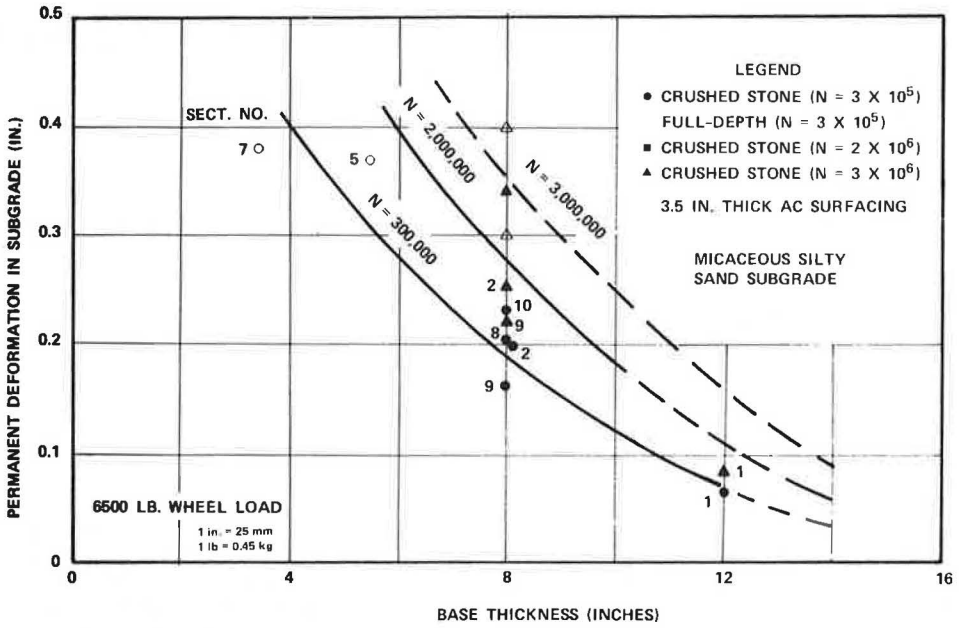

FIGURE 13 Effect of base thickness and number of load repetitions on subgrade rutting: crushed-stone base and full-depth asphalt-concrete test results.

crete surfacings can successfully withstand large numbers of heavy loadings. Full-scale field tests such as those at Lake Wales, Florida; Stockbridge, Georgia; and in North Carolina support this finding (1,9,10). The results of this study show that rutting in a properly constructed crushed-stone base can be less than that in either the asphalt-concrete surfacing or a silty-sand subgrade at a temperature of 79°F; at higher temperatures even greater amounts of rutting would occur in the asphalt concrete.

The good performance of the engineered crushed-stone base is attributed to (a) a uniform, high degree of density (100 percent of AASHTO T-180), (b) use on a well-graded crushed stone with 1- to 2-in. top size that has only 4 to 5 percent passing the No. 200 sieve, (c) practically no segregation, and (d) a relatively thin asphalt-concrete surfacing.

ACKNOWLEDGMENT

This project was sponsored by GDOT and FHWA. Specific acknowledgment is given to W.T. Stapler, GDOT state materials engineer, and to Wouter Gulden and Danny Brown for their assistance. Special acknowledgment is given to Alan Todres for designing the testing system and general assistance. Ken Thomas and Andy Fitzsimmons made many valuable contributions. Support was also given by Hugh Gauntt, Mr. Ashtiana, Ben Laughlin, and Scott Davidson. Vicki Clopton carefully typed the manuscript. The asphalt concrete was supplied by APAC Georgia, Inc. Acknowledgment is also given to E.J. Barenberg of the University of Illinois for providing the pugmill.

REFERENCES

1. R.D. Barksdale and H.A. Todres. A Study of Factors Affecting Crushed Stone Base Course Performance. GDOT Project 7603. Georgia Institute of Technology, Atlanta, March 1983, 169 pp.
2. D.A. Dasianchuk. Fatigue Considerations in the Design of Asphalt Concrete Pavements. Ph.D. thesis. University of California, Berkeley, 1966.
3. R.D. Barksdale, S. Intraprasart, and R.L. Crisp. Settlements of Footings on a Saprolite Soil. Proc., 5th Pan American Conference on Soil Mechanics and Foundations, Buenos Aires, Argentina, 1975.
4. J.B. Rauhut and T.W. Kennedy. Characterizing Fatigue Life of Asphalt Concrete Pavement. In Transportation Research Record 888, TRB, National Research Council, Washington, D.C., 1982, pp. 47-56.
5. R.D. Barksdale. Repeated Load Test Evaluation of Base Course Materials. GDOT Project 7002. Georgia Institute of Technology, Atlanta, 1972.
6. TRB Special Report 73: The AASHO Road Test. TRB, National Research Council, Washington, D.C., 1962.
7. AASHTO Interim Guide for Design of Pavement Structures, Chap. 3, rev. AASHTO, Washington, D.C., 1981.
8. Technical Considerations and Recommendations of the National Crushed Stone Association for Revision of the AASHTO Interim Guide for Design of Pavement Structures. National Crushed Stone Association, Washington, D.C., June 1983, 29 pp.
9. C.F. Potts, B.E. Ruth, and L.L. Smith. Performance of Sand-Asphalt and Limerock Pavements in Florida. In Transportation Research Record 741, TRB, National Research Council, Washington, D.C., 1980, pp. 22-34.
10. B.D. Barnes and W.G. Mullen. Evaluation of Base Courses for Flexible Pavements. Final report. School of Civil Engineering, North Carolina State University, Raleigh, 1979.

Publication of this paper sponsored by Committee on Strength and Deformation Characteristics of Pavement Sections.

Seasonal Effects on the Strength of Pavement Structures

JO A. LARY and JOE P. MAHONEY

ABSTRACT

Results are presented from monitoring and predicting changes in subgrade resilient modulus with season of the year for test sites on the U.S. Forest Service road system. Data collection involved measuring deflection, subgrade moisture content, and soil suction over an 18-month period at four test sites located in Washington and Oregon. In addition the pavement materials (asphalt concrete and base and subgrade materials) were sampled and a series of laboratory resilient modulus tests was conducted on each sample. The laboratory and field data were used to develop methods of predicting changes in subgrade stiffness (strength) over time. The two most promising methods were those obtained from regression equations developed from the laboratory test data for the pavement materials and appropriate elastic-layered computer programs and a hand-calculation method based on deflection measurements.

In analyzing pavement performance, seasonal variations caused by environmental conditions pose a difficult problem. These variations, particularly freezing and thawing and the associated soil moisture changes, result in the deterioration of the pavement structure because of a decrease in its stiffness and associated strength. This deterioration has economic impacts including maintenance and rehabilitation costs as well as user costs.

The overall objective of the study being reported was to evaluate the effect of seasonal environmental variations on pavement stiffness and strength. More specifically, the objectives were to

1. Measure changes in subgrade resilient modulus with changes in season and
2. Develop an algorithm to predict seasonal change in modulus from easily measured field data.

Easily measured field data include deflections, soil moisture content, soil suction, and weather information.

To meet these objectives, computer programs and a hand-calculation method were tested to see whether modulus values could be predicted from deflection measurements such as those obtained with a Benkelman beam or from deflection basins measured by the Dynaflect or similar equipment. In addition an attempt was made to correlate modulus with soil type, weather data, soil moisture, and soil suction.

FIELD STUDY

Site Selection

To meet the study goals, extensive use of existing U.S. Forest Service (USFS) roads was made. Several criteria were used as a basis for roadway test-site selection. They were that

1. The site must represent USFS Region 6 soil conditions, climate, and topography;
2. The site must be easily accessible; and
3. Weather data from a nearby source must be available.

Based on these criteria, four test sites were chosen: in the Olympic and Wenatchee National Forests in Washington and the Deschutes and Willamette National Forests in Oregon. Table 1 provides a summary of the site characteristics. To illustrate the differences between test sites during winter conditions, design freezing indices (1,2) were compared as follows [t°F = (t°C ÷ 0.55) + 32]:

Site	Degree-Days
Olympic	150
Wenatchee	1,000
Deschutes	800
Willamette	200

Instrumentation

A main objective of this study was to measure changes in subgrade moduli during a 2-year period. To this end, each site was instrumented with Soiltest MC-310A soil cells to measure subgrade moisture content, soil suction, and temperature (typical locations shown in Figure 1); frost tubes to measure depth of freezing (schematic view shown in Figure 2); and pavement station markers to facilitate repeatable deflection measurements. A typical schematic view of the location of the deflection points, frost tubes, and moisture-temperature cells for one of the four test sections (Olympic National Forest) is shown in Figure 3.

In addition to measurements obtained with the Dynaflect and Benkelman beam, the falling-weight deflectometer (FWD) (Dynatest Consulting, Inc.) was used to measure deflections at both the Olympic and Willamette sites.

Data-Collection Procedures

Field data were collected at all four sites over an 18-month period beginning in January 1981 with special emphasis on the spring thaw period. The following data were collected during each site visit:

1. Pavement deflection,
2. Pavement temperature,
3. Air temperature,
4. Subgrade temperature,
5. Soil cell resistivity (for moisture content), and
6. Frost penetration depth.

Tensiometer suction measurements and gravimetric water contents were also recorded at the Deschutes and Willamette sites.

TABLE 1 Summary of the Characteristics of the Four Test Sites

Forest	USFS Road No.	Elevation (ft above sea level)	Yearly Rainfall (in.)	Pavement Material	Base-Course Material	Subgrade Material
Olympic	220	≃ Sea level	150	5-in. ACP	Crushed aggregate (8 in.)	Clean silty sand with 5 percent gravel
Wenatchee	2451	2,450	24	4-in. CSS-1	Granitic sand (4-6 in.)	Granitic sand
Deschutes	2301	4,400	25	5-in. open-graded emulsion	Crushed aggregate (4.5 in. GW)	SW-SM light-brown pumice ash
Willamette	2233	2,200	70	2.4-in. ACP	Crushed aggregate (14.4 in. GP)	MH clayey silt, residual soil

Note: 1 in. = 2.54 cm; 1 ft = 0.3 m; GW, GP, SW, SM, MH = groups from Unified Soil Classification of U.S. Corps of Engineers and U.S. Bureau of Reclamation.

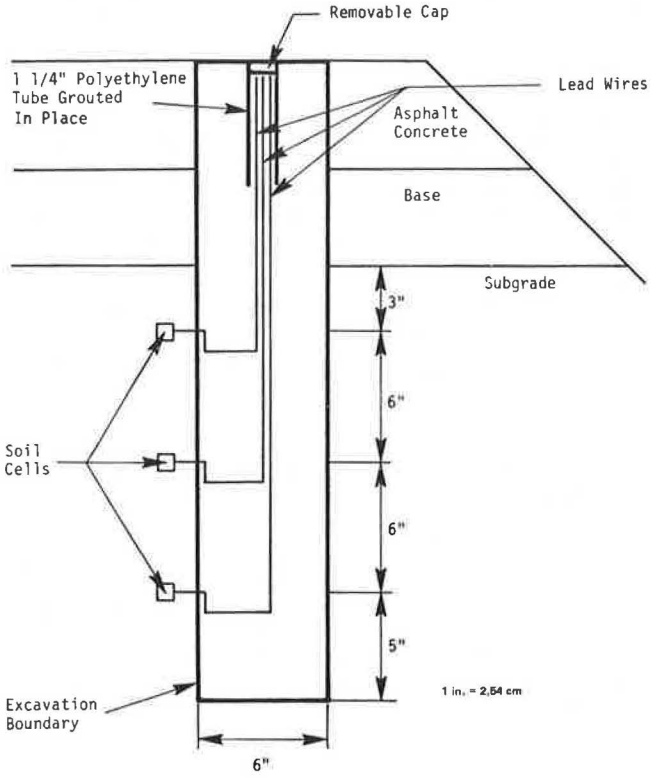

FIGURE 1 Typical soil-cell layout.

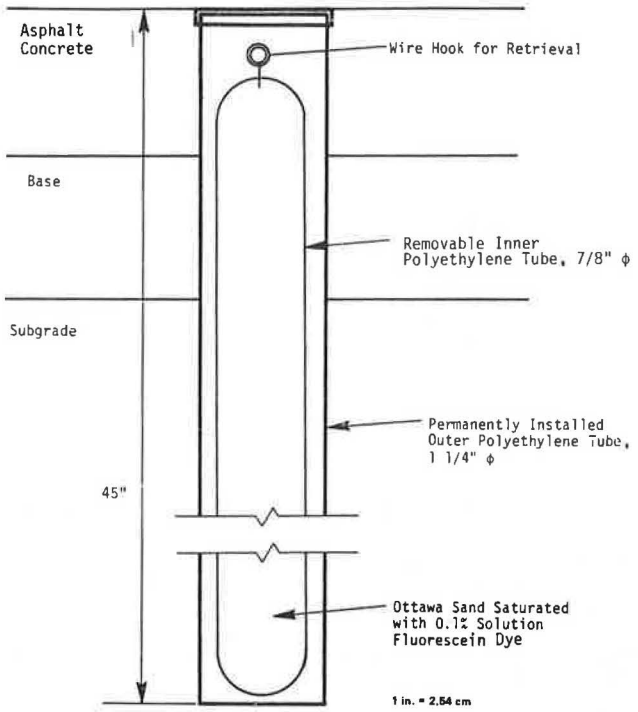

FIGURE 2 Schematic of in situ frost tube.

LABORATORY STUDY

Pavement cores and grab samples of the base and subgrade materials were obtained from each test site. Samples of each were taken for laboratory testing and moisture content determination. The moisture content samples were placed in plastic bags and sealed to prevent evaporation. In situ dry density of each soil was also determined at the time of sampling.

The laboratory testing included sieve analysis (ASTM D421 and D422), hydrometer analysis (ASTM D421 and D422), Atterberg limits (ASTM D423), and specific gravity (ASTM D854) for each soil. These tests were done to provide basic identification of the base and subgrade materials. The optimum density and moisture content for the soils was also determined by AASHTO T-99 (Standard Proctor). Much of the laboratory testing was conducted at the Department of Civil Engineering, Oregon State University.

In addition to the standard soil tests, the resilient moduli of the bases and subgrades were also determined. The soil samples were tested at several moisture contents and densities to bracket in situ conditions. The resilient moduli were then used as inputs for computer programs to predict subgrade modulus. The resilient moduli of the pavement cores were also determined by using a repeated-load diametral test apparatus at 70°F (21°C).

DATA ANALYSIS

This section contains a description of the methods used and the results obtained in predicting modulus from easily measured field data. The relationships examined were those of predicting subgrade modulus from soil moisture content and measured deflections. Soil suction was not investigated as an alternative because suction data were not available for the Olympic and Wenatchee test sites and it was determined that soil suction was no better a predictor of modulus than subgrade moisture content and was more difficult to measure.

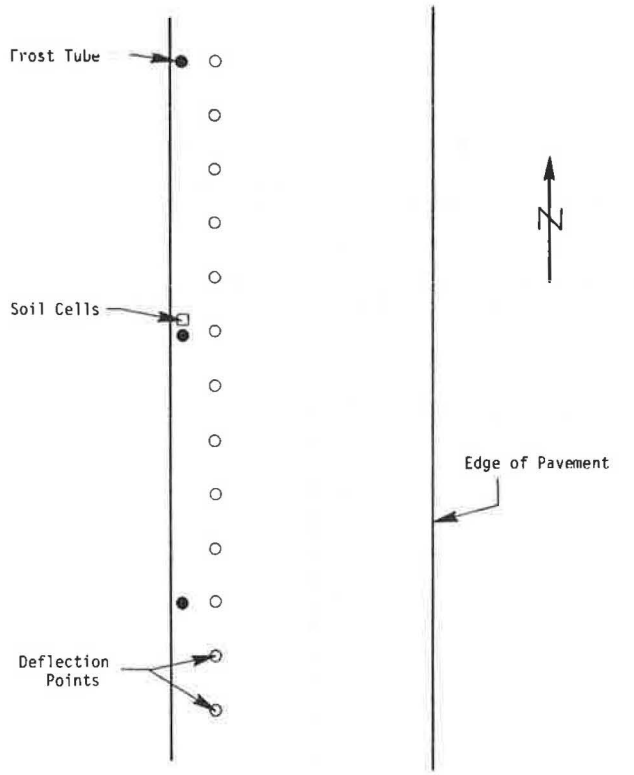

FIGURE 3 Schematic of Olympic National Forest, USFS Road 220.

Prediction of Resilient Modulus from Moisture Content

The regression equations developed from the laboratory resilient modulus test results (Table 2) can be used directly to predict resilient modulus. Equations were developed for the base course and subgrade soils of the four test sites. To use the equations, three quantities must be known:

1. Dry density of the soil,
2. Stress appropriate to a given load (either bulk or deviator depending on whether the soil is granular or fine-grained), and
3. Moisture content.

The dry density of the soil is considered to be a constant and can be determined either from the initial construction records or from field measurement. The stress required is either bulk or deviator stress. These stresses vary depending on the surface loading conditions and can be determined by use of computer programs such as PSAD2A (3) or ELSYM5 (3). The loading conditions and the appropriate pavement layer data are input into the programs. Layer data include the thickness, dry density, Poisson's ratio, and the stress relationship ($M_R = K_1\theta^{K_2}$, and so on) for each. The programs will then output stresses at the points requested, including bulk and deviator stresses. Alternatively, bulk and deviator stresses at a point in a layered system can be estimated by using other methods such as those developed by Jones and Peattie (4,5).

Once the bulk or deviator stress for a particular loading is known, along with the dry density, the regression equations can be used to calculate modulus at a given moisture content. The moisture content to input can be determined by sampling to determine gravimetric water content or obtaining resistivity measurements with instrumentation such as the Soiltest cells. To use the latter method, calibration curves of resistivity versus moisture content for the soil must be developed in the laboratory.

Such equations can be used to predict change in modulus with moisture content variation throughout the year; however, the equations are only valid for the range of stresses at which the soils were tested. The laboratory deviator stress range was from 1 to 12 psi (7 to 83 kN/m²) for the subgrade soils and 1 to 20 psi (7 to 138 kN/m²) for the base-course soils. The bulk stress range was 7 to 30 psi (48 to 207 kN/m²) for the subgrade soils and 4 to 64 psi (28 to 448 kN/m²) for the base-course soils. The behavior of the soils at lower stresses has not been determined.

Prediction of Subgrade Modulus from Deflection Measurements

To predict subgrade resilient modulus from measured deflections, three methods were chosen for analysis. Two were computer programs, PSAD2A (3), developed at the University of California, Berkeley, and BISDEF (6), developed at the U.S. Army Corps of Engineers Waterways Experiment Station in Vicksburg, Mississippi. The third, a hand-calculation method, was the dual parametric approach (7), refined at the Texas Transportation Institute by Little. Each of these will be discussed.

PSAD2A Computer Program

PSAD2A is the computer program used to analyze Benkelman beam loads. The program uses an iterative approach to determine moduli of the different layers. Several inputs are required for the program. Each layer must be characterized by

1. Poisson's ratio,
2. Dry density,

TABLE 2 Multivariate Regression Equations Developed from Laboratory Data for Predicting Resilient Modulus from Bulk or Deviator Stress, Moisture Content, and Dry Density

Site	Layer	Regression Equation	r^2
Olympic	Subgrade	$\log M_R = 0.749 + 0.673(\log\theta) - 0.0286(w/c) - 0.0008(\gamma_d)$	0.837
Olympic	Base	$\log M_R = -0.102 + 0.796(\log\theta) - 0.0124(w/c) + 0.0053(\gamma_d)$	0.845
Wenatchee	Subgrade	$\log M_R = -0.266 + 0.551(\log\theta) - 0.0554(w/c) + 0.0097(\gamma_d)$	0.894
Wenatchee	Base	$\log M_R = -0.636 + 0.581(\log\theta) - 0.0254(w/c) + 0.0102(\gamma_d)$	0.877
Deschutes	Subgrade	$\log M_R = -0.850 + 0.671(\log\theta) - 0.0122(w/c) + 0.0182(\gamma_d)$	0.895
Deschutes	Base	$\log M_R = 0.473 + 0.584(\log\theta) - 0.0324(w/c) + 0.0022(\gamma_d)$	0.930
Willamette	Subgrade	$\log M_R = 1.61 - 0.213(\log\sigma_d) - 0.0346(w/c) + 0.0130(\gamma_d)$	0.419
Willamette	Base	$\log M_R = -0.0143 + 0.645(\log\theta) - 0.0304(w/c) + 0.0035(\gamma_d)$	0.928

Note: M_R in ksi; θ and σ_d in psi (1 psi = 7 kN/m²); w/c in percent; γ_d in pcf (1 pcf = 0.16 kN/m³).

3. Thickness,
4. Stress relationship, and
5. Initial estimate of modulus.

Poisson's ratios for the individual layers were determined from average values found in the literature for similar material (8). The dry density of the asphalt concrete was assumed to be 150 pcf (24 kN/m³), and the dry densities for the soils were as measured in the field. The thicknesses of the layers were the actual thicknesses of the pavement components. The input values for each site are summarized in Table 3. The stress relationships to input were obtained from the regression equations presented in Table 2.

TABLE 3 Summary of the Layer Characteristics for the Four Test Sites

Site	Layer	Thickness (in.)	Dry Density (pcf)	Poisson's Ratio
Olympic	Asphalt	5.0	150	0.30
Olympic	Base	8.0	137	0.35
Olympic	Subgrade	212	115	0.40
Wenatchee	Asphalt	4.0	150	0.30
Wenatchee	Base	4.0	124	0.40
Wenatchee	Subgrade	212	129	0.40
Deschutes	Asphalt	5.0	150	0.30
Deschutes	Base	4.5	114.5	0.35
Deschutes	Subgrade	212	65	0.40
Willamette	Asphalt	2.4	150	0.30
Willamette	Base	14.4	127	0.35
Willamette	Subgrade	∞	—	0.45

Note: 1 in. = 2.54 cm; 1 pcf = 0.16 kN/m^3.

The base-course moisture contents were not measured in the field. For each site, the in situ base and subgrade moisture content were measured at the time of material sampling. The percentage of change in moisture content between that measured at sampling and those determined by the soil cells was assumed to be the same for the subgrade and base-course materials. In other words, the same percentage of increase or decrease in moisture content was assumed for both layers.

Because asphalt-concrete modulus changes with temperature, a temperature-corrected modulus was required. The pavement surface temperature was measured during each visit. To determine the asphalt-concrete temperature at the layer middepth, Southgate and Deen's method was used (9). This method uses air and pavement surface temperatures. Once this temperature had been determined, the correction factor (10) was multiplied by the laboratory asphalt-concrete modulus to provide the appropriate asphalt-concrete modulus at the time of deflection testing.

The load inputs were two loads of 4,500 lbf (20 kN) each, 12.7 in. (32.2 cm) apart center to center. The load radius was assumed to be 4.2 in. (10.8 cm), which corresponds to a tire pressure of 80 psi (552 kN/m²).

The output of the program consists of stresses, strains, and deflections. The outputs of primary interest were the surface deflection between the two tires, the modulus of each layer, bulk stress at the middle of the base course, bulk or deviator stress at the top of the subgrade, horizontal tensile strain at the bottom of the asphalt-concrete layer, and the vertical compressive strain at the top of the subgrade. Several runs were made for each test site, each one representing the subgrade moisture content and asphalt-concrete modulus for a particular site visit.

BISDEF Computer Program

BISDEF is a program that uses the concept of minimizing the differences between the computed and measured deflection basins to determine resilient moduli. This program was used to analyze the Dynaflect and the FWD data.

The inputs required by the program for each layer are

1. Poisson's ratio,
2. Thickness,
3. Range of allowable modulus, and
4. Initial estimate of modulus.

Poisson's ratios and layer thicknesses were the same as those used in PSAD2A.

The load inputs were those representative of Dynaflect loading, two 500-lbf (2.2-kN) loads 20 in. (51 cm) apart center to center. The loaded area per force wheel was assumed to be 4 in.² (25 cm²), giving a load radius of 1.13 in. (2.87 cm) (7). Four geophone inputs were used for all analyses.

The outputs of the program are the modulus of each layer and the stresses at any predetermined point. So that bulk and deviator stress could be determined, stress output was requested at the middle of the base and the top of the subgrade.

Dual Parametric Approach

This method is a graphical approach for subgrade modulus determination from Dynaflect deflections based on layered-elastic theory. It uses two deflection basin parameters. They are maximum deflection and spreadability.

Spreadability is defined as follows:

$$S = (d_{max} + d_1 + d_2 + d_3 + d_4)/5d_{max} \quad (1)$$

where d_{max} is the maximum pavement deflection and d_1, d_2, d_3, d_4 are deflections at 1, 2, 3, and 4 ft (0.3, 0.6, 0.9, and 1.2 m) from the center of the applied load. This approach is a modification of the Vaswani method (11).

One of the major assumptions in this method is that the spreadabilities for the deflection basin measured under Dynaflect and Benkelman beam are identical. This allows the subgrade modulus to be estimated under normal load conditions rather than under the light Dynaflect loads by obtaining only Dynaflect data.

To use the method to predict subgrade modulus a composite or average modulus of elasticity for the layers above the subgrade must be calculated. The equation used is as follows:

$$E_{avg} = (E_1h_1 + E_2h_2 + \ldots)/(h_1 + h_2 + \ldots) \quad (2)$$

where E_1, E_2, and so on, are the elastic moduli of the layers and h_1, h_2, and so on, are the corresponding thicknesses of the layers.

Once the composite modulus, spreadability, and maximum deflection are known, the subgrade modulus can be determined. This is done by using a graph such as that shown in Figure 4. For example, assume E_{avg} = 200,000 psi (1 380 000 kN/m²), the spreadability = 60, and the maximum deflection (Dynaflect converted to Benkelman beam, BB = D x 16.2) = 22.6 milli-in. This results in a subgrade modulus (E_s) of 10,000 psi (69 000 kN/m²) as illustrated in Figure 4. Moduli can be interpolated between lines.

Composite moduli were determined by using the temperature-corrected asphalt modulus and the PSAD2A-determined base-course modulus for the date being investigated.

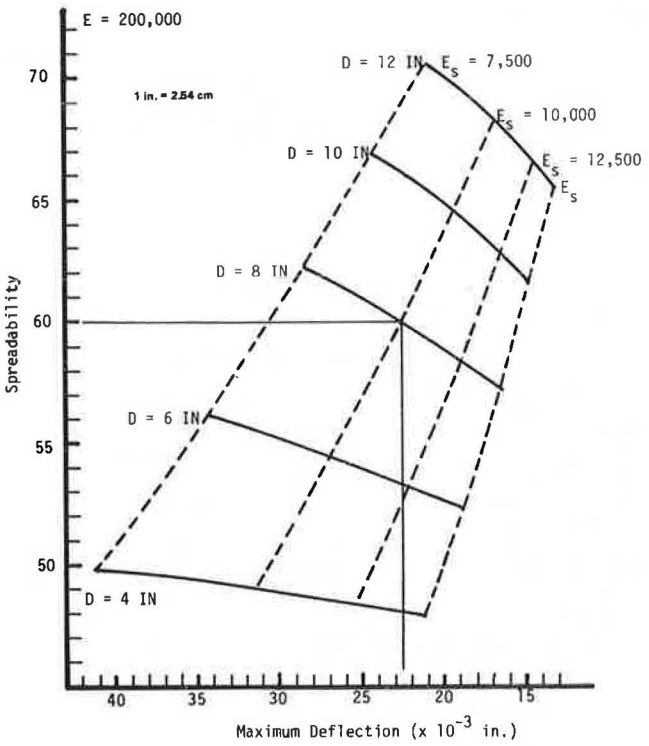

FIGURE 4 Typical graph for use with the dual parametric approach *(7)*.

Comparison of Subgrade Modulus Prediction Methods

To make comparisons it is necessary to examine the loading conditions used or assumed in the method. Benkelman beam loads were used in PSAD2A. The dual parametric approach uses Dynaflect deflections converted to Benkelman beam values. The FWD can be used to approximate essentially any loading condition. Even though all three measurement systems can be in terms of Benkelman beam loading conditions, stress-sensitive layers will not necessarily react similarly. Given this shortcoming, comparisons are presented in Table 4.

With the exception of the Olympic test site the dual parametric approach and PSAD2A results matched well. A difficulty with the dual parametric approach is that it does not, as currently developed, predict moduli less than 7,500 psi (51 800 kN/m²); however, the procedure can be easily extended to overcome this limitation.

In a comparison of the modulus predicted by using FWD data in BISDEF with that predicted by using PSAD2A, the results were favorable. This indicates that the regression equations are a good predictor of subgrade modulus because they were the basis for the output of PSAD2A. Another indication that the equations reasonably predict modulus is that the actual and predicted deflections are similar. This indicates that the equations (derived from laboratory data) reasonably matched the in situ soil conditions.

As an additional check on how well the laboratory-based equations predict modulus, the deviator stress resulting from FWD loading was placed in the regression equation for the Willamette subgrade in order to predict subgrade modulus. By using a moisture content of 51.7 percent as measured by the soil cells and a dry density of 66 pcf (10.57 kN/m³), the equation predicted a modulus of 3,370 psi (23 240 kN/m²) as compared with that of 3,410 psi (23 540 kN/m²) for BISDEF. To see whether the same predictive capability existed for the base-course equation for Willamette, it too was analyzed. By using a bulk stress of 11.4 psi (78.4 kN/m²), a moisture content of 5.2 percent, and a dry density of 127 pcf (20.34 kN/m³), the equation predicted a base-course modulus of 8,970 psi (61 890 kN/m²). This can be compared with the BISDEF-predicted modulus of 6,600 psi (45 530 kN/m²). Again the comparison was reasonable.

To see whether this trend continued, the same analysis was completed for the Olympic National Forest FWD data. Three stress levels were used at this site; thus more comparisons could be made (results are shown in Table 5). As shown, the base-course moduli are similar, whereas the equations predict subgrade moduli one-third those predicted by BISDEF. Recall that the dual parametric approach

TABLE 4 Comparison of Predicted Subgrade Modulus Values for the Four Test Sites

Date	PSAD2A (psi)	Dual Parametric Approach (psi)
USFS Road 220, Olympic National Forest		
01/29/81	12,410	26,100
11/06/81	10,510	27,000
01/28/82	9,260	31,500
02/25/82	9,060	32,000
05/11/82	10,620	32,300
USFS Road 2451, Wenatchee National Forest		
11/05/81	18,230	20,000
04/15/82	13,750	13,750
05/11/82	16,480	15,850
USFS Road 2301, Deschutes National Forest		
01/28/81	2,970	<7,500
03/24/81	4,450	<7,500
05/19/81	4,460	<7,500
11/19/81	4,090	<7,500
02/22/82	4,340	8,470
04/21/82	4,780	<7,500
05/17/82	4,850	<7,500
USFS Road 2233, Willamette National Forest		
01/27/81	1,420	<7,500
03/25/81	2,120	<7,500
04/20/81	3,280	<7,500
05/18/81	1,540	<7,500
07/16/81	3,350	
11/18/81	2,890	<7,500
04/22/82	3,260	<7,500
05/17/82	2,560	<7,500

Note: Subgrade modulus values measured with the FWD on 4/16/81 in the Olympic National Forest and 6/23/81 in Willamette National Forest were 34,503 and 3,410 psi, respectively. 1 psi = 7 kN/m².

TABLE 5 Comparison of Moduli Predicted by BISDEF for FWD Loading and by the Regression Equations, Olympic National Forest, USFS Road 220

Base θ (psi)	Subgrade θ (psi)	Base M_R from BISDEF (psi)	Base M_R from Equation[a] (psi)	Subgrade M_R from BISDEF (psi)	Subgrade M_R from Equation[b] (psi)
15.6	11.5	29,130	29,740	37,390	11,010
15.0	11.2	23,850	28,830	34,500	10,820
19.5	14.4	48,630	35,520	37,380	12,810
19.8	14.8	33,550	35,960	34,160	13,050
25.1	18.8	46,210	43,430	35,540	15,330
30.6	18.2	62,550	50,850	38,470	15,000

Note: 1 psi = 7 kN/m²; 1 pcf = 0.16 kN/m³.
[a]Using γ_d = 137 pcf, w/c = 8.1 percent.
[b]Using γ_d = 115 pcf, w/c = 11.5 percent.

also predicted subgrade moduli in the range of 30,000 psi (207 000 kN/m²), which indicates that possibly the Olympic subgrade equation is not representative of the subgrade soil behavior.

SEASONAL VARIATIONS OF MATERIAL PROPERTIES

By referring to Table 4, it is observed that the amount of change in the predicted subgrade moduli varies between test sites and with time of the year (both as one would expect). The subgrade soils at the test sites were generally coarse-grained (Olympic, Wenatchee, and Deschutes) and hence (as the predictions show) vary only small to modest amounts throughout the year. Based on the PSAD2A-predicted moduli, the percentage differences given in Table 6 were found for the four test sites. As shown in Table 6, the fine-grained subgrade at the Willamette test site varied by 40 to 50 percent during the data-collection period. Thus, a road structure designed without consideration of such variation could be easily underdesigned. However, the modest subgrade variations at the other test sites were much lower, primarily because of more granular gradation of the subgrade soils.

Table 4 also reveals another interesting observation: The critical (or weakest) period for the Deschutes test site did not occur in the early spring but in November (however, the moduli variations from that test site are low). Further, the critical period for the remaining test sites ranged from February through May. This is quite reasonable given that the frost penetration at all of the test sites was minor. Thus, the predicted moduli are primarily a function of rainfall, not of the formation and subsequent thawing of ice lenses in frost-susceptible soils.

TABLE 6 Percentage Differences for Moduli at Four Test Sites

Site	Percentage Differences: Between Maximum and Minimum Values	Percentage Differences: Between Mean and Minimum Values
Olympic	27	13
Wenatchee	25	15
Deschutes	16[a]	9
Willamette	54	43

[a]First observation not used.

SUMMARY AND CONCLUSIONS

Seasonal variations in pavement strength caused by environmental conditions pose difficult problems. These variations can cause deterioration of the pavement structure, which results in maintenance, rehabilitation, and higher user costs. This study was undertaken to evaluate the effect of seasonal variations on pavement stiffness and strength and to develop a method to predict seasonal changes in modulus from easily measured field data.

To accomplish these goals, four USFS roads were chosen to be monitored over an 18-month period beginning in January 1981 (two in Washington and two in Oregon). Surface deflections were measured by using a Dynaflect and Benkelman beam, subgrade moisture content was measured by using Soiltest moisture-temperature cells, and weather data were collected from nearby weather stations. In addition soil samples and pavement cores were obtained and subjected to resilient modulus testing.

Two major relationships were explored:

1. Prediction of subgrade resilient modulus from soil moisture content and
2. Prediction of subgrade resilient modulus from measured surface deflections.

Predicting subgrade modulus from soil moisture content was accomplished through the use of regression equations developed from the laboratory resilient modulus testing. In the equations resilient modulus is a function of soil moisture content, dry density, and bulk or deviator stress.

To predict subgrade modulus from measured deflections, three analysis methods were chosen. Two were computer programs, PSAD2A and BISDEF, and the third, a hand-calculation method, was the dual parametric approach. PSAD2A was used to analyze the Benkelman beam data and BISDEF and the dual parametric approach were used to analyze the Dynaflect data because they use deflection basins.

In addition to predicting modulus, percentage changes in modulus over time were calculated to determine seasonal variations in pavement strength for the four test sites.

The following conclusions are appropriate:

1. The regression equations (based on moisture content, soil dry density, and bulk or deviator stress) developed from laboratory resilient modulus data can be used to reasonably predict subgrade and base-course resilient modulus.
2. The dual parametric approach is an easy-to-use and accurate method of predicting subgrade modulus by using Dynaflect data. The method, however, needs to be extended to accommodate subgrade modulus values below 7,500 psi.
3. Fine-grained subgrade soils exhibit larger variations in resilient modulus throughout the year than do the more granular subgrade soils encountered in this study.
4. When frost penetration into the pavement structure is minimal, variation in modulus is primarily a function of rainfall and the minimum modulus for the year does not necessarily occur during the spring.

ACKNOWLEDGMENT

The authors gratefully acknowledge the funding of the reported study by the U.S. Forest Service, Region 6, and specifically Ron Williamson and John Stewart. Further, the study was a cooperative activity of the University of Washington and Oregon State University.

REFERENCES

1. S.W. Lee. Frost Penetration in the State of Washington. M.S. thesis. University of Washington, Seattle, 1982.
2. W.J. Ryan. Estimates of Winter Ground Freezing in the State of Oregon. M.S. thesis. University of Washington, Seattle, 1982.
3. R.G. Hicks, J.D. Swait, Jr., and E.O. Chastain. Use of Layered Theory in the Design and Evaluation of Pavement Systems, 3rd ed. Department of Civil Engineering, Oregon State University, Corvallis, Jan. 1978.
4. A. Jones. Tables of Stresses in Three-Layer Elastic Systems. Bull. 342. HRB, National Research Council, Washington, D.C., 1962, pp. 176-214.

5. K.R. Peattie. Stress and Strain Factors for Three-Layer Elastic Systems. Bull. 342. HRB, National Research Council, Washington D.C., 1962, pp. 215-252.
6. W.R. Barker and W.N. Brabston. Development of a Structural Design Procedure for Flexible Airport Pavements. Report FAA-RD-74-199. U.S. Army Corps of Engineers Waterways Experiment Station, Vicksburg, Miss., Sept. 1975.
7. D.N. Little. The Dual Parametric Approach to the Analysis of Surface Deflection Data. Texas Transportation Institute, Texas A&M University System, College Station, June 1980.
8. Flexible Pavement Design and Management, Materials Characterization. NCHRP Report 140. TRB, National Research Council, Washington, D.C., 1973.
9. H.F. Southgate and R.D. Deen. Temperature Distribution within Asphalt Pavements and Its Relationship to Pavement Deflection. Report HRP-1(3), Part II: KYHPR-64-20. Division of Research, Kentucky Department of Highways, Lexington, 1964.
10. W. Barker et al. Description of BISDEF Program. U.S. Army Corps of Engineers, Aug. 1982.
11. N.K. Vaswani. Method for Separately Evaluating Structural Performance of Subgrades and Overlying Flexible Pavements. In Highway Research Record 362, TRB, National Research Council, Washington, D.C., 1971, pp. 48-62.

Publication of this paper sponsored by Committee on Strength and Deformation Characteristics of Pavement Sections.

Stresses in Full-Depth Granular Pavements

S.R. DODDIHAL and B.B. PANDEY

ABSTRACT

Highway pavements for moderate to low-volume traffic often consist of granular materials topped with thin bituminous surfacing. The particulate bases transfer the stresses to the underlying layer by grain-to-grain interaction and cannot resist tensile stresses. The usual analysis of multilayer pavements requires the granular layers to possess tensile strength. A finite-element solution is presented for determination of stresses in pavements made up of full-depth granular layers. In this method the tensile stresses computed in the elements of the granular material by the elastic approach are eliminated during each iteration until the solution converges. The vertical stresses on the subgrade are found to be significantly higher than those obtained from linear-elastic analysis.

Design of highway and airfield pavements involves selection of materials and determination of the thickness of various layers that should be used in pavement construction so that the pavement layers are stable and carry the traffic during the design period without any major maintenance. Highway pavements in India and elsewhere for moderate to low-volume traffic consist essentially of granular materials in the form of water-bound macadam or crushed rock with thin bituminous surfacing. The pavements in such cases are practically full-depth granular construction if the strength of the thin bituminous surfacing is ignored. Analysis of such pavements requires special consideration because of the particulate nature of the materials and the absence of confinement for want of a thick bituminous surfacing.

Various organizations have developed computer programs such as BISAR (1), CHEVRON (2), ELSYM 5 (3), and so on, based on multilayer elastic theory, which requires the granular materials to withstand tensile stresses. Materials like crushed rock or water-bound macadam have little or no strength in tension. The little tensile strength that they may have is because of the interlocking and the intergranular friction. Hence the linear or nonlinear elastic analyses used by different researchers require modification to account for the limited tensile strength of granular layers of flexible pavements.

Some of the design procedures (4-6) assign definite values of elastic moduli to the granular bases depending on the thickness of the layers, and the pavement is analyzed as an elastic-layered system. The maximum tensile strain in asphalt concrete and the vertical stress or strain on the subgrade are evaluated in order to ensure the safety of the pavement from fatigue and rutting, respectively.

In this paper the development of an analytical method for estimating stresses in full-depth granular pavements is described that takes into account the limited tensile strength of granular materials.

DEVELOPMENT OF COMPUTER PROGRAM

A finite-element technique has been adopted to develop computer programs for calculation of stresses in granular pavements. A program designated EPAVE

was first developed for elastic analysis of a layered pavement. This formed the basis for development of computer programs that considered the no-tension nature of the granular layers. EPAVE was subsequently modified to account for the low tensile strength of granular materials and the modified program was termed NPAVE. When the results of NPAVE were compared with experimental values for full-depth granular pavements the NPAVE program was further refined, and the new program for the full-depth granular pavements was named MPAVE.

EPAVE Program

For developing this basic program, a layered system is idealized as an axisymmetric solid with finite boundaries in both radial and vertical directions. Nodal points on the vertical boundaries at the center line and at a distance of 12 radii from the center have been constrained from radial movement and those on the bottom boundary were not allowed to move in either the vertical or the horizontal direction. The bottom boundary has been fixed at a depth of 18 radii in the case of elastic half-space analysis and at a depth of 50 radii for layered pavements as suggested by Duncan et al. (7). The axisymmetry body has been divided into a set of 360 triangular ring elements. Meshes are closer near the axis of symmetry, and they have been gradually widened toward the boundaries as shown in Figure 1. The displacements within an element are represented by linear polynomials and one-point integration has been used for finding the stiffness of each element. The global stiffness of the system is banded and symmetric and the nodal displacements are obtained by a modified Gaussian elimination technique to suit the storage of the stiffness in half-band form. The analysis has been carried out for a single wheel load of 40 131 N (9,000 lb) distributed over a circular area with a tire pressure of 0.55 MPa (80 psi) by using a consistent load vector. The stresses calculated by this program agree well with those obtained from elastic half-space analysis (8) as shown in Figure 2 and indicate the validity of the formulation. Poisson's ratio has been taken as 0.35 for all the layers.

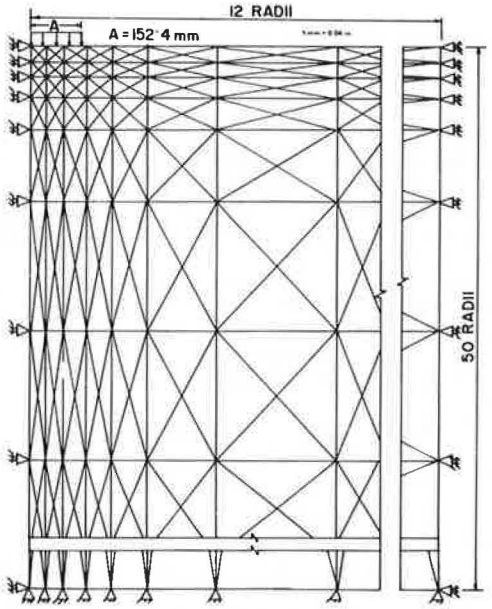

FIGURE 1 Finite-element idealization of pavement.

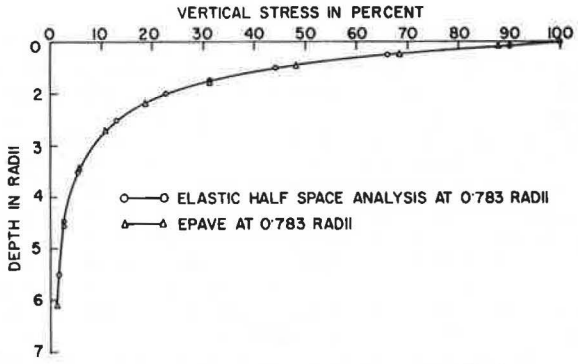

FIGURE 2 Comparison of vertical stress at 0.783 times radius of loaded region from EPAVE and elastic half-space analysis.

NPAVE Program

The elastic analysis invariably exhibits tensile stresses in unbound granular layers, which they cannot resist. These tensile stresses are eliminated by adopting the following steps based on the principle of stress transfer developed by Zienkiewicz et al. (9):

1. Elastic analysis is carried out.
2. Principal stresses (σ_1, σ_2, σ_3) at the centroid of each element in granular layers are calculated by using the formulas given as follows:

$$\sigma_1, \sigma_2 = [(\sigma_z + \sigma_r)/2] \pm \left\{[(\sigma_z - \sigma_r)/2]^2 + \tau_{rz}^2\right\}^{1/2} \quad (1)$$

$$\sigma_3 = \sigma_\theta \quad (2)$$

where σ_1, σ_2, and σ_3 are the principal stresses at the centroid of each element and σ_z, σ_r, σ_θ, and τ_{rz} are, respectively, vertical, radial, tangential, and shear stresses at the centroid of each element.

3. The angles of inclination (θ) of principal planes are determined.
4. Principal tensile and compressive stresses are identified.
5. A nominal stress of 0.0055 MPa (0.80 psi) equal to 1 percent of the applied surface pressure is taken as the limiting tensile strength of granular materials.
6. If the principal tensile stresses are greater than the limiting value, stresses (σ_z, σ_r, τ_{rz}, σ_θ) necessary on the elements to cause only principal tensile stresses are calculated from the following:

$$\sigma_z = [(\sigma_1 + \sigma_2)/2] + [(\sigma_1 - \sigma_2)/2] \cos 2\theta \quad (3)$$

$$\sigma_r = [(\sigma_1 + \sigma_2)/2] - [(\sigma_1 - \sigma_2)/2] \cos 2\theta \quad (4)$$

$$\sigma_\theta = \sigma_3 \quad (5)$$

$$\tau_{rz} = [(\sigma_1 - \sigma_2)/2] \sin 2\theta \quad (6)$$

7. The nodal forces $\{q^e\}$ required to develop stresses σ_z, σ_r, σ_θ, and τ_{rz} calculated in step 6 are found by using the following equation:

$$\{q^e\} = \int [B]^T \{\sigma\} \, d(\text{vol}) \quad (7)$$

where

$[B]^T$ = transpose of strain matrix of an element,
$\{\sigma\}$ = stress vector at the centroid of the element, and
vol = volume of the element.

8. The nodal forces obtained in step 7 are assembled to obtain the global load vector.
9. The stresses σ_z, σ_r, τ_{rz}, and σ_θ necessary on the elements to develop only principal compressive stresses are calculated.
10. Once again the elastic analysis is carried out with the load vector calculated in step 8.
11. The stresses obtained in step 10 are added to the stress found in step 9 and strains obtained in step 10 are added to those of the previous elastic analysis.
12. Steps 2 to 11 are repeated until the tensile stresses in the granular layer become equal to or less than 0.0055 MPa.

It is observed that for $E_2/E_3 = 2$ and $H_2/A = 5$, convergence occurred within four cycles, whereas for $E_2/E_3 = 20$, $H_2/A = 2$, six cycles were required for convergence. The larger the tensile stresses computed by the elastic analysis, the greater is the number of iterations for convergence.

NPAVE RESULTS

Full-depth granular pavements have been analyzed for thicknesses ranging from two to five times the radius of the loaded area and modular ratios ranging from 2 to 20. The vertical stresses on the top of the subgrade estimated by the EPAVE and NPAVE programs are given in Table 1. It is seen that the no-tension analysis (NPAVE) gives higher vertical stresses than the corresponding elastic analysis (EPAVE). In order to check the validity of the analysis, the measured values of stresses by McMahon and Yoder (10), Khanna and Mathur (11), and De (12) have been compared with those predicted by the programs EPAVE and NPAVE and are shown in Tables 2, 3, and 4. To compare the results of McMahon and Yoder (10), the modular ratio has been computed by using the equation given by Edwards and Valkering (13) because these bases were made up of crushed limestone well compacted by a gasoline-powered vibrator. The modular-ratio equation is given as follows:

$$E_2/E_3 = 0.58H_2^{0.45} \quad (8)$$

where E_2 and E_3 are the elastic moduli of the granular base and the subgrade, respectively, and H_2 is the thickness of the granular layer in millimeters.

The formula for computation of the modular ratio given by Dormon and Metcalf (14) has been adopted for comparing experimental results of Khanna and Mathur (11) and De (12), who used open-graded granular materials during their experiments. In the model tests reported by Khanna and Mathur, 25-mm (1-in.) aggregates were evenly spread to a loose depth of 100 mm (4 in.) in a tank 1.22 x 1.22 m (4 x 4 ft), and the layer was compacted dry. Subsequently 12.5-mm (0.49-in.) aggregate and moorum with 75 percent sand were added in stages and compacted first in the dry condition and then after the surface had been wet with water. The compacted depth was 75 mm (3 in.). Various layers were constructed in multiples of 75 mm. The granular layers in De's model experiments consisted of aggregates that passed through the following sieve sizes: 19, 12.5, 9.5, 4.76, and 2.36 mm (3/4, 1/2, 1/8 in. and No. 4 and No. 8). The percent passing was 100, 93, 88, 50, and 0, respectively. The modular-ratio formula is taken as follows:

$$E_2/E_3 = 0.2H_2^{0.45} \quad (9)$$

The validity of these approaches will be examined later in this paper.

Although the stresses obtained by the NPAVE program are higher than those computed by the EPAVE program, they are still significantly lower than the measured values. Hence the NPAVE program requires further modification to take into account the load-spreading behavior of granular materials.

From the pressure distribution diagrams obtained

TABLE 1 Vertical Stresses on Top of Subgrade

Slab No.	Thickness of Base Course (radii) (H_2/A)	Vertical Stresses (% compression) $E_2/E_3 = 2$ EPAVE	$E_2/E_3 = 2$ NPAVE	$E_2/E_3 = 10$ EPAVE	$E_2/E_3 = 10$ NPAVE	$E_2/E_3 = 20$ EPAVE	$E_2/E_3 = 20$ NPAVE
1	2.0	16.75	19.00	10.50	13.75	5.50	9.00
2	3.0	9.75	11.00	5.50	6.25	2.50	3.25
3	5.0	3.00	3.25	2.25	2.50	1.25	1.25

Note: A = radius of loaded area = 152.4 mm (6 in.); H_2/A = thickness of granular layer in radii; E_2/E_3 = ratio of the moduli of the granular layer and the subgrade.

TABLE 2 Comparison of Measured and Predicted Values of Vertical Stresses on Top of Subgrade: Results of McMahon and Yoder *(10)*

Slab No.	Plate Diameter and Base Thickness (mm)	H_2/A	E_2/E_3 ($0.58H_2^{0.45}$)	Vertical Stresses (% compression) McMahon and Yoder *(10)*	NPAVE	EPAVE	Elastic Half-Space Analysis[a]
1	182.6 and 101.6	1.113	4.64	51.0	52.03	44.57	60.00
2	182.6 and 203.2	2.226	6.34	17.0	12.97	11.63	23.74
3	182.6 and 304.8	3.339	7.61	12.5	5.76	5.32	12.60
4	304.8 and 203.2	1.330	6.34	38.0	33.66	28.61	48.80
5	304.8 and 304.8	2.000	7.61	26.0	14.86	12.87	28.45
6	457.2 and 304.8	1.330	7.61	38.0	31.59	26.01	48.80

Note: 1 mm = 0.04 in.
[a] $E_2/E_3 = 1$.

TABLE 3 Comparison of Measured and Predicted Values of Vertical Stresses on Top of Subgrade: Results of Khanna and Mathur *(11)*

Slab No.	Plate Diameter and Base Thickness (mm)	H_2/A	E_2/E_3 $(0.2H_2^{0.45})$	Vertical Stresses (% compression)			
				Khanna and Mathur *(11)*	NPAVE	EPAVE	Elastic Half-Space Analysis[a]
1	152.4 and 152.4	2.00	2.000	38.00	20.37	13.75	28.45
2	152.4 and 228.6	3.00	2.305	20.00	9.22	8.32	14.62

Note: 1 mm = 0.04 in.
[a]$E_2/E_3 = 1$.

TABLE 4 Comparison of Measured and Predicted Values of Vertical Stresses on Top of Subgrade: Results of De *(12)*

Slab No.	Plate Diameter and Base Thickness (mm)	H_2/A	E_2/E_3 $(0.2H_2^{0.45})$	Vertical Stresses (% compression)			
				De *(12)*	NPAVE	EPAVE	Elastic Half-Space Analysis[a]
1	330.2 and 304.8	1.846	2.623	28.80	23.24	20.28	32.63
2	228.6 and 228.6	2.000	2.305	34.00	20.37	17.72	28.45
3	152.4 and 228.6	3.000	2.305	20.00	9.22	8.32	14.62

Note: 1 mm = 0.04 in.
[a]$E_2/E_3 = 1$.

by Herner (15), Khanna and Mathur (11), and De (12), it is observed that the stress distribution in granular layers is confined to certain zones only. In the usual finite-element idealization all the elements up to 12 radii or more in the radial direction are considered for load transfer to the lower layers. It is seen from Figure 3 that the vertical pressure distribution on the subgrade due to the applied loads on the surface of the granular layers is confined within a zone formed by 45-degree lines, and hence the elements outside the zone do not participate in the stress distribution. They have been assigned a modular ratio one-tenth of their values in the NPAVE program. This makes the boundary of the zone nearly free and it simulates the stress distribution condition illustrated in Figure 3. This method of stiffness reduction is adopted so that the same NPAVE program can be used with a little modification in this case. The modified NPAVE program is termed MPAVE.

MPAVE RESULTS

Figures 4, 5, and 6 give the results of some full-depth granular pavements for both the EPAVE and the MPAVE programs. Because the vertical stress on the subgrade is a major factor to be considered in the design of such pavements, the values of the vertical stresses on the top of the subgrade are shown in Figure 7 for various modular ratios and pavement thicknesses for the EPAVE, NPAVE, and MPAVE programs. It may be seen that when H_2/A is equal to or greater than 5, all the analyses give the same results.

COMPARISON OF MPAVE STRESSES WITH MEASURED VALUES

The stresses measured by McMahon and Yoder (10) were compared with those estimated by the MPAVE program and are given in Table 5. For the comparison, the modular ratio given by Equation 8 has been used.

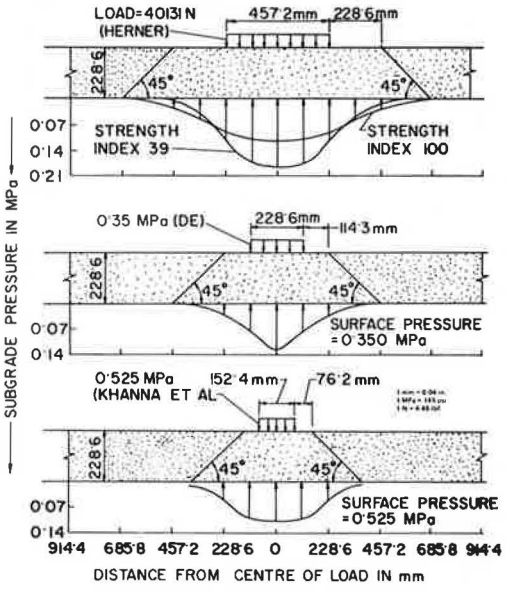

FIGURE 3 Stress distribution in granular bases.

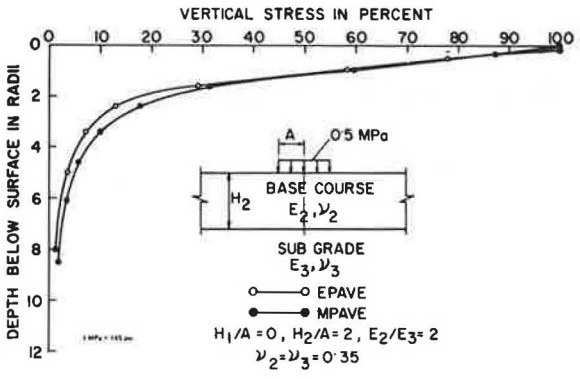

FIGURE 4 Vertical stress versus depth below surface for $H_2/A = 2$, $E_2/E_3 = 2$.

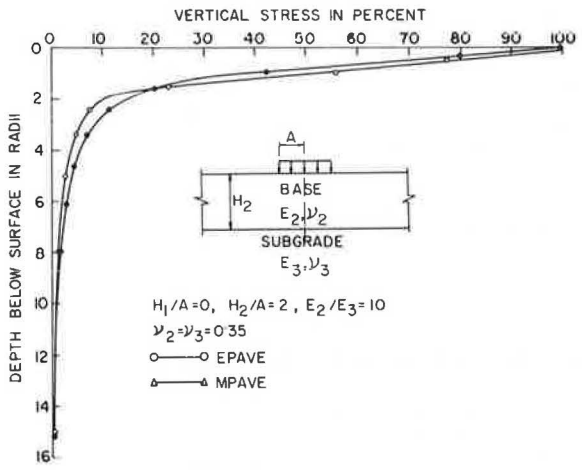

FIGURE 5 Vertical stress versus depth below surface for $H_2/A = 2$, $E_2/E_3 = 10$.

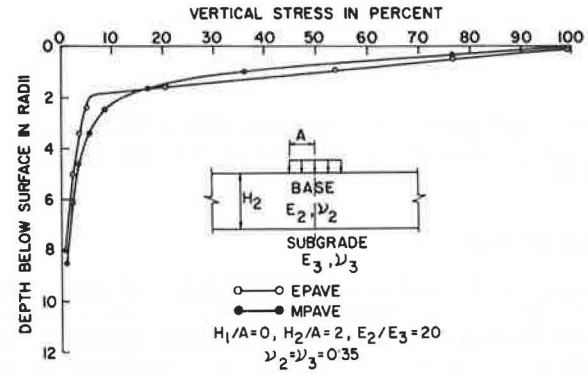

FIGURE 6 Vertical stress versus depth below surface for $H_2/A = 2$, $E_2/E_3 = 20$.

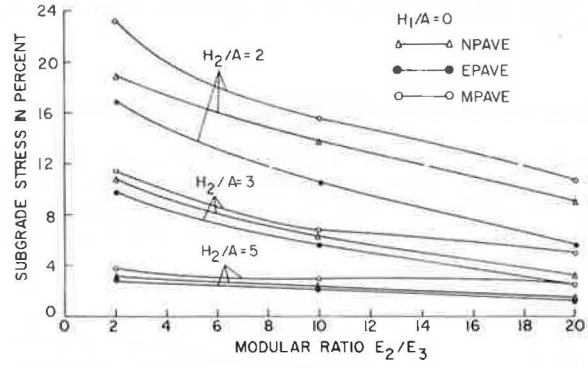

FIGURE 7 Subgrade stresses for granular pavements.

Table 5 shows clearly how the stresses on the subgrade increase as the program is improved by the consideration of the particulate nature of the base courses. The stresses predicted by MPAVE agree reasonably well with those measured by McMahon and Yoder (10) for rows 1, 2, 4, and 6, but the results in rows 3 and 5 deviate considerably from the measured values. However, it may be seen that McMahon and Yoder's results in rows 3 and 5 are close to the elastic half-space solution ($E_2/E_3 = 1$) given for those rows in the last column of Table 5. This indicates that the granular material was not effective in reducing vertical stress on the subgrade, probably because of lack of proper grading or poor compaction or both.

Stresses measured by Khanna and Mathur (11) and by De (12) are compared with those predicted by MPAVE and elastic half-space analysis. The comparison is shown in Tables 6 and 7. For these cases Equation 9 is used for modular-ratio calculation. Measured values by Khanna and Mathur (11) are considerably higher than those predicted by the elastic half-space solution ($E_2/E_3 = 1$), which indicates that the base course was of poor quality. The stress predicted by MPAVE nearly agrees with that measured by De in row 1, but other results deviate considerably from the measured values. However, it may be seen that the measured values in rows 2 and 3 are much higher than those predicted by the elastic half-space solution. This indicates that the granular layers had no strengthening effect because of lack of grading or improper compaction or both.

It is thus generally found that the vertical stresses on the top of the subgrade predicted by the MPAVE program are reasonably close to the experimental values for the base courses that are well graded and properly compacted.

It may be noted that the computation has been done with the assumption that the load is uniformly distributed over a circle, whereas experimental results were obtained from rigid-plate tests. But the numerous tests by Herner (15) on granular bases of various thicknesses indicated that the vertical pressure transmitted to the subgrades from the loads applied on the bases by rigid plates or by pneumatic tires are nearly the same, except for the tests on thin bases. In such cases the stress distribution curves from rigid-plate loading are a little flatter than those obtained from pneumatic-tire loading.

The measured values of vertical subgrade stress for the thinnest base layer in slab 1 of Table 5 are lower than the MPAVE or NPAVE values. On the basis of Herner's test results (15) discussed earlier, the experimental results of McMahon and Yoder (10) for the thin layer would have been still closer to those predicted by the MPAVE program if the load had been applied by pneumatic tires. The comparison of the theoretical values with experimental results substantiates the validity of the theory within reasonable engineering accuracy in spite of unavoidable experimental errors in pressure measurement in the

TABLE 5 Comparison of Experimental Results of McMahon and Yoder *(10)* with Computed Results

Slab No.	Plate Diameter and Base Thickness (mm)	H_2/A	E_2/E_3 $(0.58H_2^{0.45})$	Vertical Stresses (% compression)				
				McMahon and Yoder *(10)*	EPAVE	NPAVE	MPAVE	Elastic Half-Space Analysis
1	182.6 and 101.6	1.113	4.64	51.00	44.57	52.03	55.42	60.00
2	182.6 and 203.2	2.226	6.34	17.00	11.63	12.97	15.22	23.74
3	182.6 and 304.8	3.339	7.61	12.50	5.32	5.76	7.04	12.60
4	304.8 and 203.2	1.330	6.34	38.00	28.61	33.66	37.28	48.80
5	304.8 and 304.8	2.000	7.61	26.00	12.87	14.86	17.18	28.45
6	457.2 and 304.8	1.330	7.61	38.00	26.01	31.59	34.94	48.80

Note: 1 mm = 0.04 in.

subgrade. McMahon and Yoder (10) have found the experimental errors to be within 5 percent of the actual values in clay soil.

VALIDITY OF DIFFERENT PROCEDURES

The measured values of stresses obtained by McMahon and Yoder (10) for well-compacted granular bases have been compared with those calculated by MPAVE by using modular ratios given by Equations 8 and 9; they are given in Table 8. It may be seen from columns 4, 5, and 6 of Table 8 that the vertical stresses on the subgrade by using the modular-ratio formula of Edwards and Valkering (13) are generally closer to the measured values than those computed by using Equation 9. Modular-ratio values given by others (5,16) generally give vertical stress values intermediate between those in columns 5 and 6. As mentioned earlier, the experimental values of McMahon and Yoder (10) in rows 3 and 5 are close to elastic half-space analysis, and this indicates that the bases were poorly constructed. The stresses computed with the modular ratio given by Dormon and Metcalf (14) for bases in rows 3 and 5 are closer to the measured values, whereas those computed by using the modular ratios given by Edwards and Valkering (13) are much lower. Hence the modular ratios given by Dormon and Metcalf (14) are suitable for poorly graded base courses like the water-bound macadam so commonly used in India. If a good computing facility is not available, elastic half-space analysis for full-depth granular pavements similar to water-bound macadam may be carried out to obtain a reasonable estimate of the vertical stress on the top of the subgrade.

CONCLUSION

The stresses and strains predicted by the EPAVE program agree with those obtained by elastic half-space analysis. The values of the vertical stresses on the top of the subgrade predicted by the NPAVE program are higher than those predicted by the EPAVE program. The maximum increase in vertical stress on the top of the subgrade is 63.6 percent for a pavement with $H_2/A = 2.0$ and $E_2/E_3 = 20$. The difference in the vertical stress estimated by the programs decreases with greater base-course thickness, and little difference is observed if the thickness of the granular layer is equal to or greater than five times the radius of the loaded area.

Measured vertical stresses on the top of the subgrade agree well with those predicted by MPAVE except for the cases in which the measured values are nearer or higher than those predicted by elastic half-space analysis. The measured values closer to or higher than the Boussinesq solution indicate that the grading or compaction or both of base courses are poor and there is no significant strengthening effect of the granular layer.

The modular-ratio equation given by Edwards and Valkering (13) is suitable for well-graded and properly compacted base courses. The values given by Dormon and Metcalf (14) appear to be more appropriate for poorly graded granular layers.

In the absence of a good computing facility elastic half-space analysis may be used for the computation of vertical stresses on the top of the subgrade for full-depth granular pavements in which granular materials are open graded.

TABLE 6 Comparison of Experimental Results by Khanna and Mathur *(11)* with Predicted Values

Slab No.	Plate Diameter and Base Thickness (mm)	H_2/A	E_2/E_3 $(0.2H_2^{0.45})$	Vertical Stresses (% compression)		
				Khanna and Mathur *(11)*	MPAVE	Elastic Half-Space Analysis
1	152.4 and 152.4	2.00	2.000	38.00	22.87	28.45
2	152.4 and 228.6	3.00	2.305	20.00	11.12	14.62

Note: 1 mm = 0.04 in.

TABLE 7 Comparison of Experimental Results by De *(12)* with Predicted Values

Slab No.	Plate Diameter and Base Thickness (mm)	H_2/A	E_2/E_3 $(0.2H_2^{0.45})$	Vertical Stresses (% compression)		
				De *(12)*	MPAVE	Elastic Half-Space Analysis
1	330.2 and 304.8	1.846	2.623	28.80	25.47	32.63
2	228.6 and 228.6	2.000	2.305	34.00	22.52	28.45
3	152.4 and 228.6	3.000	2.305	20.00	11.12	14.62

Note: 1 mm = 0.04 in.

TABLE 8 Measured and Computed Vertical Stresses by Using Modular Ratios Calculated by Different Equations

Slab No.	Plate Diameter and Base Thickness (mm)	H_2/A	Vertical Stresses (% compression)			
			McMahon and Yoder *(10)*	Dorman and Metcalf *(14)*	Edwards and Valkering *(13)*	Elastic Half-Space Analysis
1	182.6 and 101.6	1.113	51.00	63.41	55.42	60.00
2	182.6 and 203.2	2.226	17.00	18.80	15.12	23.74
3	182.6 and 304.8	3.339	12.50	9.08	7.04	12.60
4	304.8 and 203.8	1.330	38.00	46.06	37.28	48.80
5	304.8 and 304.8	2.000	26.00	22.16	17.18	28.45
6	457.2 and 304.8	1.330	38.00	45.05	34.94	48.80

Note: 1 mm = 0.04 in.

REFERENCES

1. D.L. DeJong, M.G.F. Poutz, and A.R. Korswagon. Computer Program BISAR: Layered Systems under Normal and Tangential Surface Loads. External Report AMSR, 006.73. Koniklijke/Shell Laboratorium, Amsterdam, Netherlands, 1973.
2. J. Michelow. Analysis of Stresses and Displacements in an n-layered Elastic System under a Load Uniformly Distributed on a Circular Area. California Research Corp., Richmond, Calif., Sept. 1963.
3. G. Ahlborn. ELSYM5 Computer Program for Determining Stresses and Deformation in a Five Layer Elastic System. University of California, Berkley, 1972.
4. A.I.M. Claessen, J.M. Edwards, P. Sommer, and P. Uge. Asphalt Pavement Design: The Shell Method. Proc., 4th International Conference on the Structural Design of Asphalt Pavements, Vol. 1, University of Michigan, Ann Arbor, 1977, pp. 39-74.
5. W.R. Barker, W.N. Brabston, and Y.T. Chou. A General System for the Structural Design of Flexible Pavements. Proc., 4th International Conference on the Structural Design of Asphalt Pavements, Vol. 1, University of Michigan, Ann Arbor, 1977, pp. 209-248.
6. R.C. Deen, H.G. Southgate, and J.H. Havens. Structural Analysis of Bituminous Concrete Pavements. Research Report 305. Division of Research, Kentucky Department of Highways, Frankfort, May 1971.
7. J.M. Duncan, C.L. Monismith, and E.L. Wilson. Finite Element Analysis of Pavements. In Highway Research Record 228, HRB, National Research Council, Washington, D.C., 1968, pp. 18-33.
8. R.G. Ahlvin and H.H. Ulery. Tabulated Values for Determining the Complete Pattern of Stresses, Strains and Deflections Beneath Uniform Circular Load on a Homogeneous Half Space. Bull. 342. HRB, National Research Council, Washington, D.C., 1962, pp. 1-13.
9. O.C. Zienkiewicz, S. Valliappan, and I.P. King. Stress Analysis of Rock as a "No-Tension" Material. Geotechnique, Vol. 18, 1968, pp. 56-66.
10. T.F. McMahon and E.J. Yoder. Design of a Pressure Sensitive Cell and Model Studies of Pressures in a Flexible Pavement Subgrade. HRB Proc., Vol. 39, 1960, pp. 650-682.
11. S.K. Khanna and O.P. Mathur. Load Transmission through Base Courses of Different Types and Thicknesses. Road Research Bull. 11. Indian Roads Congress, New Delhi, 1967, pp. 1-30.
12. D.C. De. Development of Earth Pressure Cell and Study of Stress Distribution Characteristics of Granular Base Course Materials. Master's thesis. Indian Institute of Technology, Kharagpur, India, 1969.
13. J.M. Edwards and C.P. Valkering. Structural Design of Asphalt Pavements. Shell International Petroleum Co., Ltd., London, 1970.
14. G.M. Dormon and C.T. Metcalf. Design Curves for Flexible Pavements Based on Layered System Theory. In Highway Research Record 71, HRB, National Research Council, Washington, D.C., 1965, pp. 69-84.
15. R.C. Herner. Progress Report on Load Transmission Characteristics of Flexible Paving and Base Courses. HRB Proc., Vol. 31, 1952, pp. 101-120.
16. B.E. Smith and M.W. Witczak. Equivalent Granular Base Moduli: Prediction. Transportation Engineering Journal of ASCE, Vol. 107, No. TE6, 1981, pp. 635-652.

Publication of this paper sponsored by Committee on Strength and Deformation Characteristics of Pavement Sections.